POLITECNICO DI MILANO

Dipartimento di Matematica "F. Brioschi"

Ph.D. Course in Mathematical Models and Methods for Engineering

XXIV Cycle

Numerical Modelling of Flows in Fractured Porous Media by the XFEM Method

Ph.D. candidate   Alessio Fumagalli
matr.   738811

Supervisor	Prof. Luca Formaggia
Tutor	Prof. Marco Verani
Coordinator	Prof. Paolo Biscari

Milan, 27ᵀᴴ April, 2012

Acknowledgements

Contents

List of symbols

We indicate the scalar values, scalar functions and sets by normal letters, like λ and Φ. Vectors and vector value functions are typeset in lower case and bold like $\boldsymbol{u}$ and $\boldsymbol{g}$. Tensors and tensor value functions are written in upper case and bold like $\boldsymbol{K}$ and $\boldsymbol{G}$.

β_γ Inverse of the equivalent molecular diffusion in the normal direction to the fracture γ, page 116

Ca   Capillary number in the dimensionless equations of the two-phase flow, page 39

c The concentration of a passive scalar or tracer, page 109

$\boldsymbol{u}$ Total velocity, page 30

$\boldsymbol{u}_\alpha$ Darcy velocity for the α phase, page 26

$\hat{\boldsymbol{u}}$ Reduced Darcy velocity for the Darcy reduced model, page 68

$\mathcal{E}_h$ Set of all the facets of the tessellation $\mathcal{T}_h$, page 50

η_γ Inverse of the equivalent permeability in the normal direction to the fracture γ, page 70

$\boldsymbol{I}$ Identity matrix, page 34

γ_{nw} The interface tension between the wetting w and non-wetting n phase, page 34

$\hat{\beta}$ Inverse of the equivalent molecular diffusion in the tangential direction to the fracture γ, page 115

$\hat{\eta}$ Inverse of the equivalent permeability in the tangential direction to the fracture γ for the Darcy reduced model, page 69

$[\![\cdot]\!]_\gamma$ Jump of a quantity across the fracture γ, page 68

λ Total mobility, page 29

λ_α Mobility for the α phase, page 29

$[\cdot]_i$ Element in position i of the vector in the square brackets, page 29

$[\cdot]_{ij}$ Element at row i and column j of the matrix in the square brackets, page 55

Introduction

The objective of this thesis is the development and the implementation of advanced models for the simulation of two phases flows in highly heterogeneous porous medium. The work has been coordinated in collaboration with Eni s.p.a., the major Italian oil industry, which also sponsored it.

In the last few decades oil industries have resorted more and more to mathematical and numerical modelling to locate new hydrocarbon reservoirs and to exploit the existing ones at their best. The exploration of hydrocarbons is a very expensive and risky operation, with a chance of success ranging from 30 to 80%. Accurate numerical simulation of generation and migration processes can support the tracking of hydrocarbons "from source to trap" and therefore reduce the risks and costs in oil exploration.

Hydrocarbons are generated several million of years ago in layers of sediments rich in organic matter, called *source rocks*, under suitable pressure and temperature conditions. Hydrocarbons then migrate upwards through the different layers and accumulate in a reservoir, a porous layer seated by a poorly permeable layer called *cap rock*. The migration of hydrocarbons consists of two distinct stages, characterized by different physical mechanisms and time scales. During the first stage, denoted as *primary migration*, oil and gas are expelled from the source rock as the layers compact, while during *secondary migration* hydrocarbons move towards the reservoir through the porosity and fractures of the rocks. A vast literature is present for flows of hydrocarbons in the underground in terms of both laboratory experiments and numerical models. Nevertheless the commonly numerical models used by petroleum engineering, like invasion percolation or flowpath modelling, are too simplistic to resolve all the physical phenomena of the problem. The major drawback is the lack of a detailed and realistic description of the fractures, since very often they use approximated relations to describe the presence of fractures. Recently, thanks to new fast numerical solvers and the diffusion of super-computers, the attention of the scientific community has turned to the resolution of the physical governing equations for the flow previously regarded as too computationally costly. Usually finite elements or finite volume methods are applied in order to solve these equations. Even if the aforementioned technological advantages can improve the performance of a simulation some problems still remain. Using both finite element or finite volume numerical schemes a computational grid which approximates the real domain has to be constructed. In realistic applications the creation of a mesh which resolves all the fractures present in the domain is complicated also for the modern mesh generation software. Furthermore the resulting grid may have poor quality and involve several billions of grid cells yielding a problem of prohibitive computational costs even in the high perfor-

mance computing framework. On the other hand if the computational grid does not resolve the fractures the solution we obtain is poorly approximated. Finally all the data we know about the properties of the underground at the time when the secondary migration took place, *i.e.* several million of years ago, are affected by uncertainty and multiple scenario analyses are required to obtain a better forecast of the reservoir distribution.

In [2] the authors proposed a model to overcome these problems, for the single-phase flow, using a domain decomposition approach where the fractures are natural interfaces between the domains with a suitable reduced model which describes the flow inside the fracture. The numerical simulations presented in the work are two-dimensional with simple geometries and the bulk grids are conforming to the fractures, *i.e.* the mesh of the fracture is composed by contiguous edges of the bulk mesh. The model proposed can successfully address the problem of the high number of unknowns in the simulation, in the restricted case of non intersecting fractures acting as preferential paths, which completely cut the domain in separated sub-domains. An improvements to the model is given in [48] where the authors presented a new reduced model which is also able to describe the fractures that, thanks to their low permeability, act as barriers for the flow. Numerical experiments are presented showing the capability of the reduced model to capture both the behaviours. Realistic simulation in a three dimensional porous medium are presented in [3] where also suitable interface conditions are imposed on the intersecting fractures. These conditions do not take into account the different properties of the fractures involved in an intersection, *e.g.* one fracture can act as a barrier with respect to the other one, and they simply impose the conservation of mass and the continuity of the pressure. In [57] the reduced model presented previously is extended to take into account the different pressure profiles in the fracture with an additional parameter. Existence and uniqueness of the solution to the model problem are proved. While all of the aforementioned models are written in the framework of domain decomposition and cannot handle fractures with tips, in [4] the model is extended to admit fractures which do not cut entirely the domain. Numerical experiments show the correctness of the extension. To overcome the limit of the conformity between the grids of the fractures and the grid of the porous medium, in [24] the authors extended the reduced model presented in [57] to the case of non matching grids between the fractures and the porous medium. The idea is based on a previous work [39] which uses the extended finite element method (XFEM) to allow discontinuity of the pressure and the Darcy velocity inside the cut elements of the bulk grid. With this model the problems of mesh conformity and generation disappear and the reduced model can be successfully applied to realistic problems. Finally in a recent work [46] the authors extend the reduced model valid for the single-phase flow to the two phase flow problem.

The aim of this thesis is twofold. We introduce further extensions of the non matching reduced model presented in [24] in the case of single-phase flow. In particular we address the problem of gravity effects, *i.e.* how the reduced model and the coupling conditions have to be modified to take into account this new feature correctly. In the framework of non matching grids, we extend the case of crossing fractures presented in [3] where suitable interface conditions are considered to allow jump in the pressure and in the velocity. In this case the XFEM method is applied to the porous matrix as well as to the fractures whose meshes form an arbitrary set of non matching grids which intersect and communicate.

Finally using the same mathematical and numerical tools we present a reduced model for the parabolic problem governing the transport of a passive tracer in the porous medium. For all of these models we present both analytical and numerical results with an emphasis on realistic problems. The other part of the thesis consists in the parallel implementation of a three-dimensional two-phase flow solver. Numerical test will be presented to verify the correctness of the implementation and the good properties in a high performance computing framework.

The thesis is organized as follows: the first chapter presents an overview of the physical process of the secondary migration of hydrocarbons, with an highlight on the state of the art and a detailed description on the effect of faults and horizons. In the second chapter the mathematical model which describes the two-phase flow is presented with details on the numerical scheme used for its solution. The third chapter is devoted in the presentation of reduced models to handle fractures in an efficient and effective way. Both geometrical and model complexity are addressed. In the fourth chapter the computational aspects of the implementation the of two-phase solver and the reduced models are shown. Finally, the fifth chapter contains several applicative examples, in particular some examples of two-phase flows in realistic domains, together with a further analysis of the reduced models and some test in high performance computing framework. A conclusive section summarizes the results of this work and possible future studies and improvements.

Chapter 1

From the source rock to the reservoir

A "Petroleum System" is a geologic system that encompasses the hydrocarbon source rocks and all related oil and gas, and which includes all of the geologic elements and processes that are essential if a hydrocarbon accumulation is to exist [56].

An hydrocarbon is an organic compound, which consists entirely of hydrogen and carbon. In nature the hydrocarbons can be principally found in the crude oil and natural gas, liquid and gas phases formed geological eras ago by decomposition of organic matter. The sedimentary basin is a geographical feature which exhibits subsidence and consequently infilling by sedimentation. The sedimentary basins lie on the bottom of depressed areas where the erosion processes deposit various kinds of materials. Typically the type of sediments deposited varies quite suddenly in a point of view of geological scales. This process forms some well defined sedimentary layers and the mixing between the different materials is very limited. The separating interfaces between the layers are called horizons.

Due to the lithostatic pressure, which is the pressure applied by the overburden and to the possible extension of the basin, the sedimentary layers tend to fracture and to modify their reciprocal position. See Figure 1.1 for an example of a basin with horizons and faults. The typical size of the basins is of
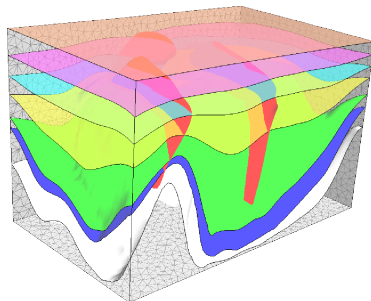
Figure 1.1: Sedimentary basin with three faults, in red, and several horizons, in different colours.

the order of 100 by 100 km in the horizontal plane and 10 km in depth. A reservoir is the portion of a sedimentary basin, usually sandstone, where hydrocarbons can migrate and accumulate. The petroleum was generated geological eras ago in the source rock, a thin layer of rock sediments rich in organic matter called kerogen, under suitable pressure and temperature conditions, usually called *oil window*. Several techniques are used to model transport and generation processes for hydrocarbon flow in order to improve the understanding and prediction of this phenomena. One of the techniques is the so-called *reservoir modelling*, *i.e.* the mathematical description of all the geological processes in a reservoir over geological time scales. Several geophysical processes are involved and the most important are: deposition, compaction, heat flow, petroleum generation and petroleum migration and accumulation. The deposition process
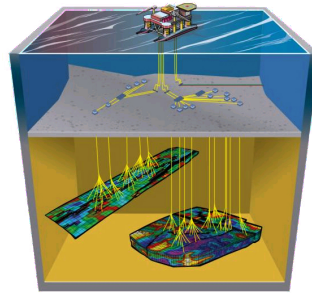
Figure 1.2: Offshore oil recovery, figure taken from Nexus® Reservoir Simulation Software.

describes the evolution of new layers of rocks on the top of the sedimentary basin, due to sedimentation and erosion phenomena. Pore pressure reduction, triggered by overburden weight due to sedimentation, entails compaction and produces changes in the geometry of the basin. Heat flow calculation is necessary to calibrate the geochemical reactions, which appear in all the geophysical processes.

The migration of hydrocarbons from source rock to trap, a part of the reservoir which is surrounded by an impermeable rock, called seal rock or cap-rock, consists of two different processes: the *primary* and the *secondary migration*. Primary migration consists in the expulsion of the hydrocarbons from the source rocks, while in the secondary migration the hydrocarbons flow from the source rock to the trap through the sedimentary basin, see Figure 1.3. Even if some
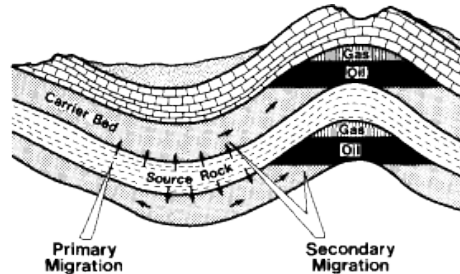
Figure 1.3: Primary and secondary migration, figure taken from [30].

physical aspects are similar, primary and secondary migration are character-

16

ized by different mechanisms, velocities and spatial scales. In this thesis our attention is principally focused on the secondary migration.

1.1 Secondary migration

The secondary migration is the movement of the hydrocarbons, composed by crude oil and natural gas, expelled from the source rock to the trap through the basin usually along horizons and faults.

Following the work of [29], [30] and [77] the secondary migration occurs by a mechanism involving two phases: petroleum, considering crude oil and natural gas as a single phase, and water. The petroleum, once expelled from the source rock, gradually accumulates as a separate phase from water, since it can be considered insoluble in water. Given that, and since the petroleum is less dense than surrounding pore water, it starts moving vertically, from bottom to top. The capillary pressure, which is the difference in pressure across an interface between two immiscible fluids, opposes the buoyancy force, discouraging the entry into smaller water-wet pores.

Reaching some low permeability regions, *e.g.* with very small pores size, the capillary pressure increases and the petroleum tends to move laterally over-coming the local capillary pressure barriers, for example in pore throats of a coarse-grained sandstone. The authors in [71] showed that the lateral migration distance for petroleum was usually about $10km$, but with a significant number of cases that exceed $80km$, while vertical distances range up to $1200m$. If no lateral path existed overpressure of the hydrocarbon would lead to break the barriers, enabling the flow of petroleum. Any time the petroleum reaches a capillary pressure heterogeneity, in the carrier bed, it starts to move in a tortuous pathway involving much of the carrier bed. However only a small part of the total carrier is exploited by the migrating petroleum [30]. Typical flow rate, based on average amount of expulsion oil, ranges from 8×10^{-15} to $8 \times 10^{-14} m^3/m^2/s$, see [30], therefore the total amount of oil involved in the secondary migration is very small. During the migration part of the oil is lost and remains immobile in the carrier: the authors in [59] studied 92 sample fields to determine the residual of oil content in reservoirs and it was found to range from 2% to 46%, with an approximate average of 15% to 20%.

The final part in the secondary migration is when hydrocarbons reach a trap and the accumulation process starts, see Figure 1.4. The geochemical composition of petroleum in the trap is constantly changing because the maturity of the source rock is varying with time. Because most reservoirs were felt from one side, there is a geochemical compositional gradient of petroleum. Over time, however, diffusion and convection can eliminate much of the inherited compositional gradients.

1.2 State of the art

Hydrocarbon migration at basin scale and geological time-scales may be modelled by several techniques. The most important and common methods used by the oil industries are: the solution of the equation governing the flow using the finite volume or the finite element method, the *flowpaths analyses* and the
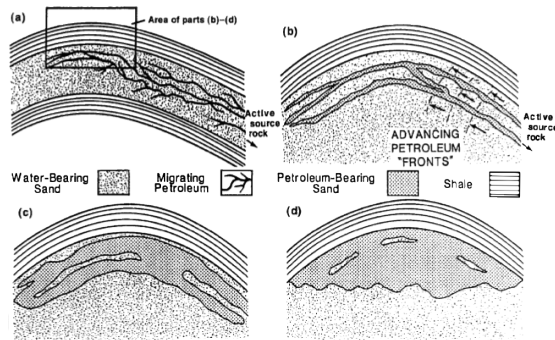
Figure 1.4: (a) Petroleum migrating into a trap from a source rock. (b) During the initial filling process, the coarsest beds are filled first with petroleum. Widespread mixing is impossible due to poor connectivity. (c) and (d) The increasing column height causes other parts of the reservoir rock to become saturated with petroleum. Figure taken from [56].

invasion percolation technique. If the simulations with the first method were sufficiently fast to allow high-resolution modelling the other method would be redundant. Both flowpaths analyses and invasion percolation are simplifications of the governing equations with the objective of increasing the spatial resolution at an affordable temporal cost. We present the models highlighting the advantages and disadvantages when they are applied in a secondary migration framework. Further details can be found in [8], [73], [21], [19] and [40].

1.2.1 Darcy flow

We call "Darcy flow" the method which solves the partial differential equations of the porous media flow and, using a finite volume method or a finite element method, gives the value of the oil saturation in each grid cell, as Figure 1.5 shows. The major advantage of the method is the simulation of all the most relevant
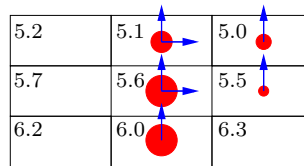
Figure 1.5: Example of a Darcy flow in a heterogeneous porous medium. The values are the oil potential. Figure taken from [40].

physical phenomena occurring in the secondary migration. Due to its complexity this method is the slowest and needs a lot of efforts to obtain the same spatial resolution of the other methods. Separate flow of non-mixing phases is usually assumed to be the dominant mechanism for secondary migration. Two or three phases are commonly used depending if we consider gas and oil as a separate phase. Chemical reactions and thermal description are needed to describe the quality of the hydrocarbon at the reservoir. In presence of a leakage from a cap rock the Darcy method will distribute hydrocarbons at low-saturation as a relatively broad chimney above the trap, because of the physical and numerical dispersion, the latter being caused by coarse grids. Chapter 2 is devoted to a

wide presentation of the Darcy flows in the secondary migration framework.

1.2.2 Flowpath modelling

The flowpath modelling, or ray-tracing method, constructs the flowpaths of the oil phase from a purely geometric analysis of the basin and indicates only the direction of the flow, as Figure 1.6 shows. Even if it is simple the construction of the method it provides an acceptable description of the secondary migration process. Ray-tracing assumes that hydrocarbon flow-rates, and therefore hydro-
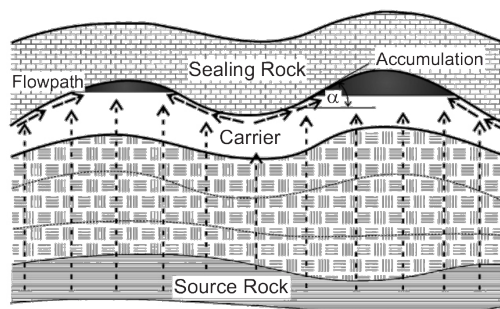
Figure 1.6: Section of a basin with the different layers. Figure taken from [40].

carbon saturation, changes very slowly compare to the chosen time step, hence a steady state model is applied. Only the buoyancy force drives the migration and the flow is modelled to occur up the steepest slop in a thin zone just below the seals of carriers, see Figure 1.7 as an example. Migration modelling
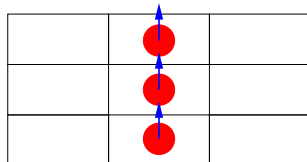
Figure 1.7: Schematic picture of the flowpath method in an homogeneous porous medium. Figure taken from [40].

with flowpaths has an implicit hight resolution because flowpaths can be constructed from interpolations of mapped grid-points. The flowpaths modelling can be applied also for multi-component systems. As Figure 1.8 shows, several flowpaths starting far from each other can end at one local height, hence all the hydrocarbons reaching the same trap have to be summed up. Due to its high efficiency the flowpath model is usually processed as a first guess model or as a crude approximation, even if the assumptions are poorly fulfilled. The major drawback of this method is its applicability to migration within mud-rocks.

1.2.3 Invasion percolation

In the invasion percolation method the flow is modelled using the entry pressure, also called threshold pressure, and assuming that the hydrocarbon saturation is
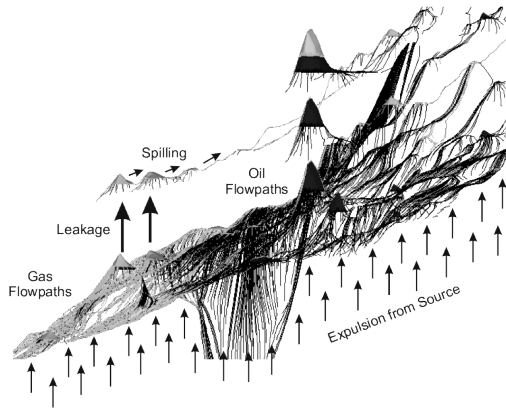
Figure 1.8: Flowpaths simulation in a basin with isolines depict the depth of the sealing interface. The values in the figure are in meters. Figure taken from [40].

constant. The driving force is the buoyancy while an additional pressure gradient can be taken into account. The migration of oil and gas from one cell to the next one is computed by looking for the neighbouring cell with the lowest resistance to the flow, *i.e.* lowest threshold pressure. All the saturation present in the cell is transferred into this neighbour cell, see Figure 1.9 for an example. At
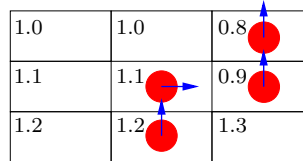
Figure 1.9: Schematic picture of the invasion percolation algorithm with the values of the entry pressure. Figure taken from [40].

the end of this process a backbone migration results and the sub-sequent migration is modelled to occur along the backbone. When a backbone reaches a cap rock an hydrocarbon column builds up, then the percolation method finds the next node with the lower entry pressure somewhere down along the migration path and continues incorporating new nodes. See Figure 1.10 for an example of invasion percolation in a permeable channel of a basin. In contrast with re-
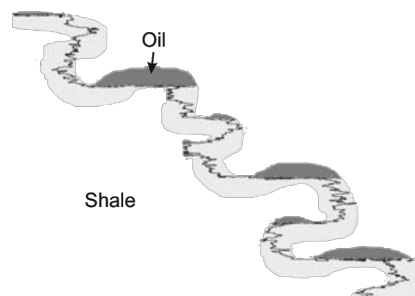
Figure 1.10: Example of the invasion percolation method in a basin. Figure taken from [40].

spect to the Darcy flow the method does not represent well the capillary leakage from the cap rocks, this imply that the hydrocarbon migration losses may be different. Due to the uncertainty on the underground properties it is difficult to model correctly the threshold pressure and its anisotropy hence in presence of heterogeneities the backbones created by the method can be different from one scenario to the others, as Figure 1.11 shows. The percolation method can be
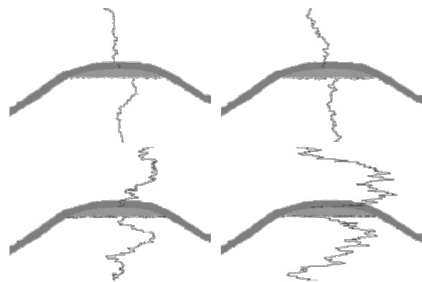
Figure 1.11: Solution with the percolation method with entry pressure heterogeneity of 10% variations and different anisotropy level. Figure taken from [40].

successfully used when the filling rates of a reservoir are very low, *e.g.* in some very old basins with very low thermal gradients, or in the assessment of multi extraction system in deltas. The major drawback of the invasion percolation method is that the dynamics of the basin, *e.g.* subsidence and compaction, is not fully incorporated and the faults geometries and properties are not represented with sufficient degrees of accuracy. Further details about the percolation method can be found in [44].

1.3 The effect of faults and horizons

Faults and horizons are important features that need to be accounted for in many geological systems to obtain a realistic behaviour of the underlying physical phenomena, nevertheless they are frequently ignored or treated in a very simplistic way. In this work we use the term *fracture* to indicate in general a localized heterogeneity such as a fault or an horizon. Faults can act as barriers or preferential paths for the flow at geological scales depending on their properties [16]. A fracture can act differently depending on the temporal window we are dealing with, in fact it can behave as a barrier at the production scale, *i.e.* years, while completely open to flow at a geological time scale.
Fractures and systems of fractures occur of different scales and with different geometries, they are principally generated by an over stress in the underground which can be lithostatic, tectonic, thermal or the result of overpressure of fluids. Tectonic fractures tend to be oriented along stress field on a regional scale, while the other types of stresses generate fractures on different scales and with different geometries. When sand or seal sequences are faulted, some of the materials is dragged into the fault plane. Clay or shale that is dragged into the fault plane will act as capillary caps to the hydrocarbons that try to flow through the very small holes of the clay stones. Hence the cross fault migration is controlled by the minimum entry pressure of the part of the fault plane that is in contact with hydrocarbons. When the thickness of the fault is large enough

Figure 1.12: Fracture network in sandstone, with horizons and faults. Figure taken from [28].

hydrocarbons may migrate along the fault plane and then they have to exceed the entry pressure of the fault plane to get out of it. Hence it is often more difficult to have migration up the fault plane than across it. The permeability
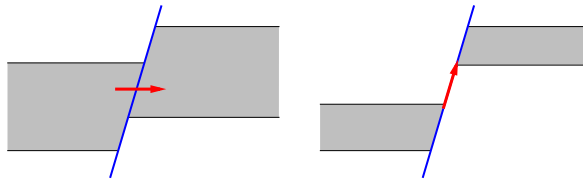
Figure 1.13: Different position of a fracture respect a low permeable layer, in grey. In the left figure the flow can take place across the fracture while in the right picture only along the fracture.

between fractures and the porous matrix spans many orders of magnitude and can vary extremely in space. Characterizing fractured system therefore requires a careful examination of the interconnections in the fracture network as well as an evaluation of the fracture matrix interaction. Further details can be found in [28].

Chapter 2

Two-phase flow

In this chapter we introduce equations governing the secondary migration in a sedimentary basin. We are interested in a very rather temporal window, we also assume a very low velocity flow and finally, since we focus on a macroscopic description of the phenomena, we can model the sedimentary basin as a porous medium [8]. We are interested in sedimentary basins which extend for several kilometres under the ground so we can suppose that the medium is saturated with water.

For simplicity we consider crude oil and natural gases as a single incompressible liquid phase, in the sequel called oil, and water as a different incompressible liquid phase. We consider oil and water as immiscible fluids.

Thanks to the previous assumptions we can model secondary migration with the *two-phase flow equations* in a porous media, considering water as the *wetting* phase and oil as the *non-wetting* phase. The set of equations for the two-phase flow is based on the Darcy's law for a fluid flow in a porous medium, which links, via the permeability tensor $\boldsymbol{K}$, the pressure p and a macroscopic velocity $\boldsymbol{u}$, usually called the Darcy's velocity.

The Darcy's law is an approximation of the conservation of momentum law [78] and is complemented with the equations for the conservation of mass for the fluids. When two immiscible fluids share the pore space experiments have shown [60] that the Darcy's law is still applicable, separately, for each phase with the addition of appropriate coupling conditions.

2.1 Two-phase flow equations

Let us consider the physical process that governs the flow of two immiscible phases in a porous medium. This two phases are the wetting phase, indicated with subscript w, and the non-wetting phase, indicated with the subscript n. The interaction between the adhesive forces, which attract the fluid molecules to the solid, and the cohesive forces, which attract the molecules of the two fluids, lead to a contact angle. The fluid which angle is less then $90°$ is the wetting phase while the other is the non-wetting phase. Here, and in the sequel, we indicate with the subscript α quantities for one of the two phases, *i.e.* $\alpha \in \{w, n\}$.

Assumption 2.1 (Porous matrix)**.** *We assume the following hypotheses, taken from [9, 23, 8], to identify the rock matrix as a porous medium:*

1. *the non-solid space of the solid porous matrix is interconnected, so no flow can take place in a disconnected void space. If unconnected pores exist they can be considered, for our purpose, as part of the solid matrix;*

2. *the smallest dimension of the pore solid space is large enough to contain fluid particles, i.e. it is large compared to the mean-free path of fluid molecules, therefore we may replace the fluid molecules in the void space by an hypothetical continuum. For example, see [49], the mean-free path of air in standard temperature is 68 nm while the mean-free path for water is 2 Å;*

3. *the dimensions of the pore space is small enough so that the fluid flow is controlled by adhesive forces at liquid-solid interfaces and cohesive forces at fluid-fluid interfaces. We exclude cases like a network of pipes.*

We focus on the study of fluid flows between the microscopic scale, *i.e.* $\sim 10^{-3}m$, and the macroscopic scale, *i.e.* $\sim 10m$, where the statistical average permits the continuum approach to the model [9]. We will use macroscopic equations that do not need an exact description of the microscopic configuration of the porous medium with its properties so, as we said, only measurable statistical properties of the porous medium and the fluids are required. Let us introduce the mathematical requests for the domain of interest.

Assumption 2.2 (Domain). *We introduce the main hypotheses for the computational domain* Ω:

1. Ω *is an open bounded measurable subset of* $\mathbb{R}^n$, *with* $n = 2$ *or* 3, *with Lipschitz boundary* $\Gamma := \partial\Omega$ *of outward unit normal* $\boldsymbol{n}$. *The interval of time is* $\mathcal{I}_T := (0, T)$, *with* $T \in \mathbb{R}^+$. *We define* $Q_T := \Omega \times \mathcal{I}_T$ *the space-time domain of interest;*

2. Γ *is partitioned in measurable sub-sets* Γ^i *and* Υ^i *where boundary conditions for the Darcy and saturation equations will be imposed. We have*

$$\overline{\Gamma} = \overline{\Gamma}^N \cup \overline{\Gamma}^E \cup \overline{\Gamma}^R \quad and \quad \mathring{\Gamma}^i \cap \mathring{\Gamma}^j = \emptyset \quad for \ i \neq j = N, E, R,$$

$$\overline{\Gamma} = \overline{\Upsilon}^N \cup \overline{\Upsilon}^E \cup \overline{\Upsilon}^R \quad and \quad \mathring{\Upsilon}^i \cap \mathring{\Upsilon}^j = \emptyset \quad for \ i \neq j = N, E, R.$$

Super scripts E, N *and* R *indicate the sub-sets where essential, natural and Robin boundary condition are imposed, respectively. We suppose that* $\Gamma^E \neq \emptyset$ *and* $\Upsilon^E \neq \emptyset$;

3. *we indicate with* $\boldsymbol{e}_i$, *for* $i = 1, \ldots, n$, *the unit normal vectors of each coordinate axis.*

To introduce the properties of the underground for our problem, it is useful to introduce the concept of *representative elementary volume* (REV), through the definition of porosity Φ of the porous medium. Let Ω_0 be a spherical sub-domain of Ω centred in x_0 with radius $\boldsymbol{r}$, see Figure 2.1 for $n = 2$, on the macroscopic level.

The void space indicator function at the microscopic level is

$$i(\boldsymbol{x}, t) := \begin{cases} 1 & \boldsymbol{x} \in \text{non-solid matrix at time } t, \\ 0 & \boldsymbol{x} \in \text{solid matrix at time } t, \end{cases} \tag{2.1}$$
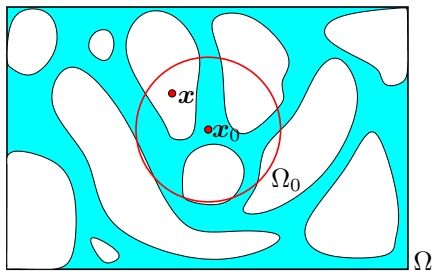
Figure 2.1: Example of averaging volume Ω_0 in a two-dimensional porous medium Ω.

then the porosity $\Phi(\boldsymbol{x}_0, t)$ of the porous medium, at time t, is defined as

$$\Phi(\boldsymbol{x}_0, t) := \frac{1}{|\Omega_0|} \int_{\Omega_0} i(\boldsymbol{x}, t) \, d\boldsymbol{x}. \tag{2.2}$$

If we plot the value of $\Phi(\boldsymbol{x}_0, t)$ at the fixed position $\boldsymbol{x}_0$ and time t and for different values of the radius $|\boldsymbol{r}|$ we obtain a behaviour as in Figure 2.2. For
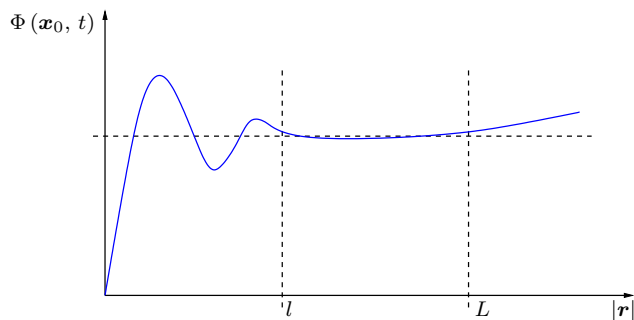
Figure 2.2: Example of the value of the porosity $\Phi(\boldsymbol{x}_0, t)$ for different value of the radius $|\boldsymbol{r}|$ of Ω_0. Figure taken from [9].

small value of the radius $|\boldsymbol{r}|$ the indicator function i produces large variations of $\Phi(\boldsymbol{x}_0, t)$, then for an interval of values of $|\boldsymbol{r}| \in [l, L]$ the average stabilizes obtaining a fixed value of $\Phi(\boldsymbol{x}_0, t)$, finally the large scale heterogeneities destabilize the value of $\Phi(\boldsymbol{x}_0, t)$ again. The averaging volume Ω_0 is called a representative elementary volume (REV) if its length scales in $[l, L]$ for all $t \in (0, T)$.

Assumption 2.3 (Wetting and non-wetting phases). *For the wetting and non-wetting phase we require that:*

1. *the two phases are distinct;*

2. *the two phases completely fill the porous medium, therefore no void spaces are allowed;*

3. *the two phases are immiscible.*

Under Assumption 2.1 and Assumption 2.3 the standard set of equations, derived for example in [18], for the two-phase flow describe the evolution of the following quantities:

- the saturation of the phase α indicated with $S_\alpha(\boldsymbol{x}, t)$ and defined as

$$S_\alpha(\boldsymbol{x}, t) := \frac{\text{volume of phase } \alpha \text{ in REV}}{\text{volume of void space in REV}} = \frac{\displaystyle\int_{\Omega_0} i_\alpha(\boldsymbol{x}, t)\, d\boldsymbol{x}}{\displaystyle\int_{\Omega_0} i(\boldsymbol{x}, t)\, d\boldsymbol{x}}, \quad (2.3)$$

in each REV centred in $\boldsymbol{x}$, see [9], where i_α is the phase α indicator function defined as

$$i_\alpha(\boldsymbol{x}, t) := \begin{cases} 1 & \boldsymbol{x} \in \text{phase } \alpha \text{ at time } t, \\ 0 & \boldsymbol{x} \notin \text{phase } \alpha \text{ at time } t. \end{cases}$$

By definition (2.3), the saturation is dimensionless with the constraints

$$S_\alpha \in \mathbb{1} \quad \text{a.e. in } Q_T,$$

with $\mathbb{1} := [0, 1]$ and, thanks to Assumption 2.3-2,

$$S_n + S_w = 1 \quad \text{a.e. in } Q_T. \quad (2.4)$$

- the Darcy velocity of each phase α, indicated with $\boldsymbol{u}_\alpha(\boldsymbol{x}, t)$ such that $\boldsymbol{u}_\alpha : Q_T \to \mathbb{R}^n$. Its unit of measure is $[m/s]$;

- the pressure of each phase α, indicated with $p_\alpha(\boldsymbol{x}, t)$ such that $p_\alpha : Q_T \to \mathbb{R}$, whose unit of measure is $[Pa]$.

Problem 2.1 (Two-phase flow equations). *The system of equations for the two-phase flow defined in Q_T reads: find S_α, $\boldsymbol{u}_\alpha$, p_α for $\alpha = n, w$ such that*

$$\begin{cases} \dfrac{\partial(\Phi \rho_\alpha S_\alpha)}{\partial t} + \nabla \cdot (\rho_\alpha \boldsymbol{u}_\alpha) = \rho_\alpha q_\alpha & \text{for } \alpha = n, w, \\[2mm] \boldsymbol{u}_\alpha = -\dfrac{k_{r\alpha}}{\mu_\alpha} \boldsymbol{K} (\nabla p_\alpha - \rho_\alpha \boldsymbol{g}) & \text{for } \alpha = n, w, \\[2mm] S_w + S_n = 1, \\[2mm] p_n - p_w = p_c(S_w). \end{cases} \quad (2.5)$$

System (2.5) is supplemented by initial data for S_α and appropriate boundary conditions, which will be discussed later. The parameters of (2.5) are detailed in Assumption 2.4.

The first equation in (2.5) is the law of conservation of mass for each phase α. The second equation is the generalized Darcy equation for each phase α, The last two equations represent the saturation constraints and the relation linking the pressure of the two phases with the capillary pressure p_c.

Assumption 2.4 (Assumptions on the data). *The data of Problem 2.1 are:*

1. *the porosity of the medium* $\Phi(\boldsymbol{x}, t)$, *defined by* (2.2). *We assume that* $\Phi \in L^\infty(Q_T)$. *The porosity is dimensionless, moreover we assume that there exist* $\phi_0, \phi_1 \in \mathbb{R}^+$ *such that* $\phi_0 < \phi_1 < 1$ *and*

$$\phi_0 \leq \Phi \leq \phi_1 \quad a.e. \ in \ Q_T.$$

Typical values of Φ *are reported in Table* 2.1;

2. *the absolute permeability of the medium* $\boldsymbol{K}(\boldsymbol{x})$. *We assume that* $\boldsymbol{K} \in [L^\infty(\Omega)]^{n \times n}$. *The absolute permeability is a symmetric and positive definite tensor with unit of measure given in* $[m^2]$. *We assume that there exists a constant* $K_0 \in \mathbb{R}^+$ *such that* $\|\boldsymbol{K}\|_{L^\infty(\Omega)} \geq K_0$. *Due to the symmetry only* $3(n-1)$ *coefficients are independent values, however in geophysical applications, see* [40] *for example,* $\boldsymbol{K}$ *is often approximated with only two independent components: the permeability along the geological layer* K_h *and the permeability across the geological layer* K_v *with an anisotropy factor* $a_K := K_h/K_v$. *Typical values of absolute permeability are reported in Table* 2.1;

| Classification | Φ | | a_K | $K_h[m^2]$ | |
	1	2		1	2
Chalk, typical	0.01	0.75	1.5	$1.8 \cdot 10^{-22}$	$9.9 \cdot 10^{-15}$
Coal, impure	0.0317	0.74	4.0	$3.1 \cdot 10^{-23}$	$9.9 \cdot 10^{-16}$
Limestone, organic-rich typical	0.01	0.51	2.0	10^{-17}	$9.9 \cdot 10^{-15}$
Limestone, chalk typical	0.01	0.70	1.5	$1.8 \cdot 10^{-22}$	$9.9 \cdot 10^{-15}$
Dolomite, typical	0.01	0.35	1.1	$1.3 \cdot 10^{-15}$	$8.2 \cdot 10^{-12}$
Sandstone, typical	0.01	0.41	5.0	$1.6 \cdot 10^{-17}$	$2.1 \cdot 10^{-11}$
Shale, typical	0.012	0.7	1.2	$3 \cdot 10^{-24}$	$9.9 \cdot 10^{-17}$

Table 2.1: Typical values of Φ, a_K and K_h for several rock types at different depth. Values taken from [40].

3. *the density for each phase* $\rho_\alpha(\boldsymbol{x}, t)$. *We assume that* $\rho_\alpha \in L^\infty(Q_T)$. *The density is given in* $[kg/m^3]$ *and there exists* $\rho_{\alpha,0} \in \mathbb{R}^+$ *such that*

$$\rho_{\alpha,0} \leq \rho_\alpha \quad a.e. \ in \ Q_T.$$

Typical values of ρ_n *are reported in Table* 2.2 *for oil and bitumen;*

Classification	Value $[m^2]$
Light oil	$\sim$800
Heavy oil and bitumen	$\sim$1000

Table 2.2: Typical values of ρ_n. Values taken from [72].

4. *the scalar source for each phase* $q_\alpha(\boldsymbol{x}, t)$ *representing possible production or destruction rate. We assume that* $q_\alpha \in L^2(Q_T)$. *The unit of measure for* q_α *is* $[s^{-1}]$;

5. the relative permeability for each phase $k_{r\alpha}(S_\alpha)$. We assume that $k_{r\alpha} \in L^\infty(\mathbb{1})$. The relative permeability is dimensionless and

$$k_{r\alpha} \in \mathbb{1} \quad a.e. \ in \ Q_T.$$

If $k_{r\alpha} = 0$ then the corresponding phase cannot flow. The shape of the relative permeabilities functions depends on the fluid types and on the porous medium, we will discuss them in section 2.1.2 in detail;

6. the dynamic viscosity for each phases $\mu_\alpha(\boldsymbol{x}, t)$, we assume that $\mu_\alpha \in L^\infty(Q_T)$. The dynamic viscosity is given in $[Pa \cdot s]$ and we assume that there exists a $\mu_{\alpha,0} \in \mathbb{R}^+$ such that

$$\mu_{\alpha,0} \leq \mu_\alpha \quad a.e. \ in \ Q_T.$$

Typical values of μ_α for water and oil are reported in Table 2.3.

Classification	Value range $[Pa \cdot s]$
Light oil	$[3 \cdot 10^{-4}, 10^{-3}]$
Medium oil	$[10^{-3}, 6 \cdot 10^{-3}]$
Moderate oil	$[6 \cdot 10^{-3}, 5 \cdot 10^{-2}]$
Very viscous oil	$[5 \cdot 10^{-2}, 1]$
Heavy oil	> 1
Water	$3.1 \cdot 10^{-4}$

Table 2.3: Typical values of μ_α for water and oil at reservoir condition, *i.e.* $28MPa - 42MPa$ and $93.3°C$. Values taken from [19].

7. the gravity acceleration $\boldsymbol{g}$ which is $\boldsymbol{g} = g\boldsymbol{e_3}$. The unit of measure for $\boldsymbol{g}$ is $[m/s^2]$;

8. the capillary pressure $p_c(S_w)$, such that $p_c \in W^{1,\infty}(\mathbb{1})$. The unit of measure for p_c is $[Pa]$. The capillary pressure describes the inter-facial tension between two adjacent immiscible phases, which is an additional fluid pressure due to geometry and contact forces. The capillary pressure depends on the fluid types and on the porous medium, we will discuss it in section 2.1.2 with more detail.

In the sequel we will indicate with $(\cdot, \cdot)_A : L^2(A) \times L^2(A) \to \mathbb{R}$ the scalar product in $L^2(A)$ given a regular domain A, defined as

$$(u, v)_A := \int_A uv,$$

with $u, v \in L^2(A)$. With an abuse of notation the same symbol indicates also the scalar product in $[L^2(B)]^n$, with B a given regular domain, defined as $(\cdot, \cdot)_B : [L^2(B)]^n \times [L^2(B)]^n \to \mathbb{R}$, *i.e.*

$$(\boldsymbol{u}, \boldsymbol{\tau})_B := \int_B \boldsymbol{u} \cdot \boldsymbol{\tau},$$

with $\boldsymbol{u}, \boldsymbol{\tau} \in [L^2(A)]^n$.

2.1.1 Fractional flow formulation

In [17] the authors have proposed a transformation that enables to rewrite system (2.5) as a parabolic equation for the saturation coupled with an elliptic equation for the pressure. This formulation is usually call *global pressure formulation* or *fractional flow formulation* and depends on the following additional requires.

Assumption 2.5 (Fractional flow). *The additional data in the fractional flow formulation are derived from the data presented in Assumption 2.4*

1. *the phase mobility for each phase $\lambda_\alpha\left(\boldsymbol{x},\, t;\, S_\alpha\right)$ defined as*

$$\lambda_\alpha\left(\boldsymbol{x},\, t;\, S_\alpha\right) := \frac{k_{r\alpha}\left(S_\alpha\right)}{\mu_\alpha\left(\boldsymbol{x},\, t\right)}\,,$$

with regularity $\lambda_\alpha \in L^\infty\left(Q_T \times \mathbb{1}\right)$. Thanks to the previous assumptions

$$\lambda_\alpha \geq 0 \ \ a.e. \ in \ Q_T \times \mathbb{1}\,.$$

The unit of measure for λ_α is $\left[\left(Pa \cdot s\right)^{-1}\right]$;

2. *the total mobility $\lambda\left(\boldsymbol{x},\, t;\, S_w,\, S_n\right)$ defined as*

$$\lambda\left(\boldsymbol{x},\, t;\, S_w,\, S_n\right) := \lambda_w\left(\boldsymbol{x},\, t;\, S_w\right) + \lambda_n\left(\boldsymbol{x},\, t;\, S_n\right)\,,$$

with regularity $\lambda \in L^\infty\left(Q_T \times \mathbb{1}\right)$. Thanks to (2.4) we may write

$$\lambda\left(\boldsymbol{x},\, t;\, S_w,\, S_n\right) = \lambda\left(\boldsymbol{x},\, t;\, S_\alpha\right) \quad with \ \alpha = n \ or \ w\,.$$

From the previous assumptions there exists $\lambda_0 \in \mathbb{R}^+$ such that

$$\lambda_0 \leq \lambda \quad a.e. \ in \ Q_T \times \mathbb{1}\,.$$

The unit of measure for λ is $\left[\left(Pa \cdot s\right)^{-1}\right]$;

3. *the fractional flow for each phase $f_\alpha\left(\boldsymbol{x},\, t;\, S_\alpha\right)$ defined as*

$$f_\alpha\left(\boldsymbol{x},\, t;\, S_\alpha\right) := \frac{\lambda_\alpha\left(\boldsymbol{x},\, t;\, S_\alpha\right)}{\lambda\left(\boldsymbol{x},\, t;\, S_\alpha\right)}\,,$$

with regularity $f_\alpha \in L^\infty\left(Q_T \times \mathbb{1}\right)$ and such that

$$f_\alpha \in \mathbb{1} \ \ a.e. \ in \ Q_T \times \mathbb{1}\,;$$

4. *the modified gravity $\boldsymbol{G}\left(\boldsymbol{x},\, t;\, S_w,\, S_n\right)$ defined as*

$$\boldsymbol{G} := \boldsymbol{g}\frac{\lambda_w\rho_w + \lambda_n\rho_n}{\lambda}\,,$$

with regularity $\boldsymbol{G} \in \left[L^\infty\left(Q_T \times \mathbb{1}\right)\right]^n$ and there exists $G_0 \leq 0$ such that

$$G_0 \geq \left[\boldsymbol{G}\right]_i \quad for \ i = 1, \dots, n \quad a.e. \ in \ Q_T \times \mathbb{1}\,,$$

where we indicate with $\left[\cdot\right]_i$ the element in position i of the vector in the square brackets. The unit of measure for $\boldsymbol{G}$ is $\left[Kg/(s^2 m^2)\right]$.

29

To derive the new set of equations we introduce two artificial variables: the total velocity $\boldsymbol{u}$,

$$\boldsymbol{u}(\boldsymbol{x},\,t) := \boldsymbol{u}_w(\boldsymbol{x},\,t) + \boldsymbol{u}_n(\boldsymbol{x},\,t)\,, \tag{2.6}$$

and the global pressure p, which is just a mathematical tool and not a physical pressure, defined as

$$p(\boldsymbol{x},\,t;\,S_w) := p_n(\boldsymbol{x},\,t) - \pi_w(\boldsymbol{x},\,t;\,S_w)\,, \tag{2.7}$$

with

$$\pi_w(\boldsymbol{x},\,t,\,S) := \int_{S_0}^{S} f_w(\boldsymbol{x},\,t,\,\xi)\,p_c'(\xi)\,d\xi + \pi_0\,. \tag{2.8}$$

The existence of the global pressure is guaranteed by Assumption 2.4 and Assumption 2.5. Suppose that there exists a value $S_0 \in \mathbb{1}$ in (2.8) such that $p_c(S_0) = 0$ so, using the last equation of system (2.5), the expression of π_0 is

$$\pi_0 = \frac{p_n + p_w}{2} - p_0\,,$$

with $p_0 = p\left(\hat{\boldsymbol{x}},\,\hat{t},\,S_0\right)$ a given reference value in $\left(\hat{\boldsymbol{x}},\,\hat{t}\right) \in Q_T$. The gradient of the total pressure, useful in the sequel, is then given by

$$\nabla p = \nabla p_n - f_w \nabla p_c\,.$$

We expand the time derivative in the first equation of (2.5) to obtain

$$\frac{\partial \Phi}{\partial t} \rho_\alpha S_\alpha + \frac{\partial \rho_\alpha}{\partial t} \Phi S_\alpha + \frac{\partial S_\alpha}{\partial t} \Phi \rho_\alpha + \nabla \cdot (\rho_\alpha \boldsymbol{u}_\alpha) = \rho_\alpha q_\alpha\,.$$

Dividing the previous equation by ρ_α and adding the contributions of each phase α we finally obtain

$$\frac{\partial \Phi}{\partial t}(S_n + S_w) + \Phi\left(\frac{S_w}{\rho_w}\frac{\partial \rho_w}{\partial t} + \frac{S_n}{\rho_n}\frac{\partial \rho_n}{\partial t}\right) + \Phi\frac{\partial(S_w + S_n)}{\partial t} +$$
$$+ \sum_{\alpha=n,w} \rho_\alpha^{-1} \nabla \cdot (\rho_\alpha \boldsymbol{u}_\alpha) = q_w + q_n\,.$$

The divergence term can be written in a more convenient way as

$$\sum_{\alpha=n,w} \rho_\alpha^{-1} \nabla \cdot (\rho_\alpha \boldsymbol{u}_\alpha) = \rho_w^{-1} \nabla \rho_w \cdot \boldsymbol{u}_w + \rho_n^{-1} \nabla \rho_n \cdot \boldsymbol{u}_n + \nabla \cdot \boldsymbol{u}_n + \nabla \cdot \boldsymbol{u}_w =$$
$$= \sum_{\alpha=n,w} \rho_\alpha^{-1} \nabla \rho_\alpha \cdot \boldsymbol{u}_\alpha + \nabla \cdot \boldsymbol{u}\,,$$

to obtain the first equation of the new formulation

$$\sum_{\alpha=n,w} \rho_\alpha^{-1}\left(\Phi S_\alpha \frac{\partial \rho_\alpha}{\partial t} + \nabla \rho_\alpha \cdot \boldsymbol{u}_\alpha\right) + \nabla \cdot \boldsymbol{u} = q_n + q_w - \frac{\partial \Phi}{\partial t}\,. \tag{2.9}$$

We derive the second equation of the new formulation by summing the generalized Darcy equations for each phase and using the capillary pressure relation, obtaining

$$\boldsymbol{u} = \boldsymbol{u}_n + \boldsymbol{u}_w = -\lambda_n \boldsymbol{K}\nabla p_n + \lambda_n \boldsymbol{K}\rho_n \boldsymbol{g} - \lambda_w \boldsymbol{K}\nabla p_w + \lambda_w \boldsymbol{K}\rho_w \boldsymbol{g} =$$
$$= -\lambda_n \boldsymbol{K}\nabla p_n - \lambda_w \boldsymbol{K}\nabla p_n + \lambda_w \boldsymbol{K}\nabla p_c(S_w) + \boldsymbol{K}\boldsymbol{g}\left(\lambda_n\rho_n + \lambda_w\rho_w\right) =$$
$$= -\lambda \boldsymbol{K}\nabla p_n + \lambda_w \boldsymbol{K}\nabla p_c(S_w) + \lambda \boldsymbol{K}\boldsymbol{G} = -\lambda \boldsymbol{K}\left[\nabla p_n - f_w \nabla p_c(S_w) - \boldsymbol{G}\right] .$$

Then, using the definition of the global pressure (2.7),

$$\boldsymbol{u} = -\lambda \boldsymbol{K}\left(\nabla p - \boldsymbol{G}\right) . \tag{2.10}$$

Performing a linear combination of the generalized Darcy's laws for $\boldsymbol{u}_n$ and $\boldsymbol{u}_w$, with coefficients $-\lambda_w$ and λ_n respectively, we obtain

$$\lambda_n \boldsymbol{u}_w - \lambda_w \boldsymbol{u}_n = -\lambda_n\lambda_w \boldsymbol{K}\nabla p_w + \lambda_n\lambda_w\rho_w \boldsymbol{g} + \lambda_n\lambda_w \boldsymbol{K}\nabla p_n - \lambda_n\lambda_w\rho_n \boldsymbol{g} =$$
$$= -\lambda_n\lambda_w \boldsymbol{K}\left[\nabla p_w - \nabla p_n + \left(\rho_n - \rho_w\right)\boldsymbol{g}\right] =$$
$$= \lambda_n\lambda_w \boldsymbol{K}\left[\nabla p_c(S_n) + \left(\rho_w - \rho_n\right)\boldsymbol{g}\right] =$$
$$= \lambda_n\lambda_w \boldsymbol{K}\left[p_c'\nabla S_n + \left(\rho_w - \rho_n\right)\boldsymbol{g}\right] . \tag{2.11}$$

Using the definition of total velocity (2.6) we find

$$\lambda_n \boldsymbol{u}_w - \lambda_w\left(\boldsymbol{u} - \boldsymbol{u}_w\right) = \lambda_n\boldsymbol{u}_w - \lambda_w\boldsymbol{u} + \lambda_w\boldsymbol{u}_w = \lambda\boldsymbol{u}_w - \lambda_w\boldsymbol{u} \tag{2.12}$$

and

$$\lambda_n\left(\boldsymbol{u} - \boldsymbol{u}_n\right) - \lambda_w\boldsymbol{u}_n = \lambda_n\boldsymbol{u} - \lambda\boldsymbol{u}_n . \tag{2.13}$$

We combine equation (2.11) with (2.12) and (2.13) to express the phase velocities as functions of $\boldsymbol{u}$ and S_n

$$\boldsymbol{u}_w = f_w\boldsymbol{u} + \frac{\lambda_n\lambda_w}{\lambda}\boldsymbol{K}\left[p_c'\nabla S_n + \left(\rho_w - \rho_n\right)\boldsymbol{g}\right] , \tag{2.14}$$
$$\boldsymbol{u}_n = f_n\boldsymbol{u} - \frac{\lambda_n\lambda_w}{\lambda}\boldsymbol{K}\left[p_c'\nabla S_n + \left(\rho_w - \rho_n\right)\boldsymbol{g}\right] .$$

Using equations (2.9), (2.10), (2.14) and the first equation of system (2.5) we find

Problem 2.2 (Fractional flow formulation)**.** *The complete system of equations for the two-phase flow in the fractional flow formulation reads: find* $\boldsymbol{u}$*,* p*,* S_n*,* $\boldsymbol{u}_n$ *such that*

$$\begin{cases} \displaystyle\sum_{\alpha=n,w} \rho_\alpha^{-1}\left(\Phi S_\alpha \frac{\partial \rho_\alpha}{\partial t} + \nabla\rho_\alpha \cdot \boldsymbol{u}_\alpha\right) + \nabla\cdot\boldsymbol{u} = q_n + q_w - \frac{\partial\Phi}{\partial t} \\[4mm] \boldsymbol{u} = -\lambda\boldsymbol{K}\left(\nabla p - \boldsymbol{G}\right) \\[3mm] \displaystyle\frac{\partial\left(\Phi\rho_n S_n\right)}{\partial t} + \nabla\cdot\left(\rho_n\boldsymbol{u}_n\right) = \rho_n q_n \\[4mm] \boldsymbol{u}_n = f_n\boldsymbol{u} - \lambda_w f_n\boldsymbol{K}\left[p_c'\nabla S_n + \left(\rho_w - \rho_n\right)\boldsymbol{g}\right] \end{cases} \quad \text{in } Q_T . \tag{2.15}$$

The system is supplemented by initial data for S_n *and appropriate boundary conditions.* S_w *and* $\boldsymbol{u}_w$ *can be eliminated from the system* (2.15) *using* (2.4) *and* (2.6)*. The first two equations are called pressure equations, while the last two equations are called saturation equations.*

We now introduce the boundary condition for the problem, in particular we impose for the global pressure and total velocity

$$\begin{cases} p = \widetilde{p} & \text{on } \Gamma^E \times \mathcal{I}_T, \\ \boldsymbol{u} \cdot \boldsymbol{n} = \widetilde{u}^N & \text{on } \Gamma^N \times \mathcal{I}_T, \\ \boldsymbol{u} \cdot \boldsymbol{n} - p = \widetilde{u}^R & \text{on } \Gamma^R \times \mathcal{I}_T, \end{cases} \tag{2.16}$$

and for the saturation and the velocity of the non-wetting phase we impose also the initial condition

$$\begin{cases} S_n = \widetilde{S}_n & \text{on } \Upsilon^E \times \mathcal{I}_T, \\ \boldsymbol{u}_n \cdot \boldsymbol{n} = \widetilde{u}_n^N & \text{on } \Upsilon^N \times \mathcal{I}_T, \\ \boldsymbol{u}_n \cdot \boldsymbol{n} - S_n = \widetilde{u}_n^R & \text{on } \Upsilon^R \times \mathcal{I}_T, \\ S_n(0) = S_{n,0} & \text{in } \Omega \times \{0\}. \end{cases} \tag{2.17}$$

Assumption 2.6 (Regularity of boundary and initial data). *The boundary and initial data in* (2.16) *and* (2.17) *fulfil the following hypotheses:*

1. $\widetilde{p} \in L^2\left(\mathcal{I}_T; H^{\frac{1}{2}}\left(\Gamma^E\right)\right)$, $\widetilde{u}^N \in L^2\left(\mathcal{I}_T; H^{-\frac{1}{2}}\left(\Gamma^N\right)\right)$ *and*
   $\widetilde{u}^R \in L^2\left(\mathcal{I}_T; L^2\left(\Gamma^R\right)\right)$;

2. $\widetilde{S}_n \in L^2\left(\mathcal{I}_T; H^{\frac{1}{2}}\left(\Upsilon^E\right)\right)$, $\widetilde{u}_n^N \in L^2\left(\mathcal{I}_T; H^{-\frac{1}{2}}\left(\Upsilon^N\right)\right)$,
   $\widetilde{u}_n^R \in L^2\left(\mathcal{I}_T; L^2\left(\Upsilon^R\right)\right)$ *and* $S_{n,0} \in L^2\left(\Omega\right)$.

The formulation in Problem 2.2 becomes particularly attractive if both phase densities ρ_w and ρ_n are constant, an assumption which is often made in oil related applications, see for instance [20] and [21]. In this case the first equation of (2.15) does not depend on S_n and $\boldsymbol{u}_n$. As a consequence a simplified version of system (2.15) can be obtained introducing also the additional assumption that the porosity Φ is constant in time.

Problem 2.3 (Fractional flow). *If ρ_w and ρ_n are constant and Φ is constant in time then the system of equations for the two-phase flow in the fractional flow formulation reads: find $\boldsymbol{u}$, p, S_n, $\boldsymbol{u}_n$ such that*

$$\begin{cases} \nabla \cdot \boldsymbol{u} = q_w + q_n \\ \boldsymbol{u} = -\lambda \boldsymbol{K}\left(\nabla p - \boldsymbol{G}\right) \\ \Phi \dfrac{\partial S_n}{\partial t} + \nabla \cdot \boldsymbol{u}_n = q_n \\ \boldsymbol{u}_n = f_n \boldsymbol{u} - \lambda_w f_n \boldsymbol{K}\left[p_c' \nabla S_n + (\rho_w - \rho_n)\boldsymbol{g}\right] \end{cases} \quad \text{in } Q_T, \tag{2.18}$$

coupled with boundary conditions for the global pressure and the total velocity

$$\begin{cases} p = \widetilde{p} & \text{on } \Gamma^E \times \mathcal{I}_T, \\ \boldsymbol{u} \cdot \boldsymbol{n} = \widetilde{u}^N & \text{on } \Gamma^N \times \mathcal{I}_T, \\ \boldsymbol{u} \cdot \boldsymbol{n} - p = \widetilde{u}^R & \text{on } \Gamma^R \times \mathcal{I}_T, \end{cases}$$

and with the boundary and initial conditions for the saturation S_n and the velocity $\boldsymbol{u}_n$ of the non-wetting phase

$$
\begin{cases}
S_n = \widetilde{S}_n & \text{on } \Upsilon^E \times \mathcal{I}_T, \\[2mm]
\boldsymbol{u}_n \cdot \boldsymbol{n} = \widetilde{u}_n^N & \text{on } \Upsilon^N \times \mathcal{I}_T, \\[2mm]
\boldsymbol{u}_n \cdot \boldsymbol{n} - S_n = \widetilde{u}_n^R & \text{on } \Upsilon^R \times \mathcal{I}_T, \\[2mm]
S_n(0) = S_{n,0} & \text{in } \Omega \times \{0\}.
\end{cases}
$$

To reconstruct the pressure for each phase we use the definition of the global pressure and the expression of the capillary pressure to find

$$
\begin{cases}
p_n = p + \pi_w(S_w), \\[2mm]
p_w = p - p_c(S_w) + \pi_w(S_w).
\end{cases}
$$

Note that we do not need to evaluate the phase pressures but for post-process purpose.

2.1.2 Capillary pressure and relative permeability

In this section we present some models for the capillary pressure and the relative permeability, for a gas and water system and for a liquid and water system.
As the porous medium is drained, the saturation of the wetting phase decreases and capillary pressure increases. At the end of this process the so called *pendular water saturation* is reached, *i.e.* the wetting phase takes the form of rings around the contact points of the grains holding them together. These are called pendular rings and have the shape of a saddle, as Figure 2.3 shows.
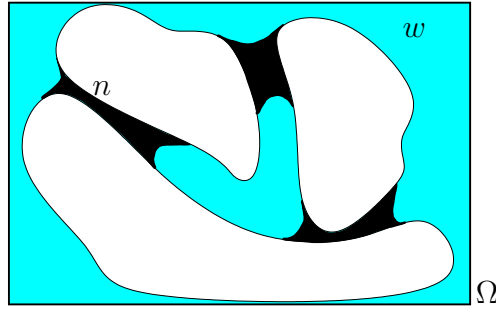
Figure 2.3: Example of pendular rings around grains.

The corresponding wetting phase saturation, usually greater than zero, is called wetting phase *residual saturation* S_{wr}. The wetting phase saturation cannot be reduced below residual saturation by pure displacement. As the residual saturation is approached the rapid increase in capillary pressure produces practically no decrease in wetting phase saturation. Generally the residual saturation, also known as *critical saturation*, is lithology dependent. Also the non-wetting phase has a residual saturation S_{nr}, with similar behaviour as wetting phase residual saturation. In a moderately water wet sandstone with oil as non-wetting phase

33

S_{nr} typically ranges in $[0.2, 0.35]$, see [19]. We can then introduce the effective saturation $\overline{S}_\alpha$ for each phase α as

$$\overline{S}_\alpha := \frac{S_\alpha - S_{\alpha r}}{1 - S_{wr} - S_{nr}} \, ,$$

such that

$$\overline{S}_\alpha \in \mathbb{1} \quad \text{a.e. in } Q_T \quad \text{and} \quad \overline{S}_n + \overline{S}_w = 1 \quad \text{a.e. in } Q_T \, .$$

From an experimental point of view and for the dimensionless formulation of the fractional flow system, it is more convenient to measure, instead of the capillary pressure, the *J-Leverett function*. The J-Leverett function is a dimensionless function, defined in an homogeneous porous medium, common to many unconsolidated sands, also known as the *J*-function, which has the form

$$J(S_w) := \frac{p_c(S_w)}{\gamma_{nw}} \sqrt{\frac{K}{\Phi}} \, ,$$

where γ_{nw} is the interface tension between the wetting and non-wetting phase, measured in $[Kg \cdot s^{-2}]$, and K is the medium permeability. We can observe that, in general, the permeability is a tensor but in this case we assume that it can be written as $\boldsymbol{K} = K\boldsymbol{I}$, with $\boldsymbol{I}$ the identity tensor.

We consider two models for the capillary pressure and the relative permeability. The first, called *Van Genuchten model*, describes a physical system with water and a gas as phases, while the second, called *Brooks-Corey model*, takes care of a physical system with water and a liquid as phases. For further details see [9], [19] and [40].

Van Genuchten model

Van Genuchten introduced in [75] a model for the capillary pressure and the relative permeability for a physical system composed by water, as wetting phase, and a gas, as non-wetting phase. For this model the proposed expression for capillary pressure p_c is

$$p_c(S_w) = \frac{1}{\alpha} \left(\overline{S}_w^{-\frac{1}{m}} - 1 \right)^{\frac{1}{n}} \, , \tag{2.19}$$

with $m = 1 - 1/n$, n and α free parameters. Typical values of n range between 2 and 5. Examples of capillary pressure curves are in Figure 2.4. The relative permeability $k_{r\alpha}$ is

$$\begin{cases} k_{rw}(S_w) = \overline{S}_w^\epsilon \left[1 - \left(1 - \overline{S}_w^{\frac{n}{n-1}} \right)^{\frac{n-1}{n}} \right]^2 \, , \\[3mm] k_{rn}(S_n) = \overline{S}_n^\gamma \left[1 - \left(1 - \overline{S}_n \right)^{\frac{n}{n-1}} \right]^{\frac{2(n-1)}{n}} \, . \end{cases}$$

with the typical choice $\epsilon = 1/2$, $\gamma = 1/3$ and n the same as in capillary pressure (2.19). Examples of relative permeability curves are in Figure 2.5
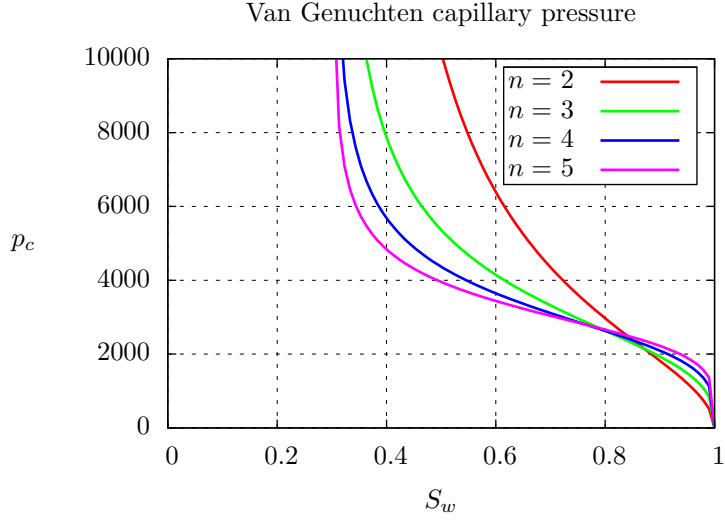
Figure 2.4: Van Genuchten capillary pressure p_c curves, with $\alpha = 3.3 \cdot 10^{-4}$, $S_{nr} = 0.0$ and $S_{wr} = 0.3$.
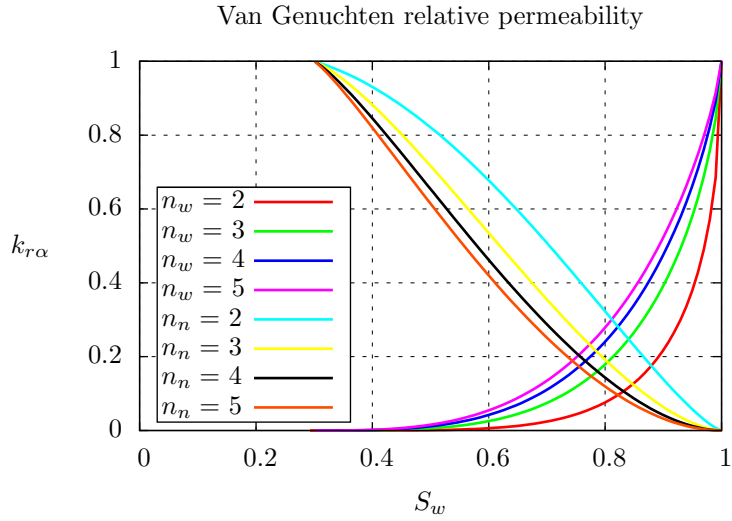
Figure 2.5: Van Genuchten relative permeability k_{rw} and k_{rn} curves, with $S_{nr} = 0.0$, $S_{wr} = 0.3$, $\epsilon = 1/2$ and $\gamma = 1/3$.

Brooks-Corey model

Brooks and Corey introduced in [12] a model for the capillary pressure and the relative permeability of a physical system composed by water, as wetting phase, and a liquid, as non-wetting phase. The capillary pressure is modelled in this case as

$$p_c(S_w) = p_d \overline{S}_w^{-\frac{1}{\lambda}}, \tag{2.20}$$

with p_d the so called *entry* or *bubbling* or *threshold pressure* of the porous medium and λ a parameter related to the pore size distribution. The entry pressure, first introduced in the same article [12], is a constant characterizing the medium. If a porous medium, as presented in Figure 2.6, is initially saturated by the wetting phase, a certain pressure must be reached for the non-wetting phase before the latter can begin to penetrate through the grains, displacing the wetting phase contained in it. More precisely the capillary pressure must be
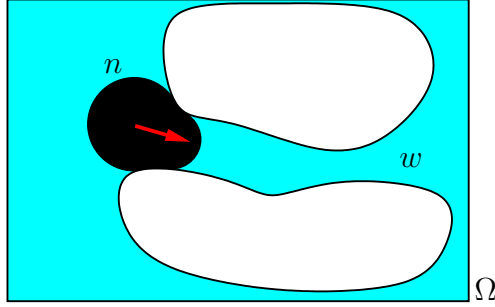
Figure 2.6: Example of porous medium with a bubble of non-wetting phase which displaces the wetting phase.

build up above the entry pressure at the interface between the two fluids before drainage of the wetting fluid starts. Values of entry pressure can be found in [74]: it ranges from $5kPa$ for $\lambda = 2$, up to $20kPa$ for $\lambda = 0.5$. According to [74] low values of λ are used for poorly sorted rocks, while large values of λ represent well-sorted rocks. The parameter λ can vary from zero to infinity but typically ranges in $\lambda \in [0.25, 4]$ for reservoir rocks. Examples of capillary pressure curves are in Figure 2.7.

For the sequel is useful to compute the derivative of the capillary pressure with respect to S_n

$$
\begin{aligned}
\frac{dp_c}{dS_n}(S_w) &= p_d \frac{d}{dS_n}\left(\frac{S_w - S_{wr}}{1 - S_{wr} - S_{nr}}\right)^{-\frac{1}{\lambda}} = \\
&= p_d \frac{d}{dS_n}\left(\frac{1 - S_n - S_{wr}}{1 - S_{wr} - S_{nr}}\right)^{-\frac{1}{\lambda}} = \\
&= \frac{p_d}{\lambda}\left(\frac{1 - S_n - S_{wr}}{1 - S_{wr} - S_{nr}}\right)^{-\frac{1}{\lambda}-1}\frac{1}{1 - S_{wr} - S_{nr}} = \\
&= \frac{p_d}{\lambda\left(1 - S_{wr} - S_{nr}\right)}\overline{S}_w^{-\frac{1}{\lambda}-1}.
\end{aligned}
$$

The relative permeability $k_{r\alpha}$, for each α phase, is

$$
\begin{cases}
k_{rw}(S_w) = \overline{S}_w^{\frac{2+3\lambda}{\lambda}}, \\
k_{rn}(S_n) = \overline{S}_n^2\left[1 - \left(1 - \overline{S}_n\right)^{\frac{2+\lambda}{\lambda}}\right].
\end{cases}
\tag{2.21}
$$

The parameter λ is the same as in the capillary pressure (2.20). Examples of relative permeability are in Figure 2.8.
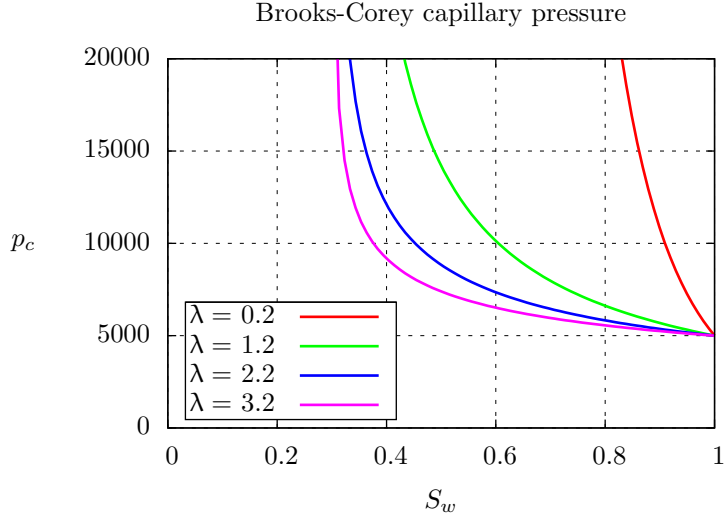
Figure 2.7: Brooks-Corey capillary pressure p_c curves, with $p_d = 5000$, $S_{nr} = 0.0$ and $S_{wr} = 0.2$.
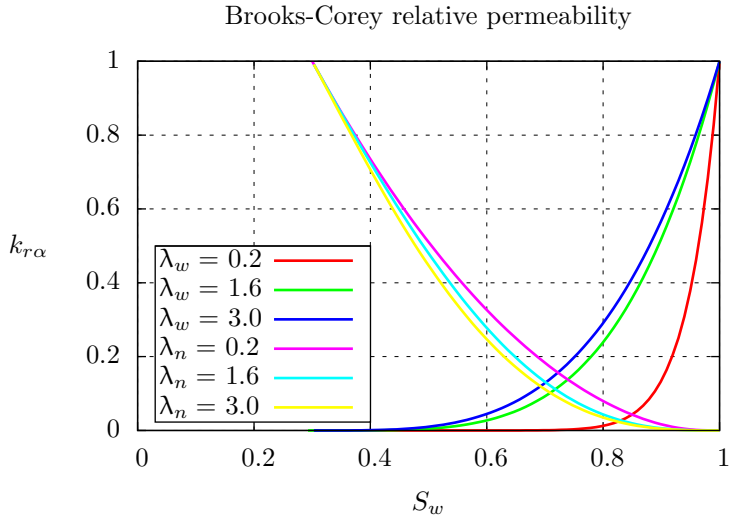
Figure 2.8: Brooks-Corey relative permeability k_{rw} and k_{rn} curves, with $S_{nr} = 0.0$ and $S_{wr} = 0.2$.

2.1.3 Fractional flow equation in dimensionless form

In this section we derive the dimensionless equations for the system (2.18), see [66] and [70], to analyse the behaviour of the system in different scenarios. We use the superscript * to indicate the dimensionless variables. Since we are dealing with a multiscale problem, *i.e.* a representative elementary volume where we have described the porous flow and the geological domain which is several orders of magnitude bigger, we use two different scaling. A reference length L

measured in $[m]$ represents the macro scale, it may be the depth of the basin, and a reference scalar permeability K_0 measured in $[m^2]$ represents the micro scale. Finally we introduce a reference velocity U measured in $[m/s]$ and a reference dynamic viscosity μ_0 measured in $[Pa \cdot s]$. The latter may be the parameters for the solution of the single-phase flow problem for the non-wetting phase in a given sample of a porous medium with permeability K_0. Correspondingly, we define the following dimensionless variables:

$$\boldsymbol{u}^* := \frac{\boldsymbol{u}}{U}, \qquad \boldsymbol{x}^* := \frac{\boldsymbol{x}}{L}, \qquad t^* := t\frac{U}{\phi L \left(1 - S_{wr} - S_{nr}\right)},$$

$$p^* := \frac{pK_0}{\mu_0 U L}, \quad S_n^* := \frac{S_n - S_{nr}}{1 - S_{wr} - S_{nr}}, \quad T^* := T\frac{U}{\phi L \left(1 - S_{wr} - S_{nr}\right)},$$

$$J := \frac{p_c}{\gamma_{nw}}\sqrt{\frac{\Phi}{K_0}},$$

with J the J-Leverett function for fixed values of p_c, γ_{nw} and Φ. The domain of interest Q_T is scaled in both space and time variables, *i.e.* $Q_T^* := \Omega^* \times (0, T^*)$ where the variables in Ω^* are scaled according to the definition of $\boldsymbol{x}^*$. We observe that the differential operators in (2.18), written in dimensionless form read

$$\nabla \cdot \boldsymbol{u} = \sum_{i=1}^n \frac{\partial}{\partial x_i} u_i = \sum_{i=1}^n \frac{\partial}{\partial x_i^*}\frac{\partial x_i^*}{\partial x_i} u_i^* U = \frac{U}{L}\sum_{i=1}^n \frac{\partial}{\partial x_i^*} u_i^* = \frac{U}{L}\nabla \cdot^* \boldsymbol{u}^*,$$

$$[\nabla p]_i = \frac{\partial}{\partial x_i} p = \frac{\partial}{\partial x_i^*}\frac{\partial x_i^*}{\partial x_i} p^*\frac{\mu_0 L U}{K_0} = \frac{U\mu_0}{K_0}\frac{\partial}{\partial x_i^*} p^* = \frac{U\mu_0}{K_0}[\nabla^* p^*]_i,$$

$$\frac{\partial}{\partial t} S_n = \frac{\partial}{\partial t^*}\frac{\partial t^*}{\partial t}\left[S_n^*\left(1 - S_{wr} - S_{nr}\right) + S_{nr}\right] =$$

$$= \frac{\partial}{\partial t^*}\frac{U}{\Phi L \left(1 - S_{wr} - S_{nr}\right)} S_n^*\left(1 - S_{wr} - S_{nr}\right) = \frac{U}{\Phi L}\frac{\partial}{\partial t^*} S_n^*,$$

$$\frac{dp_c}{dS_n} = \frac{d}{dS_n^*}\frac{dS_n^*}{dS_n} J\gamma_{nw}\sqrt{\frac{\Phi}{K_0}} = \frac{\gamma_{nw}}{\left(1 - S_{wr} - S_{nr}\right)}\sqrt{\frac{\Phi}{K_0}}\frac{dJ}{dS_n^*}.$$

The first equation of the system (2.18) becomes

$$\nabla \cdot^* \boldsymbol{u}^* = \frac{L}{U}\left(q_n + q_w\right). \tag{2.22}$$

For the second equation we use the above formula to obtain

$$\boldsymbol{u}^* U = -\lambda \boldsymbol{K}\left(\frac{U\mu_0}{K_0}\nabla^* p^* - \boldsymbol{G}\right),$$

and divide by U obtaining the dimensionless form

$$\boldsymbol{u}^* = -\lambda\mu_0\frac{\boldsymbol{K}}{K_0}\left(\nabla^* p^* - \frac{K_0\boldsymbol{G}}{U\mu_0}\right). \tag{2.23}$$

The third equation of (2.18) becomes

$$\Phi\frac{U}{\Phi L}\frac{\partial}{\partial t^*} S_n^* + \frac{U}{L}\nabla \cdot^* \boldsymbol{u}_n^* = q_n,$$

then we divide by U/L and obtain

$$\frac{\partial}{\partial t^*} S_n^* + \nabla \cdot^* \boldsymbol{u}_n^* = \frac{L}{U} q_n \,. \tag{2.24}$$

Using the expressions above, the last equation of (2.18) becomes

$$\boldsymbol{u}_n^* = f_n \boldsymbol{u}^* - \frac{\lambda_w f_n}{U} \boldsymbol{K} \left[\gamma_{nw} \sqrt{\frac{\Phi}{K_0}} \frac{dJ}{dS_n^*} \frac{\nabla^*}{L} S_n^* + (\rho_w - \rho_n) \boldsymbol{g} \right] =$$

$$= f_n \boldsymbol{u}^* - \frac{\lambda_w f_n \boldsymbol{K} \gamma_{nw}}{UL} \sqrt{\frac{\Phi}{K_0}} \frac{dJ}{dS_n^*} \nabla^* S_n^* - \lambda_w f_n \boldsymbol{K} \frac{(\rho_w - \rho_n) \boldsymbol{g}}{U} \,. \tag{2.25}$$

We normalize the values of k_{rn} and k_{rw} by scaling them with the respective maximum values to obtain $\widetilde{k_{rn}}$ and $\widetilde{k_{rw}}$

$$\widetilde{k_{rn}} := \frac{k_{rn}}{k_{rn} (1 - S_{nr})} \quad \text{and} \quad \widetilde{k_{rw}} := \frac{k_{rw}}{k_{rw} (S_{wr})} \,.$$

We introduce three dimensionless numbers that characterize the physical process of the two-phase flow, namely

$$M := \frac{\mu_w}{\mu_n} \frac{k_{rn} (1 - S_{nr})}{k_{rw} (S_{wr})} \,, \quad \text{Ca} := \frac{\mu_0 UL}{\gamma_{nw} \sqrt{K_0 \Phi}} \,, \quad \Upsilon := K_0 \frac{(\rho_w - \rho_n) g}{\mu_0 U} \,. \tag{2.26}$$

where M is the mobility ratio, Ca is the capillary number and Υ is the gravity number. In the applications of out interest the latter is strictly positive since $\rho_w > \rho_n$. We also introduce the mobility function defined as

$$\lambda_T := M \widetilde{k_{rn}} + \widetilde{k_{rw}}$$

Using these values we obtain

$$f_n = \frac{k_{rn}/\mu_n}{k_{rw}/\mu_w + k_{rn}/\mu_n} = \frac{\mu_w k_{rn} (1 - S_{nr})}{\mu_n k_{rw} (S_{wr})} \frac{\widetilde{k_{rn}}}{\widetilde{k_{rw}} + \frac{\mu_w}{\mu_n} \frac{k_{rn}(1 - S_{nr})}{k_{rw}(S_{wr})} \widetilde{k_{rn}}} =$$

$$= \frac{M \widetilde{k_{rn}}}{\lambda_T} \,,$$

$$\lambda_w f_n = \frac{k_{rw}}{\mu_w} \frac{M \widetilde{k_{rn}}}{\lambda_T} = \frac{\widetilde{k_{rw}} k_{rw} (S_{wr})}{\mu_w} \frac{\mu_w}{\mu_n} \frac{k_{rn} (1 - S_{nr})}{k_{rw} (S_{wr})} \frac{\widetilde{k_{rn}}}{\lambda_T} =$$

$$= \frac{k_{rn} (1 - S_{nr})}{\mu_n} \frac{\widetilde{k_{rw}} \widetilde{k_{rn}}}{\lambda_T} \,,$$

and

$$\frac{\lambda_w f_n \boldsymbol{K} \gamma_{nw}}{UL} \sqrt{\frac{\Phi}{K_0}} = \frac{k_{rn} (1 - S_{nr})}{\mu_n} \frac{\widetilde{k_{rw}} \widetilde{k_{rn}}}{\lambda_T} \frac{\boldsymbol{K} \gamma_{nw}}{UL} \sqrt{\frac{\Phi}{K_0}} =$$

$$= \frac{k_{rn} (1 - S_{nr}) \mu_0}{\mu_n K_0} \boldsymbol{K} \frac{\widetilde{k_{rw}} \widetilde{k_{rn}}}{\text{Ca} \lambda_T} \,,$$

$$\lambda_w f_n \boldsymbol{K} \frac{(\rho_w - \rho_n) \boldsymbol{g}}{U} = \frac{k_{rn} (1 - S_{nr})}{\mu_n} \frac{\widetilde{k_{rw}} \widetilde{k_{rn}}}{\lambda_T} \boldsymbol{K} \frac{(\rho_w - \rho_n) \boldsymbol{g}}{U} =$$

$$= \frac{k_{rn} (1 - S_{nr}) \mu_0}{\mu_n K_0} \boldsymbol{K} \Upsilon \frac{\widetilde{k_{rw}} \widetilde{k_{rn}}}{\lambda_T} \boldsymbol{e}_3 \,.$$

Then equation (2.25) becomes

$$\boldsymbol{u}_n^* = \frac{M\widetilde{k_{rn}}}{\lambda_T}\boldsymbol{u}^* - \frac{\mu_0 k_{rn}\left(1 - S_{nr}\right)}{\mu_n K_0}\boldsymbol{K}\left(\frac{\widetilde{k_{rw}}\widetilde{k_{rn}}}{\mathrm{Ca}\lambda_T}\frac{dJ}{dS_n^*}\nabla^* S_n^* + \Upsilon\frac{\widetilde{k_{rw}}\widetilde{k_{rn}}}{\lambda_T}\boldsymbol{e}_3\right)$$
(2.27)

Finally, by (2.22), (2.23), (2.24) and (2.27) the dimensionless form of system (2.18) is described by the following problem.

Problem 2.4 (Fractional flow in dimensionless form). *The system of equations for the two-phase flow in the dimensionless fractional flow formulation is defined in Q_T^* and reads: find $\boldsymbol{u}^*$, p^*, S_n^*, $\boldsymbol{u}_n^*$ such that*

$$\begin{cases}
\nabla\cdot^*\boldsymbol{u}^* = \dfrac{L}{U}\left(q_n + q_w\right), \\[2mm]
\boldsymbol{u}^* = -\lambda\mu_0\dfrac{\boldsymbol{K}}{K_0}\left(\nabla^* p^* - \dfrac{K_0\boldsymbol{G}}{U\mu_0}\right), \\[2mm]
\dfrac{\partial}{\partial t^*}S_n^* + \nabla\cdot^*\boldsymbol{u}_n^* = \dfrac{L}{U}q_n, \\[2mm]
\boldsymbol{u}_n^* = \dfrac{M\widetilde{k_{rn}}}{\lambda_T}\boldsymbol{u}^* - \dfrac{\mu_0 k_{rn}\left(1 - S_{nr}\right)}{\mu_n K_0}\boldsymbol{K}\left(\dfrac{\widetilde{k_{rw}}\widetilde{k_{rn}}}{\mathrm{Ca}\lambda_T}\dfrac{dJ}{dS_n^*}\nabla^* S_n^* + \Upsilon\dfrac{\widetilde{k_{rw}}\widetilde{k_{rn}}}{\lambda_T}\boldsymbol{e}_3\right).
\end{cases}$$

The three numbers introduced in (2.26) characterize the nature of the saturation equation. To analyse this behaviour let us make some simplifications. Let us consider a one dimensional flow parallel to the z axis, let us take $\boldsymbol{u}^*$ constant, unitary and parallel to $\boldsymbol{e}_3$, $k_{rn}\left(1 - S_{nr}\right) = 1$, no sources for the non-wetting phase $q_n \equiv 0$, the reference mobility μ_0 equal to the non-wetting phase mobility μ_n and suppose that the porous matrix is homogeneous with permeability tensor $\boldsymbol{K} = K_0\boldsymbol{I}$. With these assumptions the equation for the saturation becomes

$$\frac{\partial S_n^*}{\partial t^*} = -\frac{\partial}{\partial z^*}\left[-\frac{\widetilde{k_{rw}}\widetilde{k_{rn}}}{\mathrm{Ca}\lambda_T}\frac{dJ}{dS_n^*}\frac{\partial}{\partial z^*}S_n^* + \frac{M\widetilde{k_{rn}}}{\lambda_T}\left(1 - \Upsilon\frac{\widetilde{k_{rw}}}{M}\right)\right].$$
(2.28)

In the absence of capillary dispersion, *i.e.* for $\mathrm{Ca} \to \infty$, the equation (2.28) is a non-linear hyperbolic conservation law with flux function

$$\mathcal{F}_n := \frac{M\widetilde{k_{rn}}}{\lambda_T}\left(1 - \Upsilon\frac{\widetilde{k_{rw}}}{M}\right),$$

where the shape of the flux function depends on the value of the parameters M and Υ, as shown are in Figure 2.9 and 2.10 for the Brooks-Corey permeabilities (2.21).

We show in Figure 2.10 that for $\Upsilon > 0$, $\mathcal{F}_n$ has a positive slope for small saturation and a negative slope for large value of S_n^*. The flux function $\mathcal{F}_n$ is not a convex function, so the Riemann solution of the hyperbolic problem governing the saturation can involve both shock and rarefaction waves in a single point. See, for example, the following references [54], [14], [1], [47] for the analyses and numerical schemes to address this problem. In section 2.4 we
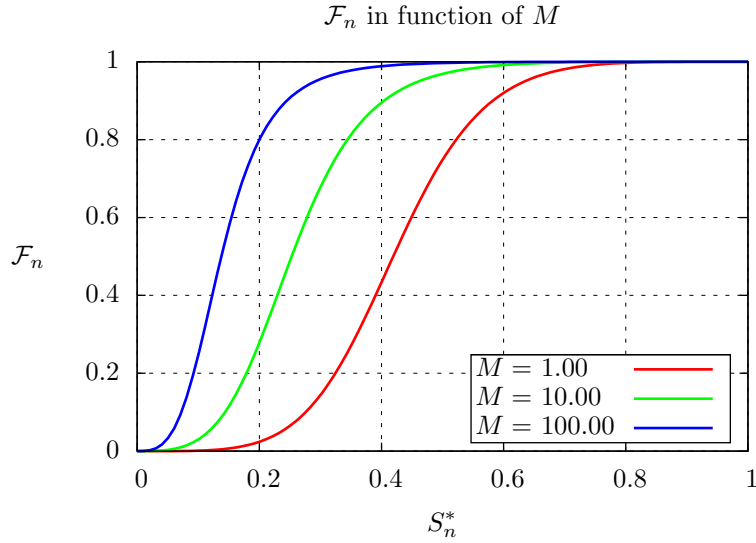
Figure 2.9: Flux function $\mathcal{F}_n$ in function of M, with fixed $\Upsilon = 1$ and $\lambda = 1.6$.
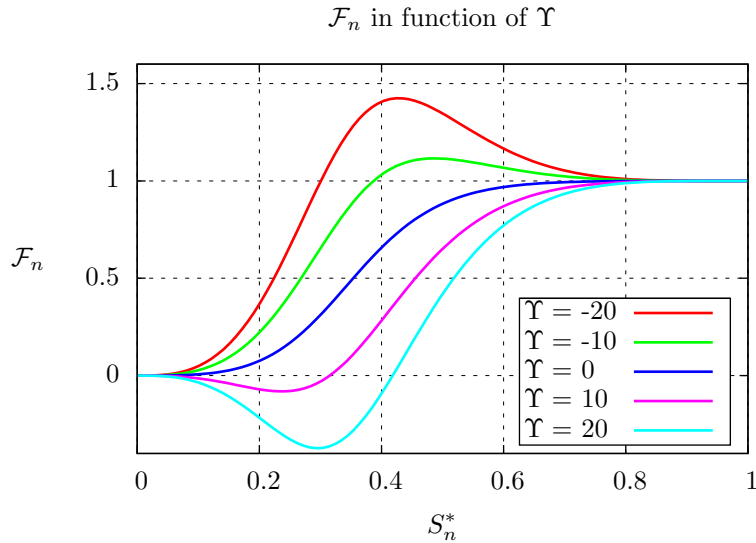
Figure 2.10: Flux function $\mathcal{F}_n$ in function of Υ, with fixed $M = 2$ and $\lambda = 1.6$.

will present some numerical results and we will compare two different numerical fluxes.

For non zero values of Ca, the saturation equation becomes a parabolic equation with the diffusion that depends on the inverse of Ca. For large values of Ca the diffusion term is small and the hyperbolic part is dominant, we obtain the same behaviour as the pure hyperbolic equation with the profile dispersed around the shock. For small value of Ca the diffusion term is dominant obtaining a purely diffusive process with a drift.

2.2 The implicit pressure explicit saturation scheme

A common scheme to solve Problem 2.3 is based on a splitting strategy denoted as *IMPES* method, that is *IM*plicit *P*ressure *E*xplicit *S*aturation method, see [18] for further details. The method splits system (2.18) in two parts: a pressure equation and a saturation equation, which will be solved in succession at each time step. Following [63] and [55], we can write Problem 2.3 in the following abstract form

$$\begin{cases} \dfrac{\partial \varphi_2}{\partial t} + \mathcal{L}\left(\boldsymbol{\varphi}\right) = \psi_p + \psi_S & \text{for } t > 0, \\[2mm] \varphi_2\left(0\right) = \overline{\varphi}_2 & \text{for } t = 0, \end{cases} \tag{2.29}$$

where $\boldsymbol{\varphi}$ is the unknown of the abstract problem of two components $\boldsymbol{\varphi} = (\varphi_1, \varphi_2)$, with $\varphi_1 = p$ and $\varphi_2 = S_n$. The differential operator $\mathcal{L}$ is defined as

$$\mathcal{L}\left(\boldsymbol{\varphi}\right) := \mathcal{L}_p\left(\boldsymbol{\varphi}\right) + \mathcal{L}_S\left(\boldsymbol{\varphi}\right) = \mathcal{L}_p(\varphi_1, \varphi_2) + \mathcal{L}_S(\varphi_1, \varphi_2),$$

with $\mathcal{L}_p$ the differential operator associated to the pressure equation and $\mathcal{L}_S$ the differential operator associated to the saturation equation. Functions ψ_p and ψ_S represent the source terms of the equation for the pressure and for the saturation, respectively, and $\overline{\varphi}_2$ the initial condition for φ_2. Thanks to the splitting of $\mathcal{L}$ equation (2.29) can be written as

$$\begin{cases} \dfrac{\partial \varphi_2}{\partial t} + \mathcal{L}_p\left(\boldsymbol{\varphi}\right) + \mathcal{L}_S\left(\boldsymbol{\varphi}\right) = \psi_p + \psi_S & \text{for } t > 0, \\[2mm] \varphi_2\left(0\right) = \overline{\varphi}_2 & \text{for } t = 0. \end{cases}$$

We consider a sub-division of the time interval $\mathcal{I}_T$ in $N + 1$ sub-intervals, (t^k, t^{k+1}) with $0 = t^0 < t^1 < \ldots < t^{N+1} = T$, and we indicate with superscript k quantities at time t^k. Using a *Yanenko*-like operator splitting [79] with a first order scheme for the time discretization, we find a system of two implicit equations, for $k \geq 0$ and $\Delta t = t^{k+1} - t^k$. The system reads

$$\begin{cases} \mathcal{L}_p\left(\varphi_1^{k+1}, \varphi_2^k\right) = \psi_p^{k+1}, \\[2mm] \dfrac{\varphi_2^{k+1} - \varphi_2^k}{\Delta t} + \mathcal{L}_S\left(\varphi_1^{k+1}, \varphi_2^{k+1}\right) = \psi_S^{k+1}, \end{cases} \tag{2.30}$$

with $\varphi_2^0 = \overline{\varphi}_2$. The following lemma gives the order of the accuracy of the method.

Lemma 2.1. *Under Assumption 2.2, Assumption 2.5 and Assumption 2.6 the consistency error of scheme (2.30) is first order with respect to Δt.*

Proof. We take the exact solution $\boldsymbol{\phi}$ of the abstract problem (2.29) and, summing both equations of (2.30), we obtain

$$\frac{\phi_2^{k+1} - \phi_2^k}{\Delta t} + \mathcal{L}_p\left(\phi_1^{k+1}, \phi_2^k\right) + \mathcal{L}_S\left(\phi_1^{k+1}, \phi_2^{k+1}\right) = \psi_p^{k+1} + \psi_S^{k+1}.$$

The local truncation error τ^{k+1} is

$$\tau^{k+1} = \frac{\phi_2^{k+1} - \phi_2^k}{\Delta t} + \mathcal{L}_p(\phi_1^{k+1}, \phi_2^k) + \mathcal{L}_S(\phi_1^{k+1}, \phi_2^{k+1}) - \psi_p^{k+1} - \psi_S^{k+1},$$

using a Taylor expansion for $\mathcal{L}_p$ and for the time derivative we obtain

$$\begin{aligned}
\tau^{k+1} =& \frac{\partial \phi_2}{\partial t} + \Delta t \phi''\left(t^{k+1}\right) + \mathcal{L}_p(\phi_1^{k+1}, \phi_2^{k+1}) - \Delta t \frac{\partial \mathcal{L}_p}{\partial \phi_2}(\phi_1^{k+1}, \phi_2^{k+1}) + \\
&+ \mathcal{L}_S(\phi_1^{k+1}, \phi_2^{k+1}) - \psi_p^{k+1} - \psi_S^{k+1} + \mathcal{O}\left(\Delta t^2\right) = \\
=& \Delta t \left[\phi''\left(t^{k+1}\right) - \frac{\partial \mathcal{L}_p}{\partial \phi_2}(\phi_1^{k+1}, \phi_2^{k+1}) \right] + \mathcal{O}\left(\Delta t^2\right).
\end{aligned}$$

$\square$

We present, in the following subsections, the pressure equation and the saturation equation decoupled with the IMPES splitting.

2.2.1 The pressure equation

Since for each time interval $\left(t^k, t^{k+1}\right)$ the saturation S_n^k is fixed, the pressure equation becomes a linear elliptic problem written in mixed form for the global pressure p^{k+1} and the total velocity $\boldsymbol{u}^{k+1}$. The total mobility λ and the modified gravity $\boldsymbol{G}$ depend on the saturation so we treat them explicitly: $\lambda = \lambda\left(S_n^k\right)$ and $\boldsymbol{G} = \boldsymbol{G}\left(S_n^k\right)$. Thus $\boldsymbol{u}^{k+1}$ and p^{k+1} are computed by solving

$$\begin{cases} \nabla \cdot \boldsymbol{u}^{k+1} = q_w + q_n, \\ \boldsymbol{u}^{k+1} = -\lambda \boldsymbol{K}\left(\nabla p^{k+1} - \boldsymbol{G}\right), \end{cases} \quad \text{in } \Omega \qquad (2.31)$$

coupled with the boundary conditions

$$\begin{cases} p^{k+1} = \widetilde{p} & \text{on } \Gamma^E, \\ \boldsymbol{u}^{k+1} \cdot \boldsymbol{n} = \widetilde{u}^N & \text{on } \Gamma^N, \\ \boldsymbol{u}^{k+1} \cdot \boldsymbol{n} - p^{k+1} = \widetilde{u}^R & \text{on } \Gamma_R, \end{cases}$$

Note that in system (2.31) there are no time derivatives. Nevertheless it is still a time dependent problem since the saturation S_n, and therefore the total mobility λ and the modified gravity $\boldsymbol{G}$, change at each time t^k.

Well posedness of the problem

For the sake of simplicity we assume that $\widetilde{u}^N \equiv 0$ or $\Gamma^N = \emptyset$, otherwise a standard lifting technique should be used. To write the weak formulation of (2.31) we introduce the functional spaces $Q = H^1(\Omega)$ and $\boldsymbol{V}$ defined as

$$\boldsymbol{V} := \left\{ \boldsymbol{\tau} \in \boldsymbol{H}_{\mathrm{div}}(\Omega) : <\boldsymbol{\tau} \cdot \boldsymbol{n}, v> = 0 \; \forall v \in H_{0,\Sigma}^1(\Omega) \text{ and } \boldsymbol{\tau} \cdot \boldsymbol{n} \in L^2\left(\Gamma^R\right) \right\},$$

with $\Sigma = \partial\Omega \backslash \Gamma^N$. Q and $\boldsymbol{V}$ are Hilbert spaces endowed with the scalar product $(\cdot, \cdot)_{H^1(\Omega)} : H^1(\Omega) \times H^1(\Omega) \to \mathbb{R}$ and $(\cdot, \cdot)_{\boldsymbol{V}} : \boldsymbol{V} \times \boldsymbol{V} \to \mathbb{R}$, defined as

$$(p, v)_{H^1(\Omega)} := (p, v)_\Omega + (\nabla p, \nabla v)_\Omega \,,$$

$$(\boldsymbol{u}, \boldsymbol{v})_{\boldsymbol{V}} := (\boldsymbol{u}, \boldsymbol{v})_\Omega + (\nabla \cdot \boldsymbol{u}, \nabla \cdot \boldsymbol{v})_\Omega + (\boldsymbol{u} \cdot \boldsymbol{n}, \boldsymbol{v} \cdot \boldsymbol{n})_{\Gamma^R} \,,$$

and norms $\|\cdot\|_{H^1(\Omega)} : H^1(\Omega) \to \mathbb{R}$ and $\|\cdot\|_{\boldsymbol{V}} : \boldsymbol{V} \to \mathbb{R}$, defined as

$$\|p\|_{H^1(\Omega)}^2 := (p, p)_{H^1(\Omega)} \quad \text{and} \quad \|\boldsymbol{u}\|_{\boldsymbol{V}}^2 := (\boldsymbol{u}, \boldsymbol{u})_{\boldsymbol{V}} \,,$$

with $\boldsymbol{u}, \boldsymbol{v} \in \boldsymbol{V}$ and $p, v \in H^1(\Omega)$. We define two bilinear forms $a(\cdot, \cdot) : \boldsymbol{V} \times \boldsymbol{V} \to \mathbb{R}$ and $b(\cdot, \cdot) : \boldsymbol{V} \times Q \to \mathbb{R}$, namely

$$a(\boldsymbol{u}, \boldsymbol{\tau}) := \left((\boldsymbol{K}\lambda)^{-1} \boldsymbol{u}, \boldsymbol{\tau}\right)_\Omega + (\boldsymbol{u} \cdot \boldsymbol{n}, \boldsymbol{\tau} \cdot \boldsymbol{n})_{\Gamma^R} \,,$$

$$b(\boldsymbol{u}, v) := -(\nabla \cdot \boldsymbol{u}, v)_\Omega \,,$$

with $\boldsymbol{u}, \boldsymbol{\tau} \in \boldsymbol{V}$ and $v \in Q$. We introduce also two functionals $F \in Q'$ and $G \in \boldsymbol{V}'$, namely

$$F(v) := (q_w + q_n, v)_\Omega \,,$$

$$G(\boldsymbol{\tau}) := (\lambda \boldsymbol{K} \boldsymbol{G}, \boldsymbol{\tau})_\Omega + (\widetilde{u}^R, \boldsymbol{\tau} \cdot \boldsymbol{n})_{\Gamma^R} - (\widetilde{p}, \boldsymbol{\tau} \cdot \boldsymbol{n})_{\Gamma^N} \,,$$

with $v \in Q$ and $\boldsymbol{\tau} \in \boldsymbol{V}$.

Problem 2.5 (Weak formulation of pressure equation). *The weak formulation of* (2.31) *is: find* $(\boldsymbol{u}^{k+1}, p^{k+1}) \in \boldsymbol{V} \times Q$ *such that*

$$\begin{cases} a(\boldsymbol{u}^{k+1}, \boldsymbol{\tau}) + b(\boldsymbol{\tau}, p^{k+1}) = G(\boldsymbol{\tau}) & \forall \boldsymbol{\tau} \in \boldsymbol{V} \,, \\ b(\boldsymbol{u}^{k+1}, v) = -F(v) & \forall v \in Q \,. \end{cases}$$

Lemma 2.2 (Well posedness). *If* $\Gamma^N \neq \emptyset$ *and under Assumption 2.2, Assumption 2.4 and Assumption 2.6 and choosing the Brooks-Corey or Van Genuchten model for the relative permeability then Problem 2.5 is well posed. Furthermore we have the following bounds*

$$\left\|\boldsymbol{u}^{k+1}\right\|_{\boldsymbol{V}} \leq \|\boldsymbol{K}\|_{L^\infty(\Omega)} \|\lambda\|_{L^\infty(\Omega)} \|G\|_{\boldsymbol{V}'} + (1 + \alpha) \|F\|_{Q'} \,,$$

$$\left\|p^{k+1}\right\|_Q \leq (1 + \alpha) \left(\|G\|_{\boldsymbol{V}'} + K_0 \lambda_0 \|F\|_{Q'}\right) \,,$$

with

$$\alpha \leq \frac{\|\boldsymbol{K}\|_{L^\infty(\Omega)} \|\lambda\|_{L^\infty(\Omega)}}{K_0 \lambda_0} \,, \quad \|F\|_{Q'} \leq \|q_w\|_{L^2(\Omega)} + \|q_n\|_{L^2(\Omega)} \,,$$

$$\|G\|_{\boldsymbol{V}'} \leq \|\boldsymbol{K}\|_{L^\infty(\Omega)} \|\lambda\|_{L^\infty(\Omega)} \|\boldsymbol{G}\|_{L^2(\Omega)} + \left\|\widetilde{u}^R\right\|_{L^2(\Gamma^R)} + \|\widetilde{p}\|_{L^2(\Gamma^N)} \,.$$

Proof. For both models we have $\lambda \in L^\infty(\Omega)$ and $\exists \lambda_0 \in \mathbb{R}^+$ such that $\lambda \geq \lambda_0$ since both relative permeabilities are positive and not zero at the same saturation value. Moreover $\boldsymbol{G} \in \left[L^2(\Omega)\right]^n$, then using the theory presented in [11] we can conclude that $\exists! (\boldsymbol{u}^{k+1}, p^{k+1}) \in \boldsymbol{V} \times Q$ solution of Problem 2.5. Furthermore

$$\left\|\boldsymbol{u}^{k+1}\right\|_{\boldsymbol{V}} \leq \frac{1}{\alpha_0} \|G\|_{\boldsymbol{V}'} + \frac{1}{k_0} \left(1 + \frac{\|a\|}{\alpha_0}\right) \|F\|_{Q'} \,,$$

$$\left\|p^{k+1}\right\|_Q \leq \frac{1}{k_0} \left(1 + \frac{\|a\|}{\alpha_0}\right) \|G\|_{\boldsymbol{V}'} + \frac{\|a\|}{k_0^2} \left(1 + \frac{\|a\|}{\alpha_0}\right) \|F\|_{Q'} \,,$$

where α_0 is the coercivity constant of the bilinear form a in the kernel of the operator B associated to the bilinear form b, $\|a\|$ is the continuity constant of the bilinear form a and k_0 is a constant which depends on the bilinear form b. In our case we have

$$\frac{1}{\alpha_0} = \|\boldsymbol{K}\|_{L^\infty(\Omega)}\|\lambda\|_{L^\infty(\Omega)}, \quad \|a\| \leq \frac{1}{K_0\lambda_0}, \quad k_0 = 1,$$

and

$$\|F\|_{Q'} \leq \|q_w\|_{L^2(\Omega)} + \|q_n\|_{L^2(\Omega)},$$
$$\|G\|_{\boldsymbol{V'}} \leq \|\boldsymbol{K}\|_{L^\infty(\Omega)}\|\lambda\|_{L^\infty(\Omega)}\|\boldsymbol{G}\|_{L^2(\Omega)} + \left\|\widetilde{u}^R\right\|_{L^2(\Gamma^R)} + \|\widetilde{p}\|_{L^2(\Gamma^N)}.$$

$\square$

2.2.2 The saturation equation

The saturation equation is a non-linear and possibly degenerate parabolic equation written in mixed form for the saturation of the non-wetting phase S_n and the Darcy velocity of the non-wetting phase $\boldsymbol{u}_n$. The non-linearities are in the transport and in the diffusion terms. The latter degenerates, *i.e.* vanishes, if $S_n = S_{nr}$ or $S_n = 1 - S_{wr}$. At each time interval (t^k, t^{k+1}), from the pressure equation (2.31) we obtain the total velocity $\boldsymbol{u}^{k+1}$ at time t^{k+1}, thus the saturation equation, defined in $\Omega \times (t^k, t^{k+1})$, reads

$$\begin{cases} \Phi\dfrac{\partial S_n}{\partial t} + \nabla{\cdot}\boldsymbol{u}_n = q_n, \\[2mm] \boldsymbol{u}_n = f_n\boldsymbol{u}^{k+1} - \lambda_w f_n \boldsymbol{K}\left[p'_c\nabla S_n + (\rho_w - \rho_n)\boldsymbol{g}\right], \end{cases} \tag{2.32}$$

coupled with boundary and initial conditions

$$\begin{cases} S_n = \overline{S}_n & \text{on } \Upsilon^N \times \left(t^k, t^{k+1}\right), \\[2mm] \boldsymbol{u}_n \cdot \boldsymbol{n} = \overline{u}_n^E & \text{on } \Upsilon^E \times \left(t^k, t^{k+1}\right), \\[2mm] \boldsymbol{u}_n \cdot \boldsymbol{n} - S_n = \overline{u}_n^R & \text{on } \Upsilon^R \times \left(t^k, t^{k+1}\right), \\[2mm] S_n\left(t^k\right) = S_n^k & \text{in } \Omega \times \left\{t^k\right\}, \end{cases}$$

and with $S_n(0) = S_n^0 = S_{n,0}$.

In reservoir simulations the transport part is dominant, so if we want to numerically solve the system of equations accurately we should stabilize it. There are several possibilities, for example using upwinding techniques [62] or by operator splitting [63]. The latter, which is a common approach to this type of problem [42, 43, 52], is based on splitting the diffusion and the transport operators leading to a non-linear purely hyperbolic equation and a non-linear purely diffusive parabolic equation. Using the same formalism of section 2.2 we introduce the abstract equation

$$\begin{cases} \dfrac{\partial\varphi}{\partial t} + \mathcal{L}_S(\varphi) = \psi & \text{for } t \in \left(t^k, t^{k+1}\right), \\[2mm] \varphi\left(t^k\right) = \overline{\varphi} & \text{for } t = t^k, \end{cases} \tag{2.33}$$

with $\varphi = S_n$ the unknown, $\overline{\varphi} = S_n^k$ the initial condition and $\psi = q_n$ the scalar source. The operator $\mathcal{L}_S$ can be decomposed as

$$\mathcal{L}_S(\varphi) := \mathcal{H}(\varphi) + \mathcal{P}(\varphi) \,,$$

where $\mathcal{P}$ is the purely elliptic part while $\mathcal{H}$ is the hyperbolic part of the saturation equation. The gravity term belongs to the hyperbolic part. We should solve first the hyperbolic equation, obtaining an intermediate value of $\varphi^{k+\frac{1}{2}}$, then solve the parabolic equation with the intermediate value $\varphi^{k+\frac{1}{2}}$. In literature we find at least two reasons to justify this splitting strategy:

- we must account for the boundary conditions of equation (2.32). In the hyperbolic step, we have to use boundary conditions compatible with an hyperbolic problem, *i.e.* just inflow and outflow type conditions. While the parabolic step uses the full set of boundary conditions. In this way if we solve the hyperbolic problem first the parabolic step "corrects" the solution at the boundary;

- a typical choice to solve an hyperbolic equation is to use an explicit scheme while for a non-linear parabolic equation it is preferable to employ an implicit scheme. Following [55] we should solve first the hyperbolic part and then the parabolic part. We obtain a global scheme which is conditionally stable for all Δt and converges to the stationary solution of the problem for sufficiently small time steps. If we solved first the parabolic equation, with an implicit scheme, and then the hyperbolic equation, with an explicit scheme, we obtain a global scheme which is unconditionally stable but does not converge to the stationary solution.

From these considerations, using a first order scheme for time discretization, we derive the following splitting

$$\begin{cases} \dfrac{\varphi^{k+\frac{1}{2}} - \varphi^k}{\Delta t} + \mathcal{H}\left(\varphi^k\right) = 0 \,, \\[3mm] \dfrac{\varphi^{k+1} - \varphi^{k+\frac{1}{2}}}{\Delta t} + \mathcal{P}\left(\varphi^{k+1}\right) = \psi^{k+1} \,, \end{cases} \tag{2.34}$$

with $\varphi^k = \overline{\varphi}$.

Lemma 2.3. *Under Assumption 2.2, Assumption 2.5 and Assumption 2.6, the consistency error of scheme (2.34) is first order with respect to Δt.*

Proof. We take the exact solution ϕ of the abstract problem (2.33), obtaining

$$\begin{cases} \dfrac{\phi^{k+\frac{1}{2}} - \phi^k}{\Delta t} + \mathcal{H}\left(\phi^k\right) = 0 \,, \\[3mm] \dfrac{\phi^{k+1} - \phi^{k+\frac{1}{2}}}{\Delta t} + \mathcal{P}\left(\phi^{k+1}\right) = \psi^{k+1} \,. \end{cases}$$

We substitute $\phi^{k+\frac{1}{2}}$ in the second equation to have

$$\phi^{k+1} = \phi^k - \Delta t \left[\mathcal{H}\left(\phi^k\right) + \mathcal{P}\left(\phi^{k+1}\right) - \psi^{k+1}\right] \,.$$

The local truncation error τ^{k+1} is then

$$\tau^{k+1} = \frac{\phi^{k+1} - \phi^k}{\Delta t} + \mathcal{H}\left(\phi^k\right) + \mathcal{P}\left(\phi^{k+1}\right) - \psi^{k+1} \,,$$

using a Taylor expansion for $\mathcal{H}$ and for the time derivative we obtain

$$\begin{aligned}
\tau^{k+1} = &\frac{\partial \phi}{\partial t} + \Delta t \phi''\left(t^{k+1}\right) + \mathcal{H}\left(\phi^{k+1}\right) + \mathcal{P}\left(\phi^{k+1}\right) - \psi^{k+1} + \\
&- \Delta t \mathcal{H}'\left(\phi^{k+1}\right) + \mathcal{O}\left(\Delta t^2\right) = \Delta t \left[\phi''\left(t^{k+1}\right) - \mathcal{H}'\left(\phi^{k+1}\right)\right] + \mathcal{O}\left(\Delta t^2\right) \,.
\end{aligned}$$

$\square$

Given the hyperbolic operator $\mathcal{H}$ we introduce the flux function

$$\boldsymbol{\mathcal{F}}(S) := f_n(S)\boldsymbol{u}^{k+1} - \lambda_w(S)f_n(S)\boldsymbol{K}\left(\rho_w - \rho_n\right)\boldsymbol{g} \,. \tag{2.35}$$

Due to the hyperbolic nature of the problem, the boundary conditions are imposed only on the inflow part of Υ, *i.e.* on

$$\Upsilon^E_{\text{inflow}} = \left\{\Upsilon^E \cap \boldsymbol{\mathcal{F}}\left(\hat{S}_n\right) \cdot \boldsymbol{n} > 0\right\} \,,$$

we impose $\hat{S}_n = \overline{S}_n$ on $\Upsilon^E_{\text{inflow}}$, where $\hat{S}_n$ is the intermediate saturation. The hyperbolic part of the saturation equation reads then

$$\begin{cases} \Phi\dfrac{\partial \hat{S}_n}{\partial t} + \nabla\cdot\boldsymbol{\mathcal{F}}\left(\hat{S}_n\right) = 0 \\ \boldsymbol{\mathcal{F}}\left(\hat{S}_n\right) = f_n \boldsymbol{u}^{k+1} - \lambda_w f_n \boldsymbol{K}\left(\rho_w - \rho_n\right)\boldsymbol{g} \end{cases} \quad \Omega \times \left(t^k,\, t^{k+1}\right) \tag{2.36}$$

coupled with boundary and initial conditions

$$\begin{cases} \hat{S}_n = \overline{S}_n & \text{on } \Upsilon^E_{\text{inflow}} \times \left(t^k,\, t^{k+1}\right), \\ \hat{S}_n^k = S_n^k & \text{in } \Omega \times \left\{t^k\right\} \end{cases}$$

provides $\hat{S}_n$. The purely parabolic equation at time step t^{k+1} then reads

$$\begin{cases} \Phi\dfrac{\partial S_n}{\partial t} + \nabla\cdot\hat{\boldsymbol{u}}_n = q_n \,, \\ \hat{\boldsymbol{u}}_n = -\lambda_w f_n \boldsymbol{K} p_c' \nabla S_n \,, \end{cases} \quad \text{in } \Omega \times \left(t^k,\, t^{k+1}\right) \tag{2.37}$$

coupled with boundary and initial conditions

$$\begin{cases} S_n = \overline{S}_n & \text{on } \Upsilon^N \times \left(t^k,\, t^{k+1}\right), \\ \boldsymbol{u}_n \cdot \boldsymbol{n} = \overline{u}_n^E & \text{on } \Upsilon^E \times \left(t^k,\, t^{k+1}\right), \\ \boldsymbol{u}_n \cdot \boldsymbol{n} - S_n = \overline{u}_n^R & \text{on } \Upsilon^R \times \left(t^k,\, t^{k+1}\right), \\ S_n\left(t^k\right) = S_n^k = \hat{S}_n\left(t^{k+1}\right) & \text{in } \Omega \times \left\{t^k\right\}. \end{cases}$$

47

Well posedness of the problem

For the sake of simplicity we assume that $\overline{u}_n^N \equiv 0$ or $\Upsilon^N = \emptyset$, otherwise a standard lifting technique should be used. To derive the weak formulation of the purely hyperbolic equation (2.36) we introduce the functional space

$$\hat{Q} = \left\{ S \in Q : S = \overline{S}^E \text{ on } \Upsilon_{\text{inflow}}^E \right\} ,$$

then the weak formulation of problem (2.36) is: find $\hat{S}_n \in \hat{Q}$ such that

$$\left(\Phi \frac{\partial \hat{S}_n}{\partial t},\, v \right)_\Omega - \left(\boldsymbol{\mathcal{F}}\left(\hat{S}_n \right),\, \nabla v \right)_\Omega = 0 \quad \forall v \in C_0^\infty \left(\Omega \right) ,$$

The study of the well posedness of the problem is complicated and not completely solved, we refer to [14] and the reference therein for a preliminary analysis.

Due to the degeneracy of the purely diffusion part of the saturation equation (2.37) the mathematical analyses is rather complex, we refer to [18] and [5] for a detailed description. To write the weak formulation of the parabolic part we introduce the functional space

$$\boldsymbol{W} := \left\{ \boldsymbol{\tau} \in \boldsymbol{H}_{\text{div}}\left(\Omega \right) : <\boldsymbol{\tau} \cdot \boldsymbol{n},\, v >= 0 \,\forall v \in H_{0,\Theta}^1 \left(\Omega \right) \text{ and } \boldsymbol{\tau} \cdot \boldsymbol{n} \in L^2 \left(\Upsilon^R \right) \right\} ,$$

with $\Theta = \partial\Omega \setminus \Upsilon^N$. We define the non-linear form $w\left(\cdot,\, \cdot,\, \cdot \right) : \boldsymbol{W} \times Q \times \boldsymbol{W} \to \mathbb{R}$ and the bilinear form $b(\cdot,\, \cdot) : \boldsymbol{W} \times Q \to \mathbb{R}$

$$w\left(\boldsymbol{u},\, z,\, \boldsymbol{\tau} \right) := \left(\left[\lambda_w(z) f_n(z) \boldsymbol{K} p_c'(z) \right]^{-1} \boldsymbol{u},\, \boldsymbol{\tau} \right)_\Omega + \left(\boldsymbol{u} \cdot \boldsymbol{n},\, \boldsymbol{\tau} \cdot \boldsymbol{n} \right)_{\Upsilon^R} ,$$

$$b(\boldsymbol{u},\, z) := -(\nabla \cdot \boldsymbol{u},\, z)_\Omega$$

with $\boldsymbol{u}, \boldsymbol{\tau} \in \boldsymbol{W}$ and $z \in Q$. We introduce also two functionals $F_S \in Q'$ and $G_S \in \boldsymbol{W}'$, namely

$$F_S\left(v \right) = (q_n,\, v)_\Omega \quad \text{and} \quad G_S\left(\boldsymbol{\tau} \right) = \left(\overline{u}_n^R,\, \boldsymbol{\tau} \cdot \boldsymbol{n} \right)_{\Upsilon^R} - \left(\overline{S}^N,\, \boldsymbol{\tau} \cdot \boldsymbol{n} \right)_{\Upsilon^N} .$$

The weak formulation reads: find $(S_n, \hat{\boldsymbol{u}}_n) \in L^2\left(t^k,\, t^{k+1};\, Q \right) \times L^2\left(t^k,\, t^{k+1};\, \boldsymbol{W} \right)$ such that $S_n' \in L^2\left(t^k,\, t^{k+1};\, Q' \right)$ and a.e. in $\left(t^k,\, t^{k+1} \right)$

$$\begin{cases} w\left(\hat{\boldsymbol{u}}_n,\, S_n,\, \boldsymbol{\tau} \right) + b\left(\boldsymbol{\tau},\, S_n \right) = G_S(\boldsymbol{\tau}) & \forall \boldsymbol{\tau} \in \boldsymbol{W}_0 , \\ b\left(\hat{\boldsymbol{u}}_n,\, v \right) - (\Phi S_n',\, v)_\Omega = -F_S(v) & \forall v \in Q . \end{cases} \quad (2.38)$$

The following lemma, taken from [18], gives the existence and uniqueness of the solution for the un-split saturation equation under stricter hypotheses on the data.

Lemma 2.4 (Existence). *If $\Upsilon^E \neq \emptyset$ and under Assumption 2.2, Assumption 2.4 and Assumption 2.6 and supposing that the parabolic part of the saturation equation (2.38) is non degenerate, i.e.*

$$S_n \neq S_{nr} \quad \text{and} \quad S_n \neq 1 - S_{wr} ,$$

the saturation equation (2.38) *admits at least one solution satisfying*

$$0 \leq S_n \leq 1 \quad a.e. \ in \ \Omega \,,$$

and

$$S_n \in L^\infty \left(\mathcal{I}_T; L^2 \left(\Omega \right) \right) \quad and \quad S_n' \in L^2 \left(\mathcal{I}_T; H^{-1} \left(\Omega \right) \right) \,.$$

Lemma 2.5 (Uniqueness)**.** *Under the hypotheses of Lemma 2.4 and assuming furthermore suppose that neither gravity nor capillary pressure heterogeneity are present, then the saturation equation* (2.32) *admits one solution, such that*

$$S_n \in L^\infty \left(\mathcal{I}_T; H^1 \left(\Omega \right) \right) \quad and \quad S_n' \in L^2 \left(\mathcal{I}_T; L^2 \left(\Omega \right) \right) \,.$$

2.3 Mixed finite element formulation

To solve numerically the pressure equation (2.31) and the parabolic part of the saturation equation (2.37) we use the dual, mixed and hybrid finite element method, we refer to [11] and [67] for a more detailed description.

Problem 2.6 (Primal formulation)**.** *The classical formulation for an elliptic partial differential equation is to find a function $p \in C^2 \left(\Omega \right)$ such that*

$$\begin{cases} -\nabla \cdot \left[\boldsymbol{K} \left(\nabla p - \boldsymbol{f}_v \right) \right] + \gamma p = f & in \ \Omega, \\ \boldsymbol{K} \nabla p \cdot \boldsymbol{n} + l p = g^R & on \ \Gamma^R, \\ p = 0 & on \ \Gamma^E. \end{cases}$$

The data are reported in Assumption 2.7.

Assumption 2.7. *We assume that:*

1. *the diffusione matrix $\boldsymbol{K} = \boldsymbol{K} \left(\boldsymbol{x} \right)$ is a symmetric and positive definite matrix such that $\boldsymbol{K} \in \left[L^\infty \left(\Omega \right) \right]^{n \times n}$;*

2. *the vector source term $\boldsymbol{f}_v = \boldsymbol{f}_v \left(\boldsymbol{x} \right)$ is such that $\boldsymbol{f}_v \in \left[L^2 \left(\Omega \right) \right]^n$;*

3. *the reactive coefficient $\gamma = \gamma \left(\boldsymbol{x} \right)$ is such that $\gamma \in L^\infty \left(\Omega \right)$;*

4. *the scalar source $f = f \left(\boldsymbol{x} \right)$ is such that $f \in L^2 \left(\Omega \right)$;*

5. *the data for the robin boundary $l = l \left(\boldsymbol{x} \right)$ and $g^R = g^R \left(\boldsymbol{x} \right)$ are such that $l \in L^\infty \left(\Gamma^R \right)$ and $g^R \in H^{-\frac{1}{2}} \left(\Gamma^R \right)$.*

2.3.1 Mixed formulation

Standard continuous finite elements are not suitable to solve neither the pressure equation nor the saturation equation, in fact they are designed for problems with smooth solutions, whereas in porous media simulations the solutions may develop sharp fronts due to convection effects. Another problem for the standard finite elements is that the velocity of the two fluids, which is an important coupling factors in the equations, is poorly approximated. More precisely the

constraint on the saturation is better reproduced if the velocity field fulfils local conservation property. Finally the typical data in the equations, for instance $\boldsymbol{K}$, may vary up to several order of magnitude from one grid cell to the nearby ones, standard finite elements can behave poorly in this case. For these reasons we use mixed finite elements for the space discretization of the pressure equation and the parabolic part of the saturation equation.

In the context of mixed methods, a problem that depends just on the unknown p is call *primal formulation* of the problem, as in Problem 2.6. Nevertheless in most practical and engineering problems, like the ones in our interest, another unknown is useful: the total flux $\boldsymbol{u}$, which is

$$\boldsymbol{u} = -\boldsymbol{K} \left(\nabla p - \boldsymbol{f}_v \right) .$$

Using the total flux Problem 2.6 can be written in the *mixed formulation*, introduced and analysed in [64].

Problem 2.7 (Mixed formulation). *The classical mixed formulation for an elliptic partial differential equation is: find $p \in C^1 \left(\Omega \right)$ and $\boldsymbol{u} \in \left[C^1 \left(\Omega \right) \right]^n$ such that*

$$\begin{cases} \boldsymbol{K}^{-1}\boldsymbol{u} + \nabla p = \boldsymbol{f}_v & \text{in } \Omega, \\[2mm] \nabla \cdot \boldsymbol{u} + \gamma p = f & \text{in } \Omega, \\[2mm] \boldsymbol{u} \cdot \boldsymbol{n} + lp = g^R & \text{on } \Gamma^R, \\[2mm] p = 0 & \text{on } \Gamma^E. \end{cases} \tag{2.39}$$

Assumption 2.8 (Computational domain and mesh). *To write equation (2.39) in a discrete form we introduce the following requests:*

1. *Ω fulfils Assumption 2.2 and is a polygonal domain;*

2. *$\mathcal{T}_h$ is the conforming tessellation of domain Ω such that*

$$\overline{\Omega} = \bigcup_{K \in \mathcal{T}_h} K \, .$$

    For an element $K \in \mathcal{T}_h$ we divide ∂K into several facet denoted with e_K. The facet shared between two elements K and K' is indicated with $e_{K-K'}$. Further we indicate with $\mathcal{E}_h$ the set of all the facets of $\mathcal{T}_h$ and with $\mathring{\mathcal{E}}_h \subset \mathcal{E}_h$ the set of all the internal facets. See Figure 2.11 for an example;

3. *the elements K are segments for $n = 1$, triangles for $n = 2$ or tetrahedra for $n = 3$; we are not considering $\mathcal{T}_h$ composed by quadrilateral nor hexahedra since the convergence rate is not guaranteed for a general mesh $\mathcal{T}_h$, see [6] and [69] for further details. We indicate with N_I the number of facets in $\mathcal{E}_h$ and with N_E the number of elements in $\mathcal{T}_h$. In addition $\boldsymbol{n}$ may be the outward unit normal to ∂K or the outward unit normal to Γ, depending on the context;*

4. *we require that $\mathcal{T}_h$ is regular, i.e.*

$$\exists \xi \geq 0 : \frac{h_K}{\rho_K} \leq \xi \ \forall K \in \mathcal{T}_h \, , \tag{2.40}$$
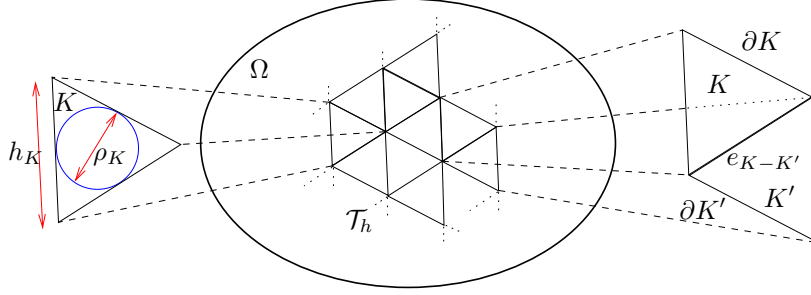
Figure 2.11: Picture of the domain Ω, its triangulation $\mathcal{T}_h$ and the element definitions.

where $h_K := \operatorname{diam}(K)$ is the diameter of K, with

$$\operatorname{diam}(K) := \max_{x,y \in K} |x - y| ,$$

and ρ_K is the diameter of the circle inscribed in K, see left part of Figure 2.11. We indicate with $h := \max_{K \in \mathcal{T}_h} h_K$.

We use the hybridization procedure to split Problem 2.7 from the entire domain to problems in each element K, and write the weak formulation for the dual problem (2.39). We introduce the following functional Hilbert spaces

$$Q := L^2(\Omega) , \qquad \boldsymbol{H}_{\operatorname{div}}(K) := \left\{ \boldsymbol{\tau} \in \left[L^2(K) \right]^n : \nabla \cdot \boldsymbol{\tau} \in L^2(K) \right\} ,$$

$$\boldsymbol{Z} := \left\{ \boldsymbol{\tau} \in \left[L^2(\Omega) \right]^n : \boldsymbol{\tau}|_K \in \boldsymbol{H}_{\operatorname{div}}(K) \text{ for } K \in \mathcal{T}_h \right\} ,$$

$$\Lambda := \left\{ \lambda \in H^{\frac{1}{2}}(\mathcal{E}_h) : \lambda = 0 \text{ on } \Gamma^E \right\} ,$$

each space is equipped with a scalar product: $(\cdot, \cdot)_Q : Q \times Q \to \mathbb{R}$, $(\cdot, \cdot)_{\boldsymbol{H}_{\operatorname{div}}(K)} : \boldsymbol{H}_{\operatorname{div}}(K) \times \boldsymbol{H}_{\operatorname{div}}(K) \to \mathbb{R}$, $(\cdot, \cdot)_{\boldsymbol{Z}} : \boldsymbol{Z} \times \boldsymbol{Z} \to \mathbb{R}$ and $(\cdot, \cdot)_\Lambda : \Lambda \times \Lambda \to \mathbb{R}$, respectively such that

$$(p, v)_Q := (p, v)_\Omega , \qquad\qquad (\boldsymbol{u}, \boldsymbol{\tau})_{\boldsymbol{H}_{\operatorname{div}}(K)} := (\boldsymbol{u}, \boldsymbol{\tau})_K + (\nabla \cdot \boldsymbol{u}, \nabla \cdot \boldsymbol{\tau})_K ,$$

$$(\boldsymbol{r}, \boldsymbol{s})_{\boldsymbol{Z}} := \sum_{K \in \mathcal{T}_h} (\boldsymbol{r}, \boldsymbol{s})_{\boldsymbol{H}_{\operatorname{div}}(K)} , \qquad (\lambda, \mu)_\Lambda := \sum_{e \in \mathcal{E}_h} (\lambda, \mu)_e ,$$

with $p, v \in Q$, $\boldsymbol{u}, \boldsymbol{\tau} \in \boldsymbol{H}_{\operatorname{div}}(K)$, $\boldsymbol{r}, \boldsymbol{s} \in \boldsymbol{Z}$ and $\lambda, \mu \in \Lambda$. The corresponding norms are $\|\cdot\|_Q : Q \to \mathbb{R}$, $\|\cdot\|_{\boldsymbol{H}_{\operatorname{div}}(K)} : \boldsymbol{H}_{\operatorname{div}}(K) \to \mathbb{R}$, $\|\cdot\|_{\boldsymbol{Z}} : \boldsymbol{Z} \to \mathbb{R}$ and $\|\cdot\|_\Lambda : \Lambda \to \mathbb{R}$

$$\|p\|_Q^2 := (p, p)_Q , \quad \|\boldsymbol{u}\|_{\boldsymbol{H}_{\operatorname{div}}(K)}^2 := (\boldsymbol{u}, \boldsymbol{u})_{\boldsymbol{H}_{\operatorname{div}}(K)} ,$$

$$\|\boldsymbol{r}\|_{\boldsymbol{Z}}^2 := (\boldsymbol{r}, \boldsymbol{r})_{\boldsymbol{Z}} , \qquad \|\lambda\|_\Lambda^2 := (\lambda, \lambda)_\Lambda .$$

The Dirichlet boundary conditions in this framework are of *essential* type, since they are imposed in the definition of the space Λ.

To write the first equation of (2.39) in a weak form, let us take a test function $\boldsymbol{\tau} \in \boldsymbol{Z}$, integrate on a single triangle K and sum on the triangulation $\mathcal{T}_h$ to

obtain

$$\sum_{K \in \mathcal{T}_h} \left(\boldsymbol{K}^{-1} \boldsymbol{u}, \, \boldsymbol{\tau} \right)_K + (\nabla p, \, \boldsymbol{\tau})_K - (\boldsymbol{f}_v, \, \boldsymbol{\tau})_K =$$

$$\sum_{K \in \mathcal{T}_h} \left(\boldsymbol{K}^{-1} \boldsymbol{u}, \, \boldsymbol{\tau} \right)_K - (p, \, \nabla \cdot \boldsymbol{\tau})_K + (\tilde{p}, \, \boldsymbol{\tau} \cdot \boldsymbol{n})_{\partial K} - (\boldsymbol{f}_v, \, \boldsymbol{\tau})_K = 0 \,.$$

The trace of a function in Q on ∂K is not well defined, so we substitute $\tilde{p}$ with $\lambda \in \Lambda$ to find

$$\sum_{K \in \mathcal{T}_h} \left(\boldsymbol{K}^{-1} \boldsymbol{u}, \, \boldsymbol{\tau} \right)_K - (p, \, \nabla \cdot \boldsymbol{\tau})_K + (\lambda, \, \boldsymbol{\tau} \cdot \boldsymbol{n})_{\partial K} - (\boldsymbol{f}_v, \, \cdot \boldsymbol{\tau})_K = 0 \quad \forall \boldsymbol{\tau} \in \boldsymbol{Z} \,. \tag{2.41}$$

To impose the requirement that $\boldsymbol{u} \in \boldsymbol{H}_{\mathrm{div}}(\Omega)$, we need to require continuity of the total flux $\boldsymbol{u}$ over $\mathring{\mathcal{E}}_h$. Following [63] we introduce the constraint

$$\sum_{e \in \mathring{\mathcal{E}}_h} (\mu, \, \boldsymbol{u} \cdot \boldsymbol{n})_e = \sum_{K \in \mathcal{T}_h} (\mu, \, \boldsymbol{u} \cdot \boldsymbol{n})_{\partial K \setminus \Gamma^R} = 0 \,, \qquad \forall \mu \in \Lambda \,. \tag{2.42}$$

To write the second equation of (2.39) in the weak form we take a test function $v \in Q$, then integrate on a single triangle K and sum on $\mathcal{T}_h$ to obtain

$$\sum_{K \in \mathcal{T}_h} -(\nabla \cdot \boldsymbol{u}, \, v)_K - (\gamma p, \, v)_K = \sum_{K \in \mathcal{T}_h} -(f, \, v)_K \quad \forall v \in Q \,. \tag{2.43}$$

The Robin boundary conditions in Γ^R are imposed weakly to give

$$\sum_{K \in \mathcal{T}_h} (\mu, \, \boldsymbol{u} \cdot \boldsymbol{n})_{\partial K \cap \Gamma^R} + (l\mu, \, \lambda)_{\partial K \cap \Gamma^R} = \sum_{K \in \mathcal{T}_h} \left(g^R, \mu \right)_{\partial K \cap \Gamma^R}, \quad \forall \mu \in \Lambda \,. \tag{2.44}$$

Gathering equations (2.41), (2.42), (2.43) and (2.44) we find the weak form for Problem 2.7: find $(\boldsymbol{u}, p, \lambda) \in \boldsymbol{Z} \times V \times \Lambda$ such that

$$\begin{cases} \displaystyle\sum_{K \in \mathcal{T}_h} \left(\boldsymbol{K}^{-1} \boldsymbol{u}, \, \boldsymbol{\tau} \right)_K - (p, \, \nabla \cdot \boldsymbol{\tau})_K + (\lambda, \, \boldsymbol{\tau} \cdot \boldsymbol{n})_{\partial K} = (\boldsymbol{f}_v, \, \boldsymbol{\tau})_\Omega & \forall \boldsymbol{\tau} \in \boldsymbol{Z} \,, \\[4mm] \displaystyle\sum_{K \in \mathcal{T}_h} -(\nabla \cdot \boldsymbol{u}, \, v)_K - (\gamma p, \, v)_K = -(f, \, v)_\Omega & \forall v \in Q \,, \\[4mm] \displaystyle\sum_{K \in \mathcal{T}_h} (\mu, \, \boldsymbol{u} \cdot \boldsymbol{n})_{\partial K \setminus \Gamma^E} + (l\mu, \, \lambda)_{\partial K \cap \Gamma^R} = \displaystyle\sum_{K \in \mathcal{T}_h} \left(g^R, \mu \right)_{\partial K \cap \Gamma^R} & \forall \mu \in \Lambda \,. \end{cases}$$

We introduce the local bilinear forms: $a_K(\cdot, \cdot) : \boldsymbol{H}_{\mathrm{div}}(K) \times \boldsymbol{H}_{\mathrm{div}}(K) \to \mathbb{R}$ and $b_K(\cdot, \cdot) : L^2(K) \times \boldsymbol{H}_{\mathrm{div}}(K) \to \mathbb{R}$ and the corresponding global bilinear forms: $a(\cdot, \cdot) : \boldsymbol{Z} \times \boldsymbol{Z} \to \mathbb{R}$ and $b(\cdot, \cdot) : Q \times \boldsymbol{Z} \to \mathbb{R}$ such that

$$a_K(\boldsymbol{u}, \, \boldsymbol{\tau}) := \left(\boldsymbol{K}^{-1} \boldsymbol{u}, \, \boldsymbol{\tau} \right)_K, \qquad b_K(p, \, \boldsymbol{\tau}) := -(p, \, \nabla \cdot \boldsymbol{\tau})_K,$$

$$a(\boldsymbol{u}, \, \boldsymbol{\tau}) := \sum_{K \in \mathcal{T}_h} a_K(\boldsymbol{u}, \, \boldsymbol{\tau}), \qquad b(p, \, \boldsymbol{\tau}) := \sum_{K \in \mathcal{T}_h} b_K(p, \, \boldsymbol{\tau}),$$

with $K \in \mathcal{T}_h$. We introduce also the following local bilinear forms: $c_e(\cdot, \cdot) :$ $H^{\frac{1}{2}}(e) \times \boldsymbol{H}_{\text{div}}(K) \to \mathbb{R}$ where $e \in \mathcal{E}_h$ is a facet of $K \in \mathcal{T}_h$, $e_K(\cdot, \cdot) : L^2(K) \times$ $L^2(K) \to \mathbb{R}$ and $h_e(\cdot, \cdot) : H^{\frac{1}{2}}(e) \times H^{\frac{1}{2}}(e) \to \mathbb{R}$ and the corresponding bilinear forms $c(\cdot, \cdot) : \Lambda \times \boldsymbol{Z} \to \mathbb{R}$, $e(\cdot, \cdot) : Q \times Q \to \mathbb{R}$ and $h(\cdot, \cdot) : \Lambda \times \Lambda \to \mathbb{R}$ such that

$$c_e(\lambda, \boldsymbol{\tau}) := (\lambda, \boldsymbol{\tau} \cdot \boldsymbol{n})_e, \qquad e_K(p, v) := (\gamma p, v)_K,$$

$$h_e(\lambda, \mu) := (l\mu, \lambda)_e, \qquad c(\lambda, \boldsymbol{\tau}) := \sum_{e \in \mathcal{E}_h} c_e(\lambda, \boldsymbol{\tau}),$$

$$e(p, v) := \sum_{K \in \mathcal{T}_h} e_K(p, v), \qquad h(\lambda, \mu) := \sum_{e \in \mathcal{E}_h \cap \Gamma^R} h_e(\lambda, \mu),$$

Finally we introduce also some local functionals: $F_{v,K} \in \boldsymbol{H}_{\text{div}}(K)'$, $F_K \in L^2(K)'$ and $G_e \in H^{\frac{1}{2}}(e)'$ and the corresponding global functionals $F_v \in \boldsymbol{Z}'$, $F \in Q'$ and $G \in \Lambda'$ such that

$$F_{v,K}(\boldsymbol{\tau}) := (\boldsymbol{f}_v, \boldsymbol{\tau})_K, \qquad F_K(v) := (f, v)_K,$$

$$G_e(\mu) := (g, \mu)_e, \qquad F_v(\boldsymbol{\tau}) := \sum_{K \in \mathcal{T}_h} F_{v,K}(\boldsymbol{\tau}),$$

$$F(v) := \sum_{K \in \mathcal{T}_h} F_K(v), \qquad G(\mu) := \sum_{e \in \mathcal{E}_h \cap \Gamma^R} G_e(\mu).$$

Problem 2.8 (Weak mixed formulation). *The weak formulation of Problem 2.7 is: find $(\boldsymbol{u}, p, \lambda) \in \boldsymbol{Z} \times Q \times \Lambda$ such that*

$$\begin{cases} a(\boldsymbol{u}, \boldsymbol{\tau}) + b(p, \boldsymbol{\tau}) + c(\lambda, \boldsymbol{\tau}) = F_v(\boldsymbol{\tau}) & \forall \boldsymbol{\tau} \in \boldsymbol{Z}, \\ b(v, \boldsymbol{u}) - e(p, v) = -F(v) & \forall v \in Q, \\ c(\mu, \boldsymbol{u}) + h(\lambda, \mu) = G(\mu) & \forall \mu \in \Lambda. \end{cases}$$

Lemma 2.6 (Well posedness). *Under Assumption 2.7 and Assumption 2.8 Problem 2.8 is well posed.*

Proof. We refer to [11] for the proof.

$\square$

2.3.2 Numerical approximation

To solve Problem 2.8 we introduce the following finite dimensional subspaces of Q, $\boldsymbol{Z}$ and Λ. We have adopted the following choices:

- piecewise Lagrangian polynomials of degree r for the scalar variables

$$Q_h := \{q_h \in Q : q_h|_K \in \mathbb{P}_r(K) \text{ for } K \in \mathcal{T}_h\} \subset Q,$$

  where we indicate with $\phi_{K,i}$ the base function of $\mathbb{P}_r(K)$ associated to the degrees of freedom $i = 1, \ldots, b_Q$ of the element $K \in \mathcal{T}_h$. The dimension of the space $\mathbb{P}_r(K)$ is

$$b_Q = \dim \mathbb{P}_r(K) = \frac{1}{n!} \prod_{k=1}^{n} (r + k),$$

therefore the dimension of Q_h is $N_E b_Q$. Given a function $q_h \in Q_h$ its expansion in the base functions of Q_h reads

$$q_h\left(\boldsymbol{x}\right) = \sum_{K \in \mathcal{T}_h} \sum_{i=1}^{b_Q} q_{K,i} \phi_{K,i}(\boldsymbol{x}) \,,$$

where $\boldsymbol{q}_K = \left(q_{K,1}, \ldots, q_{K,b_Q}\right) \in \mathbb{R}^{b_Q}$ is the vector of the local coefficients in the element $K \in \mathcal{T}_h$;

- piecewise Raviart-Thomas, introduced in [64], of degree r for the vector variables

$$\boldsymbol{Z}_h := \{\boldsymbol{z}_h \in \boldsymbol{Z} : \ \boldsymbol{z}_h|_K \in \mathbb{RT}_r\left(K\right) \ \text{for} \ K \in \mathcal{T}_h\} \subset \boldsymbol{Z} \,,$$

where we indicate with $\boldsymbol{\psi}_{K,j}$ the base function of $\mathbb{RT}_r\left(K\right)$ associated to the degrees of freedom $j = 1, \ldots, b_{\boldsymbol{Z}}$ of the element $K \in \mathcal{T}_h$. The dimension of the space $\mathbb{RT}_r(K)$ is

$$b_{\boldsymbol{Z}} = \dim \mathbb{RT}_r(K) = (r+1)(r+3) \qquad \text{for} \ n = 2 \,,$$
$$b_{\boldsymbol{Z}} = \dim \mathbb{RT}_r(K) = \frac{1}{2}(r+1)(r+2)(r+4) \quad \text{for} \ n = 3 \,,$$

therefore the dimension of $\boldsymbol{Z}_h$ is $N_E b_{\boldsymbol{Z}}$. Given a function $\boldsymbol{z}_h \in \boldsymbol{Z}_h$ its expansions in the base functions of $\boldsymbol{Z}_h$ reads

$$\boldsymbol{z}_h\left(\boldsymbol{x}\right) = \sum_{K \in \mathcal{T}_h} \sum_{j=1}^{b_{\boldsymbol{Z}}} z_{K,j} \boldsymbol{\psi}_{K,j}(\boldsymbol{x}) \,,$$

where $\boldsymbol{z}_K = (z_{K,1}, \ldots, z_{K,b_{\boldsymbol{Z}}}) \in \mathbb{R}^{b_{\boldsymbol{Z}}}$ is the vector of the local coefficients in the element $K \in \mathcal{T}_h$;

- piecewise Lagrangian polynomials of degree r on $\mathcal{E}_h$, indicated also with $R_r\left(\mathcal{E}_h\right)$, for the hybrid variables

$$\Lambda_h := R_r\left(\mathcal{E}_h\right) = \{\lambda \in \Lambda : \ \lambda|_e \in \mathbb{P}_r\left(e\right) \ \text{for} \ e \in \mathcal{E}_h\} \subset \Lambda \,,$$

where we indicate with $\xi_{e,k}$ the base function of $\mathbb{P}_r\left(e\right)$ associated to the degrees of freedom $k = 1, \ldots, b_\Lambda$ of the facet $e \in \mathcal{E}_h$. The dimension of the space $R_r(e)$ is

$$b_\Lambda = \dim R_r\left(e\right) = \frac{1}{(n-1)!} \prod_{k=1}^{n-1} (r+k) \,,$$

therefore the dimension of Λ_h is $N_I b_\Lambda$. Given a function $\lambda_h \in \Lambda_h$ its expansion in the base function of Λ_h reads

$$\lambda_h\left(\boldsymbol{x}\right) = \sum_{e \in \mathcal{E}_h} \sum_{k=1}^{b_\Lambda} \lambda_{e,k} \xi_{e,k}\left(\boldsymbol{x}\right) \,, \tag{2.45}$$

where $\boldsymbol{\lambda}_e = (\lambda_{e,1}, \ldots, \lambda_{e,b_\Lambda}) \in \mathbb{R}^{b_\Lambda}$ is the vector of the local coefficients in the element $e \in \mathcal{E}_h$.
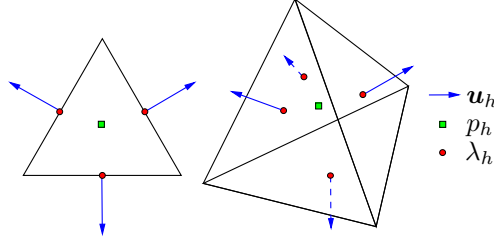
Figure 2.12: Picture of the degrees of freedom for the space $\mathbb{P}_0(K)$, $\mathbb{RT}_0(K)$ and $R_0(\partial K)$ in a triangle and in a tetrahedron.

A schematic representation for the lowest order case, *i.e.* $r = 0$, of the degrees of freedom for a function in Q_h, $\boldsymbol{Z}_h$ and Λ_h is in Figure 2.12.

Problem 2.9 (Discrete mixed formulation). *The discrete version of Problem 2.8 is: find $(\boldsymbol{u}_h, p_h, \lambda_h) \in \boldsymbol{Z}_h \times Q_h \times \Lambda_h$ such that*

$$\begin{cases} a(\boldsymbol{u}_h, \boldsymbol{\tau}_h) + b(p_h, \boldsymbol{\tau}_h) + c(\lambda_h, \boldsymbol{\tau}_h) = F_v(\boldsymbol{\tau}_h) & \forall \boldsymbol{\tau}_h \in \boldsymbol{Z}_h, \\ b(v_h, \boldsymbol{u}_h) - e(p_h, v_h) = -F(v_h) & \forall v_h \in Q_h, \\ c(\mu_h, \boldsymbol{u}_h) + h(\lambda_h, \mu_h) = G(\mu_h) & \forall \mu_h \in \Lambda_h. \end{cases}$$

Lemma 2.7 (Well posedness). *Under Assumption 2.7 and Assumption 2.8 Problem 2.9 is well posed.*

Proof. We refer to [11] for the proof. $\qquad \square$

We can write the above system in the *local matrix formulation*, to this purpose we introduce the local matrices and vectors

$$\begin{aligned} [\boldsymbol{A}]_{ij} &:= a_K(\boldsymbol{\psi}_{K,j}, \boldsymbol{\psi}_{K,i}), & [\boldsymbol{B}]_{ij} &:= b_K(\phi_{K,j}, \boldsymbol{\psi}_{K,i}), \\ [\boldsymbol{C}]_{ij} &:= \sum_{e \in \partial K} c_e(\xi_{e,i}, \boldsymbol{\psi}_{K,j}), & [\boldsymbol{E}]_{ij} &:= e_K(\phi_{K,j}, \phi_{K,i}), \\ [\boldsymbol{H}]_{ij} &:= \sum_{e \in \partial K} h_e(\xi_{e,i}, \xi_{e,j}), & [\boldsymbol{F}_v]_j &:= F_{v,K}(\boldsymbol{\psi}_{K,j}), \\ [\boldsymbol{F}]_j &:= F_K(\phi_{K,j}), & [\boldsymbol{G}]_j &:= \sum_{e \in \partial K} G_e(\xi_{e,j}), \end{aligned}$$

where we neglect to write the dependence on the element $K \in \mathcal{T}_h$ in all the matrices and vectors. We indicate with $[\cdot]_{ij}$ the element at row i and column j of the matrix in the square brackets.

Problem 2.10 (Local matrix formulation). *The local matrix formulation of Problem 2.9 in each $K \in \mathcal{T}_h$ is*

$$\begin{cases} \boldsymbol{A}\boldsymbol{u}_K + \boldsymbol{B}\boldsymbol{p}_K + \boldsymbol{C}\boldsymbol{\lambda}_K = \boldsymbol{F}_v, \\ \boldsymbol{B}^\top \boldsymbol{u}_K - \boldsymbol{E}\boldsymbol{p}_K = -\boldsymbol{F}, \\ \boldsymbol{C}^\top \boldsymbol{u}_K + \boldsymbol{H}\boldsymbol{\lambda}_K = \boldsymbol{G}. \end{cases} \tag{2.46}$$

Or alternatively

$$
\begin{bmatrix}
\boldsymbol{A} & \boldsymbol{B} & \boldsymbol{C} \\
\boldsymbol{B}^\top & -\boldsymbol{E} & \boldsymbol{0} \\
\boldsymbol{C}^\top & \boldsymbol{0} & \boldsymbol{H}
\end{bmatrix}
\begin{bmatrix}
\boldsymbol{u}_K \\
\boldsymbol{p}_K \\
\boldsymbol{\lambda}_K
\end{bmatrix}
=
\begin{bmatrix}
\boldsymbol{F}_v \\
-\boldsymbol{F} \\
\boldsymbol{G}
\end{bmatrix} .
$$

Where $\boldsymbol{u}_K$, $\boldsymbol{p}_K$ and $\boldsymbol{\lambda}_K$ denote the vectors of degrees of freedom restricted to element K of the corresponding variables.

We recall the convergence rates for the dual, mixed and hybrid method for $r = 0$, which is the most used in practice. Further details can be found in [11].

Lemma 2.8 (Convergence rates)**.** *Under Assumption 2.7, Assumption 2.8 and supposing also $\boldsymbol{f}_v \equiv 0$ and $f \in H^1(\Omega)$, the solutions $(p, \boldsymbol{u})$ of Problem 2.8 is such that $p \in H^2(\Omega)$ and the errors between the discrete solutions $(p_h, \boldsymbol{u}_h)$ of Problem 2.9 and $(p, \boldsymbol{u})$ are bounded,*

$$
\|p - p_h\|_{L^2(\Omega)} \leq C_1 h \left(\|p\|_{H^2(\Omega)} + \|f\|_{H^1(\Omega)} \right) ,
$$

$$
\|\boldsymbol{u} - \boldsymbol{u}_h\|_{\boldsymbol{H}_{\mathrm{div}}(\Omega)} \leq C_2 h \left(\|p\|_{H^2(\Omega)} + \|f\|_{H^1(\Omega)} \right) ,
$$

with the constants $C_1, C_2 \in \mathbb{R}^+$ independent of h.

2.3.3   Static condensation

The unknowns in system (2.46) are not independent since $\boldsymbol{p}_K$ and $\boldsymbol{u}_K$ may be written in function of $\boldsymbol{\lambda}_K$ alone. This technique is called *static condensation*. The main practical assumption for the static condensation is to use relatively low polynomial degree for the approximation, such that the local matrix $\boldsymbol{A}$ is simple and fast to factorize with the Cholesky algorithm.

From the first equation of system (2.46) we derive that

$$
\boldsymbol{u}_K = -\boldsymbol{A}^{-1} \left(\boldsymbol{B} \boldsymbol{p}_K + \boldsymbol{C} \boldsymbol{\lambda}_K - \boldsymbol{F}_v \right) . \tag{2.47}
$$

Using (2.47), the third equation of (2.46) becomes

$$
\begin{aligned}
&- \boldsymbol{B}^\top \boldsymbol{A}^{-1} \left(\boldsymbol{B} \boldsymbol{p}_K + \boldsymbol{C} \boldsymbol{\lambda}_K - \boldsymbol{F}_v \right) - \boldsymbol{E} \boldsymbol{p}_K = \\
&= - \left(\boldsymbol{B}^\top \boldsymbol{A}^{-1} \boldsymbol{B} + \boldsymbol{E} \right) \boldsymbol{p}_K + \boldsymbol{B}^\top \boldsymbol{A}^{-1} \boldsymbol{F}_v - \boldsymbol{B}^\top \boldsymbol{A}^{-1} \boldsymbol{C} \boldsymbol{\lambda}_K = -\boldsymbol{F} .
\end{aligned}
$$

Introducing the local matrix

$$
\boldsymbol{S} = \left(\boldsymbol{B}^\top \boldsymbol{A}^{-1} \boldsymbol{B} + \boldsymbol{E} \right)^{-1} ,
$$

we obtain a relation between $\boldsymbol{p}_K$ and $\boldsymbol{\lambda}_K$

$$
\boldsymbol{p}_K = \boldsymbol{S} \left(\boldsymbol{F} + \boldsymbol{B}^\top \boldsymbol{A}^{-1} \boldsymbol{F}_v - \boldsymbol{B}^\top \boldsymbol{A}^{-1} \boldsymbol{C} \boldsymbol{\lambda}_K \right) . \tag{2.48}
$$

We express, using the relations (2.47) and (2.48), the first term of the last equation of (2.46) as

$$
\begin{aligned}
\boldsymbol{C}^{\top}\boldsymbol{u}_K = & -\boldsymbol{C}^{\top}\boldsymbol{A}^{-1}\left(\boldsymbol{B}\boldsymbol{p}_K + \boldsymbol{C}\boldsymbol{\lambda}_K - \boldsymbol{F}_v\right) = \\
= & -\boldsymbol{C}^{\top}\boldsymbol{A}^{-1}\boldsymbol{B}\boldsymbol{p}_K - \boldsymbol{C}^{\top}\boldsymbol{A}^{-1}\boldsymbol{C}\boldsymbol{\lambda}_K + \boldsymbol{C}^{\top}\boldsymbol{A}^{-1}\boldsymbol{F}_v = \\
= & -\boldsymbol{C}^{\top}\boldsymbol{A}^{-1}\boldsymbol{B}\boldsymbol{S}\left(\boldsymbol{F} + \boldsymbol{B}^{\top}\boldsymbol{A}^{-1}\boldsymbol{F}_v - \boldsymbol{B}^{\top}\boldsymbol{A}^{-1}\boldsymbol{C}\boldsymbol{\lambda}_K\right) + \\
& + \boldsymbol{C}^{\top}\boldsymbol{A}^{-1}\boldsymbol{C}\boldsymbol{\lambda}_K + \boldsymbol{C}^{\top}\boldsymbol{A}^{-1}\boldsymbol{F}_v = \\
= & \left(\boldsymbol{C}^{\top}\boldsymbol{A}^{-1}\boldsymbol{B}\boldsymbol{S}\boldsymbol{B}^{\top}\boldsymbol{A}^{-1}\boldsymbol{C} - \boldsymbol{C}^{\top}\boldsymbol{A}^{-1}\boldsymbol{C}\right)\boldsymbol{\lambda}_K + \\
& - \boldsymbol{C}^{\top}\boldsymbol{A}^{-1}\boldsymbol{B}\boldsymbol{S}\boldsymbol{F} - \boldsymbol{C}^{\top}\boldsymbol{A}^{-1}\boldsymbol{B}\boldsymbol{S}\boldsymbol{B}^{\top}\boldsymbol{A}^{-1}\boldsymbol{F}_v + \boldsymbol{C}^{\top}\boldsymbol{A}^{-1}\boldsymbol{F}_v \,.
\end{aligned}
$$

Finally introducing the local matrix and vector for the hybrid unknown

$$
\begin{aligned}
\boldsymbol{L}_K &= \boldsymbol{C}^{\top}\boldsymbol{A}^{-1}\boldsymbol{B}\boldsymbol{S}\boldsymbol{B}^{\top}\boldsymbol{A}^{-1}\boldsymbol{C} - \boldsymbol{C}^{\top}\boldsymbol{A}^{-1}\boldsymbol{C} + \boldsymbol{H}\,, \\
\boldsymbol{r}_K &= \boldsymbol{G} + \boldsymbol{C}^{\top}\boldsymbol{A}^{-1}\boldsymbol{B}\boldsymbol{S}\boldsymbol{F} + \boldsymbol{C}^{\top}\boldsymbol{A}^{-1}\boldsymbol{B}\boldsymbol{S}\boldsymbol{B}^{\top}\boldsymbol{A}^{-1}\boldsymbol{F}_v - \boldsymbol{C}^{\top}\boldsymbol{A}^{-1}\boldsymbol{F}_v \,,
\end{aligned}
$$

we may write the third equation of (2.46) as the local system

$$
\boldsymbol{L}_K\boldsymbol{\lambda}_K = \boldsymbol{r}_K \,.
$$

To build the global system for the unknown λ_h, we use the fact that a function in Λ_h is single valued on each facet in $\mathcal{E}_h$. Summing the corresponding value for each facet for $\boldsymbol{\lambda}_K$ we obtain the following global system

$$
\boldsymbol{L}\boldsymbol{\lambda} = \boldsymbol{r} \,. \tag{2.49}
$$

Once we have solved the global system (2.49) we can locally reconstruct $\boldsymbol{p}_K$ and $\boldsymbol{u}_K$ using the relations (2.48) and (2.47). The latter operations are perfectly parallel.

2.4 Calculation of the numerical flux for the saturation equation

To solve the hyperbolic part of Problem 2.3 presented in section 2.2.2 we use an explicit finite volume scheme, *i.e.* discontinuous Galerkin [22], with a suitable numerical flux. In particular, due to the possible heterogeneity of the ground, the physical flux (2.35) may be discontinuous across grid cell boundaries, so the numerical scheme must be implemented with care.
The time step in the hyperbolic solvers is limited by the CFL condition. We could take the same time step for both the hyperbolic and the parabolic parts but this can be inefficient since the former can be very small. A common method, see for instance [32] and [43], to handle this problem is to have sub temporal iterations for the hyperbolic problem, with the time step given by the CFL condition, for each time step for the parabolic problem. The global scheme (2.36) and (2.37) is first order accurate in space and in time, see [26] and [27]. Following [47], [1] and [58] one possibility to compute the numerical flux at the interface between elements, commonly adopted by petroleum engineers, is the so called *upstream mobility flux* (UM) which is an approximation of the solution of the Riemann problem. Referring to Figure 2.13 we indicate with a superscript
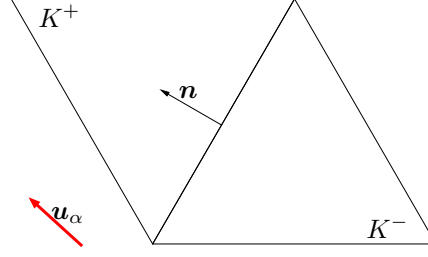
Figure 2.13: Example of two facing elements $K^+, K^- \in \mathcal{T}_h$ in the bi-dimensional case.

$^+$ quantities defined in the element K^+ and with a superscript $^-$ quantities defined in the facing element K^-. The upstream mobility flux function is

$$\mathcal{F}_{\mathrm{UM}}\left(S_n^+, S_n^-\right) = \frac{\lambda_n^*}{\lambda_w^* + \lambda_n^*} \left[\boldsymbol{u}^{k+1} - \lambda_w^* \boldsymbol{K}\left(\rho_w - \rho_n\right)\boldsymbol{g}\right] \,,$$

where λ^* are the upstream mobilities defined as

$$\lambda_\alpha^* := \begin{cases} \lambda_\alpha\left(S_\alpha^-\right) & \text{if } \boldsymbol{u}_\alpha^{k+1} \cdot \boldsymbol{n} > 0, \\[2mm] \lambda_\alpha\left(S_\alpha^+\right) & \text{if } \boldsymbol{u}_\alpha^{k+1} \cdot \boldsymbol{n} \leq 0. \end{cases}$$

Another possibility is to compute the solution of the Riemann problems at the interface using the exact Godunov (G) flux, given by

$$\mathcal{F}_{\mathrm{G}}\left(S_n^+, S_n^-\right) = \begin{cases} \displaystyle\min_{\theta \in \left[S_n^+, S_n^-\right]} \mathcal{F}\left(\theta\right) & \text{if } S_n^+ < S_n^-, \\[4mm] \displaystyle\max_{\theta \in \left[S_n^-, S_n^+\right]} \mathcal{F}\left(\theta\right) & \text{if } S_n^+ \geq S_n^- \,, \end{cases}$$

computed in both elements K^+ and K^-.

Assumption 2.9 (Two-phase flux)**.** *We assume the following hypotheses for the flux function $\mathcal{F}$*

1. *$\mathcal{F}^+$ and $\mathcal{F}^-$ are Lipschitz functions;*

2. *$\mathcal{F}^+\left(S_{nr}\right) = \mathcal{F}^-\left(S_{wr}\right) = \boldsymbol{0}$ and $\mathcal{F}^+\left(1 - S_{wr}\right) = \mathcal{F}^-\left(1 - S_{wr}\right) = \boldsymbol{u}^{k+1}$;*

3. *both $\mathcal{F}^+\left(S_n\right) \cdot \boldsymbol{n}$ and $\mathcal{F}^-\left(S_n\right) \cdot \boldsymbol{n}$ have exactly one local maximum for $S_n \in \left[S_{nr}, 1 - S_{wr}\right]$.*

Where S_{nr} and S_{wr} are the residual saturation of the non-wetting phase and wetting phase, respectively, introduced in section 2.1.2.

Under Assumption 2.9 then the Godunov flux can be re-written with the following form

$$\mathcal{F}_{\mathrm{G}}^-\left(S_n^+, S_n^-\right) = \min\left\{\mathcal{F}^-\left(\min\left\{S_n^+, \theta^-\right\}\right), \mathcal{F}^-\left(\min\left\{\theta^-, S_n^-\right\}\right)\right\} \,,$$
$$\mathcal{F}_{\mathrm{G}}^+\left(S_n^+, S_n^-\right) = \min\left\{\mathcal{F}^+\left(\min\left\{S_n^+, \theta^+\right\}\right), \mathcal{F}^+\left(\min\left\{\theta^+, S_n^-\right\}\right)\right\}$$

with

$$\theta^{\pm} = \underset{S_n \in [S_{nr},\, 1-S_{wr}]}{\text{argmax}} \boldsymbol{\mathcal{F}}^{\pm}(S_n)\,.$$

When the two phases flow in the same direction both upstream mobility and exact Godunov fluxes give the same answer but they differ when the phases flow in different directions. In fact the solutions computed using the upstream mobility flux are not consistent with the interface entropy condition given in [1], which excludes under-compressive waves at the interfaces and captures the physically relevant solutions. Finally heterogeneities in the absolute permeability $\boldsymbol{K}$ can affect the solution when the upstream mobility flux function is used.

We present some numerical tests, taken from [58], to highlight the different behaviour of the two formulations of the numerical fluxes. In both examples we suppose a one-dimensional problem with zero total velocity and zero residual saturations.

In the first example only the permeability changes, $K^{+} \equiv 1.1$ and $K^{-} \equiv 1$, while both porosity, $\Phi \equiv 1$, and relative permeabilities remain unchanged, with

$$k_{rn}(S) = 1 - S \quad \text{and} \quad k_{rw}(S) = S\,.$$

The non-wetting fluid is lighter then the wetting fluid, we choose $\rho_n g \equiv 2$ and $\rho_w g \equiv 1$. Finally the initial data is discontinuous at the interface of the two rocks $x = 0$, namely

$$S_{n0}(x) = \begin{cases} 0.65 & \text{if } x < 0, \\ 0.35 & \text{if } x > 0. \end{cases}$$

We can see from Figure 2.14 that the upstream mobility flux does not resolve
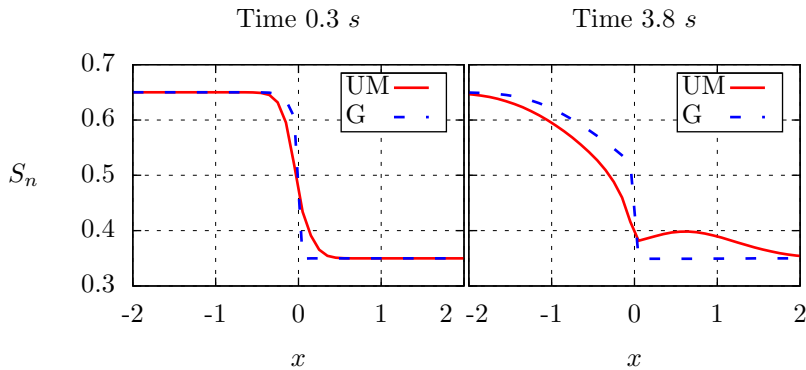
Figure 2.14: Comparison between the upstream mobility flux (UM) and the exact Godunov (G) flux at two different times for the first example. The mesh grid has spacing $h = 0.01$ and $\Delta t = 0.01$.

well the interface compared to the exact Godunov flux. Furthermore, the upstream mobility develops an unphysical travelling wave in the right rock. The reason of the incorrect behaviours of the upstream mobility flux is that it may not be consistent with the entropy interface condition, as the author pointed out in [58]. The amplitude of the wave decreases if the mesh size decreases

hence the limit solution computed by the upstream mobility flux converges to the entropy solution.

In the second example we use the same fluids as in the previous example and we leave unchanged both porosity, $\Phi \equiv 1$, and absolute permeability $K \equiv 1$. The relative permeabilities are different in the two rocks,

$$k_{rn}^{\pm} = 1 - S^2\,, \quad k_{rw}^{+} = S \quad \text{and} \quad k_{rw}^{-} = \begin{cases} 1.75S & \text{if } S \leq 0.25, \\[2mm] 0.25S + 0.375 & \text{if } S \geq 0.25. \end{cases}$$

Finally the initial condition is $S_{n0} \equiv 0.5$. Figure 2.15 shows the numerical
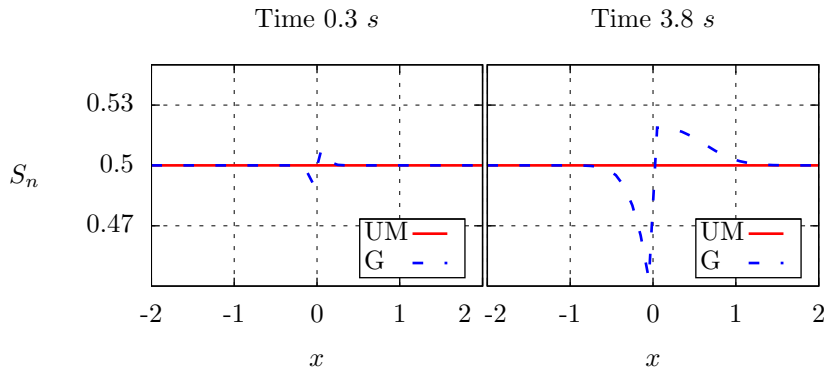
Figure 2.15: Comparison between the upstream mobility flux (UM) and the exact Godunov (G) flux at two different time for the second example. The mesh grid has spacing $h = 0.01$ and $\Delta t = 0.01$.

solution computed with the upstream mobility flux and the exact Godunov flux at two different times. The solution highlights the difference between the solution which fulfils the entropy condition [51], *i.e.* the one with the upstream mobility, and the solution which fulfils the interface entropy condition [1], the one with the exact Godunov flux. The constant solution, obtained with the upstream mobility flux in Figure 2.15, is considered in literature as unphysical [50], since the heavier fluid should flow downwards.

Chapter 3

Reduced models for faults and horizons

We introduce and analyse a reduced model that describes a single-phase flow in a fracture or fault that exchange fluids with the surrounding porous media. We will employ the term "fracture" to indicate both faults and macro fractures of the porous medium. Fault, horizons and large fractures represent preferential paths for secondary migration, and must be accurately resolved. Due to the typical size of a sedimentary basin ($200km \times 200km \times 10km$) the grid size is too coarse to capture those feature, whose characteristic width is of order of meters, unless an extreme refinement is employed, leading to unreasonably high computational costs. Thus, following [2, 57, 4, 53], we have decided to adopt a reduced model to handle this difficulties.

3.1 Single-phase Darcy equation

To introduce the reduced model we assume that the geometry and the data fulfil some requirements.

Assumption 3.1 (Domain). *We made the following requests for the domain Ω, which represents the heterogeneous porous media:*

1. *Ω is an open bounded measurable subset of $\mathbb{R}^n$, with $n = 2, 3$, with Lipschitz boundary $\Gamma := \partial\Omega$;*

2. *Ω is divided into three connected subset, called Ω_1, Ω_2 and Ω_f, such that $\mathring{\Omega}_i \cap \mathring{\Omega}_j = \emptyset$ for $i \neq j$ and $i, j = 1, 2, f$,*

$$\bigcup_{i=1,2,f} \overline{\Omega}_i = \overline{\Omega},$$

$\partial\Omega_i \cap \Gamma \neq \emptyset$ for $i = 1, 2$ and $\partial\Omega_1 \cap \partial\Omega_2 = \emptyset$, as shown for example in Figure 3.1. We define

$$\Gamma_i := \partial\Omega_i \cap \Gamma \quad \text{for } i = 1, 2, f \quad \text{and} \quad \gamma_j := \partial\Omega_j \cap \partial\Omega_f \quad \text{for } j = 1, 2.$$

We require also that each piece of the boundary is sub-divided into two disjoint parts: Γ_i^E and Γ_i^N, such that for $i = 1, 2, f$

$$\overline{\Gamma}_i = \overline{\Gamma}_i^N \cup \overline{\Gamma}_i^E, \quad and \quad \mathring{\Gamma}_i^N \cap \mathring{\Gamma}_i^E = \emptyset,$$

due to the mixed formulation of the problem on Γ_i^E we will impose essential boundary conditions, i.e. data on vector fields, while on Γ_i^N we will impose natural boundary conditions, i.e. data on scalar fields. We define

$$\Gamma^N := \bigcup_{i=1,2,f} \Gamma_i^N, \quad and \quad \Gamma^E := \bigcup_{i=1,2,f} \Gamma_i^E, \tag{3.1}$$

with the assumption $\Gamma^N \neq \emptyset$. In Figure 3.1 we put into evidence also the outward unit normal of the boundary $\boldsymbol{n}_\Gamma$. We indicate with $\boldsymbol{n}_i$ the unit normal of γ_i directed outwards with respect to Ω_i;
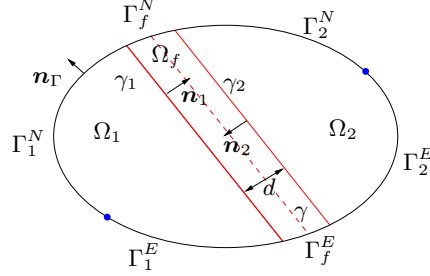
Figure 3.1: Picture of the domain Ω and the three sub-domains Ω_1, Ω_2 and Ω_f for $n = 2$.

3. furthermore, referring to Figure 3.1, we require that only one type of boundary condition, natural or essential, is imposed on the upper part of Γ_f and only one type, natural or essential, is imposed on the lower part of Γ_f, more formally we require that Γ_f^N and Γ_f^E are connected subset of $\mathbb{R}^{n-1}$ with

$$\partial\Gamma_f^N \cap \partial\Gamma_f^E = \emptyset;$$

4. for the sub-domain Ω_f, which describes the part of Ω occupied by the fracture, we suppose that exists a non auto-intersecting $n-1$ manifold γ of class C^2 such that the domain Ω_f can be written as

$$\Omega_f := \left\{ \boldsymbol{x} \in \Omega : \boldsymbol{x} = \boldsymbol{s} + r\boldsymbol{n}, \, \boldsymbol{s} \in \gamma, \, r \in \left(-\frac{d(\boldsymbol{s})}{2}, \frac{d(\boldsymbol{s})}{2} \right) \right\}, \tag{3.2}$$

with $d \in C^2(\gamma)$ the thickness of Ω_f and $\boldsymbol{n}$ the unit normal to γ, aligned as $\boldsymbol{n}_1$. We require that $\exists\, c_1, c_2 \in \mathbb{R}^+$

$$d(\boldsymbol{s}) > c_1 \quad and \quad |d'(\boldsymbol{s})| < c_2 \quad \forall \boldsymbol{s} \in \gamma,$$

with c_2 "small". See Figure 3.2 for an example of Ω_f for $n = 2$. In other words, we assume that γ does not differ too much from a plane if $n = 3$ or a straight line if $n = 2$;
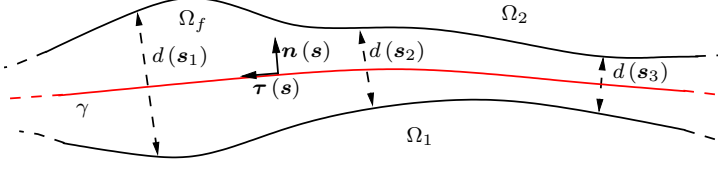
Figure 3.2: Example of Ω_f and γ for $n = 2$.

5. we define the parts of γ which belong to the natural or the essential part of the boundary as

$$\partial\gamma^N := \gamma \cap \Gamma_f^N \quad and \quad \partial\gamma^E := \gamma \cap \Gamma_f^E \,;$$

6. the domain Ω_f is "thin" compared with Ω_1 and Ω_2, i.e.

$$\mathrm{diam}\,(\Omega_i) \gg \max_{\boldsymbol{s} \in \gamma} d\,(\boldsymbol{s}) \quad for \quad i = 1, 2 \,.$$

With this assumption we can identify Ω_f with γ and we can adopt the approximations $\boldsymbol{n} \approx \boldsymbol{n}_1 \approx -\boldsymbol{n}_2$, $\Gamma_f^N \approx \partial\gamma^N$ and $\Gamma_f^E \approx \partial\gamma^E$.

The permeability tensor $\boldsymbol{K}$ can vary smoothly in each Ω_i, for $i = 1, 2, f$, but may be discontinuous across γ_j, for $j = 1, 2$. Furthermore, in the fracture $\boldsymbol{K}$ may be significantly different from that in the rest of the domain Ω.
The Darcy equations are given by

$$\begin{cases} \nabla \cdot \boldsymbol{u} = q & \text{in } \Omega \,, \\[2mm] \boldsymbol{K}^{-1}\boldsymbol{u} + \nabla p = \boldsymbol{0} & \text{in } \Omega \,, \\[2mm] p = \overline{p} & \text{on } \Gamma^N \,, \\[2mm] \boldsymbol{u} \cdot \boldsymbol{n}_\Gamma = \overline{u} & \text{on } \Gamma^E \,. \end{cases} \tag{3.3}$$

Assumption 3.2 (Data regularity). *We assume the following regularity hypotheses for the data of system* (3.3)

1. *the source term $q \in L^2\,(\Omega)$ can be decomposed as*

$$q = \sum_{i=1,2,f} q_i|_{\Omega_i} \,,$$

$q_i \in L^2\,(\Omega)$ *with* $q_i|_{\Omega_i} := q|_{\Omega_i}$ *for* $i = 1, 2, f$;

2. *the symmetric and positive definite permeability tensor $\boldsymbol{K} \in [L^\infty\,(\Omega)]^{n \times n}$ can be decomposed as*

$$\boldsymbol{K} = \sum_{i=1,2,f} \boldsymbol{K}_i|_{\Omega_i} \,,$$

$\boldsymbol{K}_i \in [L^\infty\,(\Omega)]^{n \times n}$ *with* $\boldsymbol{K}_i|_{\Omega_i} := \boldsymbol{K}|_{\Omega_i}$ *for* $i = 1, 2, f$;

63

3. *the data on the natural boundary* $\overline{p} \in H^{\frac{1}{2}}\left(\Gamma^N\right)$ *can be decomposed as*

$$\overline{p} = \sum_{i=1,2,f} \overline{p_i}\big|_{\Gamma_i^N} \ ,$$

$\overline{p_i} \in H^{\frac{1}{2}}\left(\Gamma^N\right)$ *with* $\overline{p_i}\big|_{\Gamma_i^N} := \overline{p}\big|_{\Gamma_i^N}$ *for* $i = 1, 2, f$;

4. *the data on the essential boundary* $\overline{u} \in H^{-\frac{1}{2}}\left(\Gamma^E\right)$ *can be decomposed as*

$$\overline{u} = \sum_{i=1,2,f} \overline{u_i}\big|_{\Gamma_i^E} \ ,$$

$\overline{u_i} \in H^{-\frac{1}{2}}\left(\Gamma^E\right)$ *with* $\overline{u_i}\big|_{\Gamma_i^E} := \overline{u}\big|_{\Gamma_i^E}$ *for* $i = 1, 2, f$.

In the sequel we will, with a little abuse of notation, indicate with a subscript $_i$ the restriction of a function in the i-th subset of its definition set.

Lemma 3.1 (Well posedness of (3.3)). *Under the* Assumption 3.2 *the problem* (3.3) *has one solution* $(\boldsymbol{u}, p) \in \boldsymbol{H}_{\mathrm{div}}\left(\Omega\right) \times H^1\left(\Omega\right)$.

Proof. We refer to [11] for the proof.

$\square$

Defining the restriction of the Darcy flux $\boldsymbol{u}$ and the pressure p in each sub-part Ω_i of the domain Ω as $\boldsymbol{u}_i := \boldsymbol{u}\big|_{\Omega_i}$ and $p_i := p\big|_{\Omega_i}$ for $i = 1, 2, f$, we can prove the following result.

Proposition 3.2. *The solution $(\boldsymbol{u}, p)$ of system (3.3) satisfies the following differential equations for $i = 1, 2, f$*

$$\begin{cases} \nabla \cdot \boldsymbol{u}_i = q_i \\ \boldsymbol{K}_i^{-1} \boldsymbol{u}_i + \nabla p_i = \boldsymbol{0} \end{cases} \quad in \ \Omega_i \, ,$$

equipped with the following coupling conditions for $j = 1, 2$

$$\begin{cases} \boldsymbol{u}_j \cdot \boldsymbol{n}_j = \boldsymbol{u}_f \cdot \boldsymbol{n}_j \\ p_j = p_f \end{cases} \quad on \ \gamma_j \, ,$$

and the boundary conditions for $i = 1, 2, f$

$$\begin{cases} p_i = \overline{p_i} & on \ \Gamma_i^N \, , \\ \boldsymbol{u}_i \cdot \boldsymbol{n}_\Gamma = \overline{u_i} & on \ \Gamma_i^E \, . \end{cases}$$

Proof. By standard means we can derive that a weak solution of (3.3) satisfying

$$\begin{cases} -\displaystyle\int_\Omega \boldsymbol{u} \cdot \nabla v = \int_\Omega q v & \forall v \in H_0^1\left(\Omega\right) \, , \\ \displaystyle\int_\Omega \boldsymbol{K}^{-1} \boldsymbol{u} \boldsymbol{\tau} - \int_\Omega p \nabla \cdot \boldsymbol{\tau} = 0 & \forall \boldsymbol{\tau} \in \boldsymbol{H}_{\mathrm{div},0}\left(\Omega\right) \, . \end{cases} \tag{3.4}$$

If we select $v \in H_0^1 (\Omega_i)$ for $i = 1, 2$ or f the first equation of (3.4) is equivalent to

$$-\int_{\Omega_i} \boldsymbol{u}_i \cdot \nabla v = \int_{\Omega_i} q_i v \quad \forall v \in H_0^1 (\Omega_i) \,,$$

which implies that $\nabla \cdot \boldsymbol{u}_i - q_i = 0$ in a distributional sense, *i.e.* a.e. in Ω_i. If we now take a $v \in H_0^1 (\Omega)$ with support in $\Omega_f \cup \gamma_i \cup \Omega_i$ for $i = 1$ or 2, we have

$$-\int_{\Omega_i} \boldsymbol{u}_i \cdot \nabla v - \int_{\Omega_f} \boldsymbol{u}_f \cdot \nabla v = \int_{\Omega_i} q_i v + \int_{\Omega_f} q_f v \,,$$

that is

$$_{[H^1(\Omega_i)]'}\! < \nabla \cdot \boldsymbol{u}_i - q_i, \, v >_{H^1(\Omega_1)} +_{[H^1(\Omega_f)]'}\! < \nabla \cdot \boldsymbol{u}_f - q_f, \, v >_{H^1(\Omega_f)} +$$
$$+ \int_{\gamma_i} (\boldsymbol{u}_i \cdot \boldsymbol{n}_i - \boldsymbol{u}_f \cdot \boldsymbol{n}_i) \, v = 0 \,,$$

the first two terms are zero obtaining the coupling condition for $\boldsymbol{u}$ across γ_i. If we select $\boldsymbol{\tau} \in \boldsymbol{H}_{\mathrm{div},0} (\Omega_i)$ for $i = 1, 2$ or f the second equation of (3.4) is equivalent to

$$\int_{\Omega_i} \boldsymbol{K}_i^{-1} \boldsymbol{u}_i \cdot \boldsymbol{\tau} - \int_{\Omega_i} p_i \nabla \cdot \boldsymbol{\tau} = 0 \quad \forall \boldsymbol{\tau} \in \boldsymbol{H}_{\mathrm{div},0} (\Omega_i) \,,$$

which implies $\boldsymbol{K}_i^{-1} \boldsymbol{u}_i + \nabla p_i = \boldsymbol{0}$ a.e. in Ω_i. If we take now $\boldsymbol{\tau} \in \boldsymbol{H}_{\mathrm{div},0} (\Omega)$ with support in $\Omega_f \cup \gamma_i \cup \Omega_i$ for $i = 1$ or 2, we have

$$\int_{\Omega_i} \boldsymbol{K}_i^{-1} \boldsymbol{u}_i \cdot \boldsymbol{\tau} - \int_{\Omega_i} p_i \nabla \cdot \boldsymbol{\tau} + \int_{\Omega_f} \boldsymbol{K}_f^{-1} \boldsymbol{u}_f \cdot \boldsymbol{\tau} - \int_{\Omega_f} p_f \nabla \cdot \boldsymbol{\tau} = 0 \,,$$

that is

$$_{[\boldsymbol{H}_{\mathrm{div}}(\Omega_i)]'}\! < \boldsymbol{K}_i^{-1} \boldsymbol{u}_i + \nabla p_i, \, \boldsymbol{\tau} >_{\boldsymbol{H}_{\mathrm{div}}(\Omega_i)} +$$
$$+ {}_{[\boldsymbol{H}_{\mathrm{div}}(\Omega_f)]'}\! < \boldsymbol{K}_f^{-1} \boldsymbol{u}_f + \nabla p_f, \, \boldsymbol{\tau} >_{\boldsymbol{H}_{\mathrm{div}}(\Omega_f)} - \int_{\gamma_i} (p_i - p_f) \, \boldsymbol{\tau} \cdot \boldsymbol{n}_i = 0 \,,$$

the first two terms are zero obtaining the coupling condition for p across γ_i. □

The system of equation (3.3) with the interface conditions derived in Proposition 3.2 describes the evolution in all the domain Ω of the Darcy velocity and the pressure.

Problem 3.1 (Darcy coupled problem). *The coupled problem for the single-phase Darcy system is: find $(\boldsymbol{u}, p) \in \boldsymbol{H}_{\mathrm{div}} (\Omega) \times H^1 (\Omega)$ which satisfy: for $i = 1, 2, f$*

$$\begin{cases} \nabla \cdot \boldsymbol{u}_i = q_i \\ \boldsymbol{K}_i^{-1} \boldsymbol{u}_i + \nabla p_i = \boldsymbol{0} \end{cases} \quad in \ \Omega_i \,, \tag{3.5}$$

with the coupling conditions for $j = 1, 2$

$$\begin{cases} \boldsymbol{u}_j \cdot \boldsymbol{n}_j = \boldsymbol{u}_f \cdot \boldsymbol{n}_j \\ p_j = p_f \end{cases} \quad on \ \gamma_j \tag{3.6}$$

and the boundary conditions for $i = 1, 2, f$

$$\begin{cases} p_i = \overline{p_i} & on \ \Gamma_i^N \,, \\ \boldsymbol{u}_i \cdot \boldsymbol{n}_\Gamma = \overline{u_i} & on \ \Gamma_i^E \,. \end{cases} \tag{3.7}$$

3.1.1 Projection matrix

Thanks to Assumption 3.1 the curve γ, defined in (3.2), can be parametrized as

$$\boldsymbol{g}(s) = \sum_{i=1}^{n} y_i(s)\boldsymbol{e}_i \,,$$

where s is the curvilinear abscissa, $\boldsymbol{e}_i$ are three orthonormal vectors of unit length and $y_i \in C^2(\gamma)$ represent the parametrization of γ. In the sequel, to simplify the notation, we avoid to indicate the dependence on s when it is clear from the context. On γ we can define the normal vector $\boldsymbol{n}(s)$; if s is the arc-length coordinate, then

$$\boldsymbol{n}(s) := \frac{\boldsymbol{g}''(s)}{|\boldsymbol{g}''(s)|} \,.$$

Given the normal vector we can introduce the projection matrices along the normal of γ and on the tangential space

$$\boldsymbol{N} := \boldsymbol{n} \otimes \boldsymbol{n} \quad \text{and} \quad \boldsymbol{T} := \boldsymbol{I} - \boldsymbol{N} \,,$$

with the following properties

$$\boldsymbol{N} = \boldsymbol{N}^\top \,, \quad \boldsymbol{T} = \boldsymbol{T}^\top \,, \quad \boldsymbol{N}\boldsymbol{N} = \boldsymbol{N} \,, \quad \boldsymbol{T}\boldsymbol{T} = \boldsymbol{T} \,, \quad \text{and} \quad \boldsymbol{N}\boldsymbol{T} = \boldsymbol{0} \,.$$

Furthermore the following relationships hold,

$$\boldsymbol{N}\boldsymbol{n} = \boldsymbol{n} \,, \quad \boldsymbol{N}\boldsymbol{\tau} = \boldsymbol{0} \,, \quad \boldsymbol{T}\boldsymbol{\tau} = \boldsymbol{\tau} \,, \quad \text{and} \quad \boldsymbol{T}\boldsymbol{n} = \boldsymbol{0} \,, \quad \forall \boldsymbol{\tau} \perp \boldsymbol{n} \,.$$

Given a generic vector $\boldsymbol{m}$, we can decompose $\boldsymbol{m}$ along the normal direction and the tangential space as

$$\boldsymbol{m} = \boldsymbol{N}\boldsymbol{m} + \boldsymbol{T}\boldsymbol{m} = \boldsymbol{m_n} + \boldsymbol{m_\tau} \,,$$

with $\boldsymbol{m_n} := \boldsymbol{N}\boldsymbol{m}$ and $\boldsymbol{m_\tau} := \boldsymbol{T}\boldsymbol{m}$.

3.1.2 Normal and tangential operators

In differential geometry the nabla ∇ operator can be represented as

$$\nabla = \sum_{i=1}^{n} \frac{\partial}{\partial x_i} \boldsymbol{e}_i \,.$$

We now want to use the formalism introduced in the subsection 3.1.1 to decompose the gradient and the divergence operators along the normal direction $\boldsymbol{n}$ and in the tangential space defined on γ. Given a regular scalar function $g : \Omega \to \mathbb{R}$ we define the normal and tangential gradient as

$$\nabla_{\boldsymbol{n}} g := \frac{\partial g}{\partial \boldsymbol{n}} \boldsymbol{n} = \boldsymbol{N} \nabla g \quad \text{and} \quad \nabla_{\boldsymbol{\tau}} g := \nabla g - \nabla_{\boldsymbol{n}} g = \boldsymbol{T} \nabla g \, ,$$

while, given a regular vector function $\boldsymbol{u} : \Omega \to \mathbb{R}^n$, we define the normal and tangential divergence as

$$\nabla_{\boldsymbol{n}} \cdot \boldsymbol{u} := \boldsymbol{N} : \nabla \boldsymbol{u} \quad \text{and} \quad \nabla_{\boldsymbol{\tau}} \cdot \boldsymbol{u} := \nabla \cdot \boldsymbol{u} - \nabla_{\boldsymbol{n}} \cdot \boldsymbol{u} = \boldsymbol{T} : \nabla \boldsymbol{u} \, .$$

3.1.3 Reduced conservation equation

In this section we obtain a reduced model for the conservation equation in the fracture, *i.e.* the first equation in (3.5) for $i = f$. Given a normal vector $\boldsymbol{n}$, we introduce the normal and the tangential Darcy velocity, namely

$$\boldsymbol{u}_{f,\boldsymbol{n}} := \boldsymbol{N} \boldsymbol{u}_f \quad \text{and} \quad \boldsymbol{u}_{f,\boldsymbol{\tau}} := \boldsymbol{T} \boldsymbol{u}_f \, . \tag{3.8}$$

To obtain from the conservation equation in Ω_f the corresponding reduced conservation equation along γ, we decompose the divergence into its normal and tangential part. We integrate the conservation equation along the normal direction, for a given point $\boldsymbol{s}^* \in \gamma$, see Figure 3.3.
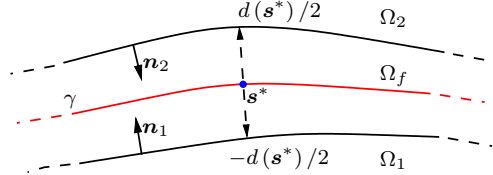
Figure 3.3: Example of a bi-dimensional fracture with the data in the normal direction.

$$\int_{-\frac{d}{2}}^{\frac{d}{2}} \nabla \cdot \boldsymbol{u}_f \, d\boldsymbol{r} = \int_{-\frac{d}{2}}^{\frac{d}{2}} \nabla_{\boldsymbol{n}} \cdot \boldsymbol{u}_f \, d\boldsymbol{r} + \int_{-\frac{d}{2}}^{\frac{d}{2}} \nabla_{\boldsymbol{\tau}} \cdot \boldsymbol{u}_f \, d\boldsymbol{r} = \int_{-\frac{d}{2}}^{\frac{d}{2}} q_f \, d\boldsymbol{r} \, ,$$

where, for convenience in notation, we omit to indicate the dependence on $\boldsymbol{s}^*$. We define the total source in a section of the fracture as

$$\hat{q}(\boldsymbol{s}) := \int_{-\frac{d(\boldsymbol{s})}{2}}^{\frac{d(\boldsymbol{s})}{2}} q_f(\boldsymbol{r}) \, d\boldsymbol{r}(\boldsymbol{s}) \, ,$$

and integrating by parts the normal divergence term we obtain

$$\boldsymbol{u}_f|_{\gamma_2} \cdot \boldsymbol{n} - \boldsymbol{u}_f|_{\gamma_1} \cdot \boldsymbol{n} + \int_{-\frac{d}{2}}^{\frac{d}{2}} \nabla_{\boldsymbol{\tau}} \cdot \boldsymbol{u}_f \, d\boldsymbol{r} = \hat{q} \, , \tag{3.9}$$

where, here and in the sequel, we indicate with $b|_{\gamma_i}$ the trace of b on γ_i. The integral in equation (3.9) is approximated as

$$\int_{-\frac{d}{2}}^{\frac{d}{2}} \nabla_{\boldsymbol{\tau}} \cdot \boldsymbol{u}_f \, d\boldsymbol{r} = \int_{-\frac{d}{2}}^{\frac{d}{2}} \boldsymbol{T} : \nabla \boldsymbol{u}_f \, d\boldsymbol{r} = \int_{-\frac{d}{2}}^{\frac{d}{2}} (\boldsymbol{TT}) : \nabla \boldsymbol{u}_f \, d\boldsymbol{r} =$$

$$= \boldsymbol{T} : \int_{-\frac{d}{2}}^{\frac{d}{2}} \boldsymbol{T} \nabla \boldsymbol{u}_f \, d\boldsymbol{r} \approx \boldsymbol{T} : \nabla \int_{-\frac{d}{2}}^{\frac{d}{2}} \boldsymbol{T} \boldsymbol{u}_f \, d\boldsymbol{r} \, ,$$

defining the flux in the tangential direction as

$$\hat{\boldsymbol{u}} \left(\boldsymbol{s} \right) := \int_{-\frac{d(\boldsymbol{s})}{2}}^{\frac{d(\boldsymbol{s})}{2}} \boldsymbol{u}_{f,\boldsymbol{\tau}} \left(\boldsymbol{r} \right) \, d\boldsymbol{r} \left(\boldsymbol{s} \right) \, , \tag{3.10}$$

equation (3.9) becomes

$$\boldsymbol{u}_f|_{\gamma_2} \cdot \boldsymbol{n} - \boldsymbol{u}_f|_{\gamma_1} \cdot \boldsymbol{n} + \nabla_{\boldsymbol{\tau}} \cdot \hat{\boldsymbol{u}} = \hat{q} \, .$$

Finally, by exploiting Assumption 3.1-6 and interface condition (3.6), we can make the approximations

$$\boldsymbol{u}_f|_{\gamma_2} \cdot \boldsymbol{n} \approx - \boldsymbol{u}_f|_{\gamma_2} \cdot \boldsymbol{n}_2 = - \boldsymbol{u}_2|_{\gamma_2} \cdot \boldsymbol{n}_2 \approx \boldsymbol{u}_2|_{\gamma} \cdot \boldsymbol{n} \, ,$$

and

$$\boldsymbol{u}_f|_{\gamma_1} \cdot \boldsymbol{n} \approx \boldsymbol{u}_f|_{\gamma_1} \cdot \boldsymbol{n}_1 = \boldsymbol{u}_1|_{\gamma_1} \cdot \boldsymbol{n}_1 \approx \boldsymbol{u}_1|_{\gamma} \cdot \boldsymbol{n} \, .$$

The conservation equation for the tangential component of the Darcy velocity in the fracture becomes

$$\nabla_{\boldsymbol{\tau}} \cdot \hat{\boldsymbol{u}} = \hat{q} + [\![\boldsymbol{u} \cdot \boldsymbol{n}]\!]_{\gamma} \quad \text{on } \gamma \, , \tag{3.11}$$

where we indicate with $[\![\cdot]\!]_{\gamma}$ the jump of a quantity across γ in the brackets

$$[\![b]\!]_{\gamma} := b_1|_{\gamma} - b_2|_{\gamma} \, ,$$

where $b_i : \Omega_i \to \mathbb{R}$, $i = 1, 2$ are functions with a well defined trace on γ. We notice that the normal $\boldsymbol{n}$ in equation (3.11) is unique.

3.1.4 Reduced Darcy equation

In this section we want to obtain a reduced model for the Darcy equation in the fracture, derived from the second equation of system (3.5) for $i = f$, and a consistency condition for the interface between the fracture and the rest of the domain.

Assumption 3.3 (Permeability $\boldsymbol{K}_f$). *We assume the following properties for the permeability tensor $\boldsymbol{K}_f$ in the fracture:*

1. *for all $\boldsymbol{s}$, tensor $\boldsymbol{K}_f$ can be written as*

$$\boldsymbol{K}_f = K_{f,\boldsymbol{n}} \boldsymbol{N} + K_{f,\boldsymbol{\tau}} \boldsymbol{T} \, ,$$

with $K_{f,\boldsymbol{n}}, K_{f,\boldsymbol{\tau}} \in L^{\infty} \left(\Omega_f \right)$ strictly positive;

2. both $K_{f,\boldsymbol{n}}$ and $K_{f,\boldsymbol{\tau}}$ are constant on each cross normal to the fracture.

As a consequence of Assumption 3.3-1 we have

$$\boldsymbol{K}_f \boldsymbol{n} = K_{f,\boldsymbol{n}}\boldsymbol{n} \quad \text{and} \quad \boldsymbol{K}_f \boldsymbol{\tau} = K_{f,\boldsymbol{\tau}}\boldsymbol{\tau} \quad \forall \boldsymbol{\tau} \perp \boldsymbol{n}.$$

For convenience we recall the Darcy equation in the fracture which reads

$$\boldsymbol{u}_f = -\boldsymbol{K}_f \nabla p_f \quad \text{in } \Omega_f.$$

Multiplying the above equation by the projection matrix $\boldsymbol{N}$ and using Assumption 3.3-1, we have

$$\boldsymbol{N}\boldsymbol{u}_f = -\boldsymbol{N}\boldsymbol{K}_f \nabla p_f = -K_{f,\boldsymbol{n}}\boldsymbol{N}\nabla p_f = -K_{f,\boldsymbol{n}}\nabla_{\boldsymbol{n}} p_f.$$

We perform the same operations multiplying by the projection matrix $\boldsymbol{T}$

$$\boldsymbol{T}\boldsymbol{u}_f = -\boldsymbol{T}\boldsymbol{K}_f \nabla p_f = -K_{f,\boldsymbol{\tau}}\boldsymbol{T}\nabla p_f = -K_{f,\boldsymbol{\tau}}\nabla_{\boldsymbol{\tau}} p_f,$$

and using definition (3.8) of normal $\boldsymbol{u}_{f,\boldsymbol{n}}$ and tangential $\boldsymbol{u}_{f,\boldsymbol{\tau}}$ Darcy velocity of the fracture, we find the following system

$$\begin{cases} \boldsymbol{u}_{f,\boldsymbol{n}} = -K_{f,\boldsymbol{n}}\nabla_{\boldsymbol{n}} p_f, \\ \boldsymbol{u}_{f,\boldsymbol{\tau}} = -K_{f,\boldsymbol{\tau}}\nabla_{\boldsymbol{\tau}} p_f. \end{cases} \tag{3.12}$$

Thanks to Assumption 3.3-2 we integrate the second equation of system (3.12) finding

$$\int_{-\frac{d}{2}}^{\frac{d}{2}} \boldsymbol{u}_{f,\boldsymbol{\tau}}\, d\boldsymbol{r} = \hat{\boldsymbol{u}} = -K_{f,\boldsymbol{\tau}}\int_{-\frac{d}{2}}^{\frac{d}{2}} \nabla_{\boldsymbol{\tau}} p_f\, d\boldsymbol{r} = -K_{f,\boldsymbol{\tau}}\boldsymbol{T}\int_{-\frac{d}{2}}^{\frac{d}{2}} \nabla p_f\, d\boldsymbol{r} \approx$$

$$\approx -K_{f,\boldsymbol{\tau}}\nabla_{\boldsymbol{\tau}}\int_{-\frac{d}{2}}^{\frac{d}{2}} p_f\, d\boldsymbol{r}.$$

Defining the mean pressure in the fracture as

$$\hat{p}(\boldsymbol{s}) := \frac{1}{d(\boldsymbol{s})} \int_{-\frac{d(\boldsymbol{s})}{2}}^{\frac{d(\boldsymbol{s})}{2}} p_f(\boldsymbol{r})\, d\boldsymbol{r}(\boldsymbol{s}), \tag{3.13}$$

and setting

$$\hat{\eta}(\boldsymbol{s}) := \frac{1}{d(\boldsymbol{s})\, K_{f,\boldsymbol{\tau}}(\boldsymbol{s})},$$

which represents the inverse of the equivalent permeability in the tangential direction to the fracture γ, we obtain the reduced Darcy equation in the fracture,

$$\hat{\eta}\hat{\boldsymbol{u}} + \nabla_{\boldsymbol{\tau}}\hat{p} = \boldsymbol{0} \quad \text{on } \gamma. \tag{3.14}$$

To derive the coupling conditions for the global problem, we consider the first equation of system (3.12). We multiply the equation by $\boldsymbol{n}$ and, using Assumption 3.3-2, we integrate in the direction normal to the fracture to obtain

$$\int_{-\frac{d}{2}}^{\frac{d}{2}} \boldsymbol{u}_{f,\boldsymbol{n}}\cdot\boldsymbol{n}\, d\boldsymbol{r} = -K_{f,\boldsymbol{n}}\int_{-\frac{d}{2}}^{\frac{d}{2}} \nabla_{\boldsymbol{n}} p_f \cdot \boldsymbol{n}\, d\boldsymbol{r} = -K_{f,\boldsymbol{n}}\left(p_f|_{\gamma_2} - p_f|_{\gamma_1}\right). \tag{3.15}$$

The integral on the left-hand side can be approximated by

$$\int_{-\frac{d}{2}}^{\frac{d}{2}} \boldsymbol{u}_{f,\boldsymbol{n}} \cdot \boldsymbol{n}\, d\boldsymbol{r} \approx \frac{d}{2}\left(\boldsymbol{u}_{f,\boldsymbol{n}}|_{\gamma_2} \cdot \boldsymbol{n} + \boldsymbol{u}_{f,\boldsymbol{n}}|_{\gamma_1} \cdot \boldsymbol{n}\right) =$$

$$= \frac{d}{2}\left(\boldsymbol{u}_2|_{\gamma_2} \cdot \boldsymbol{n} + \boldsymbol{u}_1|_{\gamma_1} \cdot \boldsymbol{n}\right) = d\,\{\!\!\{\boldsymbol{u} \cdot \boldsymbol{n}\}\!\!\}_\gamma\,, \qquad (3.16)$$

where $\{\!\!\{\cdot\}\!\!\}_\gamma$ indicates the mean of a quantity across the fracture γ in the brackets,

$$\{\!\!\{a\}\!\!\}_\gamma = \frac{1}{2}\left(a_1|_\gamma + a_2|_\gamma\right)\,,$$

with $a_i : \Omega_i \to \mathbb{R}$ a continuous function on Ω_i, for $i = 1, 2$. Using equation (3.16), condition (3.6) and Assumption 3.1-6, equation (3.15) can be written as

$$\{\!\!\{\boldsymbol{u} \cdot \boldsymbol{n}\}\!\!\}_\gamma = -K_{f,\boldsymbol{n}}\frac{p_f|_{\gamma_2} - p_f|_{\gamma_1}}{d} \approx \frac{K_{f,\boldsymbol{n}}}{d}\left(p_1|_\gamma - p_2|_\gamma\right)\,. \qquad (3.17)$$

Defining η_γ, which represent the inverse of the equivalent permeability in the normal direction to the fracture γ, as

$$\eta_\gamma\left(\boldsymbol{s}\right) := \frac{d\left(\boldsymbol{s}\right)}{K_{f,\boldsymbol{n}}\left(\boldsymbol{s}\right)}\,, \qquad (3.18)$$

we can rewrite equation (3.17) as

$$\eta_\gamma\,\{\!\!\{\boldsymbol{u} \cdot \boldsymbol{n}\}\!\!\}_\gamma = [\![p]\!]_\gamma\,, \qquad (3.19)$$

To close the reduced system we need another relation to model the effects of the variation of pressure and velocity across the fracture.
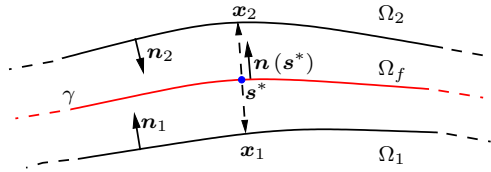
Figure 3.4: Frame of reference for the approximation of the pressure in the fracture.

In the first transversal section, see Figure 3.4, we approximate the value of the pressure inside the fracture by the following Taylor expansion

$$p_f\left(\boldsymbol{s}^*\right) = p_f(\boldsymbol{x}_1) + \frac{d}{2}\nabla p_f\left(\boldsymbol{\theta}_1\right) \cdot \boldsymbol{n}\,, \qquad (3.20)$$

where $\boldsymbol{\theta}_1 = \boldsymbol{s}^* - \xi_1\dfrac{d\left(\boldsymbol{s}^*\right)}{2}\boldsymbol{n}$ with $\xi_1 \in [0, 1]$. The point $\boldsymbol{x}_1 \in \gamma_1$ is such that $\boldsymbol{x}_1 = \boldsymbol{s}^* - \dfrac{d\left(\boldsymbol{s}^*\right)}{2}\boldsymbol{n}$. In the second transversal section we approximate the value of the pressure inside the fracture by

$$p_f\left(\boldsymbol{s}^*\right) = p_f(\boldsymbol{x}_2) - \frac{d}{2}\nabla p_f\left(\boldsymbol{\theta}_2\right) \cdot \boldsymbol{n}\,, \qquad (3.21)$$

where $\boldsymbol{\theta}_2 = \boldsymbol{s}^* + \xi_2 \dfrac{d(\boldsymbol{s}^*)}{2} \boldsymbol{n}$ with $\xi_2 \in [0, 1]$. The point $\boldsymbol{x}_2 \in \gamma_2$ is such that $\boldsymbol{x}_2 = \boldsymbol{s}^* + \dfrac{d(\boldsymbol{s}^*)}{2} \boldsymbol{n}$. Using relations (3.6), (3.12) and assuming a piecewise linear variation of $\boldsymbol{u}_{f,\boldsymbol{n}}$ we have

$$
\begin{cases}
\boldsymbol{u}_{f,\boldsymbol{n}}(\boldsymbol{\theta}_1) \cdot \boldsymbol{n} = \xi_1 \boldsymbol{u}_1 \cdot \boldsymbol{n} + (1-\xi_1)\boldsymbol{u}_2 \cdot \boldsymbol{n}, \\
\boldsymbol{u}_{f,\boldsymbol{n}}(\boldsymbol{\theta}_2) \cdot \boldsymbol{n} = \xi_2 \boldsymbol{u}_2 \cdot \boldsymbol{n} + (1-\xi_2)\boldsymbol{u}_1 \cdot \boldsymbol{n},
\end{cases}
$$

the approximate pressure in the fracture (3.20) becomes

$$
\begin{aligned}
p_f(\boldsymbol{s}^*) &\approx p_1(\boldsymbol{x}_1) - \frac{\eta_\gamma}{2}\left[\xi_1 \boldsymbol{u}_1 \cdot \boldsymbol{n} + (1-\xi_1)\boldsymbol{u}_2 \cdot \boldsymbol{n}\right] = \\
&= p_1(\boldsymbol{x}_1) - \frac{\eta_\gamma}{2}\left[\{\!\{\boldsymbol{u} \cdot \boldsymbol{n}\}\!\}_\gamma + \left(\xi_1 - \frac{1}{2}\right)[\![\boldsymbol{u} \cdot \boldsymbol{n}]\!]_\gamma\right],
\end{aligned}
\tag{3.22}
$$

while equation (3.21) gives

$$
\begin{aligned}
p_f(\boldsymbol{s}^*) &\approx p_2(\boldsymbol{x}_2) + \frac{\eta_\gamma}{2}\left[\xi_2 \boldsymbol{u}_1 \cdot \boldsymbol{n} + (1-\xi_2)\boldsymbol{u}_2 \cdot \boldsymbol{n}\right] = \\
&= p_2(\boldsymbol{x}_2) + \frac{\eta_\gamma}{2}\left[\{\!\{\boldsymbol{u} \cdot \boldsymbol{n}\}\!\}_\gamma - \left(\xi_2 - \frac{1}{2}\right)[\![\boldsymbol{u} \cdot \boldsymbol{n}]\!]_\gamma\right].
\end{aligned}
\tag{3.23}
$$

Using relation (3.19) we find

$$
\begin{aligned}
p_f(\boldsymbol{s}^*) &\approx \{\!\{p\}\!\}_\gamma - \frac{\eta_\gamma(2\xi_1 - 1)}{4}[\![\boldsymbol{u} \cdot \boldsymbol{n}]\!]_\gamma, \\
p_f(\boldsymbol{s}^*) &\approx \{\!\{p\}\!\}_\gamma - \frac{\eta_\gamma(2\xi_2 - 1)}{4}[\![\boldsymbol{u} \cdot \boldsymbol{n}]\!]_\gamma.
\end{aligned}
$$

Since the pressure in the fracture p_f is single valued at $\boldsymbol{s}^*$, the only possibility is to choose $\xi_1 = \xi_2 = \xi$, finding

$$
p_f(\boldsymbol{s}^*) \approx \{\!\{p\}\!\}_\gamma - \frac{\eta_\gamma(2\xi - 1)}{4}[\![\boldsymbol{u} \cdot \boldsymbol{n}]\!]_\gamma,
$$

Finally, integrating in the transversal section of γ and using the definition (3.13) for the reduced pressure we obtain

$$
\hat{p} = \{\!\{p\}\!\}_\gamma - \frac{\eta_\gamma(2\xi - 1)}{4}[\![\boldsymbol{u} \cdot \boldsymbol{n}]\!]_\gamma.
\tag{3.24}
$$

An alternative approach to derive (3.24) is the following. Let us assume that p is regular in Ω_f and we indicate with $p(x) = p(\boldsymbol{s}^* + x\boldsymbol{n})$ for a $\boldsymbol{s}^* \in \gamma$. We have that

$$
\hat{p} - \{\!\{p\}\!\}_\gamma = -\frac{d^2}{12}p''(\xi) \quad \text{for} \quad \xi \in \left(-\frac{d(\boldsymbol{s}^*)}{2}, \frac{d(\boldsymbol{s}^*)}{2}\right).
$$

On the other hand using Taylor expansion and relation (3.12), we obtain

$$
[\![\boldsymbol{u} \cdot \boldsymbol{n}]\!]_\gamma = dK_{f,\boldsymbol{n}}p''(0) + \mathcal{O}(d^3).
$$

Thus, neglecting higher order terms we may set

$$\llbracket \boldsymbol{u} \cdot \boldsymbol{n} \rrbracket_\gamma = dK_{f,\boldsymbol{n}} p''(0) \,,$$

and assuming $p''(\xi) = cp''(0)$, being c a particular constant, we find

$$\{\!\{p\}\!\}_\gamma - \hat{p} = -\frac{d^2}{12} cp''(0) = \frac{dc}{12 K_{f,\boldsymbol{n}}} \llbracket \boldsymbol{u} \cdot \boldsymbol{n} \rrbracket_\gamma = \eta_\gamma \frac{c}{12} \llbracket \boldsymbol{u} \cdot \boldsymbol{n} \rrbracket_\gamma \,,$$

which is equal to (3.24) if $c = 6\xi - 3$. Other approaches to derive equation (3.24) are presented in [57] and [4]. Using (3.19) and (3.24), the interface conditions on γ become

$$\begin{cases} \xi_0 \eta_\gamma \llbracket \boldsymbol{u} \cdot \boldsymbol{n} \rrbracket_\gamma = \{\!\{p\}\!\}_\gamma - \hat{p} \\ \eta_\gamma \{\!\{\boldsymbol{u} \cdot \boldsymbol{n}\}\!\}_\gamma = \llbracket p \rrbracket_\gamma \end{cases} \quad \text{on } \gamma \,, \tag{3.25}$$

with $\xi_0 := (2\xi - 1)/4$. Alternatively, the previous system can be written as

$$\begin{cases} \xi \boldsymbol{u}_1 \cdot \boldsymbol{n} + (1 - \xi) \boldsymbol{u}_2 \cdot \boldsymbol{n} = 2\eta_\gamma^{-1} (p_1 - \hat{p}) \\ (1 - \xi) \boldsymbol{u}_1 \cdot \boldsymbol{n} + \xi \boldsymbol{u}_2 \cdot \boldsymbol{n} = 2\eta_\gamma^{-1} (\hat{p} - p_2) \end{cases} \quad \text{on } \gamma \,.$$

To derive the boundary conditions for the reduced problem we use Assumption 3.1-3 and the equations (3.7) to find

$$\overline{\hat{\boldsymbol{u}}} \cdot \boldsymbol{n}_\Gamma := \int_{\Gamma_f^E} \overline{u_f} \,, \quad \text{and} \quad \overline{\hat{p}} := \frac{1}{d} \int_{\Gamma_f^N} \overline{p_f} \,. \tag{3.26}$$

Using Assumption 3.1 and Assumption 3.3, hence approximating the domain Ω reported in Figure 3.1 with the domain in Figure 3.5, the equations (3.11), (3.14), (3.25) and (3.26) form the reduced model summarized in the following problem.

Problem 3.2 (Reduced model for Darcy equation)**.** *Under Assumption 3.1, Assumption 3.2 and Assumption 3.3, the reduced formulation of the Darcy problem in a porous medium with one fracture is: find the Darcy velocity and the pressure associated to the porous matrix, respectively $\boldsymbol{u}_i$ and p_i for $i = 1, 2$, and the reduced Darcy velocity and reduced pressure associated to the fracture, respectively $\hat{\boldsymbol{u}}$ and $\hat{p}$, which satisfy the following system of partial differential equations*

$$\begin{cases} \nabla \cdot \boldsymbol{u}_i = q_i & \text{in } \Omega_i \,, \\ \boldsymbol{K}_i^{-1} \boldsymbol{u}_i + \nabla p_i = \boldsymbol{0} & \text{in } \Omega_i \,, \\ \nabla_{\boldsymbol{\tau}} \cdot \hat{\boldsymbol{u}} = \hat{q} + \llbracket \boldsymbol{u} \cdot \boldsymbol{n} \rrbracket_\gamma & \text{on } \gamma \,, \\ \hat{\eta} \hat{\boldsymbol{u}} + \nabla_{\boldsymbol{\tau}} \hat{p} = \boldsymbol{0} & \text{on } \gamma \,, \end{cases}$$

coupled with the interface conditions on γ

$$\begin{cases} \xi_0 \eta_\gamma \llbracket \boldsymbol{u} \cdot \boldsymbol{n} \rrbracket_\gamma = \{\!\{p\}\!\}_\gamma - \hat{p} \\ \eta_\gamma \{\!\{\boldsymbol{u} \cdot \boldsymbol{n}\}\!\}_\gamma = \llbracket p \rrbracket_\gamma \end{cases} \quad \text{on } \gamma \,,$$

and with the boundary conditions on $\partial\Omega$

$$\begin{cases} p_i = \overline{p_i} & on \; \Gamma_i^N \,, \\ \boldsymbol{u}_i \cdot \boldsymbol{n}_\Gamma = \overline{u_i} & on \; \Gamma_i^E \,, \\ \hat{p} = \overline{\hat{p}} & on \; \partial\gamma^N \,, \\ \hat{\boldsymbol{u}} \cdot \boldsymbol{n}_\Gamma = \overline{\hat{\boldsymbol{u}}} \cdot \boldsymbol{n}_\Gamma & in \; \partial\gamma^E \,, \end{cases}$$

for $i = 1, 2$.
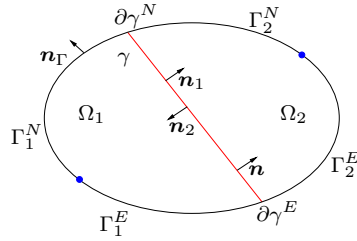
Figure 3.5: Sketch of the domain Ω, the two sub-domains Ω_1 and Ω_2 and the reduced fracture γ.

3.1.5 Gravity effects

The reduced model presented in the previous section changes in presence of the gravity, more generally in the presence of a vector source $\boldsymbol{q}$

$$\boldsymbol{u} = -\boldsymbol{K}\left(\nabla p - \boldsymbol{q}\right) \quad in \; \Omega \,.$$

The transmission conditions (3.6) remain unchanged same since we use the total flux instead the gradient as the vector variable.

Assumption 3.4 (Vector source)**.** *The source vector $\boldsymbol{q} \in \left[L^2\left(\Omega\right)\right]^n$ can be decomposed as*

$$\boldsymbol{q} = \sum_{i=1,2,f} \boldsymbol{q}_i|_{\Omega_i} \,,$$

with $\boldsymbol{q}_i \in \left[L^2\left(\Omega_i\right)\right]^n$ defined as $\boldsymbol{q}_i|_{\Omega_i} := \boldsymbol{q}|_{\Omega_i}$ for $i = 1, 2, f$. In the sequel we often will make the abuse of notation indicating with $\boldsymbol{q}_i$ its restriction on Ω_i.

Performing the same computations as in sub-section 3.1.3, system (3.12) becomes

$$\begin{cases} \boldsymbol{u}_{f,\boldsymbol{n}} = -K_{f,\boldsymbol{n}}\left(\nabla_{\boldsymbol{n}}p_f - \boldsymbol{N}\boldsymbol{q}_f\right) \,, \\ \boldsymbol{u}_{f,\boldsymbol{\tau}} = -K_{f,\boldsymbol{\tau}}\left(\nabla_{\boldsymbol{\tau}}p_f - \boldsymbol{T}\boldsymbol{q}_f\right) \,. \end{cases} \tag{3.27}$$

Then defining the reduced vector source as

$$\hat{\boldsymbol{q}}\left(\boldsymbol{s}\right) := \frac{1}{d\left(\boldsymbol{s}\right)} \int_{-\frac{d(\boldsymbol{s})}{2}}^{\frac{d(\boldsymbol{s})}{2}} \boldsymbol{T}\boldsymbol{q}_f\left(\boldsymbol{r}\right) \, d\boldsymbol{r}\left(\boldsymbol{s}\right) \,,$$

we obtain the reduced Darcy equation in the fracture

$$\hat{\eta}\hat{\boldsymbol{u}} + \nabla_{\boldsymbol{\tau}}\hat{p} = \hat{\boldsymbol{q}} \quad \text{on } \gamma. \tag{3.28}$$

To derive new coupling conditions for the global problem, we consider the first equation of system (3.27). We multiply the equation by $\boldsymbol{n}$ and, using Assumption 3.3-2, we integrate in the normal direction to the fracture to obtain

$$d\,\{\!\{\boldsymbol{u}\cdot\boldsymbol{n}\}\!\}_\gamma = K_{f,\boldsymbol{n}}\,[\![p]\!]_\gamma + K_{f,\boldsymbol{n}}\int_{-\frac{d}{2}}^{\frac{d}{2}}\boldsymbol{q}_f\cdot\boldsymbol{n}\,dr \approx$$

$$\approx K_{f,\boldsymbol{n}}\left([\![p]\!]_\gamma + d\,\{\!\{\boldsymbol{q}\cdot\boldsymbol{n}\}\!\}_\gamma\right),$$

then using definition (3.18) we obtain the new coupling condition

$$\eta_\gamma\,\{\!\{\boldsymbol{u}\cdot\boldsymbol{n}\}\!\}_\gamma = [\![p]\!]_\gamma + d\,\{\!\{\boldsymbol{q}\cdot\boldsymbol{n}\}\!\}_\gamma. \tag{3.29}$$

The closure equation (3.24) should be modified in order to take into account the vector source. In fact using the same assumption, instead of (3.22) and (3.23), we find

$$p_f\left(\boldsymbol{s}^*\right) \approx p_1(\boldsymbol{x}_1) - \frac{\eta_\gamma}{2}\left[\{\!\{\boldsymbol{u}\cdot\boldsymbol{n}\}\!\}_\gamma + \left(\xi_1 - \frac{1}{2}\right)[\![\boldsymbol{u}\cdot\boldsymbol{n}]\!]_\gamma\right] + \frac{d}{2}\boldsymbol{q}_f\left(\boldsymbol{\theta}_1\right)\cdot\boldsymbol{n},$$

$$p_f\left(\boldsymbol{s}^*\right) \approx p_2(\boldsymbol{x}_2) + \frac{\eta_\gamma}{2}\left[\{\!\{\boldsymbol{u}\cdot\boldsymbol{n}\}\!\}_\gamma - \left(\xi_2 - \frac{1}{2}\right)[\![\boldsymbol{u}\cdot\boldsymbol{n}]\!]_\gamma\right] - \frac{d}{2}\boldsymbol{q}_f\left(\boldsymbol{\theta}_2\right)\cdot\boldsymbol{n}.$$

Then approximating $\boldsymbol{q}_f\left(\boldsymbol{\theta}_i\right) \approx \boldsymbol{q}_i|_{\gamma_i}$ and using (3.29) we find

$$p_f\left(\boldsymbol{s}^*\right) \approx \{\!\{p\}\!\}_\gamma - \frac{\eta_\gamma\,(2\xi_1 - 1)}{4}[\![\boldsymbol{u}\cdot\boldsymbol{n}]\!]_\gamma - \frac{d}{4}[\![\boldsymbol{q}\cdot\boldsymbol{n}]\!]_\gamma,$$

$$p_f\left(\boldsymbol{s}^*\right) \approx \{\!\{p\}\!\}_\gamma - \frac{\eta_\gamma\,(2\xi_2 - 1)}{4}[\![\boldsymbol{u}\cdot\boldsymbol{n}]\!]_\gamma - \frac{d}{4}[\![\boldsymbol{q}\cdot\boldsymbol{n}]\!]_\gamma.$$

Since the pressure in the fracture p_f is single valued at $\boldsymbol{s}^*$, the only possibility is to choose $\xi_1 = \xi_2 = \xi$, then integrating in the transversal section of γ and using the definition (3.13) for the reduced pressure we obtain the new second coupling condition

$$\xi_0\eta_\gamma\,[\![\boldsymbol{u}\cdot\boldsymbol{n}]\!]_\gamma + \frac{d}{4}[\![\boldsymbol{q}\cdot\boldsymbol{n}]\!]_\gamma = \{\!\{p\}\!\}_\gamma - \hat{p} \text{ on } \gamma. \tag{3.30}$$

Using Assumption 3.1 and Assumption 3.3, the equations (3.11), (3.28), (3.29), (3.30) and (3.26) form the reduced model summarized in the following problem.

Problem 3.3 (Reduced model for Darcy equation with gravity)**.** *Under Assumption 3.1, Assumption 3.2 and Assumption 3.3, the reduced problem for the Darcy system with gravity is: find the Darcy velocity and the pressure associated to the porous matrix, respectively $\boldsymbol{u}_i$ and p_i for $i = 1, 2$, and the reduced Darcy velocity and reduced pressure associated to the fracture, respectively $\hat{\boldsymbol{u}}$ and $\hat{p}$, which satisfy the following system of partial differential equations*

$$\begin{cases} \nabla\cdot\boldsymbol{u}_i = q_i & \text{in } \Omega_i, \\[2mm] \boldsymbol{K}_i^{-1}\boldsymbol{u}_i + \nabla p_i = \boldsymbol{q}_i & \text{in } \Omega_i, \\[2mm] \nabla_{\boldsymbol{\tau}}\cdot\hat{\boldsymbol{u}} = \hat{q} + [\![\boldsymbol{u}\cdot\boldsymbol{n}]\!]_\gamma & \text{on } \gamma, \\[2mm] \hat{\eta}\hat{\boldsymbol{u}} + \nabla_{\boldsymbol{\tau}}\hat{p} = \hat{\boldsymbol{q}} & \text{on } \gamma, \end{cases} \tag{3.31}$$

coupled with the interface conditions on γ

$$\begin{cases} \xi_0 \eta_\gamma \, [\![\boldsymbol{u} \cdot \boldsymbol{n}]\!]_\gamma + \dfrac{d}{4} \, [\![\boldsymbol{q} \cdot \boldsymbol{n}]\!]_\gamma = \{\!\{ p \}\!\}_\gamma - \hat{p} \\[2mm] \eta_\gamma \, \{\!\{ \boldsymbol{u} \cdot \boldsymbol{n} \}\!\}_\gamma = [\![p]\!]_\gamma + d \, \{\!\{ \boldsymbol{q} \cdot \boldsymbol{n} \}\!\}_\gamma \end{cases} \qquad on \ \gamma \,, \qquad (3.32)$$

and with the boundary conditions on $\partial\Omega$

$$\begin{cases} p_i = \overline{p_i} & on \ \Gamma_i^N \,, \\[1mm] \boldsymbol{u}_i \cdot \boldsymbol{n}_\Gamma = \overline{u_i} & on \ \Gamma_i^E \,, \\[1mm] \hat{p} = \overline{\hat{p}} & on \ \partial\gamma^N \,, \\[1mm] \hat{\boldsymbol{u}} \cdot \boldsymbol{n}_\Gamma = \overline{\hat{\boldsymbol{u}}} \cdot \boldsymbol{n}_\Gamma & in \ \partial\gamma^E \,, \end{cases} \qquad (3.33)$$

for $i = 1, 2$.

3.1.6 Weak formulation

We derive the weak formulation of the global reduced Problem 3.3 and for the sake of simplicity we require $\overline{u_i} = 0$ for $i = 1, 2$ and $\widehat{\boldsymbol{u}} \cdot \boldsymbol{n}_\Gamma = 0$ or $\Gamma^E = \emptyset$, otherwise a lifting technique should be used to impose the boundary data. We define

$$D := \bigcup_{i=1}^2 \Omega_i = \Omega \setminus \gamma \,, \qquad (3.34)$$

and introduce the following functional spaces for $i = 1, 2$

$$\boldsymbol{V}_i := \Big\{ \boldsymbol{v}_i \in \boldsymbol{H}_{\mathrm{div}}(\Omega_i) : < \boldsymbol{v}_i \cdot \boldsymbol{n}_\Gamma, \, v > = 0 \ \ \forall v \in H^1_{0, \Gamma_i^N}(\Omega_i)$$

$$\text{and } \boldsymbol{v}_i \cdot \boldsymbol{n}_i \in L^2\left(\gamma \cap \partial\Omega_i\right) \Big\} \quad \text{and} \quad Q_i := H^1(\Omega_i) \,, \qquad (3.35)$$

which are Hilbert spaces, endowed with inner products $(\cdot, \cdot)_{\boldsymbol{V}_i} : \boldsymbol{V}_i \times \boldsymbol{V}_i \to \mathbb{R}$ and $(\cdot, \cdot)_{Q_i} : Q_i \times Q_i \to \mathbb{R}$, defined as

$$(\boldsymbol{u}, \boldsymbol{\tau})_{\boldsymbol{V}_i} := (\boldsymbol{u}, \boldsymbol{\tau})_{\Omega_i} + (\nabla \cdot \boldsymbol{u}, \nabla \cdot \boldsymbol{\tau})_{\Omega_i} + (\boldsymbol{u} \cdot \boldsymbol{n}_i, \boldsymbol{\tau} \cdot \boldsymbol{n}_i)_\gamma \,,$$

$$(p, q)_{Q_i} := (p, q)_{\Omega_i} + (\nabla p, \nabla q)_{\Omega_i} \,,$$

and associated norms $\|\cdot\|_{\boldsymbol{V}_i} : \boldsymbol{V}_i \to \mathbb{R}$ and $\|\cdot\|_{Q_i} : Q_i \to \mathbb{R}$, defined as

$$\|\boldsymbol{u}\|_{\boldsymbol{V}_i} := \sqrt{(\boldsymbol{u}, \boldsymbol{u})_{\boldsymbol{V}_i}} \quad \text{and} \quad \|p\|_{Q_i} := \sqrt{(p, p)_{Q_i}}$$

with $\boldsymbol{u}, \boldsymbol{\tau} \in \boldsymbol{V}_i$ and $p, q \in Q_i$. We also introduce the broken functional space $\boldsymbol{V} : D \to \mathbb{R}^n$

$$\boldsymbol{V} := \Big\{ \boldsymbol{v} : D \to \mathbb{R}^n : \boldsymbol{v}_i := \boldsymbol{v}|_{\Omega_i} \in \boldsymbol{V}_i \text{ for } i = 1, 2 \Big\} \,,$$

which is an Hilbert space endowed with the inner product $(\cdot, \cdot)_{\boldsymbol{V}} : \boldsymbol{V} \times \boldsymbol{V} \to \mathbb{R}$ and associated norm $\|\cdot\|_{\boldsymbol{V}} : \boldsymbol{V} \to \mathbb{R}$, defined as

$$(\boldsymbol{u}, \boldsymbol{v})_{\boldsymbol{V}} := \sum_{i=1}^2 (\boldsymbol{u}_i, \boldsymbol{v}_i)_{\boldsymbol{V}_i} \quad \text{and} \quad \|\boldsymbol{u}\|_{\boldsymbol{V}}^2 := \sum_{i=1}^2 \|\boldsymbol{u}_i\|_{\boldsymbol{V}_i}^2 \,,$$

with $\boldsymbol{u},\,\boldsymbol{v}\in\boldsymbol{V}$. Analogously the broken space $Q:D\to\mathbb{R}$

$$Q:=\left\{w:D\to\mathbb{R}:\,w_i:=w|_{\Omega_i}\in Q_i\text{ for }i=1,2\right\},$$

which is an Hilbert space with internal product $(\cdot,\,\cdot)_Q\,:\,Q\times Q\,\to\,\mathbb{R}$ and associated norm $\|\cdot\|_Q:Q\to\mathbb{R}$, given by

$$(p,\,w)_Q:=\sum_{i=1}^{2}(p_i,\,w_i)_{Q_i}\quad\text{and}\quad\|p\|_Q^2:=\sum_{i=1}^{2}\|p_i\|_{Q_i}^2\,,$$

with $p,\,w\in Q$. Note that $\boldsymbol{V}$ and Q may be identified with a subset of $\left[L^2\left(\Omega\right)\right]^n$ and $L^2\left(\Omega\right)$, respectively since γ is a set of zero Lebesgue measure in $\mathbb{R}^n$. Thus we will indicate for a $v\in Q$

$$\|v\|_{L^2(\Omega)}^2=\sum_{i=1}^{2}\int_{\Omega_i}v_i^2=\int_\Omega v^2\,,$$

where it is understood that v has been extended to the whole Ω. Analogously we define the $L^2\left(\Omega\right)$ norm of an element of $\boldsymbol{V}$. If we set

$$\boldsymbol{V}_\Omega:=\left\{\boldsymbol{u}\in\boldsymbol{H}_{\mathrm{div}}\left(\Omega\right):<\boldsymbol{u}\cdot\boldsymbol{n}_\Gamma,\,v>=0\,\forall v\in H_{0,\Gamma^N}^1\left(\Omega\right)\right\}\,,$$
$$Q_\Omega:=H^1\left(\Omega\right)\,,\tag{3.36}$$

to each element $\mathbf{v}\in\boldsymbol{V}_\Omega$ there is a unique $\boldsymbol{v}\in\boldsymbol{V}$ such that for $i=1,2$

$$\boldsymbol{v}|_{\Omega_i}=\mathbf{v}|_{\Omega_i}\quad\text{and}\quad[\![\mathbf{v}\cdot\boldsymbol{n}]\!]_\gamma=0\,.$$

Analogously, for each $\mathrm{w}\in Q_\Omega$ there exist a unique $w\in Q$ such that for $i=1,2$

$$w|_{\Omega_i}=\mathrm{w}|_{\Omega_i}\quad\text{and}\quad[\![\mathrm{w}]\!]_\gamma=0\,.$$

We introduce also the functional spaces for the problem in the fracture: the spaces of functions living in the tangent space, that is

$$\hat{\boldsymbol{V}}:=\left\{\hat{\boldsymbol{v}}:\,\gamma\to\mathbb{R}^n,\,\hat{\boldsymbol{v}}\in\left[L^2\left(\gamma\right)\right]^n:\,\hat{\boldsymbol{v}}\cdot\boldsymbol{n}=0,\,\nabla_{\boldsymbol{\tau}}\cdot\hat{\boldsymbol{v}}\in L^2\left(\gamma\right)\right.$$
$$\left.\text{and }<\hat{\boldsymbol{v}}\cdot\boldsymbol{n}_\Gamma,\,v>=0\,\forall v\in H_{0,\partial\gamma^N}^1\left(\gamma\right)\right\}\,,$$
$$\hat{Q}:=\left\{\hat{w}:\,\gamma\to\mathbb{R},\,\hat{w}\in L^2\left(\gamma\right):\,\nabla_{\boldsymbol{n}}\hat{w}=\boldsymbol{0}\text{ and }\nabla_{\boldsymbol{\tau}}\hat{w}\in\left[L^2\left(\gamma\right)\right]^n\right\}\,,\tag{3.37}$$

which are Hilbert spaces endowed with inner products $(\cdot,\,\cdot)_{\hat{\boldsymbol{V}}}:\hat{\boldsymbol{V}}\times\hat{\boldsymbol{V}}\to\mathbb{R}$ and $(\cdot,\,\cdot)_{\hat{Q}}:\hat{Q}\times\hat{Q}\to\mathbb{R}$, defined as

$$(\hat{\boldsymbol{u}},\,\hat{\boldsymbol{v}})_{\hat{\boldsymbol{V}}}:=(\hat{\boldsymbol{u}},\,\hat{\boldsymbol{v}})_\gamma+(\nabla_{\boldsymbol{\tau}}\cdot\hat{\boldsymbol{u}},\,\nabla_{\boldsymbol{\tau}}\cdot\hat{\boldsymbol{v}})_\gamma\,,$$
$$(\hat{p},\,\hat{w})_{\hat{Q}}:=(\hat{p},\,\hat{w})_\gamma+(\nabla_{\boldsymbol{\tau}}\hat{p},\,\nabla_{\boldsymbol{\tau}}\hat{w})_\gamma\,,$$

and norms $\|\cdot\|_{\hat{\boldsymbol{V}}}:\hat{\boldsymbol{V}}\to\mathbb{R}$ and $\|\cdot\|_{\hat{Q}}:\hat{Q}\to\mathbb{R}$, defined as

$$\|\hat{\boldsymbol{u}}\|_{\hat{\boldsymbol{V}}}^2:=(\hat{\boldsymbol{u}},\,\hat{\boldsymbol{u}})_{\hat{\boldsymbol{V}}}\quad\text{and}\quad\|\hat{p}\|_{\hat{Q}}^2:=(\hat{p},\,\hat{p})_{\hat{Q}}\,,$$

with $\hat{\boldsymbol{u}}$, $\hat{\boldsymbol{v}} \in \hat{\boldsymbol{V}}$ and $\hat{p}$, $\hat{w} \in \hat{Q}$. We define also the global space for the Darcy velocity and the global space for the pressure

$$\boldsymbol{\mathcal{V}} := \left\{ \mathbf{v} = (\boldsymbol{v},\, \hat{\boldsymbol{v}}) \in \boldsymbol{V} \times \hat{\boldsymbol{V}} \right\} \quad \text{and} \quad \mathcal{Q} := \left\{ \mathbf{w} = (w,\, \hat{w}) \in Q \times \hat{Q} \right\},$$

which are Hilbert spaces endowed with inner products $(\cdot,\, \cdot)_{\boldsymbol{\mathcal{V}}} : \boldsymbol{\mathcal{V}} \times \boldsymbol{\mathcal{V}} \to \mathbb{R}$ and $(\cdot,\, \cdot)_{\mathcal{Q}} : \mathcal{Q} \times \mathcal{Q} \to \mathbb{R}$, defined as

$$(\mathbf{u},\, \mathbf{v})_{\boldsymbol{\mathcal{V}}} := (\boldsymbol{u},\, \boldsymbol{v})_{\boldsymbol{V}} + (\hat{\boldsymbol{u}},\, \hat{\boldsymbol{v}})_{\hat{\boldsymbol{V}}} \quad \text{and} \quad (\mathrm{p},\, \mathrm{w}) := (p,\, w)_Q + (\hat{p},\, \hat{w})_{\hat{Q}},$$

and norms $\|\cdot\|_{\boldsymbol{\mathcal{V}}} : \boldsymbol{\mathcal{V}} \to \mathbb{R}$ and $\|\cdot\|_{\mathcal{Q}} : \mathcal{Q} \to \mathbb{R}$, defined as

$$\|\mathbf{u}\|_{\boldsymbol{\mathcal{V}}}^2 := (\mathbf{u},\, \mathbf{u})_{\boldsymbol{\mathcal{V}}} \quad \text{and} \quad \|\mathrm{p}\|_{\boldsymbol{\mathcal{V}}}^2 := (\mathrm{p},\, \mathrm{p})_{\mathcal{Q}},$$

with $\mathbf{u}$, $\mathbf{v} \in \boldsymbol{\mathcal{V}}$ such that $\mathbf{u} = (\boldsymbol{u},\, \hat{\boldsymbol{u}})$, $\mathbf{v} = (\boldsymbol{v},\, \hat{\boldsymbol{v}})$ and p, $\mathrm{w} \in \mathcal{Q}$ such that $\mathrm{p} = (p,\, \hat{p})$, $\mathrm{w} = (w,\, \hat{w})$. Finally we define the global space for the whole problem

$$\mathcal{D} := \{ \mathrm{z} = (\mathbf{v},\, \mathrm{w}) \in \boldsymbol{\mathcal{V}} \times \mathcal{Q} \}, \tag{3.38}$$

which is an Hilbert space endowed with the inner product $(\cdot,\, \cdot)_{\mathcal{D}} : \mathcal{D} \times \mathcal{D} \to \mathbb{R}$ and associated norm $\|\cdot\|_{\mathcal{D}}^2 : \mathcal{D} \to \mathbb{R}$, defined as

$$(\mathrm{z},\, \mathrm{t})_{\mathcal{D}} := (\mathbf{v},\, \mathbf{u})_{\boldsymbol{\mathcal{V}}} + (\mathrm{w},\, \mathrm{p})_{\mathcal{Q}} \quad \text{and} \quad \|\mathrm{z}\|_{\mathcal{D}}^2 := (\mathrm{z},\, \mathrm{z})_{\mathcal{D}},$$

with $\mathrm{z} = (\mathbf{v},\, \mathrm{w}) \in \mathcal{D}$ and $\mathrm{t} = (\mathbf{u},\, \mathrm{p}) \in \mathcal{D}$.

We derive the weak formulation of Problem 3.3, starting with the differential equation in the medium. Taking a test function $w \in Q$ multiply and integrate on Ω_i the first equation of (3.31)

$$(\nabla \cdot \boldsymbol{u}_i,\, w)_{\Omega_i} = (q_i,\, w)_{\Omega_i},$$

summing on all the domains Ω_i for $i = 1, 2$ we have

$$(\nabla \cdot \boldsymbol{u},\, w)_{\Omega} = (q,\, w)_{\Omega}.$$

Introducing the bilinear form $b(\cdot,\, \cdot) : \boldsymbol{V} \times Q \to \mathbb{R}$ and the functional $F_q \in Q'$

$$b(\boldsymbol{u},\, w) := -(\nabla \cdot \boldsymbol{u},\, w)_{\Omega} \quad \text{and} \quad F_q(w) := (q,\, w)_{\Omega}, \tag{3.39}$$

then the weak formulation of the first equation of (3.31) is

$$b(\boldsymbol{u},\, w) = -F_q(w) \quad \forall w \in Q.$$

Taking a test function $\boldsymbol{v} \in \boldsymbol{V}$ multiply and integrate on Ω_i the second equation of (3.31)

$$\left(\boldsymbol{K}_i^{-1}\boldsymbol{u}_i,\, \boldsymbol{v}\right)_{\Omega_i} + (\nabla p_i,\, \boldsymbol{v})_{\Omega_i} - (\boldsymbol{q}_i,\, \boldsymbol{v})_{\Omega_i} =$$
$$= \left(\boldsymbol{K}_i^{-1}\boldsymbol{u}_i,\, \boldsymbol{v}\right)_{\Omega_i} - (p_i,\, \nabla \cdot \boldsymbol{v})_{\Omega_i} + (p_i,\, \boldsymbol{v} \cdot \boldsymbol{n}_\Gamma)_\Gamma + (p_i,\, \boldsymbol{v} \cdot \boldsymbol{n}_i)\gamma - (\boldsymbol{q}_i,\, \boldsymbol{v})_{\Omega_i} = 0.$$

Summing the previous equation for $i = 1, 2$ and using the boundary conditions (3.33) we obtain

$$\left(\boldsymbol{K}^{-1}\boldsymbol{u},\, \boldsymbol{v}\right)_{\Omega} - (p,\, \nabla \cdot \boldsymbol{v})_{\Omega} + (\bar{p},\, \boldsymbol{v} \cdot \boldsymbol{n}_\Gamma)_{\Gamma^N} + \sum_{i=1}^{2} (p_i,\, \boldsymbol{v} \cdot \boldsymbol{n}_i)_\gamma = (\boldsymbol{q},\, \boldsymbol{v})_{\Omega}.$$

Since $\boldsymbol{n} = \boldsymbol{n}_1 = -\boldsymbol{n}_2$, using the relation $\llbracket ab \rrbracket_\gamma = \llbracket a \rrbracket_\gamma \{\!\!\{ b \}\!\!\}_\gamma + \{\!\!\{ a \}\!\!\}_\gamma \llbracket b \rrbracket_\gamma$ and the coupling conditions for γ (3.32) we have

$$
\sum_{i=1}^{2} (p_i,\, \boldsymbol{v} \cdot \boldsymbol{n}_i)_\gamma = \int_\gamma \llbracket p\boldsymbol{v} \rrbracket_\gamma \cdot \boldsymbol{n} = \left(\llbracket p \rrbracket_\gamma,\, \{\!\!\{ \boldsymbol{v} \cdot \boldsymbol{n} \}\!\!\}_\gamma \right)_\gamma + \left(\{\!\!\{ p \}\!\!\}_\gamma,\, \llbracket \boldsymbol{v} \cdot \boldsymbol{n} \rrbracket_\gamma \right)_\gamma =
$$
$$
= \left(\eta_\gamma \{\!\!\{ \boldsymbol{u} \cdot \boldsymbol{n} \}\!\!\}_\gamma,\, \{\!\!\{ \boldsymbol{v} \cdot \boldsymbol{n} \}\!\!\}_\gamma \right)_\gamma - \left(d \{\!\!\{ \boldsymbol{q} \cdot \boldsymbol{n} \}\!\!\}_\gamma,\, \{\!\!\{ \boldsymbol{v} \cdot \boldsymbol{n} \}\!\!\}_\gamma \right)_\gamma +
$$
$$
+ \xi_0 \left(\eta_\gamma \llbracket \boldsymbol{u} \cdot \boldsymbol{n} \rrbracket_\gamma,\, \llbracket \boldsymbol{v} \cdot \boldsymbol{n} \rrbracket_\gamma \right)_\gamma + \left(\frac{d}{4} \llbracket \boldsymbol{q} \cdot \boldsymbol{n} \rrbracket_\gamma,\, \llbracket \boldsymbol{v} \cdot \boldsymbol{n} \rrbracket_\gamma \right)_\gamma + \left(\hat{p},\, \llbracket \boldsymbol{v} \cdot \boldsymbol{n} \rrbracket_\gamma \right)_\gamma .
$$

Introducing the bilinear forms $a(\cdot,\, \cdot) : \boldsymbol{V} \times \boldsymbol{V} \to \mathbb{R}$ and $d(\cdot,\, \cdot) : \boldsymbol{V} \times \hat{Q} \to \mathbb{R}$ and the functionals $F_{\boldsymbol{q}} \in \boldsymbol{V}'$ as

$$
a(\boldsymbol{u},\, \boldsymbol{v}) := \left(\boldsymbol{K}^{-1} \boldsymbol{u},\, \boldsymbol{v} \right)_\Omega + \left(\eta_\gamma \{\!\!\{ \boldsymbol{u} \cdot \boldsymbol{n} \}\!\!\}_\gamma,\, \{\!\!\{ \boldsymbol{v} \cdot \boldsymbol{n} \}\!\!\}_\gamma \right)_\gamma +
$$
$$
+ \xi_0 \left(\eta_\gamma \llbracket \boldsymbol{u} \cdot \boldsymbol{n} \rrbracket_\gamma,\, \llbracket \boldsymbol{v} \cdot \boldsymbol{n} \rrbracket_\gamma \right)_\gamma ,
$$
$$
d(\boldsymbol{v},\, \hat{p}) := \left(\hat{p},\, \llbracket \boldsymbol{v} \cdot \boldsymbol{n} \rrbracket_\gamma \right)_\gamma , \tag{3.40}
$$

and

$$
F_{\boldsymbol{q}}(\boldsymbol{v}) := - (\overline{p},\, \boldsymbol{v} \cdot \boldsymbol{n}_\Gamma)_{\Gamma^N} + (\boldsymbol{q},\, \boldsymbol{v})_\Omega + \left(d \{\!\!\{ \boldsymbol{q} \cdot \boldsymbol{n} \}\!\!\}_\gamma,\, \{\!\!\{ \boldsymbol{v} \cdot \boldsymbol{n} \}\!\!\}_\gamma \right)_\gamma +
$$
$$
- \left(\frac{d}{4} \llbracket \boldsymbol{q} \cdot \boldsymbol{n} \rrbracket_\gamma,\, \llbracket \boldsymbol{v} \cdot \boldsymbol{n} \rrbracket_\gamma \right)_\gamma ,
$$

then the weak formulation of the second equation of system (3.31) with the coupling conditions on γ becomes

$$
a(\boldsymbol{u},\, \boldsymbol{v}) + b(\boldsymbol{v},\, p) + d(\boldsymbol{v},\, \hat{p}) = F_{\boldsymbol{q}}(\boldsymbol{v}) \quad \forall \boldsymbol{v} \in \boldsymbol{V} .
$$

We derive the weak formulation of the equations in the fracture, taking a test function $\hat{w} \in \hat{Q}$ multiply and integrate on γ the third equation of (3.31) becomes

$$
(\nabla_{\boldsymbol{\tau}} \cdot \hat{\boldsymbol{u}},\, \hat{w})_\gamma - \left(\llbracket \boldsymbol{u} \cdot \boldsymbol{n} \rrbracket_\gamma,\, \hat{w} \right)_\gamma = (\hat{q},\, \hat{w})_\gamma ,
$$

introducing the bilinear form $\hat{b}(\cdot,\, \cdot) : \hat{\boldsymbol{V}} \times \hat{Q} \to \mathbb{R}$ and the functional $\hat{F}_{\hat{q}} \in \hat{Q}'$

$$
\hat{b}(\hat{\boldsymbol{u}},\, \hat{w}) := -(\nabla_{\boldsymbol{\tau}} \cdot \hat{\boldsymbol{u}},\, \hat{w})_\gamma \quad \text{and} \quad \hat{F}_{\hat{q}}(\hat{w}) := (\hat{q},\, \hat{w})_\gamma , \tag{3.41}
$$

the weak formulation of the third equation of (3.31) reads

$$
\hat{b}(\hat{\boldsymbol{u}},\, \hat{w}) + d(\boldsymbol{u},\, \hat{w}) = -\hat{F}_{\hat{q}}(\hat{w}) \quad \forall \hat{w} \in \hat{Q} .
$$

Taking a test function $\hat{\boldsymbol{v}} \in \hat{\boldsymbol{V}}$ and integrating on γ, the fourth equation of (3.31) becomes

$$
(\hat{\eta} \hat{\boldsymbol{u}},\, \hat{\boldsymbol{v}})_\gamma + (\nabla_{\boldsymbol{\tau}} \hat{p},\, \hat{\boldsymbol{v}})_\gamma - (\hat{\boldsymbol{q}},\, \hat{\boldsymbol{v}})_\gamma =
$$
$$
= (\hat{\eta} \hat{\boldsymbol{u}},\, \hat{\boldsymbol{v}})_\gamma - (\hat{p},\, \nabla_{\boldsymbol{\tau}} \cdot \hat{\boldsymbol{v}})_\gamma + (\hat{p},\, \hat{\boldsymbol{v}} \cdot \boldsymbol{n}_\Gamma)_{\partial\gamma} - (\hat{\boldsymbol{q}},\, \hat{\boldsymbol{v}})_\gamma = 0 .
$$

Using the boundary conditions (3.33) and introducing the bilinear form $\hat{a}(\cdot, \cdot):$ $\hat{\boldsymbol{V}} \times \hat{\boldsymbol{V}} \to \mathbb{R}$ and the functional $\hat{F}_{\hat{q}} \in \hat{\boldsymbol{V}}'$

$$\hat{a}(\hat{\boldsymbol{u}}, \hat{\boldsymbol{v}}) := (\hat{\eta}\hat{\boldsymbol{u}}, \hat{\boldsymbol{v}})_\gamma \quad \text{and} \quad \hat{F}_{\hat{q}}(\hat{\boldsymbol{v}}) := (\hat{q}, \hat{\boldsymbol{v}})_\gamma - \left(\overline{\hat{p}}, \hat{\boldsymbol{v}} \cdot \boldsymbol{n}_\Gamma\right)_{\partial\gamma^N},$$

we obtain the weak formulation of the fourth equation of (3.31)

$$\hat{a}(\hat{\boldsymbol{u}}, \hat{\boldsymbol{v}}) + \hat{b}(\hat{\boldsymbol{v}}, \hat{p}) = \hat{F}_{\hat{q}}(\hat{\boldsymbol{v}}) \quad \forall \hat{\boldsymbol{v}} \in \hat{\boldsymbol{V}}.$$

We define the global bilinear forms for the medium and the fracture as $\alpha(\cdot, \cdot):$ $\boldsymbol{V} \times \boldsymbol{V} \to \mathbb{R}$, $\beta(\cdot, \cdot): \boldsymbol{V} \times \mathcal{Q} \to \mathbb{R}$ and $\mathcal{A}(\cdot, \cdot): \mathcal{D} \times \mathcal{D} \to \mathbb{R}$

$$\alpha(\mathbf{u}, \mathbf{v}) := a(\boldsymbol{u}, \boldsymbol{v}) + \hat{a}(\hat{\boldsymbol{u}}, \hat{\boldsymbol{v}}),$$
$$\beta(\mathbf{v}, \mathrm{p}) := b(\boldsymbol{v}, p) + \hat{b}(\hat{\boldsymbol{v}}, \hat{p}) + d(\boldsymbol{v}, \hat{p}),$$
$$\mathcal{A}[(\mathbf{u}, \mathrm{p}), (\mathbf{v}, \mathrm{w})] := \alpha(\mathbf{u}, \mathbf{v}) + \beta(\mathbf{v}, \mathrm{p}) - \beta(\mathbf{u}, \mathrm{w})$$

and the global functionals for the medium and the fracture as $\mathcal{F}_{\boldsymbol{q}} \in \boldsymbol{V}'$, $\mathcal{F}_q \in \mathcal{Q}'$ and $\mathcal{F} \in \mathcal{D}'$

$$\mathcal{F}_{\boldsymbol{q}}(\mathbf{v}) := F_{\boldsymbol{q}}(\boldsymbol{v}) + \hat{F}_{\hat{q}}(\hat{\boldsymbol{v}}) \quad \text{and} \quad \mathcal{F}_q(\mathrm{w}) := -F_q(w) - \hat{F}_{\hat{q}}(\hat{w}),$$
$$\mathcal{F}(\mathbf{v}, \mathrm{w}) := \mathcal{F}_{\boldsymbol{q}}(\mathbf{v}) + \mathcal{F}_q(\mathrm{w}).$$

Indicating with $\mathbf{u} := (\boldsymbol{u}, \hat{\boldsymbol{u}}) \in \boldsymbol{V}$ the Darcy velocity in the medium and in the fracture, $\mathrm{p} := (p, \hat{p}) \in \mathcal{Q}$ the pressure in the medium and in the fracture we introduce the following problem.

Problem 3.4 (Weak Formulation of Darcy Reduced Model). *Under Assumption 3.1, Assumption 3.2, Assumption 3.3 and Assumption 3.4 the weak formulation of Problem 3.3 is: find* $(\mathbf{u}, \mathrm{p}) \in \mathcal{D}$ *such that*

$$\begin{cases} \alpha(\mathbf{u}, \mathbf{v}) + \beta(\mathbf{v}, \mathrm{p}) = \mathcal{F}_{\boldsymbol{q}}(\mathbf{v}) & \forall \mathbf{v} \in \boldsymbol{V}, \\ \beta(\mathbf{u}, \mathrm{w}) = \mathcal{F}_q(\mathrm{w}) & \forall \mathrm{w} \in \mathcal{Q}, \end{cases}$$

or alternatively

$$\mathcal{A}[(\mathbf{u}, \mathrm{p}), (\mathbf{v}, \mathrm{w})] = \mathcal{F}(\mathbf{v}, \mathrm{w}) \quad \forall(\mathbf{v}, \mathrm{w}) \in \mathcal{D}.$$

In [57] the authors prove the following theorem of existence and uniqueness

Theorem 3.3 (Existence and uniqueness [57]). *Assume that* $\xi_0 > 0$ *then Problem 3.4 has a unique solution.*

Lemma 3.4 (Global conservation of mass). *Assume that* $q_i \equiv 0$ *and* $\hat{q} \equiv 0$ *then the solution* $\mathbf{u} \in \boldsymbol{V}$ *of Problem 3.4 satisfies*

$$\int_{\partial A} \mathbf{u} \cdot \boldsymbol{n}_A = 0 \quad \forall A \subset \Omega,$$

with A an open bounded measurable subset of $\mathbb{R}^n$ with Lipschitz boundary ∂A and with outward unit normal $\boldsymbol{n}_A$.
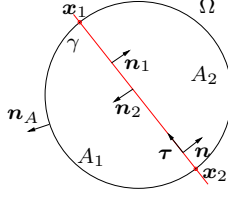
Figure 3.6: Example of domain $A \subset \Omega$ for $n = 2$.

Proof. If $A \cap \gamma = \emptyset$ then the proof is trivial. Let assume that $A \cap \gamma \neq \emptyset$ like in Figure 3.6. Then we can divide A into two connected subset called A_1 and A_2 such that

$$\overline{A} = \overline{A}_1 \cup \overline{A}_2 \quad \text{and} \quad \mathring{A}_1 \cap \mathring{A}_2 = \emptyset \,,$$

thus $\gamma = \partial A_1 \cap \partial A_2$. Taking $\mathbf{u} \in \mathcal{V}$ solution of Problem 3.4 with $\mathrm{w} \equiv 1$ we have

$$\int_A \nabla \cdot \mathbf{u} = \int_{A_1} \nabla \cdot \boldsymbol{u}_1 + \int_{A_2} \nabla \cdot \boldsymbol{u}_2 + \int_\gamma \nabla_{\boldsymbol{\tau}} \cdot \hat{\boldsymbol{u}} = \int_\gamma [\![\boldsymbol{u} \cdot \boldsymbol{n}]\!]_\gamma \,. \tag{3.42}$$

Then since $\boldsymbol{u}_i$ is solution of Problem 3.4 in A_i we have

$$\int_{A_i} \nabla \cdot \boldsymbol{u}_i = \int_{\partial A_i \setminus \gamma} \boldsymbol{u}_i \cdot \boldsymbol{n}_A + \int_\gamma \boldsymbol{u}_i \cdot \boldsymbol{n}_i \,,$$

furthermore $\hat{\boldsymbol{u}}$ is solution of Problem 3.4 in γ we obtain

$$\int_\gamma \nabla_{\boldsymbol{\tau}} \cdot \hat{\boldsymbol{u}} = \int_{\partial \gamma} \hat{\boldsymbol{u}} \cdot \boldsymbol{n}_A \,.$$

Hence we have

$$\int_A \nabla \cdot \mathbf{u} = \sum_{i=1}^2 \int_{\partial A_i \setminus \gamma} \boldsymbol{u}_i \cdot \boldsymbol{n}_A + \int_{\partial \gamma} \hat{\boldsymbol{u}} \cdot \boldsymbol{n}_A + \int_\gamma [\![\boldsymbol{u} \cdot \boldsymbol{n}]\!]_\gamma \,,$$

finally using the above relation with (3.42) we obtain the result. $\qquad \square$

3.2 Single-phase Darcy equation with intersection

In nature macro or micro fractures can intersect, we want to extend the model introduced previously to take into account this configuration. Let us consider the sketch of an intersection between fractures illustrated in Figure 3.7.
The two fractures Ω_{f_1} and Ω_{f_2} are identified by the two lines γ_1 and γ_2. We will indicate with s_1 and s_2 the curvilinear coordinate along γ_1 and γ_2, respectively. The intersection point $\boldsymbol{i}_p$ has curvilinear coordinate $s_{\boldsymbol{i}_p,1}$ and $s_{\boldsymbol{i}_p,2}$ respectively on γ_1 and γ_2. The physical fracture intersect in a region of the plane I which is modelled as a quadrilateral. In the reduced model we assume that the fluxes $\hat{\boldsymbol{u}}_1$ and $\hat{\boldsymbol{u}}_2$ along fractures and the pressure $\hat{p}_1$ and $\hat{p}_2$ are discontinuous at
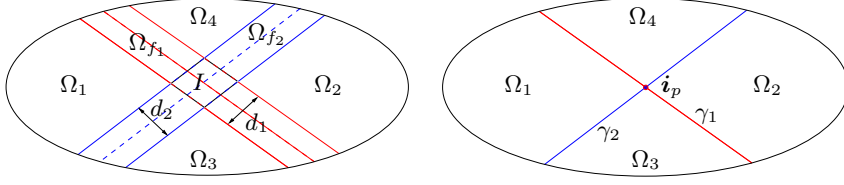
Figure 3.7: Example of a bi-dimensional domain with two fractures intersecting once and the corresponding reduced model.

the intersection point $\boldsymbol{i}_p$. We denote with $\hat{p}_I$ the value of the pressure at the intersection point. We set for $i = 1, 2$

$$\hat{\boldsymbol{u}}_{i,1} := \lim_{s_i \to s_{\boldsymbol{i}_p,i}^-} \hat{\boldsymbol{u}}_i \,, \qquad \hat{\boldsymbol{u}}_{i,2} := \lim_{s_i \to s_{\boldsymbol{i}_p,i}^+} \hat{\boldsymbol{u}}_i \,,$$

$$\hat{p}_{i,1} := \lim_{s_i \to s_{\boldsymbol{i}_p,i}^-} \hat{p}_i \,, \qquad \hat{p}_{i,2} := \lim_{s_i \to s_{\boldsymbol{i}_p,i}^+} \hat{p}_i \,,$$

more over we set

$$[\![a_i]\!]_{\boldsymbol{i}_p} := a_{i,1} - a_{i,2} \quad \text{and} \quad \{\!\{a_i\}\!\}_{\boldsymbol{i}_p} := \frac{a_{i,1} + a_{i,2}}{2} \,.$$

We start the derivation of new coupling conditions from the following requests. For the sake of simplicity we consider here only the case $n = 2$.

Assumption 3.5 (Intersecting fractures). *We require:*

1. *the problem is composed by two different fractures, for each fracture we assume that Assumption 3.1 is valid and we indicate quantities of a fracture with an additional subscript. See Figure 3.8 for an example;*
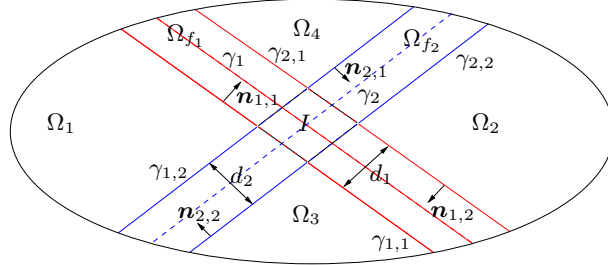

Figure 3.8: Example of a bi-dimensional domain with two fractures intersecting once.

2. *we define*

$$\partial \gamma^N := \bigcup_{i=1}^2 \partial \gamma_i^N \,, \quad \text{and} \quad \partial \gamma^E := \bigcup_{i=1}^2 \partial \gamma_i^E \,;$$

3. *the intersection area involves two different fractures Ω_{f_1} and Ω_{f_2} and*

$$I := \Omega_{f_1} \cap \Omega_{f_2} \,,$$

is a connected subset with boundary ∂I. Using Assumption 3.1-2 the domain Ω is thus divided into four disjoint parts, see Figure 3.8 for a schematic example;

81

4. we assume that I can be modelled as a quadrilateral with parallel sides. The thickness d_i of each fracture Ω_{f_i} does not change inside the intersecting region I. We introduce

$$d_i^* := \frac{d_i}{\sin \theta} = \frac{d_i}{\sqrt{1 - (\boldsymbol{\tau}_1 \cdot \boldsymbol{\tau}_2)^2}} \,,$$

see Figure 3.9 for an example. We can write the intersecting region I as

$$I = \left\{ \boldsymbol{x} \in \Omega : \boldsymbol{x} = \boldsymbol{i}_p + x_1 \boldsymbol{\tau}_1 + x_2 \boldsymbol{\tau}_2, \, x_i \in \left(-\frac{d_j^*}{2}, \frac{d_j^*}{2} \right) \text{ for } i \neq j = 1, 2 \right\} \,,$$

furthermore

$$|I| = d_1^* d_2^* |\sin \theta| = d_1^* d_2^* \sqrt{1 - (\boldsymbol{\tau}_1 \cdot \boldsymbol{\tau}_2)^2} = \frac{d_1 d_2}{\sqrt{1 - (\boldsymbol{\tau}_1 \cdot \boldsymbol{\tau}_2)^2}} \,;$$
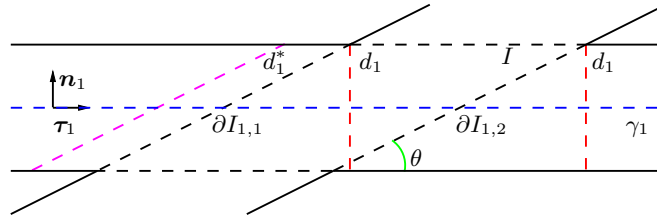

Figure 3.9: Example of a bi-dimensional intersection between two fractures.

5. we can partition the boundary ∂I into four disjoint pieces $\partial I_{i,j}$, for $i, j = 1, 2$, such that

$$\partial I_{i,1} \cup \partial I_{i,2} = \partial I \cap \Omega_{f_i} \quad \forall i = 1, 2 \,,$$

see Figure 3.9 for an example. Furthermore we assume that each $\partial I_{i,j}$ can be approximated by a straight line;

6. the permeability tensor in the intersection $\boldsymbol{K}_I$, which fulfils Assumption 3.2-2, is constant;

7. we assume Assumption 3.2-1 for the scalar source q_I, i.e. $q_i \in L^2(I)$;

8. the domain I is "smaller" than each Ω_i for $i = 1, \dots, 4$, i.e.

$$\text{diam}(\Omega_i) \gg \text{diam}(I) \quad \text{ for } i = 1, \dots, 4 \,.$$

With this assumption we can identify I with its centre point if $n = 2$ or its centre line if $n = 3$ defined as $\boldsymbol{i}_p := \gamma_1 \cap \gamma_2$, which divides each fracture into two disjoint parts

$$\mathring{\gamma}_j = \mathring{\gamma}_{j_1} \cup \boldsymbol{i}_p \cup \mathring{\gamma}_{j_2} \quad \text{ for } j = 1, 2 \,.$$

We need now to find proper matching conditions for the reduced models at point $\boldsymbol{i}_p$. First of all let us note that the mass conservation implies

$$\sum_{k=1}^{2} [\![\hat{\boldsymbol{u}}_k \cdot \boldsymbol{\tau}_k]\!]_{\boldsymbol{i}_p} = 0 \,,$$

since we neglect the contribution of the source term in I. The momentum equation of the Darcy model implies that

$$-\boldsymbol{K}_I^{-1} \boldsymbol{u}_I = \nabla p_I \quad \text{in } I \,. \tag{3.43}$$

The coupling conditions (3.6) still hold if we consider each piece of the boundary of the intersection. To derive the first coupling condition we integrate the previous equation on I and we assume

$$\int_{\partial I_{i,j}} \boldsymbol{u}_I \approx \hat{\boldsymbol{u}}_{i,j} \quad \text{and} \quad \frac{1}{d_i^*} \int_{\partial I_{i,j}} p_I \approx \hat{p}_{i,j} \,. \tag{3.44}$$

We approximate the integral involving the velocity $\boldsymbol{u}_I$ by the trapezium rule for each fracture, then using the definition (3.10) and Assumption 3.5-6 we find

$$-\int_I \boldsymbol{K}_I^{-1} \boldsymbol{u}_I = -\boldsymbol{K}_I^{-1} \int_I \boldsymbol{u}_I \approx -\boldsymbol{K}_I^{-1} \frac{|I|}{2} \sum_{i=1}^{2} \frac{\hat{\boldsymbol{u}}_{i,1} + \hat{\boldsymbol{u}}_{i,2}}{d_i^*} =$$

$$= -\boldsymbol{K}_I^{-1} |I| \sum_{i=1}^{2} \frac{1}{d_i^*} \{\!\!\{ \hat{\boldsymbol{u}}_i \}\!\!\}_{\boldsymbol{i}_p} \,. \tag{3.45}$$

Furthermore the integral of the pressure p_I in the intersection becomes

$$\int_I \nabla p_I = \int_{\partial I} p_I \boldsymbol{n}_{\partial I} = \boldsymbol{n}_2 \int_{\partial I_{1,2}} p_I - \boldsymbol{n}_2 \int_{\partial I_{1,1}} p_I + \boldsymbol{n}_1 \int_{\partial I_{2,2}} p_I - \boldsymbol{n}_1 \int_{\partial I_{2,1}} p_I \approx$$

$$\approx (\hat{p}_{1,2} - \hat{p}_{1,1}) \, \boldsymbol{n}_2 d_1^* + (\hat{p}_{2,2} - \hat{p}_{2,1}) \, \boldsymbol{n}_1 d_2^* = - [\![\hat{p}_1]\!]_{\boldsymbol{i}_p} \boldsymbol{n}_2 d_1^* - [\![\hat{p}_2]\!]_{\boldsymbol{i}_p} \boldsymbol{n}_1 d_2^* \tag{3.46}$$

Hence using the relations (3.45) and (3.46), equation (3.43) becomes

$$\boldsymbol{K}_I^{-1} |I| \sum_{i=1}^{2} \frac{1}{d_i^*} \{\!\!\{ \hat{\boldsymbol{u}}_i \}\!\!\}_{\boldsymbol{i}_p} = [\![\hat{p}_1]\!]_{\boldsymbol{i}_p} \boldsymbol{n}_2 d_1^* + [\![\hat{p}_2]\!]_{\boldsymbol{i}_p} \boldsymbol{n}_1 d_2^* \,,$$

multiplying the above relation by $\boldsymbol{\tau}_1$, or equivalently by $\boldsymbol{\tau}_2$, and using the identity $d_1 = d_1^* \boldsymbol{n}_2 \cdot \boldsymbol{\tau}_1$ we obtain a reduced model for the intersection valid for $j = 1$ and 2

$$\boldsymbol{\tau}_j^\top \cdot \boldsymbol{K}_I^{-1} \frac{|I|}{d_j} \sum_{i=1}^{2} \frac{1}{d_i^*} \{\!\!\{ \hat{\boldsymbol{u}}_i \}\!\!\}_{\boldsymbol{i}_p} = [\![\hat{p}_j]\!]_{\boldsymbol{i}_p} \quad \text{in } \boldsymbol{i}_p \,. \tag{3.47}$$

Assumption 3.6 (Orthogonal fractures)**.** *The two fractures γ_1 and γ_2 are orthogonal and the permeability tensor is diagonal, namely*

$$\boldsymbol{K}_I^{-1} = \begin{bmatrix} \eta_{\gamma_1}/d_1 & 0 \\ 0 & \eta_{\gamma_2}/d_2 \end{bmatrix} \,.$$

With these requirements the relations (3.44) are exact.

Under Assumption 3.6 the reduced model (3.47) can be simplified, for $i, j = 1, 2$ and $i \neq j$, as

$$\frac{\eta_{\gamma_i}}{d_j} \left\{\!\!\left\{ \hat{\boldsymbol{u}}_j \cdot \boldsymbol{\tau}_j \right\}\!\!\right\}_{\boldsymbol{i}_p} = [\![\hat{p}_j]\!]_{\boldsymbol{i}_p} \qquad \text{in } \boldsymbol{i}_p \,. \tag{3.48}$$

In this relation, very similar to (3.19), the jump of the pressure depends on the permeability of the other fracture i which can act as a barrier or a preferential path for the current fracture j. Furthermore decreasing the thickness of the fracture j the pressure jump increases, while increasing the thickness of the other fracture i the pressure jump decreases, and this is physically correct. Defining the pressure in the intersection region $\hat{p}_I$ as
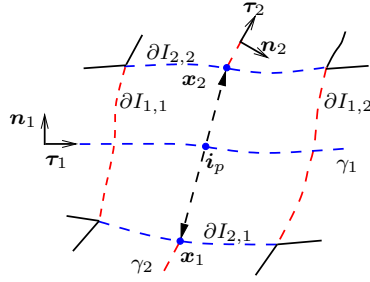

Figure 3.10: Example of a bi-dimensional intersection between two fractures.

$$\hat{p}_I := \frac{1}{|I|} \int_I p_I \,, \tag{3.49}$$

we use the same arguments as in subsection 3.1.4 to close the system. For each fracture j in the first transversal section, see Figure 3.10 for an example, we approximate the value of the pressure in the intersection point $\boldsymbol{i}_p$ by the following Taylor expansion

$$p_{f_j}(\boldsymbol{i}_p) = p_I(\boldsymbol{x}_1) + \frac{d_j^*}{2} \nabla p_I(\boldsymbol{\theta}_1) \cdot \boldsymbol{\tau}_i \quad i \neq j \,, \tag{3.50}$$

where $\boldsymbol{\theta}_1 = \boldsymbol{i}_p - \xi_1 \dfrac{d_j^*}{2} \boldsymbol{\tau}_i$ and $\xi_1 \in [0, 1]$. In the second transversal section we approximate the value of the pressure in the intersection point $\boldsymbol{i}_p$ by

$$p_{f_j}(\boldsymbol{i}_p) = p_I(\boldsymbol{x}_2) - \frac{d_j^*}{2} \nabla p_I(\boldsymbol{\theta}_2) \cdot \boldsymbol{\tau}_i \quad i \neq j \,, \tag{3.51}$$

where $\boldsymbol{\theta}_2 = \boldsymbol{i}_p + \xi_2 \dfrac{d_j^*}{2} \boldsymbol{\tau}_i$ and $\xi_2 \in [0, 1]$. Using the relation (3.6) we find $p_I(\boldsymbol{x}_k) = p_{f_i}|_{\partial I_{i,k}}$, for $k = 1, 2$ and with (3.43) equations (3.50) and (3.51) become

$$p_{f_j}(\boldsymbol{i}_p) = p_i|_{\partial I_{i,1}} - \frac{d_j^*}{2} \boldsymbol{\tau}_i^\top \cdot \boldsymbol{K}_I^{-1} \boldsymbol{u}_I(\boldsymbol{\theta}_1) \,,$$

$$p_{f_j}(\boldsymbol{i}_p) = p_i|_{\partial I_{i,2}} + \frac{d_j^*}{2} \boldsymbol{\tau}_i^\top \cdot \boldsymbol{K}_I^{-1} \boldsymbol{u}_I(\boldsymbol{\theta}_2) \,.$$

The values of $\boldsymbol{u}_I$ in $\boldsymbol{\theta}_k$ for $k = 1, 2$ are unknown, therefore using (3.6) we express them by the following combination

$$\boldsymbol{u}_I (\boldsymbol{\theta}_1) = \xi_1 \, \boldsymbol{u}_i|_{\partial I_{i,1}} + (1 - \xi_1) \, \boldsymbol{u}_i|_{\partial I_{i,2}} + \frac{1}{2} \, \boldsymbol{u}_j|_{\partial I_{j,1}} + \frac{1}{2} \, \boldsymbol{u}_j|_{\partial I_{j,2}} \text{ for } \xi_1 \in [0, \, 1],$$

$$\boldsymbol{u}_I (\boldsymbol{\theta}_2) = \xi_2 \, \boldsymbol{u}_i|_{\partial I_{i,2}} + (1 - \xi_2) \, \boldsymbol{u}_i|_{\partial I_{i,1}} + \frac{1}{2} \, \boldsymbol{u}_j|_{\partial I_{j,1}} + \frac{1}{2} \, \boldsymbol{u}_j|_{\partial I_{j,2}} \text{ for } \xi_2 \in [0, \, 1].$$

Using the previous expression the pressure of the fracture j in the intersection becomes

$$p_{f_j} (\boldsymbol{i}_p) = p_i|_{\partial I_{i,1}} - \frac{d_j^*}{2} \boldsymbol{\tau}_i^\top \cdot \boldsymbol{K}_I^{-1} \left[\xi_1 \, \boldsymbol{u}_i|_{\partial I_{i,1}} + (1 - \xi_1) \, \boldsymbol{u}_i|_{\partial I_{i,2}} + \right.$$
$$\left. + \frac{1}{2} \, \boldsymbol{u}_j|_{\partial I_{j,1}} + \frac{1}{2} \, \boldsymbol{u}_j|_{\partial I_{j,2}} \right],$$

and

$$p_{f_j} (\boldsymbol{i}_p) = p_i|_{\partial I_{i,2}} + \frac{d_j^*}{2} \boldsymbol{\tau}_i^\top \cdot \boldsymbol{K}_I^{-1} \left[\xi_2 \, \boldsymbol{u}_i|_{\partial I_{i,2}} + (1 - \xi_2) \, \boldsymbol{u}_i|_{\partial I_{i,1}} + \right.$$
$$\left. + \frac{1}{2} \, \boldsymbol{u}_j|_{\partial I_{j,1}} + \frac{1}{2} \, \boldsymbol{u}_j|_{\partial I_{j,2}} \right].$$

Integrating the above relations in I and using the midpoint rule to approximate (3.49) we find

$$\hat{p}_I |I| \approx d_i^* d_j \hat{p}_{i,1} - \frac{d_j^*}{2} \boldsymbol{\tau}_i^\top \cdot \boldsymbol{K}_I^{-1} \left[d_j \, \{\!\{ \hat{\boldsymbol{u}}_i \}\!\}_{\boldsymbol{i}_p} + d_i \, \{\!\{ \hat{\boldsymbol{u}}_j \}\!\}_{\boldsymbol{i}_p} + d_j \left(\xi_1 - \frac{1}{2} \right) [\![\hat{\boldsymbol{u}}_i]\!]_{\boldsymbol{i}_p} \right],$$

$$\hat{p}_I |I| \approx d_i^* d_j \hat{p}_{i,2} + \frac{d_j^*}{2} \boldsymbol{\tau}_i^\top \cdot \boldsymbol{K}_I^{-1} \left[d_j \, \{\!\{ \hat{\boldsymbol{u}}_i \}\!\}_{\boldsymbol{i}_p} + d_i \, \{\!\{ \hat{\boldsymbol{u}}_j \}\!\}_{\boldsymbol{i}_p} - d_j \left(\xi_2 - \frac{1}{2} \right) [\![\hat{\boldsymbol{u}}_i]\!]_{\boldsymbol{i}_p} \right].$$

Using the coupling condition (3.47)

$$\hat{p}_I = \hat{p}_{i,1} - \frac{d_j}{d_i} \frac{1}{2} \boldsymbol{\tau}_i^\top \cdot \boldsymbol{K}_I^{-1} \left[\{\!\{ \hat{\boldsymbol{u}}_i \}\!\}_{\boldsymbol{i}_p} + \frac{d_i}{d_j} \, \{\!\{ \hat{\boldsymbol{u}}_j \}\!\}_{\boldsymbol{i}_p} + \left(\xi_1 - \frac{1}{2} \right) [\![\hat{\boldsymbol{u}}_i]\!]_{\boldsymbol{i}_p} \right] =$$
$$= \hat{p}_{i,1} - \frac{1}{2} [\![\hat{p}_i]\!]_{\boldsymbol{i}_p} - \frac{d_j}{d_i} \frac{(2\xi_1 - 1)}{4} \boldsymbol{\tau}_i^\top \cdot \boldsymbol{K}_I^{-1} [\![\hat{\boldsymbol{u}}_i]\!]_{\boldsymbol{i}_p} =$$
$$= \{\!\{ \hat{p}_i \}\!\}_{\boldsymbol{i}_p} - \frac{d_j}{d_i} \frac{(2\xi_1 - 1)}{4} \boldsymbol{\tau}_i^\top \cdot \boldsymbol{K}_I^{-1} [\![\hat{\boldsymbol{u}}_i]\!]_{\boldsymbol{i}_p} \, ,$$

and

$$\hat{p}_I = \{\!\{ \hat{p}_i \}\!\}_{\boldsymbol{i}_p} - \frac{d_j}{d_i} \frac{(2\xi_2 - 1)}{4} \boldsymbol{\tau}_i^\top \cdot \boldsymbol{K}_I^{-1} [\![\hat{\boldsymbol{u}}_i]\!]_{\boldsymbol{i}_p} \, .$$

The pressure $\hat{p}_I$ is single value thus $\xi_1 = \xi_2 = \xi$. In conclusion the second coupling condition is

$$\hat{\xi}_0 \frac{d_j}{d_i} \boldsymbol{\tau}_i^\top \cdot \boldsymbol{K}_I^{-1} [\![\hat{\boldsymbol{u}}_i]\!]_{\boldsymbol{i}_p} = \{\!\{ \hat{p}_i \}\!\}_{\boldsymbol{i}_p} - \hat{p}_I \quad \text{in } \boldsymbol{i}_p, \tag{3.52}$$

with $\hat{\xi}_0 := (2\xi - 1)/4$. Furthermore using Assumption 3.6 we obtain the following simplified relation

$$\hat{\xi}_0 \frac{\eta_{\gamma_j}}{d_i} [\![\hat{\boldsymbol{u}}_i \cdot \boldsymbol{\tau}_i]\!]_{\boldsymbol{i}_p} = \{\!\{ \hat{p}_i \}\!\}_{\boldsymbol{i}_p} - \hat{p}_I \quad \text{in } \boldsymbol{i}_p, \tag{3.53}$$

Using Assumption 3.5, hence approximating the domain Ω reported in Figure 3.8 to the domain in Figure 3.11, then Problem 3.2 written for each fracture coupled with (3.47) and (3.52) forms the reduced model with intersections summarized in the following problem.

Problem 3.5 (Reduced Model for Darcy Equation with Intersection). *Under Assumption 3.5, the reduced problem for the Darcy system of equation with two fractures intersecting once is: find the Darcy velocity and the pressure associated to the porous matrix, respectively $\boldsymbol{u}_i$ and p_i for $i = 1, \ldots, 4$, the reduced Darcy velocity and reduced pressure associated to each fracture, respectively $\hat{\boldsymbol{u}}_j$ and $\hat{p}_j$ for $j = 1, 2$ and the reduced pressure associated to the intersection point $\hat{p}_I$, which satisfy the following system of partial differential equations*

$$\begin{cases} \nabla \cdot \boldsymbol{u}_i = q_i & in \ \Omega_i, \\[2mm] \boldsymbol{K}_i^{-1} \boldsymbol{u}_i + \nabla p_i = \boldsymbol{0} & in \ \Omega_i, \\[2mm] \nabla_{\boldsymbol{\tau}_j} \cdot \hat{\boldsymbol{u}}_j = \hat{q}_j + [\![\boldsymbol{u} \cdot \boldsymbol{n}_j]\!]_{\gamma_j} & on \ \gamma_j, \\[2mm] \hat{\eta}_j \hat{\boldsymbol{u}}_j + \nabla_{\boldsymbol{\tau}_j} \hat{p}_j = \boldsymbol{0} & on \ \gamma_j, \end{cases} \tag{3.54}$$

coupled with the interface conditions for the matrix-fracture system for $j = 1, 2$

$$\begin{cases} \xi_{0j} \eta_{\gamma_j} [\![\boldsymbol{u} \cdot \boldsymbol{n}_j]\!]_{\gamma_j} = \{\!\!\{ p \}\!\!\}_{\gamma_j} - \hat{p}_j \\[2mm] \eta_{\gamma_j} \{\!\!\{ \boldsymbol{u} \cdot \boldsymbol{n}_j \}\!\!\}_{\gamma_j} = [\![p]\!]_{\gamma_j} \end{cases} \quad on \ \gamma_j \,, \tag{3.55}$$

and the coupling conditions for the fracture-fracture system for $i \neq j = 1, 2$

$$\begin{cases} \boldsymbol{\tau}_j^\top \cdot \boldsymbol{K}_I^{-1} \dfrac{|I|}{d_j} \sum_{i=1}^2 \dfrac{1}{d_i^*} \{\!\!\{ \hat{\boldsymbol{u}}_i \}\!\!\}_{\boldsymbol{i}_p} = [\![\hat{p}_j]\!]_{\boldsymbol{i}_p} \\[4mm] \hat{\xi}_0 \dfrac{d_j}{d_i} \boldsymbol{\tau}_i^\top \cdot \boldsymbol{K}_I^{-1} [\![\hat{\boldsymbol{u}}_i]\!]_{\boldsymbol{i}_p} = \{\!\!\{ \hat{p}_i \}\!\!\}_{\boldsymbol{i}_p} - \hat{p}_I & in \ \boldsymbol{i}_p \,, \\[4mm] \sum_{k=1}^2 [\![\hat{\boldsymbol{u}}_k \cdot \boldsymbol{\tau}_k]\!]_{\boldsymbol{i}_p} = 0 \end{cases} \tag{3.56}$$

and with the boundary conditions on $\partial\Omega$ for $i, j = 1, 2$

$$\begin{cases} p_i = \overline{p_i} & on \ \Gamma_i^N, \\[2mm] \boldsymbol{u}_i \cdot \boldsymbol{n}_\Gamma = \overline{u_i} & on \ \Gamma_i^E, \\[2mm] \hat{p}_j = \overline{\hat{p}_j} & on \ \partial\gamma_j^N, \\[2mm] \hat{\boldsymbol{u}}_j \cdot \boldsymbol{\tau}_j = \overline{\hat{\boldsymbol{u}}_j} \cdot \boldsymbol{\tau}_j & on \ \partial\gamma_j^E. \end{cases}$$

3.2.1 Weak formulation

We derive the weak formulation of the global reduced Problem 3.5 and for the sake of simplicity we require $\overline{u_i} = 0$ for $i = 1, \ldots, 4$ and $\overline{\hat{\boldsymbol{u}}_j} \cdot \boldsymbol{\tau}_j = 0$, for $j = 1, 2$ or
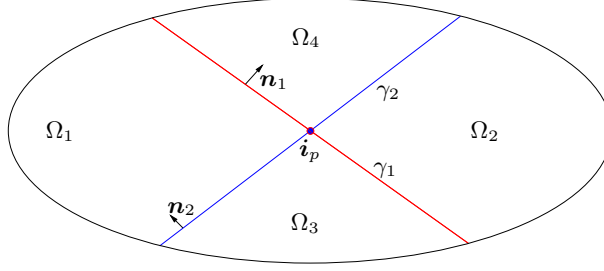
Figure 3.11: Example of the reduced bi-dimensional domain with two fractures intersecting once, from the original domain presented in Figure 3.8.

$\Gamma^E = \emptyset$, otherwise a lifting technique should be used. Furthermore to simplify the derivation of the weak formulation we assume Assumption 3.6. Indicating with

$$\gamma_j := \bigcup_{k=1}^{2} \gamma_{j,k}, \quad \gamma := \bigcup_{j=1}^{2} \gamma_j \quad \text{and} \quad D := \bigcup_{i=1}^{4} \Omega_i,$$

then we consider the functional space defined in (3.35) for $i = 1, \ldots, 4$. We introduce the broken functional space $\boldsymbol{V} : D \to \mathbb{R}^n$

$$\boldsymbol{V} := \left\{ \boldsymbol{v} : D \to \mathbb{R}^n : \ \boldsymbol{v}|_{\Omega_i} \in \boldsymbol{V}_i \text{ for } i = 1, \ldots, 4 \right\}, \tag{3.57}$$

which is an Hilbert space endowed with the inner product $(\cdot, \cdot)_{\boldsymbol{V}} : \boldsymbol{V} \times \boldsymbol{V} \to \mathbb{R}$ and associated norm $\|\cdot\|_{\boldsymbol{V}} : \boldsymbol{V} \to \mathbb{R}$, defined as

$$(\boldsymbol{u}, \boldsymbol{v})_{\boldsymbol{V}} := \sum_{i=1}^{4} (\boldsymbol{u}_i, \boldsymbol{v}_i)_{\boldsymbol{V}_i} \quad \text{and} \quad \|\boldsymbol{u}\|_{\boldsymbol{V}}^2 := \sum_{i=1}^{4} \|\boldsymbol{u}_i\|_{\boldsymbol{V}_i}^2.$$

Analogously the broken space $Q : D \to \mathbb{R}$

$$Q := \left\{ w : D \to \mathbb{R} : \ w|_{\Omega_i} \in Q_i \text{ for } i = 1, \ldots, 4 \right\}, \tag{3.58}$$

which is an Hilbert space with internal product $(\cdot, \cdot)_Q : Q \times Q \to \mathbb{R}$ and associated norm $\|\cdot\|_Q : Q \to \mathbb{R}$, defined as

$$(p, w)_Q := \sum_{i=1}^{4} (p_i, w_i)_{Q_i} \quad \text{and} \quad \|p\|_Q^2 := \sum_{i=1}^{4} \|p_i\|_{Q_i}^2.$$

Note that $\boldsymbol{V}$ and Q may be identified with a subset of $\left[L^2(\Omega) \right]^n$ and $L^2(\Omega)$, respectively since

$$\gamma = \bigcap_{i=1}^{4} \partial \Omega_i \setminus \{\boldsymbol{i}_p\}$$

is a set of zero Lebesgue measure in $\mathbb{R}^n$. Thus we will indicate for a $v \in Q$

$$\|v\|_{L^2(\Omega)}^2 = \sum_{i=1}^{4} \int_{\Omega_i} v_i^2 = \int_{\Omega} v^2,$$

where it is understood that v has been extended to the whole Ω. Analogously we define the $L^2(\Omega)$ norm of an element of $\boldsymbol{V}$. Considering the space $\boldsymbol{V}_\Omega$ in (3.36) then for a $\mathbf{v} \in \boldsymbol{V}_\Omega$ there is a unique $\boldsymbol{v} \in \boldsymbol{V}$ such that for $i = 1, \ldots, 4$ and $j = 1, 2$

$$\boldsymbol{v}|_{\Omega_i} = \mathbf{v}|_{\Omega_i} \quad \text{and} \quad [\![\mathbf{v} \cdot \boldsymbol{n}_j]\!]_{\gamma_j} = 0.$$

Analogously, considering the space Q_Ω in (3.36), for each $\mathrm{p} \in Q_\Omega$ there exist a unique $p \in \boldsymbol{V}$ such that for $i = 1, \ldots, 4$ and $j = 1, 2$

$$p|_{\Omega_i} = \mathrm{p}|_{\Omega_i} \quad \text{and} \quad [\![\mathrm{p}]\!]_{\gamma_j} = 0.$$

We consider also the functional spaces for the problem in each fractures: on each γ_j we consider a space of vector functions living in the tangent space, that is

$$\hat{\boldsymbol{V}}_{j,k} := \Big\{ \hat{\boldsymbol{v}} : \ \gamma_{j,k} \to \mathbb{R}^n, \ \hat{\boldsymbol{v}} \in \left[L^2\left(\gamma_{j,k}\right) \right]^n : \ \hat{\boldsymbol{v}} \cdot \boldsymbol{n}_j = 0,$$
$$\nabla_{\boldsymbol{\tau}_j} \cdot \hat{\boldsymbol{v}} \in L^2\left(\gamma_{j,k}\right) \ \text{and} \ < \hat{\boldsymbol{v}} \cdot \boldsymbol{n}_\Gamma, v > = 0 \, \forall v \in H^1_{0,\partial\gamma_j^N}\left(\gamma_j\right) \Big\},$$

and the space of scalar functions living in the tangent space

$$\hat{Q}_{j,k} := \Big\{ \hat{w} : \ \gamma_{j,k} \to \mathbb{R}, \ \hat{w} \in L^2\left(\gamma_{j,k}\right) : \ \nabla_{\boldsymbol{n}_j} \hat{w} = \boldsymbol{0} \ \text{and} \ \nabla_{\boldsymbol{\tau}_j} \hat{w} \in \left[L^2\left(\gamma_{j,k}\right) \right]^n \Big\}.$$

Both spaces are Hilbert spaces endowed with inner products $(\cdot, \cdot)_{\hat{\boldsymbol{V}}_{j,k}} : \ \hat{\boldsymbol{V}}_{j,k} \times \hat{\boldsymbol{V}}_{j,k} \to \mathbb{R}$ and $(\cdot, \cdot)_{\hat{Q}_{j,k}} : \ \hat{Q}_{j,k} \times \hat{Q}_{j,k} \to \mathbb{R}$, defined as

$$(\hat{\boldsymbol{u}}, \hat{\boldsymbol{v}})_{\hat{\boldsymbol{V}}_{j,k}} := (\hat{\boldsymbol{u}}, \hat{\boldsymbol{v}})_{\gamma_{j,k}} + \left(\nabla_{\boldsymbol{\tau}_j} \cdot \hat{\boldsymbol{u}}, \nabla_{\boldsymbol{\tau}_j} \cdot \hat{\boldsymbol{v}}\right)_{\gamma_{j,k}},$$
$$(\hat{p}, \hat{w})_{\hat{Q}_{j,k}} := (\hat{p}, \hat{w})_{\gamma_{j,k}} + \left(\nabla_{\boldsymbol{\tau}_j} \hat{p}, \nabla_{\boldsymbol{\tau}_j} \hat{w}\right)_{\gamma_{j,k}},$$

and norms $\|\cdot\|_{\hat{\boldsymbol{V}}_{j,k}} : \ \hat{\boldsymbol{V}}_{j,k} \to \mathbb{R}$ and $\|\cdot\|_{\hat{Q}_{j,k}} : \ \hat{Q}_{j,k} \to \mathbb{R}$, defined as

$$\|\hat{\boldsymbol{v}}\|^2_{\hat{\boldsymbol{V}}_{j,k}} := (\hat{\boldsymbol{v}}, \hat{\boldsymbol{v}})_{\hat{\boldsymbol{V}}_{j,k}} \quad \text{and} \quad \|\hat{w}\|^2_{\hat{Q}_{j,k}} := (\hat{w}, \hat{w})_{\hat{Q}_{j,k}}.$$

We will also use the broken space for vector value function on each piece of the fractures $\hat{\boldsymbol{V}}_j : \ \gamma_j \to \mathbb{R}^n$

$$\hat{\boldsymbol{V}}_j := \Big\{ \hat{\boldsymbol{v}} : \ \gamma_j \to \mathbb{R}^n : \ \hat{\boldsymbol{v}}_k := \hat{\boldsymbol{v}}|_{\gamma_{j,k}} \in \hat{\boldsymbol{V}}_{j,k} \Big\},$$

which is an Hilbert space endowed with inner product $(\cdot, \cdot)_{\hat{\boldsymbol{V}}_j} : \ \hat{\boldsymbol{V}}_j \times \hat{\boldsymbol{V}}_j \to \mathbb{R}$ and associated norm $\|\cdot\|_{\hat{\boldsymbol{V}}_j} : \ \hat{\boldsymbol{V}}_j \to \mathbb{R}$, defined as

$$(\hat{\boldsymbol{u}}, \hat{\boldsymbol{v}})_{\hat{\boldsymbol{V}}_j} := \sum_{k=1}^2 (\hat{\boldsymbol{u}}_k, \hat{\boldsymbol{v}}_k)_{\hat{\boldsymbol{V}}_{j,k}} \quad \text{and} \quad \|\hat{\boldsymbol{u}}\|^2_{\hat{\boldsymbol{V}}_j} := \sum_{k=1}^2 \|\hat{\boldsymbol{u}}_k\|^2_{\hat{\boldsymbol{V}}_{j,k}}.$$

Analogously the broken space $\hat{Q}_j : \ \gamma_j \to \mathbb{R}$

$$\hat{Q}_j := \Big\{ \hat{w} : \ \gamma_j \to \mathbb{R} : \ \hat{w}_k := \hat{w}|_{\gamma_{j,k}} \in \hat{Q}_{j,k} \Big\},$$

which is an Hilbert space endowed with inner product $(\cdot, \cdot)_{\hat{Q}_j} : \hat{Q}_j \times \hat{Q}_j \to \mathbb{R}$ and associated norm $\|\cdot\|_{\hat{Q}_j} : \hat{Q}_j \to \mathbb{R}$, defined as

$$(\hat{p}, \hat{w})_{\hat{Q}_j} := \sum_{k=1}^{2} (\hat{p}_k, \hat{w}_k)_{\hat{Q}_{j,k}} \quad \text{and} \quad \|\hat{p}\|_{\hat{Q}_j}^2 := \sum_{k=1}^{2} \|\hat{p}_k\|_{\hat{Q}_{j,k}}^2 .$$

Note that $\hat{V}_j$ and $\hat{Q}_j$ may be identified with a subset of $\left[L^2(\gamma_j) \right]^n$ and $L^2(\gamma_j)$, respectively since $\boldsymbol{i}_p$ is a set of zero Lebesgue measure in $\mathbb{R}^{n-1}$. Thus we will indicate for a $v \in \hat{Q}_j$

$$\|v\|_{L^2(\gamma_j)}^2 = \sum_{k=1}^{2} \int_{\gamma_{j,k}} v_k^2 = \int_{\gamma_j} v^2 ,$$

where it is understood that v has been extended to the whole γ_j. Analogously we define the $L^2(\gamma_j)$ norm of an element of $\hat{V}_j$. Note that the normal component $\boldsymbol{v} \cdot \boldsymbol{n}_j$ of a function $\boldsymbol{v} \in \boldsymbol{V}$ is discontinuous across γ_j and a function $\hat{\boldsymbol{v}} \in \hat{V}_j$ is discontinuous across $\boldsymbol{i}_p$. We define also the global space for the Darcy velocity and the global space for the pressure including the reduce pressure at the interface I

$$\boldsymbol{\mathcal{V}} := \left\{ \mathbf{v} = (\boldsymbol{v}, \hat{\boldsymbol{v}}_1, \hat{\boldsymbol{v}}_2) \in \boldsymbol{V} \times \hat{V}_1 \times \hat{V}_2 \right\} ,$$

$$\mathcal{Q} := \left\{ \mathrm{w} = (w, \hat{w}_1, \hat{w}_2, c) \in Q \times \hat{Q}_1 \times \hat{Q}_2 \times \mathbb{R} \right\} ,$$

equipped with scalar products $(\cdot, \cdot)_{\boldsymbol{\mathcal{V}}} : \boldsymbol{\mathcal{V}} \times \boldsymbol{\mathcal{V}} \to \mathbb{R}$ and $(\cdot, \cdot)_{\mathcal{Q}} : \mathcal{Q} \times \mathcal{Q} \to \mathbb{R}$, defined as

$$(\mathbf{u}, \mathbf{v})_{\boldsymbol{\mathcal{V}}} := (\boldsymbol{u}, \boldsymbol{v})_{\boldsymbol{V}} + \sum_{j=1}^{2} (\hat{\boldsymbol{u}}_j, \hat{\boldsymbol{v}}_j)_{\hat{V}_j} ,$$

$$(\mathrm{p}, \mathrm{w})_{\mathcal{Q}} := (p, w)_Q + \sum_{j=1}^{2} (\hat{p}_j, \hat{w}_j)_{\hat{Q}_j} + c_1 c_2$$

with $\mathrm{p} = (p, \hat{p}_1, \hat{p}_2, c_1) \in \mathcal{Q}$ and similarly for w. The associated norms $\|\cdot\|_{\boldsymbol{\mathcal{V}}} : \boldsymbol{\mathcal{V}} \to \mathbb{R}$ and $\|\cdot\|_{\mathcal{Q}} : \mathcal{Q} \to \mathbb{R}$, defined as

$$\|\mathbf{v}\|_{\boldsymbol{\mathcal{V}}}^2 := (\mathbf{v}, \mathbf{v})_{\boldsymbol{\mathcal{V}}} \quad \text{and} \quad \|\mathrm{w}\|_{\mathcal{Q}}^2 := (\mathrm{w}, \mathrm{w})_{\mathcal{Q}} .$$

With this definition of $\boldsymbol{\mathcal{V}}$ and $\mathcal{Q}$, we finally introduce the global space $\mathcal{D}$ for the problem as in (3.38).

The derivation of the weak formulation for the first two equation of (3.54) is similar to the one presented in the section 2.3, but in this case we do not use the hybridization procedure leaving the system in the mixed form.

Taking a test function $w \in Q$ and integrating in Ω_i the first equation of (3.54) becomes for $i = 1, \ldots, 4$

$$(\nabla \cdot \boldsymbol{u}_i, w)_{\Omega_i} = (q_i, w)_{\Omega_i} \quad \forall w \in Q ,$$

then sum on all the domains Ω_i for $i = 1, \ldots, 4$ we find

$$(\nabla \cdot \boldsymbol{u}, w)_{\Omega} = (q, w)_{\Omega} \quad \forall w \in Q .$$

Introducing the bilinear form $b(\cdot,\,\cdot) :\, \boldsymbol{V} \times Q \to \mathbb{R}$ and the functional $F_q \in Q'$, defined as

$$b(\boldsymbol{u},\,w) := -(\nabla\cdot\boldsymbol{u},\,w)_\Omega \quad \text{and} \quad F_q(w) := (q,\,w)_\Omega\,,$$

the weak formulation of the first equation of (3.54) is

$$b(\boldsymbol{u},\,w) = -F_q(w) \quad \forall w \in Q\,. \tag{3.59}$$

Taking a test function $\boldsymbol{v} \in \boldsymbol{V}$ and integrating in Ω_i the second equation of (3.54) reads for $i = 1,\ldots,4$

$$\left(\boldsymbol{K}_i^{-1}\boldsymbol{u}_i,\,\boldsymbol{v}\right)_{\Omega_i} + (\nabla p_i,\,\boldsymbol{v})_{\Omega_i} = \left(\boldsymbol{K}_i^{-1}\boldsymbol{u}_i,\,\boldsymbol{v}\right)_{\Omega_i} - (p_i,\,\nabla\cdot\boldsymbol{v})_{\Omega_i} + (p_i,\,\boldsymbol{v}\cdot\boldsymbol{n}_\Gamma)_{\Gamma_i} +$$
$$+ \sum_{j=1}^{2} (p_i,\,\boldsymbol{v}\cdot\boldsymbol{n}_{j,i})_{\gamma_j\cap\partial\Omega_i} = 0 \quad \forall\boldsymbol{v} \in \boldsymbol{V}\,.$$

Summing the previous equation on all the domains Ω_i for $i = 1,\ldots,4$ and using the boundary condition we obtain

$$\left(\boldsymbol{K}^{-1}\boldsymbol{u},\,\boldsymbol{v}\right)_\Omega - (p,\,\nabla\cdot\boldsymbol{v})_\Omega + (\bar{p},\,\boldsymbol{v}\cdot\boldsymbol{n}_\Gamma)_{\Gamma^N} +$$
$$+ \sum_{i=1}^{4}\sum_{j=1}^{2} (p_i,\,\boldsymbol{v}\cdot\boldsymbol{n}_{j,i})_{\gamma_j\cap\partial\Omega_i} = 0 \quad \forall\boldsymbol{v} \in \boldsymbol{V}\,.$$

Since $\boldsymbol{n}_j = \boldsymbol{n}_{j,1} = -\boldsymbol{n}_{j,2}$ for $j = 1,2$, using the relation $[\![ab]\!]_{\gamma_j} = [\![a]\!]_{\gamma_j}\{\!\{b\}\!\}_{\gamma_j} + \{\!\{a\}\!\}_{\gamma_j}[\![b]\!]_{\gamma_j}$ and the coupling conditions for γ_j (3.55), the last integral becomes

$$\sum_{i=1}^{4}\sum_{j=1}^{2}(p_i,\,\boldsymbol{v}\cdot\boldsymbol{n}_{j,i})_{\gamma_j\cap\partial\Omega_i} = \sum_{j=1}^{2}\int_{\gamma_j}[\![p\boldsymbol{v}]\!]_{\gamma_j}\cdot\boldsymbol{n}_j = \sum_{j=1}^{2}\left([\![p]\!]_{\gamma_j},\,\{\!\{\boldsymbol{v}\cdot\boldsymbol{n}_j\}\!\}_{\gamma_j}\right)_{\gamma_j} +$$
$$+ \left(\{\!\{p\}\!\}_{\gamma_j},\,[\![\boldsymbol{v}\cdot\boldsymbol{n}_j]\!]_{\gamma_j}\right)_{\gamma_j} = \sum_{j=1}^{2}\left(\eta_{\gamma_j}\{\!\{\boldsymbol{u}\cdot\boldsymbol{n}_j\}\!\}_{\gamma_j},\,\{\!\{\boldsymbol{v}\cdot\boldsymbol{n}_j\}\!\}_{\gamma_j}\right)_{\gamma_j} +$$
$$+ \left(\hat{p}_j,\,[\![\boldsymbol{v}\cdot\boldsymbol{n}_j]\!]_{\gamma_j}\right)_{\gamma_j} + \xi_{0j}\left(\eta_{\gamma_j}[\![\boldsymbol{u}\cdot\boldsymbol{n}_j]\!]_{\gamma_j},\,[\![\boldsymbol{v}\cdot\boldsymbol{n}_j]\!]_{\gamma_j}\right)_{\gamma_j}\,.$$

We finally obtain

$$\left(\boldsymbol{K}^{-1}\boldsymbol{u},\,\boldsymbol{v}\right)_\Omega - (p,\,\nabla\cdot\boldsymbol{v})_\Omega + \sum_{j=1}^{2}\left(\eta_{\gamma_j}\{\!\{\boldsymbol{u}\cdot\boldsymbol{n}_j\}\!\}_{\gamma_j},\,\{\!\{\boldsymbol{v}\cdot\boldsymbol{n}_j\}\!\}_{\gamma_j}\right)_{\gamma_j} +$$
$$+ \xi_{0j}\left(\eta_{\gamma_j}[\![\boldsymbol{u}\cdot\boldsymbol{n}_j]\!]_{\gamma_j},\,[\![\boldsymbol{v}\cdot\boldsymbol{n}_j]\!]_{\gamma_j}\right)_{\gamma_j} + \left(\hat{p}_j,\,[\![\boldsymbol{v}\cdot\boldsymbol{n}_j]\!]_{\gamma_j}\right)_{\gamma_j} =$$
$$= -(\bar{p},\,\boldsymbol{v}\cdot\boldsymbol{n}_\Gamma)_{\Gamma^N} \quad \forall\boldsymbol{v} \in \boldsymbol{V}\,.$$

Introducing the bilinear forms $a(\cdot,\,\cdot) :\, \boldsymbol{V} \times \boldsymbol{V} \to \mathbb{R}$ and $d(\cdot,\,\cdot) :\, \boldsymbol{V} \times \hat{Q}_j \to \mathbb{R}$ and functionals

$$a(\boldsymbol{u},\,\boldsymbol{v}) := \left(\boldsymbol{K}^{-1}\boldsymbol{u},\,\boldsymbol{v}\right)_\Omega + \sum_{j=1}^{2}\left(\eta_{\gamma_j}\{\!\{\boldsymbol{u}\cdot\boldsymbol{n}_j\}\!\}_{\gamma_j},\,\{\!\{\boldsymbol{v}\cdot\boldsymbol{n}_j\}\!\}_{\gamma_j}\right)_{\gamma_j} +$$
$$+ \xi_{0j}\left(\eta_{\gamma_j}[\![\boldsymbol{u}\cdot\boldsymbol{n}_j]\!]_{\gamma_j},\,[\![\boldsymbol{v}\cdot\boldsymbol{n}_j]\!]_{\gamma_j}\right)_{\gamma_j}\,,$$
$$d(\boldsymbol{v},\,\hat{p}_j)_{\gamma_j} := \left(\hat{p}_j,\,[\![\boldsymbol{v}\cdot\boldsymbol{n}_j]\!]_{\gamma_j}\right)_{\gamma_j} \quad \text{and} \quad F_{\boldsymbol{q}}(\boldsymbol{v}) := -(\bar{p},\,\boldsymbol{v}\cdot\boldsymbol{n}_\Gamma)_{\Gamma^N}\,,$$

then the weak formulation of the second equation of system (3.54) together with the coupling conditions on γ_i becomes

$$a(\boldsymbol{u},\,\boldsymbol{v}) + b(\boldsymbol{v},\,p) + \sum_{j=1}^{2} d(\boldsymbol{v},\,\hat{p}_j) = F_{\boldsymbol{q}}\left(\boldsymbol{v}\right) \quad \forall \boldsymbol{v} \in \boldsymbol{V}. \tag{3.60}$$

We derive the weak formulation of the equations in the fractures, *i.e.* the third and fourth equation of (3.54). Taking a test function $\hat{w} \in \hat{Q}_j$ and integrating on $\gamma_{j,k}$ for $k,j = 1,2$, the third equation of (3.54) becomes

$$\left(\nabla_{\boldsymbol{\tau}_j} \cdot \hat{\boldsymbol{u}}_j,\,\hat{w}\right)_{\gamma_{j,k}} - \left(\llbracket \boldsymbol{u}\cdot\boldsymbol{n}_j\rrbracket_{\gamma_j},\,\hat{w}\right)_{\gamma_{j,k}} = (\hat{q}_j,\,\hat{w})_{\gamma_{j,k}} \quad \forall \hat{w} \in \hat{Q}_j,$$

then summing for $k = 1,2$ we find for $j = 1,2$

$$\left(\nabla_{\boldsymbol{\tau}_j} \cdot \hat{\boldsymbol{u}}_j,\,\hat{w}\right)_{\gamma_j} - \left(\llbracket \boldsymbol{u}\cdot\boldsymbol{n}_j\rrbracket_{\gamma_j},\,\hat{w}\right)_{\gamma_j} = (\hat{q}_j,\,\hat{w})_{\gamma_j} \quad \forall \hat{w} \in \hat{Q}_j.$$

Introducing the bilinear from $\hat{b}_j(\cdot,\,\cdot): \hat{\boldsymbol{V}}_j \times \hat{Q}_j \to$ and the functional $\hat{F}_{\hat{q},j} \in \hat{Q}_j'$, defined as

$$\hat{b}_j(\hat{\boldsymbol{u}}_j,\,\hat{w}) := -\left(\nabla_{\boldsymbol{\tau}_j} \cdot \hat{\boldsymbol{u}}_j,\,\hat{w}\right)_{\gamma_j} \quad \text{and} \quad \hat{F}_{\hat{q},j}\left(\hat{w}\right) := (\hat{q}_j,\,\hat{w})_{\gamma_j},$$

the weak formulation of the third equation of (3.54) reads for $j = 1,2$

$$\hat{b}_j(\hat{\boldsymbol{u}}_j,\,\hat{w}) + d(\boldsymbol{u},\,\hat{w}) = -\hat{F}_{\hat{q},j}\left(\hat{w}\right) \quad \forall \hat{w} \in \hat{Q}_j. \tag{3.61}$$

Taking a test function $\hat{\boldsymbol{v}} \in \hat{\boldsymbol{V}}_j$ and integrating on $\gamma_{j,k}$ for $k,j = 1,2$, the fourth equation of (3.54) becomes

$$(\hat{\eta}_j\hat{\boldsymbol{u}}_j,\,\hat{\boldsymbol{v}})_{\gamma_{j,k}} + \left(\nabla_{\boldsymbol{\tau}_j}\hat{p}_j,\,\hat{\boldsymbol{v}}\right)_{\gamma_{j,k}} = (\hat{\eta}_j\hat{\boldsymbol{u}}_j,\,\hat{\boldsymbol{v}})_{\gamma_{j,k}} - \left(\hat{p}_j,\,\nabla_{\boldsymbol{\tau}_j}\cdot\hat{\boldsymbol{v}}\right)_{\gamma_{j,k}} + $$
$$+ (\hat{p}_j,\,\hat{\boldsymbol{v}}\cdot\boldsymbol{\tau}_j)_{\partial\gamma_{j,k}} = 0 \quad \forall \hat{\boldsymbol{v}} \in \hat{\boldsymbol{V}}_j.$$

Summing the previous equations for $k = 1,2$ and using the boundary conditions with $\boldsymbol{n}_\Gamma \approx \boldsymbol{\tau}_j$, we find for $j = 1,2$

$$(\hat{\eta}_j\hat{\boldsymbol{u}}_j,\,\hat{\boldsymbol{v}})_{\gamma_j} - \left(\hat{p}_j,\,\nabla_{\boldsymbol{\tau}_j}\cdot\hat{\boldsymbol{v}}\right)_{\gamma_j} + \llbracket\hat{p}_j\hat{\boldsymbol{v}}\rrbracket_{\boldsymbol{i}_p}\cdot\boldsymbol{\tau}_j = -\overline{\hat{p}_j\hat{\boldsymbol{v}}}\big|_{\partial\gamma_j^N}\cdot\boldsymbol{n}_\Gamma \quad \forall \hat{\boldsymbol{v}} \in \hat{\boldsymbol{V}}_j.$$

The term with the jump operator can be decomposed using the interface conditions on $\boldsymbol{i}_p$ (3.56) for $j = 1,2$

$$\llbracket\hat{p}_j\hat{\boldsymbol{v}}\rrbracket_{\boldsymbol{i}_p}\cdot\boldsymbol{\tau}_j = \llbracket\hat{p}_j\rrbracket_{\boldsymbol{i}_p}\{\!\{\hat{\boldsymbol{v}}\}\!\}_{\boldsymbol{i}_p}\cdot\boldsymbol{\tau}_j + \{\!\{\hat{p}_j\}\!\}_{\boldsymbol{i}_p}\llbracket\hat{\boldsymbol{v}}\rrbracket_{\boldsymbol{i}_p}\cdot\boldsymbol{\tau}_j =$$
$$= \frac{\eta_{\gamma_i}}{d_j}\{\!\{\hat{\boldsymbol{u}}_j\cdot\boldsymbol{\tau}_j\}\!\}_{\boldsymbol{i}_p}\{\!\{\hat{\boldsymbol{v}}\cdot\boldsymbol{\tau}_j\}\!\}_{\boldsymbol{i}_p} + \hat{\xi}_0\frac{\eta_{\gamma_i}}{d_j}\llbracket\hat{\boldsymbol{u}}_j\cdot\boldsymbol{\tau}_j\rrbracket_{\boldsymbol{i}_p}\llbracket\hat{\boldsymbol{v}}\cdot\boldsymbol{\tau}_j\rrbracket_{\boldsymbol{i}_p} + \hat{p}_I\llbracket\hat{\boldsymbol{v}}\cdot\boldsymbol{\tau}_j\rrbracket_{\boldsymbol{i}_p},$$

then we find for $j = 1,2$

$$(\hat{\eta}_j\hat{\boldsymbol{u}}_j,\,\hat{\boldsymbol{v}})_{\gamma_j} - \left(\hat{p}_j,\,\nabla_{\boldsymbol{\tau}_j}\cdot\hat{\boldsymbol{v}}\right)_{\gamma_j} + \frac{\eta_{\gamma_i}}{d_j}\{\!\{\hat{\boldsymbol{u}}_j\cdot\boldsymbol{\tau}_j\}\!\}_{\boldsymbol{i}_p}\{\!\{\hat{\boldsymbol{v}}\cdot\boldsymbol{\tau}_j\}\!\}_{\boldsymbol{i}_p} + \hat{p}_I\llbracket\hat{\boldsymbol{v}}\cdot\boldsymbol{\tau}_j\rrbracket_{\boldsymbol{i}_p}$$
$$+ \hat{\xi}_0\frac{\eta_{\gamma_i}}{d_j}\llbracket\hat{\boldsymbol{u}}_j\cdot\boldsymbol{\tau}_j\rrbracket_{\boldsymbol{i}_p}\llbracket\hat{\boldsymbol{v}}\cdot\boldsymbol{\tau}_j\rrbracket_{\boldsymbol{i}_p} = -\overline{\hat{p}_j\hat{\boldsymbol{v}}}\big|_{\partial\gamma_j^N}\cdot\boldsymbol{n}_\Gamma \quad \forall \hat{\boldsymbol{v}} \in \hat{\boldsymbol{V}}_j.$$

Introducing the bilinear forms $\hat{a}_j(\cdot,\,\cdot) : \hat{\boldsymbol{V}}_j \times \hat{\boldsymbol{V}}_j \to \mathbb{R}$ and $\hat{d}_j(\cdot,\,\cdot) : \hat{\boldsymbol{V}}_j \times \mathbb{R} \to \mathbb{R}$ and the functional $\hat{F}_{\hat{\boldsymbol{q}},j} \in \hat{\boldsymbol{V}}_j'$, defined as

$$\hat{a}_j(\hat{\boldsymbol{u}}_j,\,\hat{\boldsymbol{v}}) := (\hat{\eta}_j \hat{\boldsymbol{u}}_j,\,\hat{\boldsymbol{v}})_{\gamma_j} + \frac{\eta_{\gamma_i}}{d_j} \left\{\!\!\left\{ \hat{\boldsymbol{u}}_j \cdot \boldsymbol{\tau}_j \right\}\!\!\right\}_{\boldsymbol{i}_p} \left\{\!\!\left\{ \hat{\boldsymbol{v}} \cdot \boldsymbol{\tau}_j \right\}\!\!\right\}_{\boldsymbol{i}_p} +$$

$$+ \hat{\xi}_0 \frac{\eta_{\gamma_i}}{d_j} [\![\hat{\boldsymbol{u}}_j \cdot \boldsymbol{\tau}_j]\!]_{\boldsymbol{i}_p} [\![\hat{\boldsymbol{v}} \cdot \boldsymbol{\tau}_j]\!]_{\boldsymbol{i}_p} \,,$$

$$\hat{d}_j(\hat{\boldsymbol{v}},\,\hat{p}_I) := \hat{p}_I [\![\hat{\boldsymbol{v}} \cdot \boldsymbol{\tau}_j]\!]_{\boldsymbol{i}_p} \quad \text{and} \quad \hat{F}_{\hat{\boldsymbol{q}},j}(\hat{\boldsymbol{v}}) := - \left. \overline{\hat{p}_j} \hat{\boldsymbol{v}} \right|_{\partial\gamma_j^N} \cdot \boldsymbol{n}_\Gamma \,,$$

we obtain the weak formulation of the fourth equation of (3.54) for $j = 1, 2$

$$\hat{a}_j(\hat{\boldsymbol{u}}_j,\,\hat{\boldsymbol{v}}) + \hat{b}_j(\hat{\boldsymbol{v}},\,\hat{p}_j) + \hat{d}_j(\hat{\boldsymbol{v}},\,\hat{p}_I) = \hat{F}_{\hat{\boldsymbol{q}},j}(\hat{\boldsymbol{v}}) \quad \forall \hat{\boldsymbol{v}} \in \hat{\boldsymbol{V}}_j \,. \qquad (3.62)$$

The weak formulation of the coupling condition of the two fractures at the intersection point $\boldsymbol{i}_p$, i.e. the third equation of (3.56), is

$$\sum_{j=1}^{2} \hat{w}_I [\![\hat{\boldsymbol{u}}_j \cdot \boldsymbol{\tau}_j]\!]_{\boldsymbol{i}_p} = 0 \quad \forall \hat{w}_I \in \mathbb{R} \,.$$

Using the definition of the bilinear form $\hat{d}_j$ we obtain

$$\sum_{j=1}^{2} \hat{d}_j(\hat{\boldsymbol{u}}_j,\,\hat{w}_I) = 0 \quad \forall \hat{w}_I \in \mathbb{R} \,. \qquad (3.63)$$

Defining the global bilinear forms for the medium and the fractures as $\alpha(\cdot,\,\cdot) : \boldsymbol{\mathcal{V}} \times \boldsymbol{\mathcal{V}} \to \mathbb{R}$, $\beta(\cdot,\,\cdot) : \boldsymbol{\mathcal{V}} \times \mathcal{Q} \to \mathbb{R}$ and $\mathcal{A}(\cdot,\,\cdot) : \mathcal{D} \times \mathcal{D} \to \mathbb{R}$

$$\alpha(\mathbf{u},\,\mathbf{v}) := a(\boldsymbol{u},\,\boldsymbol{v}) + \sum_{j=1}^{2} \hat{a}_j(\hat{\boldsymbol{u}}_j,\,\hat{\boldsymbol{v}}) \,,$$

$$\beta(\mathbf{v},\,\mathrm{p}) := b(\boldsymbol{v},\,p) + \sum_{j=1}^{2} \hat{b}_j(\hat{\boldsymbol{v}},\,\hat{p}_j) + d(\boldsymbol{v},\,\hat{p}_j) + \hat{d}_j(\hat{\boldsymbol{v}},\,\hat{p}_I) \,,$$

$$\mathcal{A}\left[(\mathbf{u},\,\mathrm{p}),\,(\mathbf{v},\,\mathrm{w})\right] := \alpha(\mathbf{u},\,\mathbf{v}) + \beta(\mathbf{v},\,\mathrm{p}) - \beta(\mathbf{u},\,\mathrm{w})$$

and the global functionals for the medium and the fractures as $\mathcal{F}_{\boldsymbol{q}} \in \boldsymbol{\mathcal{V}}'$, $\mathcal{F}_q \in \mathcal{Q}'$ and $\mathcal{F} \in \mathcal{D}'$

$$\mathcal{F}_{\boldsymbol{q}}(\mathbf{v}) := F_{\boldsymbol{q}}(\boldsymbol{v}) + \sum_{j=1}^{2} \hat{F}_{\hat{\boldsymbol{q}},j}(\hat{\boldsymbol{v}}_j) \,, \qquad \mathcal{F}_q(\mathrm{w}) := -F_q(w) - \sum_{j=1}^{2} \hat{F}_{\hat{q},j}(\hat{w}_j) \,,$$

$$\mathcal{F}(\mathbf{v},\,\mathrm{w}) := \mathcal{F}_{\boldsymbol{q}}(\mathbf{v}) + \mathcal{F}_q(\mathrm{w}) \,,$$

with $\mathbf{u} := (\boldsymbol{u},\,\hat{\boldsymbol{u}}_1,\,\hat{\boldsymbol{u}}_2) \in \boldsymbol{\mathcal{V}}$ the Darcy velocity in the medium and in each fracture, $\mathrm{p} := (p,\,\hat{p}_1,\,\hat{p}_2,\,\hat{p}_I) \in \mathcal{Q}$ the pressure in the medium, in each fracture and in the intersection point $\boldsymbol{i}_p$, therefore using the equations (3.59), (3.60), (3.61), (3.62) and (3.63) we obtain the following problem.

Problem 3.6 (Weak Formulation of Darcy Reduced Model with Intersection)**.** *The weak formulation of Problem 3.5 is: find* $(\mathbf{u},\,\mathrm{p}) \in \mathcal{D}$ *such that*

$$\begin{cases} \alpha(\mathbf{u},\,\mathbf{v}) + \beta(\mathbf{v},\,\mathrm{p}) = \mathcal{F}_{\boldsymbol{q}}(\mathbf{v}) & \forall \mathbf{v} \in \boldsymbol{\mathcal{V}} \,, \\[2mm] \beta(\mathbf{u},\,\mathrm{w}) = \mathcal{F}_q(\mathrm{w}) & \forall \mathrm{w} \in \mathcal{Q} \,, \end{cases}$$

or alternatively

$$\mathcal{A}\left[(\mathbf{u},\, \mathrm{p}),\, (\mathbf{v},\, \mathrm{w})\right] = \mathcal{F}(\mathbf{v},\, \mathrm{w}) \quad \forall (\mathbf{v},\, \mathrm{w}) \in \mathcal{D}\,.$$

3.2.2   Enriched finite elements spaces

To introduce the enriched finite elements spaces for the discrete formulation of the system presented in Problem 3.6 we consider a family of regular tessellation $\mathcal{T}_h$ such that

$$\overline{\Omega} \approx \mathcal{T}_h := \bigcup_j K_j \quad \text{and} \quad \partial\mathcal{T}_h := \{e \in \partial K,\, K \in \mathcal{T}_h\}\,,$$

with h the largest diameter of elements of $\mathcal{T}_h$ and K_j a generic triangle, moreover $\partial\mathcal{T}_h$ is the collection of all the edges in the triangulation. For each fracture i we introduce a family of regular tessellation $\gamma_{\hat{h},i}$ such that

$$\overline{\gamma}_i \approx \gamma_{\hat{h},i} := \bigcup_j l_j\,,$$

with $\hat{h}$ the maximum length of the segments of $\gamma_{\hat{h},i}$ and l_j a generic segment. Note that $\mathcal{T}_h$ may not be conformal with $\gamma_{\hat{h},i}$, since elements of $\mathcal{T}_h$ may be cut by $\gamma_{\hat{h},i}$ as reported in Figure 3.12. Also element of $\gamma_{\hat{h},1}$ may not be conformal with elements of $\gamma_{\hat{h},2}$.
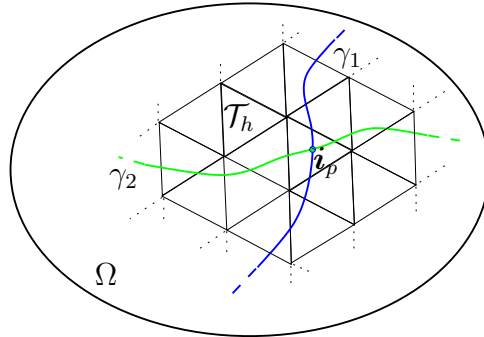
Figure 3.12: Example of a bi-dimensional triangulation $\mathcal{T}_h$ of Ω crossed by two intersecting fractures.

To introduce the enriched finite elements spaces we require the following assumptions, pointing out also when there are present more then two fractures and more then one intersection point.

Assumption 3.7. *We suppose the following properties for $\mathcal{T}_h$ and $\gamma_{\hat{h},i}$, for $i = 1, 2$*

1. *the bi-dimensional mesh $\mathcal{T}_h$ is composed by triangles and is regular, i.e. it satisfies (2.40);*

2. *if a fracture intersect a triangle $K \in \mathcal{T}_h$ then it intersect exactly two edges. Situations reported in Figure 3.13 are excluded;*

93

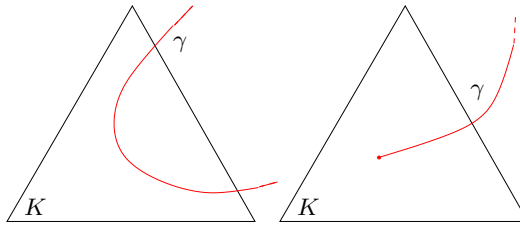**Figure 3.13:** Example of not allowed crossings between fracture γ and triangle K.

3. for the sake of simplicity we suppose that at most two fractures cross inside a triangle $K \in \mathcal{T}_h$;

4. the intersection point $\boldsymbol{i}_p$ of two fractures belongs to the interior of a triangle $\boldsymbol{i}_p \in \mathring{K}$, for $K \in \mathcal{T}_h$. The fracture meshes may intersect each other in a non-conforming way. If they intersect more then once, the intersection points belongs to different triangles, the situation in Figure 3.14 is not allowed;
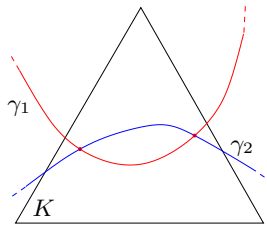
Figure 3.14: Example of multiple intersections in a triangle not allowed.

5. we approximate the curve γ_i describing the fracture i by its piecewise rectilinear interpolation $\widetilde{\gamma}_i$, each piece belonging to a triangle, see Figure 3.15 for an example. Therefore the mono-dimensional meshes $\gamma_{\hat{h},i}$ is constructed on $\widetilde{\gamma}_i$ by segments, for $i = 1, 2$.
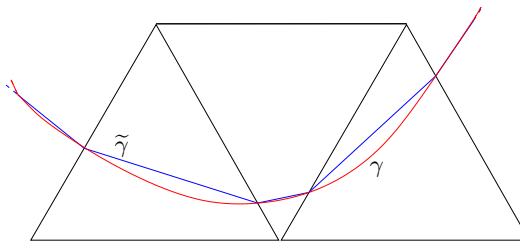
Figure 3.15: Example of the interpolation $\widetilde{\gamma}$ of the fracture γ, in $2D$.

6. let $\gamma_{\hat{h},i}$, for $i = 1, 2$ be the straight line segment connecting the points of intersection between γ_i and ∂K. We assume that $\gamma_i|_K$ is a function of

94

length on $\gamma_{\hat{h},i}$. In particular, in local coordinates (s, t) we have

$$\gamma_{\hat{h},i} = \left\{ (s, t) : 0 < s < \left| \gamma_{\hat{h},i} \right|, t = 0 \right\} ,$$
$$\gamma_i|_K = \left\{ (s, t) : 0 < s < \left| \gamma_{\hat{h},i} \right|, t = \delta(s) \right\} ,$$

where δ_i is positive in the direction of $\boldsymbol{n}_i$, i.e.

$$\boldsymbol{n}_i (s) = \frac{\left(-\delta_i' (s), 1 \right)^\top}{\left(\delta_i' (s)^2 + 1 \right)^2} ,$$

in local coordinates. This hypotheses is fulfilled on sufficiently small meshes if γ_i has bounded curvature. Assumption taken from [24].

Thanks to the above assumptions, we report in Figure 3.16 situations that are allowed.
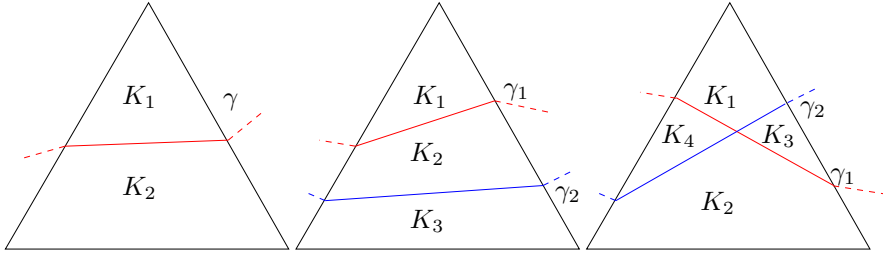
Figure 3.16: Example of possible intersections of a triangle and the system of fractures.

We denote by for $i = 1, 2$

$$\mathcal{G}_{h,i} := \left\{ K \in \mathcal{T}_h : K \cap \gamma_i \neq \emptyset \wedge K \cap \gamma_j = \emptyset, j \neq i \right\} ,$$

the collection of elements that are crossed only by fracture i, while we denote by

$$\mathcal{M}_h := \left\{ K \in \mathcal{T}_h : K \cap \gamma_i \neq \emptyset \wedge K \cap \gamma_j \neq \emptyset \wedge \gamma_i \cap \gamma_j = \emptyset, j \neq i \right\} ,$$

the set of elements that are crossed by the two fractures, but the fractures do not intersect each other. We define also the set

$$\mathcal{I}_h := \left\{ K \in \mathcal{T}_h : \gamma_i \cap \gamma_j \in K, j \neq i \right\} ,$$

which is the collection of elements that contain an intersection point. Finally we introduce

$$\mathcal{CR}_h := \mathcal{M}_h \cup \mathcal{I}_h \cup \bigcup_{i=1}^2 \mathcal{G}_{h,i} \quad \text{and} \quad \mathcal{N}_h := \mathcal{T}_h \setminus \mathcal{CR}_h ,$$

which are the cut region and the collection of elements in $\mathcal{T}_h$ not crossed by any fracture, respectively; see Figure 3.17 for an example. For finite elements with
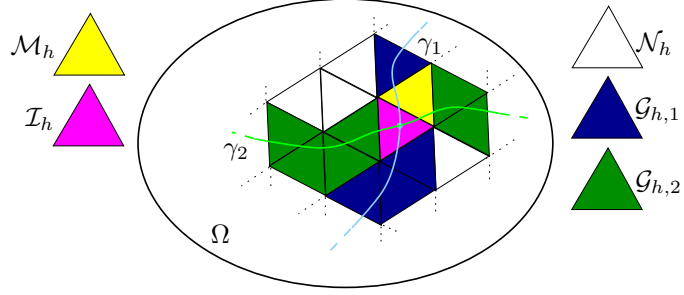
Figure 3.17: Example of subdivision of $\mathcal{T}_h$ in $\mathcal{G}_{h,1}$, $\mathcal{G}_{h,2}$, $\mathcal{M}_h$, $\mathcal{I}_h$ and $\mathcal{N}_h$, in a bi-dimensional domain Ω.

degrees of freedom defined on the edges of a triangle, it is useful to define the following sets for $i = 1, 2$

$$\partial \mathcal{I}_h := \{e \in \partial K, \, K \in \mathcal{I}_h\} \,, \qquad \partial \mathcal{M}_h := \{e \in \partial K, \, K \in \mathcal{M}_h\} \setminus \partial \mathcal{I}_h \,,$$

$$\partial \mathcal{G}_{h,i} := \{e \in \partial K, \, K \in \mathcal{G}_{h,i}\} \setminus \partial \mathcal{M}_h \,, \, \partial \mathcal{N}_h := \{e \in \partial K, \, K \in \mathcal{N}_h\} \setminus \bigcup_{i=1}^{2} \partial \mathcal{G}_{h,i} \,.$$

We split also the mesh of the fractures into intersected elements and non intersected elements, in particular we define for $i = 1, 2$

$$\mathcal{C}_{\hat{h},i} := \left\{ l \in \gamma_{\hat{h},i} : l \cap \boldsymbol{i}_p \neq \emptyset \right\} \quad \text{and} \quad \mathcal{B}_{\hat{h},i} := \gamma_{\hat{h},i} \setminus \mathcal{C}_{\hat{h},i} \,,$$
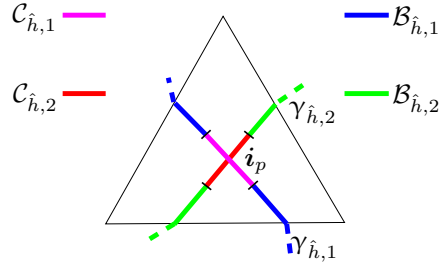
see Figure 3.18 for an example.

Figure 3.18: Example of subdivision of $\gamma_{\hat{h},i}$ in $\mathcal{C}_{\hat{h},i}$ and $\mathcal{B}_{\hat{h},i}$, for $i = 1, 2$, in the triangle K.

As done previously we introduce the following sets of points

$$\partial \mathcal{B}_{\hat{h},i} := \left\{ p \in \partial l, \, l \in \mathcal{B}_{\hat{h},i} \right\} \quad \text{and} \quad \partial \mathcal{C}_{\hat{h},i} := \left\{ p \in \partial l, \, l \in \mathcal{C}_{\hat{h},i} \right\} \setminus \partial \mathcal{B}_{\hat{h},i} \,.$$

In our applications, to numerically solve Problem 3.6 with finite elements it is common to choose the $(\mathbb{RT}_0, \mathbb{P}_0)$ pair, which is locally conservative and robust with respect to the heterogeneity of the coefficients [64]. For these reasons we choose $\mathbb{RT}_0$ finite elements to approximate the Darcy velocity, both in the medium and in the fractures, while $\mathbb{P}_0$ finite elements are used to approximate the pressure, both in the medium and in the fractures. To account for the presence of fractures and coupling terms we have to enrich the standard $\mathbb{RT}_0$

and $\mathbb{P}_0$ spaces with additional base functions. Following the idea presented in [24] we handle discontinuous functions where the jump is inside an element. In particular the solution in $K \in \mathcal{G}_{h,i}$, for $i = 1, 2$, can be discontinuous once, the solution in $K \in \mathcal{M}_h$ is discontinuous two times, while the solution in $K \in \mathcal{I}_h$ is discontinuous three times and finally the solution $K \in \mathcal{N}_h$ have no jumps. To this purpose we enrich the finite elements space by doubling the degrees of freedom in each element $K \in \mathcal{G}_{h,i}$ for $i = 1, 2$, three times in each element $K \in \mathcal{M}_h$ and four times in each element $K \in \mathcal{I}_h$. A similar enrichment have to be done for the fractures, in particular we double the base functions in each element $l \in \mathcal{C}_{\hat{h},i}$ for $i = 1, 2$ to allow jumps for both the velocity and the pressure. We introduce the following enriched finite elements spaces for the medium

$$\widetilde{\mathbb{RT}}_0\left(\mathcal{T}_h\right) := \mathbb{RT}_0\left(\mathcal{N}_h\right) \oplus \bigcup_{k,j=1}^{2} \mathbb{RT}_0\left(\mathcal{G}_{h,k}\right) \oplus \bigcup_{m=1}^{3} \mathbb{RT}_0\left(\mathcal{M}_h\right) \oplus \bigcup_{l=1}^{4} \mathbb{RT}_0\left(\mathcal{I}_h\right) ,$$

$$\widetilde{\mathbb{P}}_0\left(\mathcal{T}_h\right) := \mathbb{P}_0\left(\mathcal{N}_h\right) \oplus \bigcup_{k,j=1}^{2} \mathbb{P}_0\left(\mathcal{G}_{h,k}\right) \oplus \bigcup_{m=1}^{3} \mathbb{P}_0\left(\mathcal{M}_h\right) \oplus \bigcup_{l=1}^{4} \mathbb{P}_0\left(\mathcal{I}_h\right) .$$

A function $\boldsymbol{v}_h \in \widetilde{\mathbb{RT}}_0\left(\mathcal{T}_h\right)$ can be expanded using the base functions of $\widetilde{\mathbb{RT}}_0\left(\mathcal{T}_h\right)$

$$\boldsymbol{v}_h\left(\boldsymbol{x}\right) = \sum_{e \in \partial \mathcal{N}_h} v_{e,1} \boldsymbol{\psi}_e\left(\boldsymbol{x}\right) + \sum_{i,k=1}^{2} \sum_{e \in \partial \mathcal{G}_{h,k}} v_{e,i} \left.\boldsymbol{\psi}_e\left(\boldsymbol{x}\right)\right|_{K_i} +$$

$$+ \sum_{m=1}^{3} \sum_{e \in \partial \mathcal{M}_h} v_{e,m} \left.\boldsymbol{\psi}_e\left(\boldsymbol{x}\right)\right|_{K_m} + \sum_{l=1}^{4} \sum_{e \in \partial \mathcal{I}_h} v_{e,l} \left.\boldsymbol{\psi}_e\left(\boldsymbol{x}\right)\right|_{K_l} , \qquad (3.64)$$

where K_i, K_m and K_l are the sub-divisions in two, three and four pieces of the generic triangle K, see Figure 3.16 for an example of the sub-divisions of the triangle $K \in \mathcal{T}_h$. Where we indicate with $\vec{\boldsymbol{v}} = (\dots, v_{i,j}, \dots) \in \mathbb{R}^{N_v}$ the vector of the degrees of freedom associated to the finite element function $\boldsymbol{v}_h$ and with $N_{\boldsymbol{v}}$ the total number of degrees of freedom for $\widetilde{\mathbb{RT}}_0\left(\mathcal{T}_h\right)$. A function $w_h \in \widetilde{\mathbb{P}}_0\left(\mathcal{T}_h\right)$ can be expanded using the base functions of $\widetilde{\mathbb{P}}_0\left(\mathcal{T}_h\right)$

$$w_h\left(\boldsymbol{x}\right) = \sum_{K \in \mathcal{N}_h} w_{K,1} \phi_K\left(\boldsymbol{x}\right) + \sum_{i,k=1}^{2} \sum_{K \in \mathcal{G}_{h,k}} w_{K,i} \left.\phi_K\left(\boldsymbol{x}\right)\right|_{K_i} +$$

$$+ \sum_{m=1}^{3} \sum_{K \in \mathcal{M}_h} w_{K,m} \left.\phi_K\left(\boldsymbol{x}\right)\right|_{K_m} + \sum_{l=1}^{4} \sum_{K \in \mathcal{I}_h} w_{K,l} \left.\phi_K\left(\boldsymbol{x}\right)\right|_{K_l} ,$$

where K_i, K_m and K_l are the sub-divisions in two, three and four pieces of the generic triangle K. As for $\boldsymbol{v}_h$, we indicate with $\vec{w} = (\dots, w_{i,j}, \dots) \in \mathbb{R}^{N_q}$ the vector of the degrees of freedom associated to the finite element function w_h and with N_q the total number of degrees of freedom for $\widetilde{\mathbb{P}}_0\left(\mathcal{T}_h\right)$.
For each fracture $i = 1, 2$ the enriched finite elements spaces are

$$\widetilde{\mathbb{RT}}_0\left(\gamma_{\hat{h},i}\right) := \mathbb{RT}_0\left(\mathcal{B}_{\hat{h},i}\right) \oplus \bigcup_{k=1}^{2} \mathbb{RT}_0\left(\mathcal{C}_{\hat{h},i}\right) ,$$

$$\widetilde{\mathbb{P}}_0\left(\gamma_{\hat{h},i}\right) := \mathbb{P}_0\left(\mathcal{B}_{\hat{h},i}\right) \oplus \bigcup_{k=1}^{2} \mathbb{P}_0\left(\mathcal{C}_{\hat{h},i}\right) .$$

A function $\hat{\boldsymbol{v}}_{h,i} \in \widetilde{\mathbb{R}\mathbb{T}}_0\left(\gamma_{\hat{h},i}\right)$ can be expanded using the base functions of $\widetilde{\mathbb{R}\mathbb{T}}_0\left(\gamma_{\hat{h},i}\right)$ for $i = 1, 2$

$$\hat{\boldsymbol{v}}_{h,i}\left(\boldsymbol{x}\right) = \sum_{p\in\partial\mathcal{C}_{\hat{h},i}} \hat{v}_{p,1}\boldsymbol{\psi}_p\left(\boldsymbol{x}\right) + \sum_{k=1}^2 \sum_{p\in\partial\mathcal{B}_{\hat{h},i}} \hat{v}_{p,k}\left.\boldsymbol{\psi}_p\left(\boldsymbol{x}\right)\right|_{l_k} ,$$

where l_k is the sub-division in two pieces of the generic segment l. As in precedence we indicate with $\vec{\hat{\boldsymbol{v}}}_i = (\ldots, \hat{v}_{j,k}, \ldots) \in \mathbb{R}^{N_{\hat{v}}}$ the vector of the degrees of freedom associated to the finite element function $\hat{\boldsymbol{v}}_{h,i}$ and with $N_{\hat{v}}$ the total number of degrees of freedom for $\widetilde{\mathbb{R}\mathbb{T}}_0\left(\gamma_{\hat{h},i}\right)$. Finally a function $\hat{w}_{h,i} \in \widetilde{\mathbb{P}}_0\left(\gamma_{\hat{h},i}\right)$ can be expanded using the base functions of $\widetilde{\mathbb{P}}_0\left(\gamma_{\hat{h},i}\right)$ for $i = 1, 2$

$$\hat{w}_{h,i}\left(\boldsymbol{x}\right) = \sum_{l\in\mathcal{B}_{\hat{h},i}} \hat{w}_{l,1}\phi_l\left(\boldsymbol{x}\right) + \sum_{k=1}^2 \sum_{l\in\mathcal{C}_{\hat{h},i}} \hat{w}_{l,k}\left.\phi_l\left(\boldsymbol{x}\right)\right|_{l_k} ,$$

where l_k is the sub-division in two pieces of the generic segment l. We indicate with $\vec{\hat{w}}_i = (\ldots, \hat{w}_{j,k}, \ldots) \in \mathbb{R}^{N_{\hat{q}}}$ the vector of the degrees of freedom associated to the finite element function $\hat{w}_{h,i}$ and with $N_{\hat{q}}$ the total number of degrees of freedom for $\widetilde{\mathbb{P}}_0\left(\gamma_{\hat{h},i}\right)$.

The choice of these expansions is due that the base functions involved have the support on the whole of each element $K \in \mathcal{T}_h$ and not just on each sub-element K_i, hence the error between the exact solution and the computed depends on the strach of K and not on K_i.

3.2.3 Discrete formulation

We use the Nitsche's method to impose essential boundary conditions on Γ^E and $\partial\gamma^E$, which is a flexible tool to impose essential boundary conditions directly on the weak formulation of the problem. Reference of this approach can be found in [13] and [25]. We introduce the following h-dependent norm valid for the medium and the fractures

$$\|u\|_{h,\pm\frac{1}{2},\Sigma} := h^{\mp\frac{1}{2}}\sqrt{\int_\Sigma u^2} , \tag{3.65}$$

and the $\boldsymbol{H}_{\mathrm{div}}$-weighted norm

$$\|\boldsymbol{v}\|_{\boldsymbol{H}_{\mathrm{div}}(\Sigma),f}^2 := \|f\boldsymbol{v}\|_{L^2(\Sigma)}^2 + \|f\nabla\cdot\boldsymbol{v}\|_{L^2(\Sigma)}^2$$

where $f \in L^\infty\left(\Sigma\right)$ is the weight function.

To introduce the discrete formulation of Problem 3.6, we define the following functional spaces

$$\boldsymbol{V}_h := \boldsymbol{V} \cap \widetilde{\mathbb{R}\mathbb{T}}_0\left(\mathcal{T}_h\right) \qquad \text{and} \quad Q_h := Q \cap \widetilde{\mathbb{P}}_0\left(\mathcal{T}_h\right) ,$$
$$\hat{\boldsymbol{V}}_{h,j} := \hat{\boldsymbol{V}}_j \cap \widetilde{\mathbb{R}\mathbb{T}}_0\left(\gamma_{\hat{h},j}\right) \quad \text{and} \quad \hat{Q}_{h,j} := \hat{Q}_j \cap \widetilde{\mathbb{P}}_0\left(\gamma_{\hat{h},j}\right) ,$$

which are Hilbert spaces, which we endow with the following problem dependent norms $\|\cdot\|_{\boldsymbol{V}_h} : \boldsymbol{V}_h \to \mathbb{R}$ and $\|\cdot\|_{Q_h} : Q_h \to \mathbb{R}$, which also take into account the penalization terms due to the Nitsche's method, defined as

$$
\|\boldsymbol{v}_h\|_{\boldsymbol{V}_h}^2 := \sum_{i=1}^4 \|\boldsymbol{v}_{h,i}\|_{\boldsymbol{H}_{\mathrm{div}}(\Omega_i),\rho_{\boldsymbol{K}_i}^{-\frac{1}{2}}}^2 + \|\boldsymbol{v}_{h,i} \cdot \boldsymbol{n}_\Gamma\|_{h,+\frac{1}{2},\Gamma_i^E}^2 +
$$
$$
+ \sum_{j=1}^2 \left\| \eta_{\gamma_j}^{\frac{1}{2}} \{\!\{ \boldsymbol{v}_h \cdot \boldsymbol{n}_j \}\!\}_{\gamma_j} \right\|_{L^2(\gamma_{\hat{h},j})}^2 + \xi_{0j} \left\| \eta_{\gamma_j}^{\frac{1}{2}} [\![\boldsymbol{v}_h \cdot \boldsymbol{n}_j]\!]_{\gamma_j} \right\|_{L^2(\gamma_{\hat{h},j})}^2 ,
$$
$$
\|w_h\|_{Q_h}^2 := \sum_{i=1}^4 \left\| \rho_{\boldsymbol{K}_i}^{\frac{1}{2}} w_{h,i} \right\|_{L^2(\Omega_i)}^2 , \tag{3.66}
$$

where $\rho_{\boldsymbol{K}_i}$ is the spectral radius of the permeability tensor $\boldsymbol{K}_i$ in the sub-domain Ω_i. The norms for the space defined on the fractures $\|\cdot\|_{\hat{\boldsymbol{V}}_{h,j}} : \hat{\boldsymbol{V}}_{h,j} \to \mathbb{R}$ and $\|\cdot\|_{\hat{Q}_{h,j}} : \hat{Q}_{h,j} \to \mathbb{R}$ read

$$
\|\hat{\boldsymbol{v}}_h\|_{\hat{\boldsymbol{V}}_{h,j}}^2 := \|\hat{\boldsymbol{v}}_h \cdot \boldsymbol{n}_\Gamma\|_{\hat{h},+\frac{1}{2},\partial\gamma_j^E}^2 + \hat{\xi}_0 \eta_{\gamma_i} [\![\hat{\boldsymbol{v}}_h \cdot \boldsymbol{\tau}_i]\!]_{\boldsymbol{i}_p}^2 + \eta_{\gamma_i} \{\!\{ \hat{\boldsymbol{v}}_h \cdot \boldsymbol{\tau}_i \}\!\}_{\boldsymbol{i}_p}^2 +
$$
$$
+ \sum_{k=1}^2 \|\hat{\boldsymbol{v}}_{h,k}\|_{\boldsymbol{H}_{\mathrm{div}}(\gamma_{\hat{h},j,k}),\eta_{\boldsymbol{\tau}_j}^{\frac{1}{2}}}^2 ,
$$
$$
\|\hat{w}_{h,j}\|_{\hat{Q}_{h,j}} := \sum_{k=1}^2 \left\| \eta_{\boldsymbol{\tau}_j}^{-\frac{1}{2}} \hat{w}_{h,j} \right\|_{L^2(\gamma_{\hat{h},j_k})} ,
$$

with $i \neq j$ in the weight η_{γ_i} of the jump and average terms. We define also the global discrete spaces as

$$
\boldsymbol{\mathcal{V}}_h := \left\{ \mathbf{v}_h = (\boldsymbol{v}_h, \hat{\boldsymbol{v}}_{h,1}, \hat{\boldsymbol{v}}_{h,2}) \in \boldsymbol{V}_h \times \hat{\boldsymbol{V}}_{h,1} \times \hat{\boldsymbol{V}}_{h,2} \right\} \subset \boldsymbol{\mathcal{V}} ,
$$
$$
\mathcal{Q}_h := \left\{ \mathbf{w}_h = (w_h, \hat{w}_{h,1}, \hat{w}_{h,2}, c) \in Q_h \times \hat{Q}_{h,1} \times \hat{Q}_{h,2} \times \mathbb{R} \right\} \subset \mathcal{Q} ,
$$
$$
\mathcal{D}_h := \boldsymbol{\mathcal{V}}_h \times \mathcal{Q}_h \subset \mathcal{D} ,
$$

which are Hilbert spaces endowed with the norms $\|\cdot\|_{\boldsymbol{\mathcal{V}}_h} : \boldsymbol{\mathcal{V}}_h \to \mathbb{R}$, $\|\cdot\|_{\mathcal{Q}_h} : \mathcal{Q}_h \to \mathbb{R}$ and $\|\cdot\|_{\mathcal{D}_h} : \mathcal{D}_h \to \mathbb{R}$, defined as

$$
\|\mathbf{v}_h\|_{\boldsymbol{\mathcal{V}}_h}^2 := \|\boldsymbol{v}_h\|_{\boldsymbol{V}_h}^2 + \sum_{j=1}^2 \|\hat{\boldsymbol{v}}_{h,j}\|_{\hat{\boldsymbol{V}}_{h,j}}^2 ,
$$
$$
\|\mathbf{w}_h\|_{\mathcal{Q}_h}^2 := \|w_h\|_{Q_h}^2 + \sum_{j=1}^2 \|\hat{w}_{h,j}\|_{\hat{Q}_{h,j}}^2 + |c|^2 ,
$$
$$
\|(\mathbf{v}_h, \mathbf{w}_h)\|_{\mathcal{D}_h}^2 := \|\mathbf{v}_h\|_{\boldsymbol{\mathcal{V}}_h}^2 + \|\mathbf{w}_h\|_{\mathcal{Q}_h}^2
$$

To implement the Nitsche's method we modify the bilinear forms and the functionals to take into account the boundary terms. The bilinear forms for the

99

medium become

$$a_h(\boldsymbol{u}_h,\,\boldsymbol{v}_h) := a(\boldsymbol{u}_h,\,\boldsymbol{v}_h) + \sum_{i=1}^{4} \mu h^{-1}(\boldsymbol{u}_{h,i} \cdot \boldsymbol{n}_\Gamma,\,\boldsymbol{v}_h \cdot \boldsymbol{n}_\Gamma)_{\Gamma_i^E}\,,$$

$$b_h(\boldsymbol{u}_h,\,w_h) := b(\boldsymbol{u}_h,\,w_h) + \sum_{i=1}^{4} (\boldsymbol{u}_{h,i} \cdot \boldsymbol{n}_\Gamma,\,w_h)_{\Gamma_i^E}\,,$$

with $\mu \in \mathbb{R}^+$ a penalty parameter. The functionals become

$$F_{h,q}\,(w_h) := F_q\,(w_h) - \sum_{i=1}^{4} (w_h,\,\overline{u_i})_{\Gamma_i^E}\,,$$

$$F_{h,\boldsymbol{q}}\,(\boldsymbol{v}_h) := F_{\boldsymbol{q}}\,(\boldsymbol{v}_h) + \sum_{i=1}^{4} \mu h^{-1}(\overline{u_i},\,\boldsymbol{v}_h \cdot \boldsymbol{n}_\Gamma)_{\Gamma_i^E}\,,$$

while for the fractures the bilinear forms become for $j = 1, 2$

$$\hat{a}_{h,j}(\hat{\boldsymbol{u}}_{h,j},\,\hat{\boldsymbol{v}}_h) := \hat{a}_j(\hat{\boldsymbol{u}}_{h,j},\,\hat{\boldsymbol{v}}_h) + \mu \hat{h}^{-1}\,\hat{\boldsymbol{u}}_{h,j} \cdot \boldsymbol{n}_\Gamma \hat{\boldsymbol{v}}_h\big|_{\partial \gamma_j^E} \cdot \boldsymbol{n}_\Gamma\,,$$

$$\hat{b}_{h,j}(\hat{\boldsymbol{u}}_{h,j},\,\hat{w}_h) := \hat{b}_j(\hat{\boldsymbol{u}}_{h,j},\,\hat{w}_h) + \hat{w}_h \hat{\boldsymbol{u}}_{h,j}\big|_{\partial \gamma_j^E} \cdot \boldsymbol{n}_\Gamma\,,$$

and the functionals read

$$\hat{F}_{h,\hat{q},j}\,(\hat{w}_j) := \hat{F}_{\hat{q},j}\,(\hat{w}_j) - \overline{\hat{\boldsymbol{u}}_j} \cdot \boldsymbol{n}_\Gamma \hat{w}_j\big|_{\partial \gamma_j^E}\,,$$

$$\hat{F}_{h,\hat{\boldsymbol{q}},j}\,(\hat{\boldsymbol{v}}_h) := \hat{F}_{\hat{\boldsymbol{q}},j}\,(\hat{\boldsymbol{v}}_h) + \mu \hat{h}^{-1}\,\overline{\hat{\boldsymbol{u}}_j} \cdot \boldsymbol{n}_\Gamma \hat{\boldsymbol{v}}_h\big|_{\partial \gamma_j^E} \cdot \boldsymbol{n}_\Gamma\,.$$

Finally the global bilinear forms for the discrete problem are

$$\alpha_h(\mathbf{u}_h,\,\mathbf{v}_h) := a_h(\boldsymbol{u}_h,\,\boldsymbol{v}_h) + \sum_{j=1}^{2} \hat{a}_{h,j}(\hat{\boldsymbol{u}}_{h,j},\,\hat{\boldsymbol{v}}_h)\,,$$

$$\beta_h(\mathbf{v}_h,\,\mathrm{p}_h) := b_h(\boldsymbol{v}_h,\,p_h) + \sum_{j=1}^{2} \hat{b}_{h,j}(\hat{\boldsymbol{v}}_h,\,\hat{p}_{h,j}) + d(\boldsymbol{v}_h,\,\hat{p}_{h,j}) +$$

$$+ \hat{d}_j(\hat{\boldsymbol{v}}_h,\,\hat{p}_{h,I})\,,$$

$$\mathcal{A}_h\,[(\mathbf{u}_h,\,\mathrm{p}_h),\,(\mathbf{v}_h,\,\mathrm{w}_h)] := \alpha_h(\mathbf{u}_h,\,\mathbf{v}_h) + \beta_h(\mathbf{v}_h,\,\mathrm{p}_h) - \beta_h(\mathbf{u}_h,\,\mathrm{w}_h)$$

while the global functionals are

$$\mathcal{F}_{h,\boldsymbol{q}}\,(\mathbf{v}_h) := F_{h,\boldsymbol{q}}\,(\boldsymbol{v}_h) + \sum_{j=1}^{2} \hat{F}_{h,\hat{\boldsymbol{q}},j}\,(\hat{\boldsymbol{v}}_{h,j})\,,$$

$$\mathcal{F}_{h,q}\,(\mathrm{w}_h) := -\,F_{h,q}(w) - \sum_{j=1}^{2} \hat{F}_{\hat{q},j}\,(\hat{w}_j)\,,$$

$$\mathcal{F}_h(\mathbf{v}_h,\,\mathrm{w}_h) := \mathcal{F}_{h,\boldsymbol{q}}\,(\mathbf{v}_h) + \mathcal{F}_{h,q}\,(\mathrm{w}_h)\,,$$

with $\mathbf{u}_h := (\boldsymbol{u}_h,\,\hat{\boldsymbol{u}}_{h,1},\,\hat{\boldsymbol{u}}_{h,2}) \in \boldsymbol{\mathcal{V}}_h$ the discrete Darcy velocity in the medium and in each fracture, $\mathrm{p}_h := (p_h,\,\hat{p}_{h,1},\,\hat{p}_{h,2},\,\hat{p}_{h,I}) \in \mathcal{Q}_h$ the discrete pressure in the medium, in each fracture and in the intersection point $\boldsymbol{i}_p$. Using the above operators we obtain

Problem 3.7 (Discrete Formulation of Darcy Reduced Model with Intersection). *The discrete formulation of Problem 3.6 is: find $(\mathbf{u}_h, \mathrm{p}_h) \in \mathcal{D}_h$ such that*

$$\begin{cases} \alpha_h(\mathbf{u}_h,\, \mathbf{v}_h) + \beta_h(\mathbf{v}_h, \mathrm{p}_h) = \mathcal{F}_{h,\boldsymbol{q}}\,(\mathbf{v}_h) & \forall \mathbf{v}_h \in \boldsymbol{\mathcal{V}}_h\,, \\ \beta_h(\mathbf{u}_h,\, \mathrm{w}_h) = \mathcal{F}_{h,q}\,(\mathrm{w}_h) & \forall \mathrm{w}_h \in \mathcal{Q}_h\,, \end{cases}$$

or alternatively

$$\mathcal{A}_h\left[(\mathbf{u}_h,\, \mathrm{p}_h),\, (\mathbf{v}_h,\, \mathrm{w}_h)\right] = \mathcal{F}_h(\mathbf{v}_h,\, \mathrm{w}_h) \quad \forall (\mathbf{v}_h,\, \mathrm{w}_h) \in \mathcal{D}_h\,.$$

We recall an important theorem from [24] valid if the fractures do not intersect each other and if the pressures in the fractures $\hat{p}_{h,i}$ are known.

Theorem 3.5 (Convergence [24]). *Let $(\mathbf{u}, \mathrm{p}) \in \mathcal{D}$ be the solution of Problem 3.4. If the fractures do not intersect each other and $\hat{p}_{h,i}$ are known, then there exist a unique discrete solution $(\mathbf{u}_h, \mathrm{p}_h) \in \mathcal{D}_h$ of Problem 3.7. Furthermore*

$$\|(\mathbf{u}_h - \mathbf{u},\, \mathrm{p}_h - \mathrm{p})\|_{\mathcal{D}_h} \leq M_\gamma \inf_{(\mathbf{v}_h,\, \mathrm{w}_h) \in \mathcal{D}_h} \|(\mathbf{v}_h - \mathbf{u},\, \mathrm{w}_h - \mathrm{p})\|_{\mathcal{D}_h}\,,$$

with $M_\gamma := \max\left\{1, h\sqrt{\eta_\gamma / \min\left\{\lambda_{\boldsymbol{K}}^{-1}\right\}}\right\}$ and $\lambda_{\boldsymbol{K}}$ is the minimum eigenvalue of $\boldsymbol{K}$ on D.

The following results are an extension of the results presented in [24] when the fractures intersect and the pressures in the fractures and in the intersection points are known. The proofs are similar to the one presented in [24], where the key is the construction of *patches of elements* in the cut region $\mathcal{CR}_h$.

Under Assumption 3.7 a sub-element $K_j = K \cap \Omega_j \neq \emptyset$ of $K \in \mathcal{CR}_h$ can be a triangle, a quadrangle or a pentagon. See Figure 3.19 as an example.
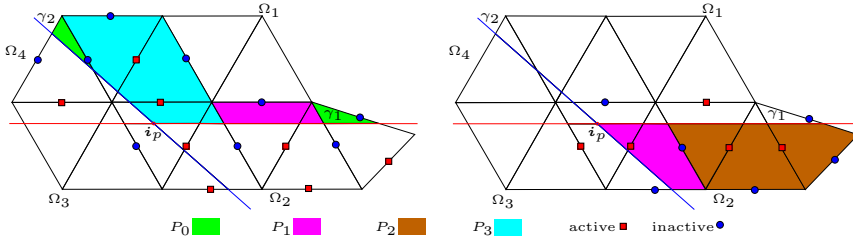
Figure 3.19: In the left the patches for the domain Ω_1, in the right the patches for the domain Ω_2. In both cases there are indicated also the active and inactive edges for $\boldsymbol{v}_p$.

We enrich the definition of patches given in [24] to our problem. For each $K \in \cup_i \mathcal{G}_{h,i}$ let e_K the only edge, which we call *active edge*, of K that is not cut by γ_i. There are only two possibilities: either $e_K \cap \Omega_j = \emptyset$ or $e_K \subset \partial \mathcal{T}_h \cap \partial \mathcal{G}_{h,i}$. In the first case K_j is a triangle, we say that K is of type T and we write $K \sim T$. In the other case K_j is a quadrangle, we say that K is of type Q and we write $K \sim Q$. In the region $\mathcal{M}_h$ the sub-element K_j can be a pentagon then we say that K is of type R and we write $K \sim R$, a quadrangle then $K \sim Q$, or a triangle then $K \sim T$. In the last case the triangle K_j always shares a

vertex V with K. We call the active edge e_K the edge of K opposite to V. We indicate with $K \sim \{Q, R\}$ the fact that $K \sim Q$ or $K \sim R$. Finally if $K \in \mathcal{I}_h$ the sub-element K_j can be a quadrangle then $K \sim Q$, a pentagon then $K \sim R$ or a triangle then $K \sim T$. In the last case the triangle K_j shares only a part of an edge e_{sh} of K, then we call the active edge e_K one of the two edges in the set $\partial K \setminus e_{sh}$.

We split $\mathcal{CR}_h$ in the following types of patch:

- patches of type P_0 are formed by a single element $K \sim T$;

- patches of type P_n are formed by one element $K' \sim T$ and n elements $K \sim \{Q, R\}$;

- patches of type S_n are formed by n elements $K \sim Q$.

Assumption 3.8 (Shape regularity). *Let K^1 and K^2 be two adjacent elements in $\mathcal{CR}_h$. There exist two constant $c, C \in \mathbb{R}^+$, dependent only on γ_i, such that*

$$\left| K_j^1 \right| \leq C \left| K_j^2 \right| \qquad \text{if } K^1 \sim T \text{ and } K^2 \sim \{Q, R\},$$
$$c \left| K_j^1 \right| \leq \left| K_j^2 \right| \leq C \left| K_j^1 \right| \qquad \text{if } K^1, K^2 \sim \{Q, R\}.$$

Lemma 3.6 (Inf-sup condition). *Under Assumption 3.8 and if $\hat{p}_{h,i}$ and $\hat{p}_{h,I}$ are known, then for any pressure $p_h \in Q_h$ there exists $\boldsymbol{v}_p \in \boldsymbol{V}_h$ such that*

$$b(\boldsymbol{v}_p, \, p_h) \gtrsim \|p_h\|_{Q_h}^2 \quad \text{and} \quad \|\boldsymbol{v}_p\|_{\boldsymbol{V}_h} \lesssim M_\gamma \|p_h\|_{Q_h} \, ,$$

moreover $\boldsymbol{v}_p = \boldsymbol{0}$ on Γ^E. The h-dependent constant M_γ is the same as in Theorem 3.5.

Proof. We can identify a patch of type S_n to a patch of type P_n simply choosing as the active edge of the patch the uncut edge of an element. An example of S_n is reported in Figure 3.20.
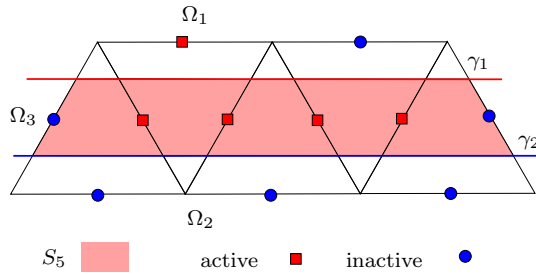
Figure 3.20: Example of a patch of type S_n for the domain Ω_3 with the active and inactive edges for $\boldsymbol{v}_p$.

With the new definition of patches we can apply the proof of [24] as it is, where the edge E_K in [24] is substituted with the active edge e_K defined above and where elements $K \sim Q$ are now elements $K \sim \{Q, R\}$.

$\square$

Thanks to [Lemma 3.6](#) and following [24] we can proof a stability and a convergence theorem analogous to those in [24].

The following lemmas are extensions of the lemmas presented in [24] when the fractures intersect and the pressures in the fractures and in the intersection point are unknowns of the problem.

Lemma 3.7 (Consistency). *Let* $(\mathbf{u}, \mathrm{p}) \in \mathcal{D}$ *be solution of [Problem 3.6](#) and let* $(\mathbf{u}_h, \mathrm{p}_h) \in \boldsymbol{\mathcal{V}}_h \times \mathcal{Q}_h$ *be the solution of [Problem 3.7](#), if* $\overline{\Omega} = \mathcal{T}_h$ *and* $\overline{\gamma}_i = \gamma_{\hat{h},i}$ *for* $i = 1, 2$, *then*

$$\mathcal{A}_h\left[(\mathbf{u} - \mathbf{u}_h, \mathrm{p} - \mathrm{p}_h), (\mathbf{v}_h, \mathrm{w}_h)\right] = 0 \quad \forall (\mathbf{v}_h, \mathrm{w}_h) \in \boldsymbol{\mathcal{V}}_h \times \mathcal{Q}_h.$$

Proof. Due to the linearity of the problem if we can show that

$$\mathcal{A}_h\left[(\mathbf{u}, \mathrm{p}), (\mathbf{v}_h, \mathrm{w}_h)\right] = \mathcal{F}_h(\mathbf{v}_h, \mathrm{w}_h) \quad \forall (\mathbf{v}_h, \mathrm{w}_h) \in \boldsymbol{\mathcal{V}}_h \times \mathcal{Q}_h,$$

the proof is complete. Using the Green's theorem in the bulk and in the fractures we obtain for $j = 1, 2$

$$b_h(\boldsymbol{v}_h, p) = (\nabla p, \boldsymbol{v}_h)_\Omega - (p, \boldsymbol{v}_h \cdot \boldsymbol{n}_\Gamma)_{\Gamma^N} - \sum_{j=1}^{2} \int_{\gamma_j} [\![p\boldsymbol{v}_h \cdot \boldsymbol{n}_j]\!]_{\gamma_j},$$

$$\hat{b}_{h,j}(\hat{\boldsymbol{v}}_h, \hat{p}_j) = \left(\nabla_{\boldsymbol{\tau}_j} \hat{p}_j, \hat{\boldsymbol{v}}_h\right)_{\gamma_j} - \hat{p}_j \hat{\boldsymbol{v}}_h\big|_{\partial \gamma_j^N} \cdot \boldsymbol{n}_\Gamma - [\![\hat{p}_j \hat{\boldsymbol{v}}_h \cdot \boldsymbol{\tau}_j]\!]_{\boldsymbol{i}_p}.$$

Since $(\mathbf{u}, \mathrm{p})$ is the solution of [Problem 3.6](#), then

$$\mathcal{A}_h\left[(\mathbf{u}, \mathrm{p}), (\mathbf{v}_h, \mathrm{w}_h)\right] = (q, \mathrm{w}_h)_\Omega - (\overline{p}, \boldsymbol{v}_h \cdot \boldsymbol{n}_\Gamma)_{\Gamma^N} - \sum_{k=1}^{4} (\overline{u}_k, \mathrm{w}_h)_{\Gamma_k^E} +$$

$$+ \sum_{i=1}^{2} \left(\eta_{\gamma_i} \{\!\!\{ \boldsymbol{u} \cdot \boldsymbol{n}_i \}\!\!\}_{\gamma_i}, \{\!\!\{ \boldsymbol{v}_h \cdot \boldsymbol{n}_i \}\!\!\}_{\gamma_i} \right)_{\gamma_i} + \xi_{0i} \left(\eta_{\gamma_i} [\![\boldsymbol{u} \cdot \boldsymbol{n}_i]\!]_{\gamma_i}, [\![\boldsymbol{v}_h \cdot \boldsymbol{n}_i]\!]_{\gamma_i} \right)_{\gamma_i} +$$

$$+ \mu h^{-1}(\boldsymbol{u}_k \cdot \boldsymbol{n}_\Gamma, \boldsymbol{v}_h \cdot \boldsymbol{n}_\Gamma)_{\Gamma_k^E} + (\hat{q}_i, \hat{w}_h)_{\gamma_i} - \overline{\hat{p}_i} \hat{\boldsymbol{v}}_h\big|_{\partial \gamma_i^N} \cdot \boldsymbol{n}_\Gamma - \overline{\hat{u}_i} \cdot \boldsymbol{n}_\Gamma \hat{w}_h\big|_{\partial \gamma_i^E} +$$

$$+ \frac{\eta_{\gamma_j}}{d_i} \{\!\!\{ \hat{\boldsymbol{u}}_i \cdot \boldsymbol{\tau}_i \}\!\!\}_{\boldsymbol{i}_p} \{\!\!\{ \hat{\boldsymbol{v}}_h \cdot \boldsymbol{\tau}_i \}\!\!\}_{\boldsymbol{i}_p} + \hat{\xi}_0 \frac{\eta_{\gamma_j}}{d_i} [\![\hat{\boldsymbol{u}}_i \cdot \boldsymbol{\tau}_i]\!]_{\boldsymbol{i}_p} [\![\hat{\boldsymbol{v}}_h \cdot \boldsymbol{\tau}_i]\!]_{\boldsymbol{i}_p} +$$

$$+ \mu \hat{h}^{-1} \hat{\boldsymbol{u}}_i\big|_{\partial \gamma_i^E} \cdot \boldsymbol{n}_\Gamma \hat{v}_h\big|_{\partial \gamma_i^E} \cdot \boldsymbol{n}_\Gamma + \left(\hat{p}_i, [\![\boldsymbol{v}_h \cdot \boldsymbol{n}_i]\!]_{\gamma_i} \right)_{\gamma_i} + \hat{p}_I [\![\hat{\boldsymbol{v}}_h \cdot \boldsymbol{\tau}_i]\!]_{\boldsymbol{i}_p} +$$

$$- \int_{\gamma_i} [\![p\boldsymbol{v}_h \cdot \boldsymbol{n}_i]\!]_{\gamma_i} - [\![\hat{p}_i \hat{\boldsymbol{v}}_h \cdot \boldsymbol{\tau}_i]\!]_{\boldsymbol{i}_p}, \tag{3.67}$$

thanks to the interface conditions [(3.55)](#) and [(3.56)](#) for $i = 1, 2$ the last two terms become

$$\int_{\gamma_i} [\![p\boldsymbol{v}_h \cdot \boldsymbol{n}_i]\!]_{\gamma_i} = \left([\![p]\!]_{\gamma_i}, \{\!\!\{ \boldsymbol{v}_h \cdot \boldsymbol{n}_i \}\!\!\}_{\gamma_i} \right)_{\gamma_i} + \left(\{\!\!\{ p \}\!\!\}_{\gamma_i}, [\![\boldsymbol{v}_h \cdot \boldsymbol{n}_i]\!]_{\gamma_i} \right)_{\gamma_i} =$$

$$= \left(\eta_{\gamma_i} \{\!\!\{ \boldsymbol{u} \cdot \boldsymbol{n}_i \}\!\!\}_{\gamma_i}, \{\!\!\{ \boldsymbol{v}_h \cdot \boldsymbol{n}_i \}\!\!\}_{\gamma_i} \right)_{\gamma_i} + \xi_{0i} \left(\eta_{\gamma_i} [\![\boldsymbol{u} \cdot \boldsymbol{n}_i]\!]_{\gamma_i}, [\![\boldsymbol{v}_h \cdot \boldsymbol{n}_i]\!]_{\gamma_i} \right)_{\gamma_i} +$$

$$+ \left(\hat{p}_i, [\![\boldsymbol{v}_h \cdot \boldsymbol{n}_i]\!]_{\gamma_i} \right)_{\gamma_i},$$

and

$$\llbracket \hat{p}_i \boldsymbol{v}_h \cdot \boldsymbol{\tau}_i \rrbracket_{\boldsymbol{i}_p} = \llbracket \hat{p}_i \rrbracket_{\boldsymbol{i}_p} \{\!\!\{ \boldsymbol{\hat{v}}_h \cdot \boldsymbol{\tau}_i \}\!\!\}_{\boldsymbol{i}_p} + \{\!\!\{ \hat{p}_i \}\!\!\}_{\boldsymbol{i}_p} \llbracket \boldsymbol{\hat{v}}_h \cdot \boldsymbol{\tau}_i \rrbracket_{\boldsymbol{i}_p} =$$

$$= \frac{\eta_{\gamma_j}}{d_i} \{\!\!\{ \boldsymbol{\hat{u}}_i \cdot \boldsymbol{\tau}_i \}\!\!\}_{\boldsymbol{i}_p} \{\!\!\{ \boldsymbol{\hat{v}}_h \cdot \boldsymbol{\tau}_i \}\!\!\}_{\boldsymbol{i}_p} + \hat{\xi}_0 \frac{\eta_{\gamma_j}}{d_i} \llbracket \boldsymbol{\hat{u}}_i \cdot \boldsymbol{\tau}_i \rrbracket_{\boldsymbol{i}_p} \llbracket \boldsymbol{\hat{v}}_h \cdot \boldsymbol{\tau}_i \rrbracket_{\boldsymbol{i}_p} +$$

$$+ \hat{p}_I \llbracket \boldsymbol{\hat{v}}_h \cdot \boldsymbol{\tau}_i \rrbracket_{\boldsymbol{i}_p}$$

then equation (3.67) becomes

$$\mathcal{A}_h \left[(\mathbf{u}, \, \mathrm{p}), \, (\mathbf{v}_h, \, \mathrm{w}_h) \right] = (q, \, w_h) - (\overline{p}, \, \boldsymbol{v}_h \cdot \boldsymbol{n}_\Gamma)_{\Gamma^N} - \sum_{k=1}^4 (\overline{u}_k, \, w_h)_{\Gamma_k^E} +$$

$$+ \mu h^{-1} (\overline{u_k}, \, \boldsymbol{v}_h \cdot \boldsymbol{n}_\Gamma)_{\Gamma_k^E} + \sum_{i=1}^2 (\hat{q}_i, \, \hat{w}_h)_{\gamma_i} - \overline{\hat{p}_i \boldsymbol{v}_h}\big|_{\partial \gamma_i^N} \cdot \boldsymbol{n}_\Gamma +$$

$$- \overline{\boldsymbol{\hat{u}}_i} \cdot \boldsymbol{n}_\Gamma \hat{w}_h \big|_{\partial \gamma_i^E} + \mu \hat{h}^{-1} \, \overline{\boldsymbol{\hat{u}}_i} \cdot \boldsymbol{n}_\Gamma \hat{v}_h \big|_{\partial \gamma_i^E} \cdot \boldsymbol{n}_\Gamma = \mathcal{F}_h (\mathbf{v}_h, \, \mathrm{w}_h) \,.$$

$\square$

Lemma 3.8 ($\mathcal{F}_h$-Boundedness)**.** *If $\xi_{0i} > 0$ for $i = 1, 2$ and $\hat{\xi} > 0$ then exists a constant C_h, depending also on h, such that*

$$|\mathcal{F}_h (\mathbf{v}_h, \, \mathrm{w}_h)| \leq C_h \|(\mathbf{v}_h, \, \mathrm{w}_h)\|_{\mathcal{D}_h} \,,$$

where the constant C_h is

$$C_h = \sum_{i=1}^4 C_{\Omega_i} \left\| \rho_{\boldsymbol{K}_i}^{\frac{1}{2}} \overline{p}_i \right\|_{H^{\frac{1}{2}} \left(\Gamma_i^N \right)} + \mu \|\overline{u}_i\|_{h, +\frac{1}{2}, \Gamma_i^E} + \left\| \rho_{\boldsymbol{K}_i}^{-\frac{1}{2}} q_i \right\|_{L^2(\Omega_i)} +$$

$$+ \left\| \rho_{\boldsymbol{K}_i}^{-\frac{1}{2}} \overline{u}_i \right\|_{L^2 \left(\Gamma_i^E \right)} + \sum_{j=1}^2 \hat{C}_{\gamma_{j,k}} \left\| \hat{\eta}_j^{-\frac{1}{2}} \overline{\hat{p}_j} \right\|_{H^{\frac{1}{2}} \left(\partial \gamma_j^N \right)} + \mu \left\| \overline{\boldsymbol{\hat{u}}_j} \cdot \boldsymbol{\tau}_j \right\|_{\hat{h}, +\frac{1}{2}, \partial \gamma_j^E} +$$

$$+ \left\| \hat{\eta}_j^{\frac{1}{2}} \hat{q}_j \right\|_{L^2(\gamma_j)} + \left\| \hat{\eta}_j^{\frac{1}{2}} \overline{\boldsymbol{\hat{u}}_j} \cdot \boldsymbol{\tau}_j \right\|_{L^2 \left(\partial \gamma_j^E \right)} \,.$$

Proof. Using the definition of $\mathcal{F}_h$ and the triangle inequality we find

$$|\mathcal{F}_h (\mathbf{v}_h, \, \mathrm{w}_h)| \leq \sum_{i=1}^4 \left| \left(\rho_{\boldsymbol{K}_i}^{\frac{1}{2}} \overline{p}_i, \, \rho_{\boldsymbol{K}_i}^{-\frac{1}{2}} \boldsymbol{v}_h \cdot \boldsymbol{n}_\Gamma \right)_{\Gamma_i^N} \right| +$$

$$+ \mu \left| \left(h^{-\frac{1}{2}} \overline{u}_i, \, h^{-\frac{1}{2}} \boldsymbol{v}_h \cdot \boldsymbol{n}_\Gamma \right)_{\Gamma_i^E} \right| + \sum_{j=1}^2 \left| \left(\hat{\eta}_j^{-\frac{1}{2}} \overline{\hat{p}_j}, \, \hat{\eta}_j^{\frac{1}{2}} \boldsymbol{\hat{v}}_h \cdot \boldsymbol{n}_\Gamma \right)_{\partial \gamma_j^N} \right| +$$

$$+ \mu \left| \left(\hat{h}^{-\frac{1}{2}} \overline{\boldsymbol{\hat{u}}_j} \cdot \boldsymbol{n}_\Gamma, \, \hat{h}^{-\frac{1}{2}} \boldsymbol{\hat{v}}_h \cdot \boldsymbol{n}_\Gamma \right)_{\partial \gamma_j^E} \right| + \left| \left(\rho_{\boldsymbol{K}_i}^{-\frac{1}{2}} q_i, \, \rho_{\boldsymbol{K}_i}^{\frac{1}{2}} w_h \right)_{\Omega_i} \right| +$$

$$+ \left| \left(\rho_{\boldsymbol{K}_i}^{-\frac{1}{2}} \overline{u}_i, \, \rho_{\boldsymbol{K}_i}^{\frac{1}{2}} w_h \right)_{\Gamma_i^E} \right| + \left| \left(\hat{\eta}_j^{\frac{1}{2}} \hat{q}_j, \, \hat{\eta}_j^{-\frac{1}{2}} \hat{w}_h \right)_{\gamma_j} \right| + \left| \left(\hat{\eta}_j^{\frac{1}{2}} \overline{\boldsymbol{\hat{u}}_j} \cdot \boldsymbol{n}_\Gamma, \, \hat{\eta}_j^{-\frac{1}{2}} \hat{w}_h \right)_{\partial \gamma_j^E} \right| \,.$$

By using Cauchy-Schwartz inequality, the weighted trace inequality in $\boldsymbol{H}_{\mathrm{div}}$ and

104

the definition (3.65) we obtain

$$
\begin{aligned}
|\mathcal{F}_h(\mathbf{v}_h, \mathrm{w}_h)| \leq &\sum_{i=1}^{4} C_{\Omega_i} \left\| \rho_{\boldsymbol{K}_i}^{\frac{1}{2}} \overline{p}_i \right\|_{H^{\frac{1}{2}}\left(\Gamma_i^N\right)} \|\boldsymbol{v}_h\|_{\boldsymbol{H}_{\mathrm{div}}(\Omega_i), \rho_{\boldsymbol{K}_i}^{-\frac{1}{2}}} + \\
&+ \mu \|\overline{u}_i\|_{h, +\frac{1}{2}, \Gamma_i^E} \|\boldsymbol{v}_h \cdot \boldsymbol{n}_\Gamma\|_{h, +\frac{1}{2}, \Gamma_i^E} + \\
&+ \sum_{j=1}^{2} \hat{C}_{\gamma_{j,k}} \left\| \hat{\eta}_j^{-\frac{1}{2}} \overline{\hat{p}}_j \right\|_{H^{\frac{1}{2}}\left(\partial\gamma_j^N\right)} \|\hat{\boldsymbol{v}}_h\|_{\boldsymbol{H}_{\mathrm{div}}(\gamma_j), \hat{\eta}_j^{\frac{1}{2}}} + \\
&+ \mu \left\| \overline{\hat{\boldsymbol{u}}_j \cdot \boldsymbol{\tau}_j} \right\|_{\hat{h}, +\frac{1}{2}, \partial\gamma_j^E} \|\hat{\boldsymbol{v}}_h \cdot \boldsymbol{\tau}_j\|_{\hat{h}, +\frac{1}{2}, \partial\gamma_j^E} + \left\| \rho_{\boldsymbol{K}_i}^{-\frac{1}{2}} q_i \right\|_{L^2(\Omega_i)} \left\| \rho_{\boldsymbol{K}_i}^{\frac{1}{2}} w_h \right\|_{L^2(\Omega_i)} + \\
&+ \left\| \rho_{\boldsymbol{K}_i}^{-\frac{1}{2}} \overline{u}_i \right\|_{L^2\left(\Gamma_i^E\right)} \left\| \rho_{\boldsymbol{K}_i}^{\frac{1}{2}} w_h \right\|_{L^2(\Omega_i)} + \sum_{j=1}^{2} \left\| \hat{\eta}_j^{\frac{1}{2}} \hat{q}_j \right\|_{L^2(\gamma_j)} \left\| \hat{\eta}_j^{-\frac{1}{2}} \hat{w}_h \right\|_{L^2(\gamma_j)} + \\
&+ \left\| \hat{\eta}_j^{\frac{1}{2}} \overline{\hat{\boldsymbol{u}}_j \cdot \boldsymbol{\tau}_j} \right\|_{L^2\left(\partial\gamma_j^E\right)} \left\| \hat{\eta}_j^{-\frac{1}{2}} \hat{w}_h \right\|_{L^2(\gamma_j)}
\end{aligned}
$$

with $C_{\Omega_i} \in \mathbb{R}^+$ the constant for the trace inequality for the sub-domain Ω_i and $\hat{C}_{\gamma_{j,k}} \in \mathbb{R}^+$ the constant for the trace inequality for the sub-domain $\gamma_{j,k}$.

$\square$

Lemma 3.9 ($\mathcal{A}_h$-Boundedness)*. The bilinear form $\mathcal{A}_h$ is bounded in $\mathcal{D}_h$, that is*

$$
|\mathcal{A}_h\left[(\mathbf{u}_h, \mathrm{p}_h), (\mathbf{v}_h, \mathrm{w}_h)\right]| \leq C \|(\mathbf{u}_h, \mathrm{p}_h)\|_{\mathcal{D}_h} \|(\mathbf{v}_h, \mathrm{w}_h)\|_{\mathcal{D}_h},
$$

where the constant $C \in \mathbb{R}^+$ depends on the penalty parameter μ and the thickness of the fracture d_j.

Proof.

$$
|\mathcal{A}_h\left[(\mathbf{u}_h, \mathrm{p}_h), (\mathbf{v}_h, \mathrm{w}_h)\right]| \leq |\alpha_h(\mathbf{u}_h, \mathbf{v}_h)| + |\beta_h(\mathbf{v}_h, \mathrm{p}_h)| + |\beta_h(\mathbf{u}_h, \mathrm{w}_h)|,
$$

we estimate each piece of the previous inequality.

$$
\begin{aligned}
|\alpha_h(\mathbf{u}_h, \mathbf{v}_h)| \leq &|a_h(\boldsymbol{u}_h, \boldsymbol{v}_h)| + \sum_{j=1}^{2} |\hat{a}_{h,j}(\hat{\boldsymbol{u}}_{h,j}, \hat{\boldsymbol{v}}_h)| \leq |a(\boldsymbol{u}_h, \boldsymbol{v}_h)| + \\
&+ \sum_{i=1}^{4} \left| \mu h^{-1}(\boldsymbol{u}_{h,i} \cdot \boldsymbol{n}_\Gamma, \boldsymbol{v}_h \cdot \boldsymbol{n}_\Gamma)_{\Gamma_i^E} \right| + \sum_{j=1}^{2} |\hat{a}_j(\hat{\boldsymbol{u}}_{h,j}, \hat{\boldsymbol{v}}_h)| + \\
&+ \left| \mu \hat{h}^{-1} \hat{\boldsymbol{u}}_{h,j} \cdot \boldsymbol{n}_\Gamma \hat{v}_h|_{\partial\gamma_j^E} \cdot \boldsymbol{n}_\Gamma \right|,
\end{aligned}
$$

the first term is bounded by

$$|a(\boldsymbol{u}_h, \boldsymbol{v}_h)| \leq \left|(\boldsymbol{K}^{-1}\boldsymbol{u}_h, \boldsymbol{v}_h)_\Omega\right| + \sum_{j=1}^{2}\left|\left(\eta_{\gamma_j}\{\!\!\{\boldsymbol{u}_h\cdot\boldsymbol{n}_j\}\!\!\}_{\gamma_j}, \{\!\!\{\boldsymbol{v}_h\cdot\boldsymbol{n}_j\}\!\!\}_{\gamma_j}\right)_{\gamma_j}\right| +$$

$$+\,\xi_{0j}\left|\left(\eta_{\gamma_j}[\![\boldsymbol{u}_h\cdot\boldsymbol{n}_j]\!]_{\gamma_j}, [\![\boldsymbol{v}_h\cdot\boldsymbol{n}_j]\!]_{\gamma_j}\right)_{\gamma_j}\right| \leq$$

$$\leq \sum_{i=1}^{4}\left\|\rho_{\boldsymbol{K}_i}^{-\frac{1}{2}}\boldsymbol{u}_{h,i}\right\|_{L^2(\Omega_i)}\left\|\rho_{\boldsymbol{K}_i}^{-\frac{1}{2}}\boldsymbol{v}_{h,i}\right\|_{L^2(\Omega_i)} +$$

$$+\sum_{j=1}^{2}\left\|\hat{\eta}_j^{\frac{1}{2}}\{\!\!\{\boldsymbol{u}_h\cdot\boldsymbol{n}_j\}\!\!\}_{\gamma_j}\right\|_{L^2(\gamma_{\hat{h},j})}\left\|\hat{\eta}_j^{\frac{1}{2}}\{\!\!\{\boldsymbol{v}_h\cdot\boldsymbol{n}_j\}\!\!\}_{\gamma_j}\right\|_{L^2(\gamma_{\hat{h},j})} +$$

$$+\,\xi_{0j}\left\|\eta_{\gamma_j}^{\frac{1}{2}}[\![\boldsymbol{v}_h\cdot\boldsymbol{n}_j]\!]_{\gamma_j}\right\|_{L^2(\gamma_{\hat{h},j})}\left\|\eta_{\gamma_j}^{\frac{1}{2}}[\![\boldsymbol{u}_h\cdot\boldsymbol{n}_j]\!]_{\gamma_j}\right\|_{L^2(\gamma_{\hat{h},j})} \leq \|\boldsymbol{u}_h\|_{\boldsymbol{V}_h}\|\boldsymbol{v}_h\|_{\boldsymbol{V}_h}\,.$$

The penalisation term in the medium is bounded by

$$\left|\mu h^{-1}(\boldsymbol{u}_{h,i}\cdot\boldsymbol{n}_\Gamma, \boldsymbol{v}_h\cdot\boldsymbol{n}_\Gamma)_{\Gamma_i^E}\right| \leq \mu\|\boldsymbol{u}_{h,i}\cdot\boldsymbol{n}_\Gamma\|_{h,+\frac{1}{2},\Gamma_i^E}\|\boldsymbol{v}_{h,i}\cdot\boldsymbol{n}_\Gamma\|_{h,+\frac{1}{2},\Gamma_i^E} \leq$$

$$\leq \mu\|\boldsymbol{u}_h\|_{\boldsymbol{V}_h}\|\boldsymbol{v}_h\|_{\boldsymbol{V}_h}\,.$$

The bilinear form $\hat{a}_j$ is bounded by

$$|\hat{a}_j(\hat{\boldsymbol{u}}_{h,j}, \hat{\boldsymbol{v}}_h)| \leq \left|(\hat{\eta}_j\hat{\boldsymbol{u}}_{h,j}, \hat{\boldsymbol{v}}_h)_{\gamma_j}\right| + \frac{\eta_{\gamma_i}}{d_j}\left|\{\!\!\{\hat{\boldsymbol{u}}_{h,j}\cdot\boldsymbol{\tau}_j\}\!\!\}_{\boldsymbol{i}_p}\{\!\!\{\hat{\boldsymbol{v}}_h\cdot\boldsymbol{\tau}_j\}\!\!\}_{\boldsymbol{i}_p}\right| +$$

$$+\,\hat{\xi}_0\frac{\eta_{\gamma_i}}{d_j}\left|[\![\hat{\boldsymbol{u}}_{h,j}\cdot\boldsymbol{\tau}_j]\!]_{\boldsymbol{i}_p}[\![\hat{\boldsymbol{v}}_h\cdot\boldsymbol{\tau}_j]\!]_{\boldsymbol{i}_p}\right| \leq$$

$$\leq \sum_{k=1}^{2}\left\|\eta_{\boldsymbol{\tau}_j}^{\frac{1}{2}}\hat{\boldsymbol{u}}_{h,j,k}\right\|_{L^2(\gamma_{\hat{h},j,k})}\left\|\eta_{\boldsymbol{\tau}_j}^{\frac{1}{2}}\hat{\boldsymbol{v}}_{h,k}\right\|_{L^2(\gamma_{\hat{h},j,k})} +$$

$$+\frac{\eta_{\gamma_i}}{d_j}\left|\{\!\!\{\hat{\boldsymbol{u}}_{h,j}\cdot\boldsymbol{\tau}_j\}\!\!\}_{\boldsymbol{i}_p}\right|\left|\{\!\!\{\hat{\boldsymbol{v}}_h\cdot\boldsymbol{\tau}_j\}\!\!\}_{\boldsymbol{i}_p}\right| +$$

$$+\,\hat{\xi}_0\frac{\eta_{\gamma_i}}{d_j}\left|[\![\hat{\boldsymbol{u}}_{h,j}\cdot\boldsymbol{\tau}_j]\!]_{\boldsymbol{i}_p}\right|\left|[\![\hat{\boldsymbol{v}}_h\cdot\boldsymbol{\tau}_j]\!]_{\boldsymbol{i}_p}\right| \leq \|\hat{\boldsymbol{u}}_{h,j}\|_{\hat{\boldsymbol{V}}_{h,j}}\|\hat{\boldsymbol{v}}_h\|_{\hat{\boldsymbol{V}}_{h,j}}\,.$$

The penalisation term for each fracture j is bounded by

$$\left|\mu\hat{h}^{-1}\,\hat{\boldsymbol{u}}_{h,j}\cdot\boldsymbol{n}_\Gamma\hat{\boldsymbol{v}}_h|_{\partial\gamma_j^E}\cdot\boldsymbol{n}_\Gamma\right| \leq \mu\|\hat{\boldsymbol{u}}_{h,j}\cdot\boldsymbol{n}_\Gamma\|_{\hat{h},+\frac{1}{2},\partial\gamma_j^E}\|\hat{\boldsymbol{v}}_h\cdot\boldsymbol{n}_\Gamma\|_{\hat{h},+\frac{1}{2},\partial\gamma_j^E} \leq$$

$$\leq \mu\|\hat{\boldsymbol{u}}_{h,j}\|_{\hat{\boldsymbol{V}}_{h,j}}\|\hat{\boldsymbol{v}}_h\|_{\hat{\boldsymbol{V}}_{h,j}}$$

The bilinear forms β_h are bounded by

$$|\beta_h(\mathbf{v}_h, \mathrm{p}_h)| \leq |b_h(\boldsymbol{v}_h, p_h)| + \sum_{j=1}^{2}\left|\hat{b}_{h,j}(\hat{v}_h, \hat{p}_{h,j})\right| + |d(\boldsymbol{v}_h, \hat{p}_{h,j})| +$$

$$+\left|\hat{d}_j(\hat{\boldsymbol{v}}_h, \hat{p}_{h,I})\right|\,,$$

we now bound each piece of the previous inequality

$$|b_h(\boldsymbol{v}_h,\, p_h)| \leq |b(\boldsymbol{v}_h,\, p_h)| + \sum_{i=1}^{4} \left|(\boldsymbol{v}_h \cdot \boldsymbol{n}_\Gamma,\, p_{h,i})_{\Gamma_i^E}\right| \leq \sum_{i=1}^{4} \left|(\nabla{\cdot}\boldsymbol{v}_h,\, p_{h,i})_{\Omega_i}\right| +$$

$$+\, \|\boldsymbol{v}_h \cdot \boldsymbol{n}_\Gamma\|_{L^2\left(\Gamma_i^E\right)} \|p_{h,i}\|_{L^2\left(\Gamma_i^E\right)} \leq \|\boldsymbol{v}_h\|_{\boldsymbol{V}_h} \|p_h\|_{Q_h} + C_\Omega \|\boldsymbol{v}_h\|_{\boldsymbol{V}_h} \|p_h\|_{Q_h} =$$

$$= (1 + C_\Omega) \|\boldsymbol{v}_h\|_{\boldsymbol{V}_h} \|p_h\|_{Q_h}\,,$$

where $C_\Omega \in \mathbb{R}^+$ is maximum of the trace constants in each Ω_i.

$$\left|\hat{b}_{h,j}(\hat{\boldsymbol{v}}_h,\, \hat{p}_{h,j})\right| \leq \left|\hat{b}_j(\hat{\boldsymbol{v}}_h,\, \hat{p}_{h,j})\right| + \left|\hat{p}_{h,j}\hat{\boldsymbol{v}}_h|_{\partial\gamma_j^E} \cdot \boldsymbol{n}_\Gamma\right| \leq$$

$$\leq \left|\left(\nabla_{\boldsymbol{\tau}_j} \cdot \hat{\boldsymbol{v}}_h,\, \hat{p}_{h,j}\right)_{\gamma_j}\right| + \left|\hat{p}_{h,j}|_{\partial\gamma_j^E}\right|\left|\hat{\boldsymbol{v}}_h|_{\partial\gamma_j^E} \cdot \boldsymbol{n}_\Gamma\right| \leq$$

$$\leq \|\hat{\boldsymbol{v}}_h\|_{\hat{\boldsymbol{V}}_{h,j}} \|\hat{p}_{h,j}\|_{\hat{Q}_{h,j}} + \hat{C}_{\gamma_j} \|\hat{\boldsymbol{v}}_h\|_{\hat{\boldsymbol{V}}_{h,j}} \|\hat{p}_{h,j}\|_{\hat{Q}_{h,j}} =$$

$$= \left(1 + \hat{C}_{\gamma_j}\right) \|\hat{\boldsymbol{v}}_h\|_{\hat{\boldsymbol{V}}_{h,j}} \|\hat{p}_{h,j}\|_{\hat{Q}_{h,j}}\,.$$

where $\hat{C}_{\gamma_j} \in \mathbb{R}^+$ is maximum of the trace constants in each $\gamma_{j,k}$. Furthermore we have

$$|d(\boldsymbol{v}_h,\, \hat{p}_{h,j})| = \left|\left(\hat{p}_j,\, [\![\boldsymbol{v} \cdot \boldsymbol{n}_j]\!]_{\gamma_j}\right)_{\gamma_j}\right| \leq \|\hat{p}_j\|_{L^2(\gamma_j)} \left\|[\![\boldsymbol{v}_h \cdot \boldsymbol{n}_j]\!]_{\gamma_j}\right\|_{L^2(\gamma_j)} \leq$$

$$\leq \|\hat{p}_j\|_{\hat{Q}_{h,j}} \|\boldsymbol{v}_h\|_{\boldsymbol{V}_h}\,,$$

and finally

$$\left|\hat{d}_j(\hat{\boldsymbol{v}}_h,\, \hat{p}_{h,I})\right| = \left|\hat{p}_I\, [\![\hat{\boldsymbol{v}} \cdot \boldsymbol{\tau}_j]\!]_{\boldsymbol{i}_p}\right| \leq |\hat{p}_I|\left|[\![\hat{\boldsymbol{v}} \cdot \boldsymbol{\tau}_j]\!]_{\boldsymbol{i}_p}\right| \leq |\hat{p}_I|\, \|\hat{\boldsymbol{v}}\|_{\hat{\boldsymbol{V}}_{h,j}}\,.$$

We can bound $\beta_h(\mathbf{u}_h,\, \mathbf{w}_h)$ in the same way as $\beta_h(\mathbf{v}_h,\, \mathbf{p}_h)$ obtaining the result. $\qquad\square$

Lemma 3.10 ($\mathcal{A}_h$-Positivity). *If $\mu \geq 1$ then the bilinear form $\mathcal{A}_h$ is positive, that is*

$$\mathcal{A}_h\left[(\mathbf{v}_h,\, \mathbf{w}_h),\, (\mathbf{v}_h,\, \mathbf{w}_h)\right] \geq \|\mathbf{v}_h\|_*^2\,,$$

where $\|\cdot\|_* : \boldsymbol{\mathcal{V}}_h \to \mathbb{R}$ is defined as

$$\|\mathbf{v}_h\|_* := \|\mathbf{v}_h\|_{\boldsymbol{\mathcal{V}}_h} - \sum_{i=1}^{4} \|\boldsymbol{v}_{h,i}\|_{\boldsymbol{H}_{\mathrm{div}}(\Omega_i),\rho_{\boldsymbol{K}_i}^{-\frac{1}{2}}} - \sum_{k=1}^{2} \|\hat{\boldsymbol{v}}_{h,k}\|_{\boldsymbol{H}_{\mathrm{div}}\left(\gamma_{\hat{h},j,k}\right),\eta_{\boldsymbol{\tau}_j}^{\frac{1}{2}}}\,.$$

Proof. If $\mu \geq 1$, then we have

$$\mathcal{A}_h\left[(\mathbf{v}_h,\, \mathbf{w}_h),\, (\mathbf{v}_h,\, \mathbf{w}_h)\right] = \alpha_h(\mathbf{v}_h,\, \mathbf{v}_h) \geq \|\mathbf{v}_h\|_*^2\,.$$

$\qquad\square$

3.2.4 Algebraic formulation

We now introduce the matrices and the vectors associated to the bilinear forms of Problem 3.7. For the medium we set

$$[\boldsymbol{A}]_{ij} := a_h(\boldsymbol{\psi}_j, \boldsymbol{\psi}_i), \qquad [\boldsymbol{B}]_{ij} := b_h(\boldsymbol{\psi}_i, \phi_j),$$
$$[\boldsymbol{F_q}]_i := F_{\boldsymbol{q},h}(\boldsymbol{\psi}_i), \qquad [\boldsymbol{F_q}]_i := F_{q,h}(\phi_i),$$

while, for each fracture $k = 1, 2$ we have

$$\left[\hat{\boldsymbol{A}}_k\right]_{ij} := \hat{a}_{h,k}\left(\hat{\boldsymbol{\psi}}_j, \hat{\boldsymbol{\psi}}_i\right), \qquad \left[\hat{\boldsymbol{B}}_k\right]_{ij} := \hat{b}_{h,k}\left(\hat{\boldsymbol{\psi}}_i, \hat{\phi}_j\right),$$
$$\left[\hat{\boldsymbol{F}}_{\hat{\boldsymbol{q}},k}\right]_i := \hat{F}_{h,\hat{\boldsymbol{q}},k}\left(\hat{\boldsymbol{\psi}}_i\right), \qquad \left[\hat{\boldsymbol{F}}_{\hat{q},k}\right]_i := \hat{F}_{h,\hat{q},k}\left(\hat{\phi}_i\right),$$

and for the medium-fracture interaction

$$[\boldsymbol{E}]_{ij} := d\left(\boldsymbol{\psi}_i, \hat{\phi}_j\right).$$

Finally, for the fracture-fracture interaction we set

$$\left[\hat{\boldsymbol{E}}_k\right]_{ij} := \hat{d}_k(\boldsymbol{\psi}_i, 1).$$

The global algebraic system is then

$$
\begin{bmatrix}
\boldsymbol{A} & \boldsymbol{B} & \boldsymbol{0} & \boldsymbol{E}_1 & \boldsymbol{0} & \boldsymbol{E}_2 & \boldsymbol{0} \\
\boldsymbol{B}^\top & \boldsymbol{0} & \boldsymbol{0} & \boldsymbol{0} & \boldsymbol{0} & \boldsymbol{0} & \boldsymbol{0} \\
\boldsymbol{0} & \boldsymbol{0} & \hat{\boldsymbol{A}}_1 & \hat{\boldsymbol{B}}_1 & \boldsymbol{0} & \boldsymbol{0} & \hat{\boldsymbol{E}}_1 \\
\boldsymbol{E}_1^\top & \boldsymbol{0} & \hat{\boldsymbol{B}}_1^\top & \boldsymbol{0} & \boldsymbol{0} & \boldsymbol{0} & \boldsymbol{0} \\
\boldsymbol{0} & \boldsymbol{0} & \boldsymbol{0} & \boldsymbol{0} & \hat{\boldsymbol{A}}_2 & \hat{\boldsymbol{B}}_2 & \hat{\boldsymbol{E}}_2 \\
\boldsymbol{E}_2^\top & \boldsymbol{0} & \boldsymbol{0} & \boldsymbol{0} & \hat{\boldsymbol{B}}_2^\top & \boldsymbol{0} & \boldsymbol{0} \\
\boldsymbol{0} & \boldsymbol{0} & \hat{\boldsymbol{E}}_2^\top & \boldsymbol{0} & \hat{\boldsymbol{E}}_2^\top & \boldsymbol{0} & \boldsymbol{0}
\end{bmatrix}
\begin{bmatrix}
\vec{\boldsymbol{u}} \\
\vec{p} \\
\vec{\hat{\boldsymbol{u}}}_1 \\
\vec{\hat{p}}_1 \\
\vec{\hat{\boldsymbol{u}}}_2 \\
\vec{\hat{p}}_2 \\
\vec{\hat{p}}_I
\end{bmatrix}
=
\begin{bmatrix}
\boldsymbol{F_q} \\
\boldsymbol{F_q} \\
\hat{\boldsymbol{F}}_{\hat{q},1} \\
\hat{\boldsymbol{F}}_{\hat{q},1} \\
\hat{\boldsymbol{F}}_{\hat{q},2} \\
\hat{\boldsymbol{F}}_{\hat{q},2} \\
\boldsymbol{0}
\end{bmatrix}.
$$

It is easy to verify that the matrix is symmetric.

3.3 Passive transport equation

We now consider the model of a passive scalar or tracer transported by an external field in a porous media. The external field can be computed by solving a Darcy problem or can be a given data.

Assumption 3.9 (Passive scalar transport). *We assume the following,*

1. *the domain of interest Ω satisfies Assumption 3.1;*

2. *we indicate the interval of time of interest with $\mathcal{I}_T := (0, T)$, with $T \in \mathbb{R}^+$. We set, as in Assumption 2.2-1, $Q_T := \Omega \times \mathcal{I}_T$. Figure 3.21 shows an example for $n = 2$;*
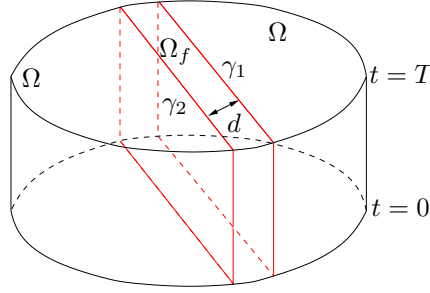
Figure 3.21: Picture of the spatial-temporal cylinder Q_T with the three spatial sub-domains Ω_1, Ω_2 and Ω_f for $n = 2$.

3. *the external convective vector field is the Darcy velocity, of the medium $\boldsymbol{u}$ and the fracture $\hat{\boldsymbol{u}}$, solution of* Problem 3.1.

We indicate with c the concentration of the passive scalar which is dimensionless with the constraint

$$c \in \mathbb{1} \quad \text{a.e. in } Q_T.$$

We indicate with $\boldsymbol{\chi}$ the total flux of the concentration c, defined as

$$\boldsymbol{\chi} := -\boldsymbol{D}\nabla c + \boldsymbol{u}c, \tag{3.68}$$

where $\boldsymbol{D}$ is the molecular diffusion of the tracer given in $[m^2/s]$. The tensor $\boldsymbol{D}$ can vary smoothly in each sub-domain Ω_i, for $i = 1, 2, f$, but may be discontinuous across γ_j, for $j = 1, 2$. Furthermore, in the fracture $\boldsymbol{D}$ may be significantly different from the rest of the domain Ω. The equations which describe the evolution of c in Q_T are given, in mixed form, by

$$
\begin{cases}
\Phi\dfrac{\partial c}{\partial t} + \nabla\!\cdot\!\boldsymbol{\chi} = g & \text{in } Q_T, \\[2mm]
\boldsymbol{D}^{-1}\boldsymbol{\chi} + \nabla c - \boldsymbol{D}^{-1}\boldsymbol{u}c = \boldsymbol{0} & \text{in } Q_T, \\[2mm]
c = \bar{c} & \text{on } \Gamma^N \times \mathcal{I}_T, \\[2mm]
\boldsymbol{\chi} \cdot \boldsymbol{n}_\Gamma = \overline{\chi} & \text{on } \Gamma^E \times \mathcal{I}_T, \\[2mm]
c = c_0 & \text{in } \Omega \times \{0\}.
\end{cases}
\tag{3.69}
$$

Assumption 3.10 (Regularity of the data). *We assume the following regularity hypotheses for the data of system* (3.69)

1. *the source term $g \in L^2(Q_T)$ which can be decomposed as*

$$g = \sum_{i=1,2,f} g_i|_{\Omega_i},$$

with $g_i \in L^2(Q_T)$ defined as $g_i|_{\Omega_i} := g|_{\Omega_i}$ for $i = 1, 2, f$;

2. the symmetric and positive defined molecular diffusion tensor constant in time $\boldsymbol{D} \in [L^\infty (\Omega)]^{n \times n}$, which can be decomposed as

$$\boldsymbol{D} = \sum_{i=1,2,f} \boldsymbol{D}_i \big|_{\Omega_i} \, ,$$

with $\boldsymbol{D}_i \in [L^\infty (\Omega)]^{n \times n}$ defined as $\boldsymbol{D}_i \big|_{\Omega_i} := \boldsymbol{D} \big|_{\Omega_i}$ for $i = 1, 2, f$. We assume the same hypotheses of $\boldsymbol{K}_f$ for $\boldsymbol{D}_f$ reported in Assumption 3.3, so we can write

$$\boldsymbol{D}_f = D_{f,\boldsymbol{n}} \boldsymbol{N} + D_{f,\boldsymbol{\tau}} \boldsymbol{T} \, ,$$

with $D_{f,\boldsymbol{n}}, D_{f,\boldsymbol{\tau}} \in L^\infty (\Omega_f)$ bounded away from zero;

3. the data for the natural boundary condition, $\overline{c} \in L^2 \left(\mathcal{I}_T; H^{\frac{1}{2}} \left(\Gamma^N \right) \right)$ and can be decomposed as

$$\overline{c} = \sum_{i=1,2,f} \overline{c_i} \big|_{\Gamma_i^N} \, ,$$

with $\overline{c_i} \in L^2 \left(\mathcal{I}_T; H^{\frac{1}{2}} \left(\Gamma^N \right) \right)$ defined as $\overline{c_i} \big|_{\Gamma_i^N} := \overline{c} \big|_{\Gamma_i^N}$ for $i = 1, 2, f$;

4. the data for the essential boundary condition, $\overline{\chi} \in L^2 \left(\mathcal{I}_T; H^{-\frac{1}{2}} \left(\Gamma^E \right) \right)$ and can be decomposed as

$$\overline{\chi} = \sum_{i=1,2,f} \overline{\chi_i} \big|_{\Gamma_i^E} \, ,$$

with $\overline{\chi_i} \in L^2 \left(\mathcal{I}_T; H^{-\frac{1}{2}} \left(\Gamma^E \right) \right)$ defined as $\overline{\chi_i} \big|_{\Gamma_i^E} := \overline{\chi} \big|_{\Gamma_i^E}$ for $i = 1, 2, f$;

5. the porosity $\Phi \in L^\infty (\Omega)$ which fulfils Assumption 2.4-1 and can be decomposed as

$$\Phi = \sum_{i=1,2,f} \Phi_i \big|_{\Omega_i} \, ,$$

with $\Phi_i \in L^\infty (\Omega_i)$ defined as $\Phi_i \big|_{\Omega_i} := \Phi \big|_{\Omega_i}$ for $i = 1, 2, f$;

6. the initial condition $c_0 \in L^2 (\Omega)$ can be decomposed as

$$c_0 = \sum_{i=1,2,f} c_{0,i} \big|_{\Omega_i} \, ,$$

with $c_{0,i} \in L^2 (\Omega)$ defined as $c_{0,i} \big|_{\Omega_i} := c_0 \big|_{\Omega_i}$ for $i = 1, 2, f$;

In the sequel we will, with a little abuse of notation, indicate with a subscript i the restriction of a function in the i-th subset of its definition set.

Defining the restriction of the flux $\boldsymbol{\chi}$ and the concentration c in each sub-part Ω_i, for $i = 1, 2, f$, of the domain Ω, i.e. $\boldsymbol{\chi}_i := \boldsymbol{\chi} \big|_{\Omega_i}$ and $c_i := c \big|_{\Omega_i}$ for $i = 1, 2, f$, we can proof the following result.

Proposition 3.11. *The solution* $(\boldsymbol{\chi}, c)$ *of system* (3.69) *satisfies the following differential equations for* $i = 1, 2, f$

$$\begin{cases} \Phi_i \dfrac{\partial c_i}{\partial t} + \nabla\cdot\boldsymbol{\chi}_i = g_i \\[2mm] \boldsymbol{D}_i^{-1}\boldsymbol{\chi}_i + \nabla c_i - \boldsymbol{D}_i^{-1}\boldsymbol{u}_i c_i = \boldsymbol{0} \end{cases} \qquad in \; Q_T \,,$$

equipped with the following coupling conditions for $j = 1, 2$

$$\begin{cases} \boldsymbol{\chi}_j \cdot \boldsymbol{n}_j = \boldsymbol{\chi}_f \cdot \boldsymbol{n}_j \\[2mm] c_j = c_f \end{cases} \qquad on \; \gamma_j \times \mathcal{I}_T \,,$$

and the boundary and initial conditions for $i = 1, 2, f$

$$\begin{cases} c_i = \overline{c_i} & on \; \Gamma_i^N \times \mathcal{I}_T, \\[2mm] \boldsymbol{\chi}_i \cdot \boldsymbol{n}_\Gamma = \overline{\chi_i} & on \; \Gamma_i^E \times \mathcal{I}_T, \\[2mm] c_i = c_{0,i} & in \; \Omega_i \times \{0\}. \end{cases}$$

Proof. By standard means the weak formulation of (3.69) satisfies

$$\begin{cases} \displaystyle\int_\Omega \Phi \dfrac{\partial c}{\partial t} v - \int_\Omega \boldsymbol{\chi} \cdot \nabla v = \int_\Omega gv & \forall v \in H_0^1(\Omega), \\[4mm] \displaystyle\int_\Omega \boldsymbol{D}^{-1}\boldsymbol{\chi}\boldsymbol{\tau} - \int_\Omega c\nabla\cdot\boldsymbol{\tau} - \int_\Omega \boldsymbol{D}^{-1}\boldsymbol{u}c\boldsymbol{\tau} = 0 & \forall \boldsymbol{\tau} \in \boldsymbol{H}_{\mathrm{div},0}(\Omega). \end{cases} \tag{3.70}$$

If we select $v \in H_0^1(\Omega_i)$ for $i = 1, 2$ or f the first equation of (3.70) is equivalent to

$$\int_{\Omega_i} \Phi_i \dfrac{\partial c_i}{\partial t} v - \int_{\Omega_i} \boldsymbol{\chi}_i \cdot \nabla v = \int_{\Omega_i} g_i v \quad \forall v \in H_0^1(\Omega_i) \,,$$

which implies that $\Phi_i \dfrac{\partial c_i}{\partial t} + \nabla\cdot\boldsymbol{\chi}_i - g_i = 0$ in a distributional sense, *i.e.* a.e. in Ω_i. If we now take a $v \in H_0^1(\Omega)$ with support in $\Omega_f \cup \gamma_i \cup \Omega_i$ for $i = 1$ or 2, we have

$$\int_{\Omega_i} \Phi_i \dfrac{\partial c_i}{\partial t} v - \int_{\Omega_i} \boldsymbol{\chi}_i \cdot \nabla v + \int_{\Omega_f} \Phi_f \dfrac{\partial c_f}{\partial t} v - \int_{\Omega_f} \boldsymbol{\chi}_f \cdot \nabla v = \int_{\Omega_i} g_i v + \int_{\Omega_f} g_f v \,, \tag{3.71}$$

that is

$$\begin{aligned} {}_{[H^1(\Omega_i)]'}&< \Phi_i \dfrac{\partial c_i}{\partial t} + \nabla\cdot\boldsymbol{\chi}_i - g_i, \, v >_{H^1(\Omega_1)} + \\[2mm] &+ {}_{[H^1(\Omega_f)]'}< \Phi_f \dfrac{\partial c_f}{\partial t} + \nabla\cdot\boldsymbol{\chi}_f - g_f, \, v >_{H^1(\Omega_f)} + \\[2mm] &+ \int_{\gamma_i} (\boldsymbol{\chi}_i \cdot \boldsymbol{n}_i - \boldsymbol{\chi}_f \cdot \boldsymbol{n}_i) \, v = 0 \,, \end{aligned}$$

but the first two terms are zero because (3.71), obtaining the coupling condition for $\boldsymbol{\chi}$ across γ_i. If we select $\boldsymbol{\tau} \in \boldsymbol{H}_{\mathrm{div},0}\left(\Omega_i\right)$ for $i = 1, 2$ or f the second equation of (3.70) is equivalent to

$$
\int_{\Omega_i} \boldsymbol{D}_i^{-1} \boldsymbol{\chi}_i \cdot \boldsymbol{\tau} - \int_{\Omega_i} c_i \nabla \cdot \boldsymbol{\tau} - \int_{\Omega_i} \boldsymbol{D}_i^{-1} \boldsymbol{u}_i c_i \boldsymbol{\tau} = 0 \quad \forall \boldsymbol{\tau} \in \boldsymbol{H}_{\mathrm{div},0}\left(\Omega_i\right), \quad (3.72)
$$

which implies $\boldsymbol{D}_i^{-1} \boldsymbol{\chi}_i + \nabla c_i - \boldsymbol{D}_i^{-1} \boldsymbol{u}_i c_i = \boldsymbol{0}$ a.e. in Ω_i. If we take now $\boldsymbol{\tau} \in \boldsymbol{H}_{\mathrm{div},0}\left(\Omega\right)$ with support in $\Omega_f \cup \gamma_i \cup \Omega_i$ for $i = 1$ or 2, we have

$$
\int_{\Omega_i} \boldsymbol{D}_i^{-1} \boldsymbol{\chi}_i \cdot \boldsymbol{\tau} - \int_{\Omega_i} c_i \nabla \cdot \boldsymbol{\tau} - \int_{\Omega_i} \boldsymbol{D}_i^{-1} \boldsymbol{u}_i c_i \boldsymbol{\tau} + \int_{\Omega_f} \boldsymbol{D}_f^{-1} \boldsymbol{\chi}_f \cdot \boldsymbol{\tau} +
$$
$$
- \int_{\Omega_f} c_f \nabla \cdot \boldsymbol{\tau} - \int_{\Omega_f} \boldsymbol{D}_f^{-1} \boldsymbol{u}_f c_f \boldsymbol{\tau} = 0,
$$

that is

$$
{}_{[\boldsymbol{H}_{\mathrm{div}}(\Omega_i)]'} < \boldsymbol{D}_i^{-1} \boldsymbol{\chi}_i + \nabla c_i - \boldsymbol{D}_i^{-1} \boldsymbol{u}_i c_i, \, \boldsymbol{\tau} >_{\boldsymbol{H}_{\mathrm{div}}(\Omega_i)} +
$$
$$
+ {}_{[\boldsymbol{H}_{\mathrm{div}}(\Omega_f)]'} < \boldsymbol{D}_f^{-1} c_f + \nabla c_f \boldsymbol{D}_f^{-1} \boldsymbol{u}_f c_f, \, \boldsymbol{\tau} >_{\boldsymbol{H}_{\mathrm{div}}(\Omega_f)} - \int_{\gamma_i} (c_i - c_f) \boldsymbol{\tau} \cdot \boldsymbol{n}_i = 0,
$$

the first two terms are zero because of (3.72), obtaining the coupling condition for c across γ_i.

$\qquad \square$

The system of equation (3.69) with the interface conditions derived in Proposition 3.11 describes the evolution in Ω of the total flux and the concentration.

Problem 3.8 (Transport coupled problem). *The coupled problem for the transport of a tracer in a porous medium is: find $(\boldsymbol{\chi}_i, c_i) \in L^2\left(\mathcal{I}_T; \boldsymbol{H}_{\mathrm{div}}\left(\Omega_i\right)\right) \times L^2\left(\mathcal{I}_T; H^1\left(\Omega_i\right)\right)$ for $i = 1, 2, f$ which satisfy for $i = 1, 2, f$*

$$
\begin{cases} \Phi_i \dfrac{\partial c_i}{\partial t} + \nabla \cdot \boldsymbol{\chi}_i = g_i \\[2mm] \boldsymbol{D}_i^{-1} \boldsymbol{\chi}_i + \nabla c_i - \boldsymbol{D}_i^{-1} \boldsymbol{u}_i c_i = \boldsymbol{0} \end{cases} \qquad in \ Q_T, \qquad (3.73)
$$

together with the coupling conditions for $j = 1, 2$

$$
\begin{cases} \boldsymbol{\chi}_j \cdot \boldsymbol{n}_j = \boldsymbol{\chi}_f \cdot \boldsymbol{n}_j \\[2mm] c_j = c_f \end{cases} \qquad in \ \gamma_j \times \mathcal{I}_T, \qquad (3.74)
$$

and the boundary and initial conditions for $i = 1, 2, f$

$$
\begin{cases} c_i = \overline{c_i} & on \ \Gamma_i^N \times \mathcal{I}_T, \\[2mm] \boldsymbol{\chi}_i \cdot \boldsymbol{n}_\Gamma = \overline{\chi_i} & on \ \Gamma_i^E \times \mathcal{I}_T, \\[2mm] c_i = c_{0,i} & in \ \Omega_i \times \{0\}. \end{cases} \qquad (3.75)
$$

We can notice that the coupling conditions on γ_j, for $j = 1, 2$, of Problem 3.8 are similar to the ones of Problem 3.1 because we have chosen the total flux in the definition (3.68) instead the ordinary flux.

3.3.1 Reduced conservation equation

We now obtain a reduced model form for the conservation equation in the fracture, *i.e.* the first equation in (3.73) for $i = f$. Given the normal vector $\boldsymbol{n}$ along the fracture γ, we introduce the normal flux and tangential flux, namely

$$\boldsymbol{\chi}_{f,\boldsymbol{n}} := \boldsymbol{N}\boldsymbol{\chi}_f \quad \text{and} \quad \boldsymbol{\chi}_{f,\boldsymbol{\tau}} := \boldsymbol{T}\boldsymbol{\chi}_f. \tag{3.76}$$

To obtain the reduced conservation equation, we decompose the divergence in a normal part and a tangential part with respect to γ. We integrate in the normal direction for a fixed point $\boldsymbol{s} = \boldsymbol{s}^*$ with $\boldsymbol{s} \in \gamma$ and fixed time $t = t^*$ with $t^* \in [0, T]$, see Figure 3.22. We get,
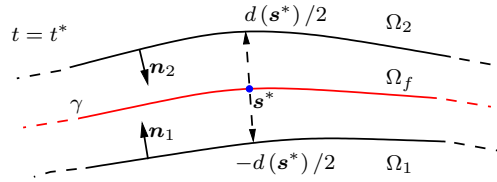
Figure 3.22: Example of a bi-dimensional fracture with the data in the normal direction.

$$\int_{-\frac{d}{2}}^{\frac{d}{2}} \Phi_f \frac{\partial c_f}{\partial t} \, d\boldsymbol{r} + \int_{-\frac{d}{2}}^{\frac{d}{2}} \nabla \cdot \boldsymbol{\chi}_f \, d\boldsymbol{r} =$$

$$\int_{-\frac{d}{2}}^{\frac{d}{2}} \Phi_f \frac{\partial c_f}{\partial t} \, d\boldsymbol{r} + \int_{-\frac{d}{2}}^{\frac{d}{2}} \nabla_{\boldsymbol{n}} \cdot \boldsymbol{\chi}_f \, d\boldsymbol{r} + \int_{-\frac{d}{2}}^{\frac{d}{2}} \nabla_{\boldsymbol{\tau}} \cdot \boldsymbol{\chi}_f \, d\boldsymbol{r} = \int_{-\frac{d}{2}}^{\frac{d}{2}} g_f \, d\boldsymbol{r}.$$

where, for convenience in notation, we drop the dependence on $\boldsymbol{s}^*$ and t^* when it is clear from the context. Defining the total source in a section of the fracture as

$$\hat{g}(\boldsymbol{s}, t) := \int_{-\frac{d(\boldsymbol{s})}{2}}^{\frac{d(\boldsymbol{s})}{2}} g_f(\boldsymbol{r}, t) \, d\boldsymbol{r}(\boldsymbol{s}),$$

and integrating by parts the normal divergence term we have that

$$\int_{-\frac{d}{2}}^{\frac{d}{2}} \Phi_f \frac{\partial c_f}{\partial t} \, d\boldsymbol{r} + \boldsymbol{\chi}_f|_{\gamma_2} \cdot \boldsymbol{n} - \boldsymbol{\chi}_f|_{\gamma_1} \cdot \boldsymbol{n} + \int_{-\frac{d}{2}}^{\frac{d}{2}} \nabla_{\boldsymbol{\tau}} \cdot \boldsymbol{\chi}_f \, d\boldsymbol{r} = \hat{g}. \tag{3.77}$$

The integral with the tangential divergence, in the above equation, becomes

$$\int_{-\frac{d}{2}}^{\frac{d}{2}} \nabla_{\boldsymbol{\tau}} \cdot \boldsymbol{\chi}_f \, d\boldsymbol{r} = \int_{-\frac{d}{2}}^{\frac{d}{2}} \boldsymbol{T} : \nabla \boldsymbol{\chi}_f \, d\boldsymbol{r} = \int_{-\frac{d}{2}}^{\frac{d}{2}} (\boldsymbol{T}\boldsymbol{T}) : \nabla \boldsymbol{\chi}_f \, d\boldsymbol{r} =$$

$$= \boldsymbol{T} : \int_{-\frac{d}{2}}^{\frac{d}{2}} \boldsymbol{T} \nabla \boldsymbol{\chi}_f \, d\boldsymbol{r} \approx \boldsymbol{T} : \nabla \int_{-\frac{d}{2}}^{\frac{d}{2}} \boldsymbol{T} \boldsymbol{\chi}_f \, d\boldsymbol{r},$$

We define the reduced flux in the fracture as

$$\hat{\boldsymbol{\chi}}(\boldsymbol{s}, t) := \int_{-\frac{d(\boldsymbol{s})}{2}}^{\frac{d(\boldsymbol{s})}{2}} \boldsymbol{\chi}_{f,\boldsymbol{\tau}}(\boldsymbol{r}, t) \, d\boldsymbol{r}(\boldsymbol{s}), \tag{3.78}$$

obtaining

$$\boldsymbol{T} : \nabla \int_{-\frac{d}{2}}^{\frac{d}{2}} \boldsymbol{T} \boldsymbol{\chi}_f \, d\boldsymbol{r} = \nabla_{\boldsymbol{\tau}} \cdot \hat{\boldsymbol{\chi}} \, .$$

Assumption 3.11 (Porosity). *We assume the porosity Φ_f is constant in each transversal section of the fracture Ω_f.*

Defining the mean concentration in the fracture as

$$\hat{c}\left(\boldsymbol{s}, \, t\right) := \frac{1}{d\left(\boldsymbol{s}\right)} \int_{-\frac{d(\boldsymbol{s})}{2}}^{\frac{d(\boldsymbol{s})}{2}} c_f\left(\boldsymbol{r}, \, t\right) \, d\boldsymbol{r}\left(\boldsymbol{s}\right) \, , \qquad (3.79)$$

with Assumption 3.11 the integral with time derivative in (3.77) becomes

$$\int_{-\frac{d}{2}}^{\frac{d}{2}} \Phi_f \frac{\partial c_f}{\partial t} \, d\boldsymbol{r} = \Phi_f \frac{\partial}{\partial t} \left(\int_{-\frac{d}{2}}^{\frac{d}{2}} c_f \, d\boldsymbol{r} \right) = d\Phi_f \frac{\partial \hat{c}}{\partial t} \, .$$

Then (3.77) reads

$$d\Phi_f \frac{\partial \hat{c}}{\partial t} + \boldsymbol{\chi}_f \cdot \boldsymbol{n}\big|_{\gamma_2} - \boldsymbol{\chi}_f \cdot \boldsymbol{n}\big|_{\gamma_1} + \nabla_{\boldsymbol{\tau}} \cdot \hat{\boldsymbol{\chi}} = \hat{g} \, .$$

Finally using Assumption 3.9-1 and the interface condition (3.74), we find

$$\boldsymbol{\chi}_f\big|_{\gamma_2} \cdot \boldsymbol{n} \approx - \boldsymbol{\chi}_f\big|_{\gamma_2} \cdot \boldsymbol{n}_2 = - \boldsymbol{\chi}_2\big|_{\gamma_2} \cdot \boldsymbol{n}_2 \approx \boldsymbol{\chi}_2\big|_{\gamma_2} \cdot \boldsymbol{n} \, ,$$

and

$$\boldsymbol{\chi}_f\big|_{\gamma_1} \cdot \boldsymbol{n} \approx \boldsymbol{\chi}_f\big|_{\gamma_1} \cdot \boldsymbol{n}_1 = \boldsymbol{\chi}_1\big|_{\gamma_1} \cdot \boldsymbol{n}_1 \approx \boldsymbol{\chi}_1\big|_{\gamma_1} \cdot \boldsymbol{n} \, .$$

The conservation equation for the tangential component of the velocity in the fracture becomes

$$d\Phi_f \frac{\partial \hat{c}}{\partial t} + \nabla_{\boldsymbol{\tau}} \cdot \hat{\boldsymbol{\chi}} = \hat{g} + [\![\boldsymbol{\chi} \cdot \boldsymbol{n}]\!]_{\gamma} \qquad \text{on } \gamma \times \mathcal{I}_T \, . \qquad (3.80)$$

3.3.2 Reduced total flux equation

We now want to obtain a reduced model for the total flux equation in the fracture, *i.e.* the second equation in the system (3.73) for $i = f$, and a consistency condition for the interfaces between the fracture and the rest of the domain. Multiplying the equation by the projection matrix $\boldsymbol{N}$ and using Assumption 3.10-2, we have

$$\boldsymbol{N} \boldsymbol{\chi}_f = -\boldsymbol{N} \boldsymbol{D}_f \nabla c_f + \boldsymbol{N} \boldsymbol{u}_f c_f = -D_{f,\boldsymbol{n}} \boldsymbol{N} \nabla c_f + \boldsymbol{N} \boldsymbol{u}_f c_f = $$
$$= -D_{f,\boldsymbol{n}} \nabla_{\boldsymbol{n}} c_f + \boldsymbol{u}_{f, \, \boldsymbol{n}} c_f \, .$$

We perform the same operations multiplying by the projection matrix $\boldsymbol{T}$

$$\boldsymbol{T} \boldsymbol{\chi}_f = -\boldsymbol{T} \boldsymbol{D}_f \nabla c_f + \boldsymbol{T} \boldsymbol{u}_f c_f = -D_{f,\boldsymbol{\tau}} \boldsymbol{T} \nabla c_f + \boldsymbol{T} \boldsymbol{u}_f c_f = $$
$$= -D_{f,\boldsymbol{\tau}} \nabla_{\boldsymbol{\tau}} c_f + \boldsymbol{u}_{f, \, \boldsymbol{\tau}} c_f \, ,$$

and using the definition (3.76) we find the following system

$$
\begin{cases}
\boldsymbol{\chi}_{f,\boldsymbol{n}} = -D_{f,\boldsymbol{n}}\nabla_{\boldsymbol{n}}c_f + \boldsymbol{u}_{f,\boldsymbol{n}}c_f\,, \\
\boldsymbol{\chi}_{f,\boldsymbol{\tau}} = -D_{f,\boldsymbol{\tau}}\nabla_{\boldsymbol{\tau}}c_f + \boldsymbol{u}_{f,\boldsymbol{\tau}}c_f\,.
\end{cases}
\tag{3.81}
$$

Thanks to Assumption 3.10-2 we can integrate the second equation of system (3.81) to find

$$
\int_{-\frac{d}{2}}^{\frac{d}{2}} \boldsymbol{\chi}_{f,\boldsymbol{\tau}}\,d\boldsymbol{r} = \hat{\boldsymbol{\chi}} = -D_{f,\boldsymbol{\tau}}\int_{-\frac{d}{2}}^{\frac{d}{2}}\nabla_{\boldsymbol{\tau}}c_f\,d\boldsymbol{r} + \int_{-\frac{d}{2}}^{\frac{d}{2}}\boldsymbol{u}_{f,\boldsymbol{\tau}}c_f\,d\boldsymbol{r} =
$$

$$
= -D_{f,\boldsymbol{\tau}}\boldsymbol{T}\int_{-\frac{d}{2}}^{\frac{d}{2}}\nabla c_f\,d\boldsymbol{r} + \int_{-\frac{d}{2}}^{\frac{d}{2}}\boldsymbol{u}_{f,\boldsymbol{\tau}}c_f\,d\boldsymbol{r} \approx
$$

$$
\approx -D_{f,\boldsymbol{\tau}}\nabla_{\boldsymbol{\tau}}\int_{-\frac{d}{2}}^{\frac{d}{2}}c_f\,d\boldsymbol{r} + \int_{-\frac{d}{2}}^{\frac{d}{2}}\boldsymbol{u}_{f,\boldsymbol{\tau}}c_f\,d\boldsymbol{r}\,.
$$

Assuming that

$$
\int_{-\frac{d}{2}}^{\frac{d}{2}}\boldsymbol{u}_{f,\boldsymbol{\tau}}c_f\,d\boldsymbol{r} \approx d\hat{\boldsymbol{u}}\hat{c}\,,
\tag{3.82}
$$

we obtain the reduced equation for the total flux in the fracture

$$
\hat{\beta}\hat{\boldsymbol{\chi}} + \nabla_{\boldsymbol{\tau}}\hat{c} - d\hat{\beta}\hat{\boldsymbol{u}}\hat{c} = \boldsymbol{0} \quad \text{on } \gamma \times \mathcal{I}_T\,,
\tag{3.83}
$$

where

$$
\hat{\beta}\left(\boldsymbol{s}\right) := \frac{1}{d\left(\boldsymbol{s}\right)D_{f,\boldsymbol{\tau}}\left(\boldsymbol{s}\right)}\,,
$$

which represent the inverse of the equivalent molecular diffusion in the tangential direction to the fracture γ.

To derive the coupling conditions for the global problem, we consider the first equation of system (3.81). We multiply the equation by $\boldsymbol{n}$ and, using Assumption 3.10-2 and (3.74), we integrate in the normal direction the fracture to obtain

$$
\int_{-\frac{d}{2}}^{\frac{d}{2}}\boldsymbol{\chi}_{f,\boldsymbol{n}}\cdot\boldsymbol{n}\,d\boldsymbol{r} = -D_{f,\boldsymbol{n}}\int_{-\frac{d}{2}}^{\frac{d}{2}}\nabla_{\boldsymbol{n}}c_f\cdot\boldsymbol{n}\,d\boldsymbol{r} + \int_{-\frac{d}{2}}^{\frac{d}{2}}c_f\boldsymbol{u}_f\cdot\boldsymbol{n}\,d\boldsymbol{r} =
$$

$$
= -D_{f,\boldsymbol{n}}\left(\left.c_f\right|_{\gamma_2} - \left.c_f\right|_{\gamma_1}\right) + \int_{-\frac{d}{2}}^{\frac{d}{2}}c_f\boldsymbol{u}_f\cdot\boldsymbol{n}\,d\boldsymbol{r}
$$

$$
= -D_{f,\boldsymbol{n}}\left(\left.c_2\right|_{\gamma_2} - \left.c_1\right|_{\gamma_1}\right) + \int_{-\frac{d}{2}}^{\frac{d}{2}}c_f\boldsymbol{u}_f\cdot\boldsymbol{n}\,d\boldsymbol{r}
$$

$$
= D_{f,\boldsymbol{n}}\left[\!\left[c\right]\!\right]_\gamma + \int_{-\frac{d}{2}}^{\frac{d}{2}}c_f\boldsymbol{u}_f\cdot\boldsymbol{n}\,d\boldsymbol{r}\,.
\tag{3.84}
$$

The integral, in the left-hand side, can be approximated by

$$
\int_{-\frac{d}{2}}^{\frac{d}{2}}\boldsymbol{\chi}_{f,\boldsymbol{n}}\cdot\boldsymbol{n}\,d\boldsymbol{r} \approx \frac{d}{2}\left(\left.\boldsymbol{\chi}_{f,\boldsymbol{n}}\right|_{\gamma_2}\cdot\boldsymbol{n} + \left.\boldsymbol{\chi}_{f,\boldsymbol{n}}\right|_{\gamma_1}\cdot\boldsymbol{n}\right) =
$$

$$
= \frac{d}{2}\left(\left.\boldsymbol{\chi}_2\right|_{\gamma_2}\cdot\boldsymbol{n} + \left.\boldsymbol{\chi}_1\right|_{\gamma_1}\cdot\boldsymbol{n}\right) = d\left\{\!\left\{\boldsymbol{\chi}\cdot\boldsymbol{n}\right\}\!\right\}_\gamma\,,
$$

while, using the same approximation of equation (3.82) but for the normal component of $\boldsymbol{u}_f$, the integral in the right-hand side of equation (3.84) becomes

$$\int_{-\frac{d}{2}}^{\frac{d}{2}} c_f \boldsymbol{u}_f \cdot \boldsymbol{n} \, d\boldsymbol{r} \approx 0 \,,$$

since the normal component of the reduced velocity inside the fracture γ is assumed to be zero. Finally equation (3.84) becomes

$$\{\!\{\boldsymbol{\chi} \cdot \boldsymbol{n}\}\!\}_\gamma = \frac{D_{f,\boldsymbol{n}}}{d} \, [\![c]\!]_\gamma \,.$$

Defining β_γ as

$$\beta_\gamma (\boldsymbol{s}) := \frac{d\,(\boldsymbol{s})}{D_{f,\boldsymbol{n}}\,(\boldsymbol{s})} \,,$$

which represent the inverse of the equivalent molecular diffusion in the normal direction to the fracture γ, we can write the above equation as

$$\beta_\gamma \{\!\{\boldsymbol{\chi} \cdot \boldsymbol{n}\}\!\}_\gamma = [\![c]\!]_\gamma \qquad \text{on } \gamma \times \mathcal{I}_T \,. \tag{3.85}$$

To close the reduced system we need another relation which needs to model the variation of the concentration and total flux across the fracture. We proceed as
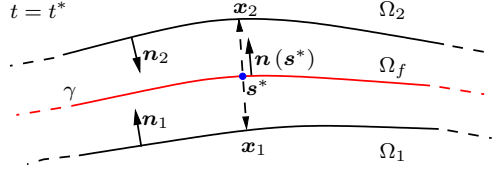
Figure 3.23: Approximation of the pressure in the fracture.

in subsection 3.1.4, *i.e.* in the first transversal section, see Figure 3.23 for an example, we approximate the value of the concentration inside the fracture by the following Taylor expansion

$$c_f\,(\boldsymbol{s}^*) = c_f(\boldsymbol{x}_1) + \frac{d}{2}\nabla c_f\,(\boldsymbol{\theta}_1) \cdot \boldsymbol{n} \,, \tag{3.86}$$

where $\boldsymbol{\theta}_1 = \boldsymbol{s}^* - \xi_1 \frac{d}{2}\boldsymbol{n}$ and $\xi_1 \in [0,\,1]$. In the second transversal section we approximate the value of the concentration inside the fracture by

$$c_f\,(\boldsymbol{s}^*) = c_f(\boldsymbol{x}_2) - \frac{d}{2}\nabla c_f\,(\boldsymbol{\theta}_2) \cdot \boldsymbol{n} \,, \tag{3.87}$$

where $\boldsymbol{\theta}_2 = \boldsymbol{s}^* + \xi_2 \frac{d}{2}\boldsymbol{n}$ and $\xi_2 \in [0,\,1]$. Using relations (3.74), (3.81) and assuming a piecewise linear combination of normal component of the total flux $\boldsymbol{\chi}_{f,\boldsymbol{n}}$

$$\begin{cases} \boldsymbol{\chi}_{f,\boldsymbol{n}}\,(\boldsymbol{\theta}_1) \cdot \boldsymbol{n} = \xi_1 \boldsymbol{\chi}_1 \cdot \boldsymbol{n} + (1 - \xi_1)\,\boldsymbol{\chi}_2 \cdot \boldsymbol{n} \,, \\ \boldsymbol{\chi}_{f,\boldsymbol{n}}\,(\boldsymbol{\theta}_2) \cdot \boldsymbol{n} = \xi_2 \boldsymbol{\chi}_2 \cdot \boldsymbol{n} + (1 - \xi_2)\,\boldsymbol{\chi}_1 \cdot \boldsymbol{n} \,, \end{cases}$$

the approximate concentration in the fracture (3.86) becomes

$$c_f\left(\boldsymbol{s}^*\right) \approx c_1(\boldsymbol{x}_1) - \frac{\beta_\gamma}{2}\left[\xi_1\boldsymbol{\chi}_1\cdot\boldsymbol{n} + (1-\xi_1)\,\boldsymbol{\chi}_2\cdot\boldsymbol{n}\right] =$$
$$= c_1(\boldsymbol{x}_1) - \frac{\beta_\gamma}{2}\left[\{\!\{\boldsymbol{\chi}\cdot\boldsymbol{n}\}\!\}_\gamma + \left(\xi_1-\frac{1}{2}\right)[\![\boldsymbol{\chi}\cdot\boldsymbol{n}]\!]_\gamma\right],$$

and equation (3.87) becomes

$$c_f\left(\boldsymbol{s}^*\right) \approx c_2(\boldsymbol{x}_2) + \frac{\beta_\gamma}{2}\left[\xi_2\boldsymbol{\chi}_1\cdot\boldsymbol{n} + (1-\xi_2)\,\boldsymbol{\chi}_2\cdot\boldsymbol{n}\right] =$$
$$= c_2(\boldsymbol{x}_2) + \frac{\beta_\gamma}{2}\left[\{\!\{\boldsymbol{\chi}\cdot\boldsymbol{n}\}\!\}_\gamma - \left(\xi_2-\frac{1}{2}\right)[\![\boldsymbol{\chi}\cdot\boldsymbol{n}]\!]_\gamma\right].$$

Using relation (3.85) we find

$$c_f\left(\boldsymbol{s}^*\right) \approx \{\!\{c\}\!\}_\gamma - \frac{\beta_\gamma\,(2\xi_1-1)}{4}[\![\boldsymbol{\chi}\cdot\boldsymbol{n}]\!]_\gamma,$$
$$c_f\left(\boldsymbol{s}^*\right) \approx \{\!\{c\}\!\}_\gamma - \frac{\beta_\gamma\,(2\xi_2-1)}{4}[\![\boldsymbol{\chi}\cdot\boldsymbol{n}]\!]_\gamma.$$

Since the concentration in the fracture c_f is single value at $\boldsymbol{s}^*$, the only possibility is to choose $\xi_1 = \xi_2 = \xi$ to find the coupling condition for $c_f\left(\boldsymbol{s}^*\right)$

$$c_f\left(\boldsymbol{s}^*\right) \approx \{\!\{c\}\!\}_\gamma - \frac{\beta_\gamma\,(2\xi-1)}{4}[\![\boldsymbol{\chi}\cdot\boldsymbol{n}]\!]_\gamma,$$

finally integrating in the transversal section of γ and using the definition (3.79) for the reduced pressure we obtain

$$\hat{c} = \{\!\{c\}\!\}_\gamma - \frac{\beta_\gamma\,(2\xi-1)}{4}[\![\boldsymbol{\chi}\cdot\boldsymbol{n}]\!]_\gamma \qquad \text{on } \gamma\times\mathcal{I}_T. \tag{3.88}$$

Using (3.85) and (3.88), the interface conditions on γ become

$$\begin{cases} \xi_0\eta_\gamma\,[\![\boldsymbol{\chi}\cdot\boldsymbol{n}]\!]_\gamma = \{\!\{c\}\!\}_\gamma - \hat{c} \\[2mm] \eta_\gamma\,\{\!\{\boldsymbol{\chi}\cdot\boldsymbol{n}\}\!\}_\gamma = [\![c]\!]_\gamma \end{cases} \qquad \text{on } \gamma\times\mathcal{I}_T, \tag{3.89}$$

with $\xi_0 := (2\xi-1)/4$. Or alternatively, summing and subtracting each equation of (3.89), we find

$$\begin{cases} \xi\boldsymbol{\chi}_1\cdot\boldsymbol{n} + (1-\xi)\,\boldsymbol{\chi}_2\cdot\boldsymbol{n} = 2\beta_\gamma^{-1}\,(c_1-\hat{c}) \\[2mm] (1-\xi)\,\boldsymbol{\chi}_1\cdot\boldsymbol{n} + \xi\boldsymbol{\chi}_2\cdot\boldsymbol{n} = 2\beta_\gamma^{-1}\,(\hat{c}-c_2) \end{cases} \qquad \text{on } \gamma\times\mathcal{I}_T.$$

To derive the boundary condition for the reduced problem we use (3.75)

$$\overline{\hat{\boldsymbol{\chi}}}\cdot\boldsymbol{n}_\Gamma := \int_{\Gamma_f^E}\overline{\chi_f} \quad \text{and} \quad \overline{\hat{c}} := \int_{\Gamma_f^N}\overline{c_f}. \tag{3.90}$$

Furthermore, the reduced initial condition for c using (3.78) becomes

$$\hat{c}_0 := \frac{1}{d}\int_{-\frac{d}{2}}^{\frac{d}{2}} c_{0,f}\,d\boldsymbol{r} \tag{3.91}$$

Using Assumption 3.9 hence approximating the domain Ω reported in Figure 3.21 to the domain in Figure 3.24, the equations (3.80), (3.83), (3.89), (3.90) and (3.91) form the reduced model summarize in the following problem.

Problem 3.9 (Reduced Model for Transport Equation)**.** *Given Assumption 3.9, Assumption 3.10 and Assumption 3.11, the reduced problem for the transport of a tracer is: given $\boldsymbol{u}_i$ for $i = 1, 2$ and $\hat{\boldsymbol{u}}$ from Problem 3.4, find the total flux and the concentration associated to the porous matrix, respectively $\boldsymbol{\chi}_i$ and c_i for $i = 1, 2$, and the reduced total flux and the reduced concentration associated to the fracture, respectively $\hat{\boldsymbol{\chi}}$ and $\hat{c}$, which satisfy the following system of partial differential equations for $i = 1, 2$*

$$
\begin{cases}
\Phi_i \dfrac{\partial c_i}{\partial t} + \nabla\cdot\boldsymbol{\chi}_i = g_i & in\ Q_T, \\[2mm]
\boldsymbol{D}_i^{-1}\boldsymbol{\chi}_i + \nabla c_i - \boldsymbol{D}_i^{-1}\boldsymbol{u}_i c_i = \boldsymbol{0} & in\ Q_T, \\[2mm]
d\Phi_f \dfrac{\partial \hat{c}}{\partial t} + \nabla_{\boldsymbol{\tau}} \cdot \hat{\boldsymbol{\chi}} = \hat{g} + [\![\boldsymbol{\chi} \cdot \boldsymbol{n}]\!]_\gamma & on\ \gamma \times \mathcal{I}_T, \\[2mm]
\hat{\beta}\hat{\boldsymbol{\chi}} + \nabla_{\boldsymbol{\tau}}\hat{c} - d\hat{\beta}\hat{\boldsymbol{u}}\hat{c} = \boldsymbol{0} & on\ \gamma \times \mathcal{I}_T,
\end{cases}
\tag{3.92}
$$

coupled with the interface conditions on $\gamma \times \mathcal{I}_T$

$$
\begin{cases}
\xi_0 \beta_\gamma [\![\boldsymbol{\chi} \cdot \boldsymbol{n}]\!]_\gamma = \{\!\{c\}\!\}_\gamma - \hat{c} \\[2mm]
\beta_\gamma \{\!\{\boldsymbol{\chi} \cdot \boldsymbol{n}\}\!\}_\gamma = [\![c]\!]_\gamma
\end{cases}
on\ \gamma \times \mathcal{I}_T \,,
\tag{3.93}
$$

with the boundary conditions on $\partial\Omega \times \mathcal{I}_T$ for $i = 1, 2$

$$
\begin{cases}
c_i = \overline{c_i} & on\ \Gamma_i^N \times \mathcal{I}_T, \\[2mm]
\boldsymbol{\chi}_i \cdot \boldsymbol{n}_\Gamma = \overline{\chi_i} & on\ \Gamma_i^E \times \mathcal{I}_T, \\[2mm]
\hat{c} = \overline{\hat{c}} & on\ \partial\gamma^N \times \mathcal{I}_T, \\[2mm]
\hat{\boldsymbol{\chi}} \cdot \boldsymbol{n}_\Gamma = \overline{\hat{\boldsymbol{\chi}}} \cdot \boldsymbol{n}_\Gamma & in\ \partial\gamma^E \times \mathcal{I}_T,
\end{cases}
\tag{3.94}
$$

and the initial condition for the concentration for $i = 1, 2$

$$
\begin{cases}
c_i = c_{0,i} & in\ \Omega \times \{0\}, \\[2mm]
\hat{c} = \hat{c}_0 & on\ \gamma \times \{0\}.
\end{cases}
$$
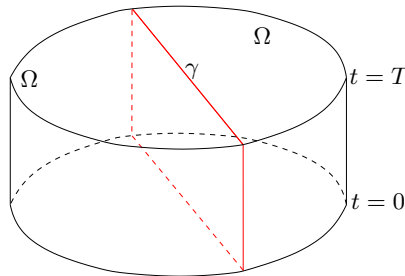
Figure 3.24: Picture of the domain Q_T with the reduced fracture for $n = 2$.

3.3.3 Weak formulation

We derive the weak formulation of Problem 3.9 and, for the sake of simplicity, we require $\overline{\chi_i} = 0$ for $i = 1, 2$ and $\widehat{\overline{\chi}} \cdot \boldsymbol{n}_\Gamma = 0$ or $\Gamma^E = \emptyset$, otherwise a standard lifting technique should be used. We indicate with

$$D_T := D \times \mathcal{I}_T \,,$$

where D is defined by (3.34). We introduce the following functional spaces for each piece of the domain $i = 1, 2$

$$\boldsymbol{U}_i := L^2\left(\mathcal{I}_T; \boldsymbol{V}_i\right) \quad \text{and} \quad J_i := L^2\left(\mathcal{I}_T; Q_i\right) \,,$$

where $\boldsymbol{V}_i$ and Q_i are defined in (3.35). We introduce the broken functional space $\boldsymbol{U} : D_T \to \mathbb{R}^n$ and $J : D_T \to \mathbb{R}$

$$\boldsymbol{U} := \left\{\boldsymbol{v} : D_T \to \mathbb{R}^n : \boldsymbol{v}|_{\Omega_i} \in \boldsymbol{U}_i \text{ for } i = 1, 2\right\} \,,$$
$$J := \left\{w : D_T \to \mathbb{R} : w|_{\Omega_i} \in J_i \text{ for } i = 1, 2\right\} \,.$$

We introduce the functional spaces for the problem in the fracture: the spaces of functions living in the tangent space, that is

$$\hat{U} := L^2\left(\mathcal{I}_T; \hat{\boldsymbol{V}}\right) \quad \text{and} \quad \hat{J} := L^2\left(\mathcal{I}_T; \hat{Q}\right) \,,$$

where $\hat{\boldsymbol{V}}$ and $\hat{Q}$ are defined in (3.37). We define also the global space for the flux and the global space for the concentration

$$\boldsymbol{\mathcal{U}} := \left\{\mathbf{x} = (\boldsymbol{\chi}, \hat{\boldsymbol{\chi}}) \in \boldsymbol{U} \times \hat{U}\right\} \quad \text{and} \quad \mathcal{J} := \left\{\mathbf{c} = (c, \hat{c}) \in J \times \hat{J}\right\} \,.$$

We derive the weak formulation of Problem 3.9, starting with the differential equation in the medium. Taking a test function $w \in Q$ multiply and integrate on Ω_i the first equation of (3.92)

$$\left(\Phi_i c_i', w\right)_{\Omega_i} + \left(\nabla \cdot \boldsymbol{\chi}_i, w\right)_{\Omega_i} = \left(g_i, w\right)_{\Omega_i} \,,$$

where we indicate with c' instead of $\dfrac{dc}{dt}(\boldsymbol{x})$. Summing on all the domain Ω_i for $i = 1, 2$ we have

$$\left(\Phi c', w\right)_\Omega + \left(\nabla \cdot \boldsymbol{\chi}, w\right)_\Omega = \left(g, w\right)_\Omega \,.$$

Using the bilinear form defined in (3.39) and introducing the functional $F_g \in Q'$

$$F_g(w) := -(g, w)_\Omega$$

with $w \in Q$, then the weak formulation of the first equation of (3.92) reads for a.e. $t \in \mathcal{I}_T$

$$-(\Phi c', w)_\Omega + b(\boldsymbol{\chi}, w) = -F_g(w) \quad \forall w \in Q \,.$$

Taking a test function $\boldsymbol{v} \in \boldsymbol{V}$ multiply and integrate on Ω_i the second equation of (3.92)

$$\left(\boldsymbol{D}_i^{-1} \boldsymbol{\chi}_i, \boldsymbol{v}\right)_{\Omega_i} + \left(\nabla c_i, \boldsymbol{v}\right)_{\Omega_i} - \left(\boldsymbol{D}_i^{-1} \boldsymbol{u}_i c_i, \boldsymbol{v}\right)_{\Omega_i} = \left(\boldsymbol{D}_i^{-1} \boldsymbol{\chi}_i, \boldsymbol{v}\right)_{\Omega_i} +$$
$$- (c_i, \nabla \cdot \boldsymbol{v})_{\Omega_i} + (c_i, \boldsymbol{v} \cdot \boldsymbol{n}_\Gamma)_\Gamma + (c_i, \boldsymbol{v} \cdot \boldsymbol{n}_i)\gamma - \left(\boldsymbol{D}_i^{-1} \boldsymbol{u}_i c_i, \boldsymbol{v}\right)_{\Omega_i} = 0 \,.$$

Summing the previous equation for $i = 1, 2$ and using boundary conditions (3.94) we have

$$\left(\boldsymbol{D}^{-1}\boldsymbol{\chi},\,\boldsymbol{v}\right)_\Omega - (c,\,\nabla\cdot\boldsymbol{v})_\Omega + (\bar{c},\,\boldsymbol{v}\cdot\boldsymbol{n}_\Gamma)_{\Gamma^N} +$$
$$+ \sum_{i=1}^{2}(c_i,\,\boldsymbol{v}\cdot\boldsymbol{n}_i)_\gamma - \left(\boldsymbol{D}^{-1}\boldsymbol{u}c,\,\boldsymbol{v}\right)_\Omega = 0\,.$$

Since $\boldsymbol{n} = \boldsymbol{n}_1 = -\boldsymbol{n}_2$, using relation $[\![ab]\!]_\gamma = [\![a]\!]_\gamma\,\{\!\{b\}\!\}_\gamma + \{\!\{a\}\!\}_\gamma\,[\![b]\!]_\gamma$ and the coupling conditions (3.93) for γ we have

$$\sum_{i=1}^{2}(c_i,\,\boldsymbol{v}\cdot\boldsymbol{n}_i)_\gamma = \int_\gamma [\![c\boldsymbol{v}]\!]_\gamma\cdot\boldsymbol{n} = \left([\![c]\!]_\gamma,\,\{\!\{\boldsymbol{v}\cdot\boldsymbol{n}\}\!\}_\gamma\right)_\gamma + \left(\{\!\{c\}\!\}_\gamma,\,[\![\boldsymbol{v}\cdot\boldsymbol{n}]\!]_\gamma\right)_\gamma =$$
$$= \left(\beta_\gamma\,\{\!\{\boldsymbol{\chi}\cdot\boldsymbol{n}\}\!\}_\gamma,\,\{\!\{\boldsymbol{v}\cdot\boldsymbol{n}\}\!\}_\gamma\right)_\gamma + \xi_0\left(\beta_\gamma\,[\![\boldsymbol{\chi}\cdot\boldsymbol{n}]\!]_\gamma,\,[\![\boldsymbol{v}\cdot\boldsymbol{n}]\!]_\gamma\right)_\gamma +$$
$$+ \left(\hat{c},\,[\![\boldsymbol{v}\cdot\boldsymbol{n}]\!]_\gamma\right)_\gamma\,.$$

Introducing the bilinear forms $a(\cdot,\,\cdot):\boldsymbol{V}\times\boldsymbol{V}\to\mathbb{R}$ and $e(\cdot,\,\cdot):\boldsymbol{V}\times Q\to\mathbb{R}$

$$a(\boldsymbol{\chi},\,\boldsymbol{v}) := \left(\boldsymbol{D}^{-1}\boldsymbol{\chi},\,\boldsymbol{v}\right)_\Omega + \left(\beta_\gamma\,\{\!\{\boldsymbol{\chi}\cdot\boldsymbol{n}\}\!\}_\gamma,\,\{\!\{\boldsymbol{v}\cdot\boldsymbol{n}\}\!\}_\gamma\right)_\gamma +$$
$$+ \xi_0\left(\beta_\gamma\,[\![\boldsymbol{\chi}\cdot\boldsymbol{n}]\!]_\gamma,\,[\![\boldsymbol{v}\cdot\boldsymbol{n}]\!]_\gamma\right)_\gamma,$$
$$e(\boldsymbol{v},\,c) := -\left(\boldsymbol{D}^{-1}\boldsymbol{u}c,\,\boldsymbol{v}\right)_\Omega,$$

and the functional $F_{\boldsymbol{g}}\in\boldsymbol{V}'$,

$$F_{\boldsymbol{g}}\left(\boldsymbol{v}\right) := -(\bar{c},\,\boldsymbol{v}\cdot\boldsymbol{n}_\Gamma)_{\Gamma^N}\,,$$

and using the bilinear form d defined in (3.40), the weak formulation of the second equation of system (3.92) becomes, for a.e. $t\in\mathcal{I}_T$

$$a(\boldsymbol{\chi},\,\boldsymbol{v}) + b(\boldsymbol{v},\,c) + e(\boldsymbol{v},\,c) + d(\boldsymbol{v},\,\hat{c}) = F_{\boldsymbol{g}}\left(\boldsymbol{v}\right)\quad\forall\boldsymbol{v}\in\boldsymbol{V}\,.$$

We derive the weak formulation for the equations in the fracture, taking a test function $\hat{w}\in\hat{Q}$ multiplying and integrating on γ the third equation of (3.92). We obtain

$$(d\Phi_f\hat{c}',\,\hat{w})_\gamma + (\nabla_{\boldsymbol{\tau}}\cdot\hat{\boldsymbol{\chi}},\,\hat{w})_\gamma - \left([\![\boldsymbol{\chi}\cdot\boldsymbol{n}]\!]_\gamma,\,\hat{w}\right)_\gamma = (\hat{g},\,\hat{w})_\gamma\,.$$

where we indicate $\dfrac{d\hat{c}}{dt}\left(\boldsymbol{x}\right)$ with $\hat{c}'$. Using the bilinear form introduced in (3.41) and defining the functional $\hat{F}_{\hat{g}}\in\hat{Q}'$

$$\hat{F}_{\hat{g}}\left(\hat{w}\right) := -(\hat{g},\,\hat{w})_\gamma\,,$$

the weak formulation of the third equation of (3.92) is: for a.e. $t\in\mathcal{I}_T$,

$$-(d\Phi_f\hat{c}',\,\hat{w})_\gamma + \hat{b}(\hat{\boldsymbol{\chi}},\,\hat{w}) + d(\boldsymbol{\chi},\,\hat{w}) = -\hat{F}_{\hat{g}}\left(\hat{w}\right)\quad\forall\hat{w}\in\hat{Q}\,.$$

Taking a test function $\hat{\boldsymbol{v}} \in \hat{\boldsymbol{V}}$ and integrating on γ, the fourth equation of (3.92) becomes

$$\left(\hat{\beta}\hat{\boldsymbol{\chi}},\, \hat{\boldsymbol{v}}\right)_\gamma + (\nabla_{\boldsymbol{\tau}}\hat{c},\, \hat{\boldsymbol{v}})_\gamma - \left(d\hat{\beta}\hat{\boldsymbol{u}}\hat{c},\, \hat{\boldsymbol{v}}\right)_\gamma =$$
$$= \left(\hat{\beta}\hat{\boldsymbol{\chi}},\, \hat{\boldsymbol{v}}\right)_\gamma - (\hat{c},\, \nabla_{\boldsymbol{\tau}}\cdot\hat{\boldsymbol{v}})_\gamma + (\hat{c},\, \hat{\boldsymbol{v}}\cdot\boldsymbol{n}_\Gamma)_{\partial\gamma} - \left(d\hat{\beta}\hat{\boldsymbol{u}}\hat{c},\, \hat{\boldsymbol{v}}\right)_\gamma = 0\,.$$

Using the boundary conditions (3.94) and introducing the bilinear forms $\hat{a}(\cdot,\,\cdot):$ $\hat{\boldsymbol{V}}\times\hat{\boldsymbol{V}}\to\mathbb{R}$, $\hat{e}(\cdot,\,\cdot):\,\hat{\boldsymbol{V}}\times\hat{Q}\to\mathbb{R}$

$$\hat{a}(\hat{\boldsymbol{\chi}},\, \hat{\boldsymbol{v}}) := \left(\hat{\beta}\hat{\boldsymbol{\chi}},\, \hat{\boldsymbol{v}}\right)_\gamma \quad\text{and}\quad \hat{e}(\hat{\boldsymbol{v}},\, \hat{c}) := -\left(d\hat{\beta}\hat{\boldsymbol{u}}\hat{c},\, \hat{\boldsymbol{v}}\right)_\gamma\,,$$

and the functional $\hat{F}_{\hat{\boldsymbol{g}}}\in\hat{\boldsymbol{V}}'$

$$\hat{F}_{\hat{\boldsymbol{g}}}\left(\hat{\boldsymbol{v}}\right) := -(\hat{c},\, \hat{\boldsymbol{v}}\cdot\boldsymbol{n}_\Gamma)_{\partial\gamma}\,,$$

we obtain the weak formulation of the fourth equation of (3.92) for a.e. $t\in\mathcal{I}_T$

$$\hat{a}(\hat{\boldsymbol{\chi}},\, \hat{\boldsymbol{v}}) + \hat{b}(\hat{\boldsymbol{v}},\, \hat{c}) + \hat{e}(\hat{\boldsymbol{v}},\, \hat{c}) = \hat{F}_{\hat{\boldsymbol{g}}}\left(\hat{\boldsymbol{v}}\right)\,.$$

We define the global bilinear forms for the medium and the fracture as $\alpha(\cdot,\,\cdot):$ $\boldsymbol{\mathcal{V}}\times\boldsymbol{\mathcal{V}}\to\mathbb{R}$, $\epsilon(\cdot,\,\cdot):\,\boldsymbol{\mathcal{V}}\times\mathcal{Q}\to\mathbb{R}$ and $\beta(\cdot,\,\cdot):\,\boldsymbol{\mathcal{V}}\times\mathcal{Q}\to\mathbb{R}$

$$\alpha(\mathbf{x},\, \mathbf{v}) := a(\boldsymbol{\chi},\, \boldsymbol{v}) + \hat{a}(\hat{\boldsymbol{\chi}},\, \hat{\boldsymbol{v}}) \quad\text{and}\quad \epsilon(\mathbf{v},\, \mathrm{c}) := e(\boldsymbol{v},\, c) + \hat{e}(\hat{\boldsymbol{v}},\, \hat{c})\,,$$
$$\beta(\mathbf{v},\, \mathrm{c}) := b(\boldsymbol{v},\, c) + \hat{b}(\hat{\boldsymbol{v}},\, \hat{c}) + d(\boldsymbol{v},\, \hat{c})\,.$$

We introduce also the bilinear form $\tau(\cdot,\,\cdot):\,\mathcal{Q}\times\mathcal{Q}\to\mathbb{R}$ as

$$\tau(\mathrm{c}',\, \mathrm{w}) := (\Phi c',\, w)_\Omega + (d\Phi_f\hat{c}',\, \hat{w})_\gamma\,.$$

Finally we define the global functionals for the medium and the fracture as $\mathcal{F}_{\boldsymbol{q}}\in\boldsymbol{\mathcal{V}}'$ and $\mathcal{F}_q\in\mathcal{Q}'$

$$\mathcal{F}_{\boldsymbol{g}}\left(\mathbf{v}\right) := F_{\boldsymbol{g}}\left(\boldsymbol{v}\right) + \hat{F}_{\hat{\boldsymbol{g}}}\left(\hat{\boldsymbol{v}}\right) \quad\text{and}\quad \mathcal{F}_g\left(\mathrm{w}\right) := -F_g\left(w\right) - \hat{F}_{\hat{g}}\left(\hat{w}\right)\,,$$

Indicating with $\mathbf{x} := (\boldsymbol{\chi},\, \hat{\boldsymbol{\chi}})\in\boldsymbol{\mathcal{U}}$ the flux in the medium and in the fracture, $\mathrm{c} := (c,\, \hat{c})\in\mathcal{J}$ the concentration in the medium and in the fracture we introduce the following problem.

Problem 3.10 (Weak Formulation of Transport Reduced Model). *Find* $(\mathbf{x},\, \mathrm{c})\in$ $\boldsymbol{\mathcal{U}}\times\mathcal{J}$ *such that* $\mathrm{c}'\in L^2\left(\mathcal{I}_T;\,\mathcal{Q}\right)$ *and for a.e.* $t\in\mathcal{I}_T$

$$\begin{cases} \alpha(\mathbf{x},\, \mathbf{v}) + \beta(\mathbf{v},\, \mathrm{c}) + \epsilon(\mathbf{v},\, \mathrm{c}) = \mathcal{F}_{\boldsymbol{q}}\left(\mathbf{v}\right) & \forall\mathbf{v}\in\boldsymbol{\mathcal{V}}\,, \\ \beta(\mathbf{x},\, \mathrm{w}) - \tau(\mathrm{c}',\, \mathrm{w}) = \mathcal{F}_q\left(\mathrm{w}\right) & \forall\mathrm{w}\in\mathcal{Q}\,, \end{cases}$$

coupled with the initial condition

$$\mathrm{c} = \mathrm{c}_0 \quad \text{a.e. in } \Omega$$

where $\mathrm{c}_0 := (c_0,\, \hat{c}_0)$.

Lemma 3.12 (Global conservation of mass). *Assume that $g_i \equiv 0$ and $\hat{g} \equiv 0$ then the solution $\mathbf{x} \in \mathcal{U}$ of Problem 3.10 satisfy a.e. $t \in \mathcal{I}_T$*

$$\int_{\partial A} \mathbf{x} \cdot \boldsymbol{n}_A = -\sum_{i=1}^{2} \frac{d}{dt} \int_{A_i} \Phi_i c_i - \frac{d}{dt} \int_{\gamma} \Phi_f \hat{c} \quad \forall A \subset \Omega \,,$$

with A any open bounded measurable subset of $\mathbb{R}^n$ with Lipschitz boundary ∂A and outward unit normal $\boldsymbol{n}_A$, such that $A \cap \gamma \neq \emptyset$ and

$$\overline{A} = \overline{A}_1 \cup \overline{A}_2 \quad while \quad \mathring{A}_1 \cap \mathring{A}_2 = \emptyset \,.$$

Proof. Taking $\mathbf{x} \in \mathcal{U}$ solution of Problem 3.10 with $w \equiv 1$ we have

$$\int_{A} \nabla \cdot \mathbf{x} = \int_{A_1} \nabla \cdot \boldsymbol{\chi}_1 + \int_{A_2} \nabla \cdot \boldsymbol{\chi}_2 + \int_{\gamma} \nabla_{\boldsymbol{\tau}} \cdot \hat{\boldsymbol{\chi}} =$$

$$= \int_{\gamma} [\![\boldsymbol{\chi} \cdot \boldsymbol{n}]\!]_{\gamma} - \sum_{i=1}^{2} \frac{d}{dt} \int_{A_i} \Phi_i c_i - \frac{d}{dt} \int_{\gamma} \Phi_f \hat{c} \quad \forall A \subset \Omega \,. \qquad (3.95)$$

Then since $\boldsymbol{\chi}_i$ is solution of Problem 3.10 in A_i we have

$$\int_{A_i} \nabla \cdot \boldsymbol{\chi}_i = \int_{\partial A_i \setminus \gamma} \boldsymbol{\chi}_i \cdot \boldsymbol{n}_A + \int_{\gamma} \boldsymbol{\chi}_i \cdot \boldsymbol{n}_i \,,$$

furthermore $\hat{\boldsymbol{\chi}}$ is solution of Problem 3.10 in γ we obtain

$$\int_{\gamma} \nabla_{\boldsymbol{\tau}} \cdot \hat{\boldsymbol{\chi}} = \int_{\partial \gamma} \hat{\boldsymbol{\chi}} \cdot \boldsymbol{n}_A \,.$$

Hence we have

$$\int_{A} \nabla \cdot \mathbf{x} = \sum_{i=1}^{2} \int_{\partial A_i \setminus \gamma} \boldsymbol{\chi}_i \cdot \boldsymbol{n}_A + \int_{\partial \gamma} \hat{\boldsymbol{\chi}} \cdot \boldsymbol{n}_A + \int_{\gamma} [\![\boldsymbol{\chi} \cdot \boldsymbol{n}]\!]_{\gamma} \,,$$

finally using the above relation with (3.95) we obtain the result.

$\square$

Chapter 4

Implementation aspects

In this chapter we present the implementation aspects we used to problems of chapters 2 and 3. In particular we discuss the implementation of the two-phase flow system of equations presented in Problem 2.3, highlighting the aspects associated with high performance computing. Furthermore we present the difficulties and the strategies we adopted to solve the reduced models presented in Problem 3.4, Problem 3.6 and Problem 3.10.

4.1 The LifeV library

We present some implementation aspects to solve Problem 2.3 with the numerical schemes presented in chapter 2. While the computational grid should have a typical size of several kilometres, it is evident that the number of degrees of freedom involved in the computation is too large to be efficiently handled by standard computers. An implementation which use parallel paradigms is thus mandatory to obtain results in a reasonable time. For this purpose we have decided to adopt as development platform the library of finite element LifeV [33] which provides implementations of state of the art mathematical and numerical methods in a parallel setting. LifeV is the joint collaboration between four institutions: École Polytechnique Fédérale de Lausanne (CMCS) in Switzerland, Politecnico di Milano (MOX) in Italy, INRIA (REO, ESTIME) in France and Emory University (Sc. Comp) in the U.S.A.
LifeV is a library, written in C++ language, which uses modern and advanced techniques in programming to implement solvers in several fields of apply mathematics. Templates programming, inheritance structures, factories and other design pattern techniques are used to obtain a fast and versatile software. LifeV is principally based on the Trilinos library suite [41], which provides sparse and distributed matrix and vector in the package Epetra and fast and parallel preconditioned linear solvers, package Ifpack [68], robust algebraic preconditioners, and the package ML [37], for multi-grid preconditioners. Furthermore Trilinos offers filters to export the solution common formats like Ensight, VTK or HDF5. Finally Trilinos is tested and tuned for high performance computing. Others libraries are connected to LifeV, for example some functionalities of the *boost*, shared pointers and the binding of functions. Finally to partition the global mesh for each sub-domains LifeV includes the library Parmetis which can parti-

tion complex meshes minimizing the connectivity graph to decrease the number of communication in the matrix assembly.

To solve Problem 2.3 with the IMPES method we have written several physical solvers. In particular we have implemented four different generalized Darcy solvers: a Darcy linear solver, a Darcy transient solver, a Darcy non-linear solver with the non-linearities in the permeability matrix and a Darcy transient and non-linear solver. We decided to use the inheritance technique to derive the transient and the non-linear solvers from the linear solvers, since most of the code is the same. Further the transient and non-linear solver inherits from both the transient and the non-linear solver. The inheritance graph is reported
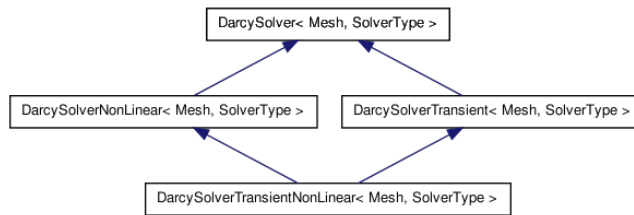
Figure 4.1: Inheritance graph of the generalized Darcy solver.

in Figure 4.1 which shows the so called *diamond problem* typical in the crossing public inheritance. To avoid redundant duplications of the attributes presented in the base class we use the virtual public inheritance technique, obtaining a code very flexible and easy to extend. The static condensation technique, presented in the sub-section 2.3.3, is performed with the BLAS and LAPACK library which can handle matrix and vectors operations in a very fast way. The temporal scheme used in the transient solver is a BDF scheme implemented in an external class, while the non-linear solver is a fixed point method implemented in the non-linear Darcy solver class. The solvers have been tested with different exact solutions and the error computed scales as the theory predicts. Furthermore the code has been tested on several super-computers showing a good performance, see section 5.3 for the examples.

We have implemented also an hyperbolic non-linear solver to address the hyperbolic part of the saturation equation. The solver can handle a generic hyperbolic problem and use an exact Godunov scheme, with a Brant algorithm for the minimization procedure to solve the Riemann problems at each facet of the mesh, for further details see [10]. This method is quite expensive, since it is applied for each facet of the mesh, and can be automatically overwritten using a problem dependent Godunov solver. The CFL condition is computed to obtain the correct time step. Finally we have used some typical techniques of functional programming to obtain the one dimensional Riemann problems, in the normal direction of each facet of the mesh, from a user implementation of the numerical flux. We use also this techniques for the CFL computation. The solver has been tested with different solutions, both with linear and non-linear physical flux functions, obtaining the correct error scale. Like the Darcy solvers we have performed some scalability tests.

4.2 Reduced models

In this section we present the relevant computational aspects for all the reduced model of chapter 3. Each fracture is represented with a level set. This is a powerful tool since, given a fracture, we can divide the domain into two different parts: where the level set function is strictly positive and where the level set function is strictly negative. The fracture is represented by the line, or surface, where the level set function is zero. If more then one fracture are present we can combine the signs of the level set functions to obtain different separated regions, as in Figure 4.2. To program the reduced model we have used the Getfem++
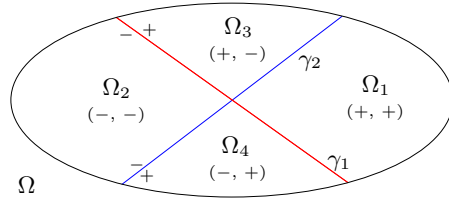
Figure 4.2: Division of the domain Ω into four different sub-regions according to the signs of the level set functions associated to the fractures γ_1 and γ_2.

library of finite elements, while we have started the extension of LifeV [33] to include also the XFEM method.

4.2.1 Degrees of freedom

One of the major problem in the implementation of the XFEM method is the handling of the degrees of freedom. In fact when a level set cut an element K of the triangulation $\mathcal{T}_h$, under Assumption 3.5, it divides K into two sub-elements K_1 and K_2 which K_1 or K_2 is not a triangle. To represent a function $f \in \widetilde{\mathbb{P}}_0(\mathcal{T}_h)$ we need to enrich the space $\mathbb{P}_0$ with new functions, $i.e.$ we need to add new degrees of freedom. Since we are using a piecewise polynomial approximation each element $K \in \mathcal{T}_h$ has the degrees of freedom inside itself and not shared with the neighbouring elements. Hence the enriching procedure of $\mathbb{P}_0$ is adding one extended degrees of freedom, for each element in $K \in \mathcal{G}_{h,j}$, associated to the fracture γ_j. Considering Figure 4.3, we should have a policy common to every
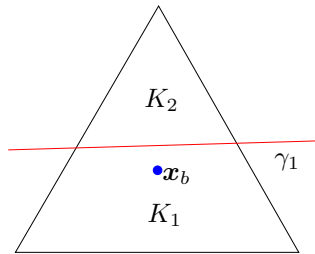
Figure 4.3: Enriching of the space $\mathbb{P}(K)$ with $K \in \mathcal{G}_{h,1}$.

element K to link the base, $i.e.$ the degree of freedom coming from $\mathbb{P}_0(K)$, and the extended degree of freedom to some geometrical properties of the triangle K. In our implementation we have chosen to assign the base degree of freedom

to the sub-element which contains the barycentre $\boldsymbol{x}_g$ of K, *e.g.* K_1 for the example in Figure 4.3, and the extended degree of freedom to the other part of K, *e.g.* K_2 for the example in Figure 4.3. Now, using the expansion (3.64), we can represent a discontinuity inside the element K. It is more involved to handle the degrees of freedom of intersecting fractures, instead to characterize the base and extended degrees of freedom to the position of the barycentre, referring to Figure 4.4, we can divide K into at least four sub-elements K_i characterized by different signs of the two level sets. We have to chose an order, based on the
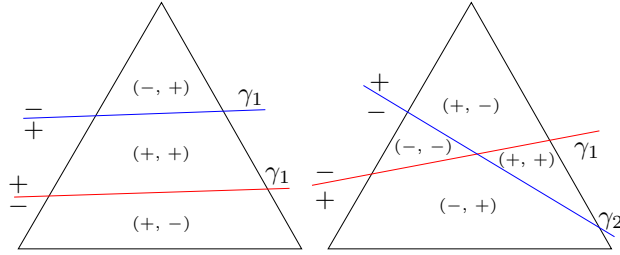
Figure 4.4: Different possibilities of regions, according to the signs of the level sets.

signs, for the sub-region to link a degree of freedom to the corresponding region. As a convention we have chosen the following order

$$\text{①}\ (+,\,+)\quad \text{②}\ (-,\,-)\quad \text{③}\ (+,\,-)\quad \text{④}\ (-,\,+) \tag{4.1}$$

where the first sign is referred to γ_1 and the second to γ_2. Note that it may happens that one of the region is not present, in this case we rescale the numbering. If an element K belongs to $\mathcal{M}_h$ to have two discontinuity we have to enrich K with two extended degrees of freedom. In this case, according to convention (4.1), we assign the base degree of freedom to the first available region, the first extended degree of freedom to the second available region while the second extended degree of freedom to the last available region. Finally if an element $K \in \mathcal{I}_h$ we have to add three degrees of freedom to represent correctly four discontinuity in its interior. According to convention (4.1) we assign the base degree of freedom to the region ①, the first extended degree of freedom to the region ②, the second extended degree of freedom to the region ③ and finally the extra degree of freedom is assigned to the region ④. To represent a function $\hat{f} \in \widetilde{\mathbb{P}}_0\left(\gamma_{\hat{h},j}\right)$ we have to enrich the polynomial space $\mathbb{P}_0\left(\gamma_{\hat{h},j}\right)$ for both the fractures j. We have chosen the same policy adopted for the elements $K \in \mathcal{G}_{h,i}$, based on the barycentre position.

The construction of the enriched space $\widetilde{\mathbb{RT}}_0\left(\mathcal{T}_h\right)$ is more involved since the degrees of freedom are on the edges of the mesh and are shared by two elements. The difficulty is to correctly decide the numeration to be coherent for all the neighbouring elements. If an element $K \in \mathcal{G}_{h,j}$, for each fracture γ_j, we use the same policy to construct $\widetilde{\mathbb{RT}}_0\left(K\right)$ as in $\widetilde{\mathbb{P}}_0\left(K\right)$ case. That is, for each edges of the triangle K, we assign the base degree of freedom to the edge of the sub-element which contains its midpoint. The extended degrees of freedom are assigned consequently to complete the degrees of freedom of each sub-element. Referring to Figure 4.5 we assign the base degree of freedom 1 to the sub-element K_1, while the base degrees of freedom 2 and 3 to K_2. Furthermore we assign the
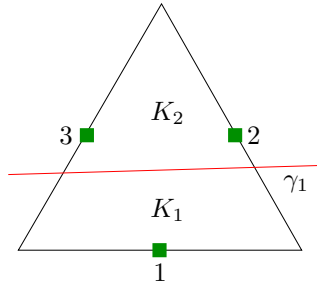
Figure 4.5: Example of local numeration of the degrees of freedom for the element $K \in \mathcal{G}_{h,1}$ cut by fracture γ_1.

extended degrees of freedom 2 and 3 to K_1 and the extend degree of freedom 1 to the sub-element K_2. This procedure ensure the continuity of a function $f \in \widetilde{\mathbb{RT}}_0\left(\mathcal{G}_{h,j}\right)$ in each part of the mesh separated by the fracture γ_j. If an element $K \in \mathcal{M}_h$ or $K \in \mathcal{I}_h$, following the idea for $\widetilde{\mathbb{P}}_0\left(\mathcal{M}_h\right)$, we need to add two more extended degrees of freedom and one extra degree of freedom for each base degree of freedom. If an edge of the sub-element K_i contains the midpoint
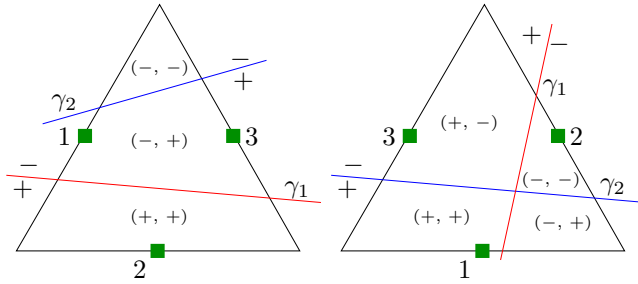
Figure 4.6: $K \in \mathcal{M}_h$.

of the edge e, of the element K, then the base degree of freedom associated to the edge e belongs to K_i. If an edge of the sub-element K_i does not contain the midpoint of e we have to check how many signs, of the level sets which intersect the element K, do change. If just one sign changes then we assign the extend degree of freedom associated to which level set changes the sign, while if two signs change we assign the extra degree of freedom, *e.g.* referring to the left part of Figure 4.6 we have the subdivision of the degrees of freedom, for an element $K \in \mathcal{M}_h$, reported in Table 4.1 for each region. While considering the

	$(+,+)$	$(-,-)$	$(+,-)$	$(-,+)$
1	extended γ_1	extended γ_2	not present	base
2	base	extra	not present	extended γ_1
3	extended γ_1	extended γ_2	not present	base

Table 4.1: Subdivision of the degrees of freedom for the left triangle of Figure 4.6.

right part of Figure 4.6 we have the subdivision of the degrees of freedom, for an element $K \in \mathcal{I}_h$ reported in Table 4.2 for each region. In all of the cases the

	$(+,+)$	$(-,-)$	$(+,-)$	$(-,+)$
1	base	extra	extended γ_2	extended γ_1
2	extra	base	extended γ_1	extended γ_2
3	extended γ_2	extended γ_1	base	extra

Table 4.2: Subdivision of the degrees of freedom for the right triangle of Figure 4.6.

continuity is guaranteed in each part of the mesh delimited by the fractures. To enrich the space $\mathbb{R}\mathbb{T}_0\left(\gamma_{\hat{h},j}\right)$, for each fracture j, to obtain $\widetilde{\mathbb{R}\mathbb{T}}_0\left(\gamma_{\hat{h},j}\right)$ we have chosen the same policy adopted for the elements $K \in \mathcal{G}_{h,i}$, based on the midpoint position.

4.2.2 Quadrature rule on the cut grid

The solution of Problem 3.4, Problem 3.7 or Problem 3.10 requires to compute integrals on the cut elements, which are not in general triangles, or tetrahedra. One possibility is to use quadrature rules which works over arbitrary polygonal domains, as in [61], an alternative is to divide the cut element into several triangles or tetrahedra only for the quadrature. The first choice is more general since it can handle non-convex domains but more complex to program and less standard. Since, thanks to Assumption 3.7 we have only convex elements from a cut element we preferred the second procedure. We choose to divide a cut element into triangles or tetrahedra, as Figure 4.7 shows. To this purpose we
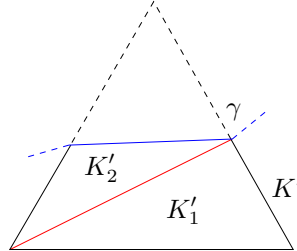
Figure 4.7: Triangulation of a cut element.

adopted the Qhull library [7] which can divide a general convex polygon into triangles, or tetrahedra, with a very fast algorithm. Furthermore we can divide each triangle or tetrahedra independently from the others the sub-triangulation is used just for the integration. Another benefit is that the parallelization of this procedure is trivial. We can observe that the quadrature error is not influenced by the "quality" of the domain, [31].

To exporting the computed solution for post-processing we use the same mesh we generated for the integration, to get the result on a "standard" mesh, therefore easy to open with standard software for scientific visualization.

Chapter 5

Applicative examples

In this chapter we apply the methods presented in chapters 2, 3 and 4, to significant test cases to asses the proposed techniques highlighting strong points and possible limits. The first section is devoted to the application of the two-phase flow model for different problems related to oil migration. In the second section we analyse different aspects of the reduced models for different aspects, *e.g.* the behaviour of the error, and we provide some realistic examples. Finally, in the third section we present some results about the performance of the algorithms.

5.1 Numerical simulations

We present some numerical results concerning the two-phase flow solver presented in Chapter 2. We focus our attention on some physical problems related to oil secondary migration which is an ideal application for the method. In particular we consider two different scenarios:

1. a single fault, acting as a barrier that stops the oil which tends to flow along it;

2. a cap-rock which captures the oil, forming an accumulation.

In the final subsection we will present a numerical test to compare, in a transmission problem similar to [38], the advantages of the XFEM method with respect the classical FEM.

5.1.1 Flow along a fracture

We present a two-phase flow problem for a water-oil system in the presence of a fault. The fracture, which acts as a barrier, is resolved by the computational grid. Figure 5.1 represents a transversal section of the domain Ω, which is obtained by extrusion along the y axis and has the dimensions

$$\Omega = (0,\, 4000) \times (0,\, 200) \times (0,\, 2000) \, .$$

The mesh $\mathcal{T}_h$, composed by 72892 tetrahedra, is conforming with the fault and more refined therein. At initial time the medium is completely filled with water, and we impose, until $t < 1900$ years an inflow of oil saturation, $S_n^{inflow} = 0.9$ in
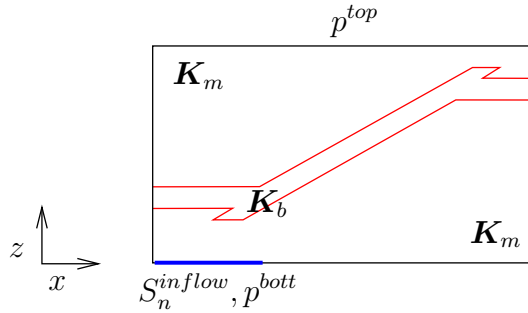
Figure 5.1: Schematic representation of the computational domain.

the left bottom part of the boundary $\partial \Omega$ of the domain, *i.e.* marked in blue in Figure 5.1, while on the top of the domain we impose zero saturation. For the pressure we impose natural boundary condition at the top $p^{top} = 1MPa$, at the bottom left part $p^{bott} = 40MPa$ of the domain and at the bottom right part we impose $10MPa$. Homogeneous boundary conditions for the flux, for both pressure and saturation equation, on the remaining part of the boundary. The data of the problem are listed in the Table 5.1.

$\boldsymbol{K}_m = 10^{-13}\,m^2$	$\boldsymbol{K}_b = 10^{-18}\,m^2$	$\mu_w = 10^{-3}\,Pa \cdot s$
$\mu_n = 2 \cdot 10^{-3}\,Pa \cdot s$	$\rho_w = 980\,Kg/m^3$	$\rho_n = 700\,Kg/m^3$
$S_{\alpha r} = 0$	$\lambda = 2$	$p_d = 1200\,Pa$
$\Phi = 0.4$	$p^{top} = 40\,MPa$	$p^{bott} = 10\,MPa$

Table 5.1: Data for the problem of two-phase flow along a fracture.

Figure 5.2 represents the saturation S_n of the oil at two different times. On the left, at $t = 630$ years, the saturation is higher along the fracture and fills the left-bottom part of the domain, under the impermeable layer. On the right, at $t = 2540$ years, the inflow of saturation has stopped and, since the oil is lighter then water, it has accumulated under the two impermeable layers. It can be observed also that the lower accumulation starts slowly to flow inside the barrier. Figure 5.3 shows the global pressure field at $t = 2540$ years. We
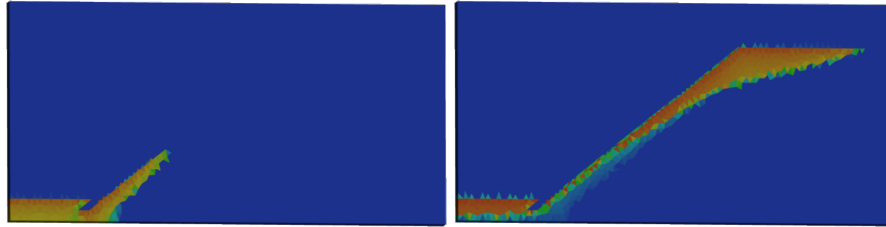
Figure 5.2: The saturation of the liquid at two different times: on the left at $t = 630$ years, on the right at $t = 2540$ years. The colour scale ranges from blue, $S_n = 0$, to red, $S_n = 1$.

can observe that the fracture support a strong gradient of the pressure across it. The pressure experiences a small variation during the simulation due to the changes in the relative permeabilities.
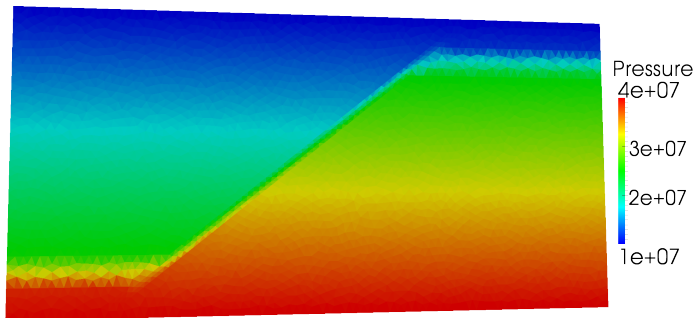
Figure 5.3: The global pressure at $t = 2540$ years.

5.1.2 Schematic cap rock

We now consider a two-phase flow for a water-oil system in presence of a cap rock resolved by the computational grid $\mathcal{T}_h$. The simulation is based on the real problem presented in [76]. Figure 5.4 represents a transversal section of the domain Ω where the flow takes place. The computational domain is obtained by its extrusion along the y axis and has dimension $2000\,\mathrm{m} \times 400\,\mathrm{m} \times 3200\,\mathrm{m}$. The mesh, composed by 120865 tetrahedra, is conforming to the cap rock. At the
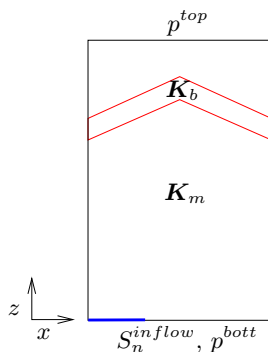
Figure 5.4: Schematic representation of the computational domain.

initial time the medium is completely filled with water. We impose an inflow condition $S_n^{inflow} = 0.9$ for $t < 1900$ years in the bottom part of the domain, marked in blue in Figure 5.4. The boundary conditions and the data are the same as in the previous example, reported in Table 5.1.

Figure 5.5 represents the saturation at three different times. In the left figure, for $t = 1500$ years, the oil starts invading the domain and, since it does not reach the cap rock, the flow is governed by the gravity force. In the second snapshot, for $t = 2400$ years, the oil reaches the cap rock and, since it is almost impermeable the oil starts to accumulate under the cap rock. In the right picture, for $t = 3000$ years, almost all the oil accumulates under the cap rock. Even if this example is schematic it represents well the process of the accumulation and trapping of the oil in a sedimentary basin. Figure 5.6 shows the global pressure field at the final time $t = 3000$ years, we can see that the pressure varies almost linearly along the vertical with a small variation near the cap rock.
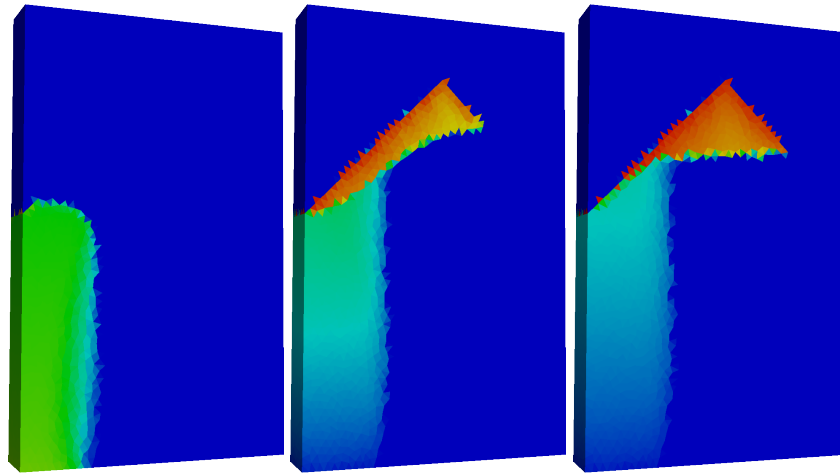
Figure 5.5: The saturation of the oil at three different times: on the left at $t = 1500$ years, in the centre at time 2400 years on the right part at $t = 3000$ years. The color scale ranges from blue, $S_n = 0$, to red, $S_n = 1$.
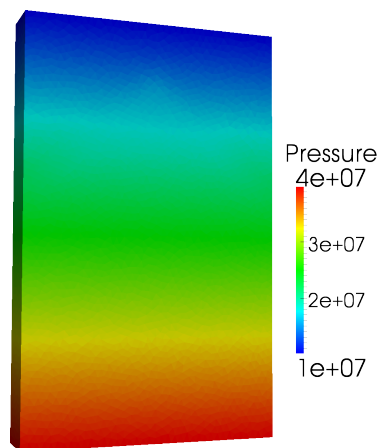
Figure 5.6: The global pressure of the oil at $t = 3000$ years.

5.1.3 Fitted and unfitted discontinuities

In realistic applications permeability coefficient can be, as shown in the previous examples, discontinuous across internal interfaces. To solve numerically this type of problems, it is common to take the discontinuity of the data into account by enforcing mesh lines or surface along the interface, otherwise we have sub-optimal convergence, as [38] shown. Let us consider a domain $\Omega \in \mathbb{R}^3$, divided into two sub-domains Ω_1 and Ω_2 by the interface γ, see Figure 5.7 for an example. Then the problem is
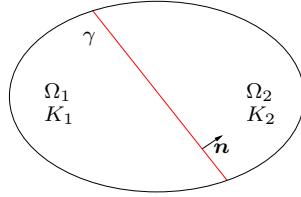
Figure 5.7: Sketch of a bi-dimensional domain for a Darcy problem with discontinuous coefficients across γ.

$$\begin{cases} -\nabla \cdot K \nabla p = q & \text{in } \Omega_1 \cup \Omega_2, \\ [\![p]\!]_\gamma = 0 & \text{on } \gamma, \\ [\![K\nabla p \cdot \boldsymbol{n}]\!]_\gamma = g & \text{on } \gamma, \\ p = 0 & \text{on } \partial\Omega, \end{cases}$$

where $K \in L^\infty(\Omega)$ can be discontinuous across γ. We want to reproduce with a $3D$ code the test case proposed in [38] in $1D$, reading

$$-\sum_{i=1}^{2} \frac{d}{dz}\left(K_i \frac{dp_i}{dz}\right) = 1 \quad \text{in } \mathcal{I},$$

where $\mathcal{I} = (0, 1)$ and $\gamma = \{z \in \mathcal{I} : z = 0.5\}$ and subject to the coupling conditions

$$\begin{cases} [\![p]\!]_\gamma = 0 \\ \left[\!\left[K\dfrac{dp}{dz}\right]\!\right]_\gamma = 0 \end{cases} \quad \text{on } \gamma,$$

and with the following boundary conditions

$$\begin{cases} p_1(0) = 0 & \text{for } z = 0, \\ p_2(1) = 0 & \text{for } z = 1. \end{cases}$$

To solve this problem in $\Omega = (0, 1)^3$, following [45] we employ homogeneous natural boundary condition in $x = 0$, $x = 1$, $y = 0$ and $y = 1$, while the jump of

the co-normal derivative is imposed in the plane $z = 1/2$. The analytic solution of the problem is

$$
\begin{cases}
p_1\left(\boldsymbol{x}\right) = \dfrac{(3K_1 + K_2)z}{4K_1^2 + 4K_1 K_2} - \dfrac{z^2}{2K_1} & \text{in } \Omega_1, \\[4mm]
p_2\left(\boldsymbol{x}\right) = \dfrac{K_2 - K_1 + (3K_1 + K_2)z}{4K_2^2 + 4K_1 K_2} - \dfrac{z^2}{2K_2} & \text{in } \Omega_2.
\end{cases}
$$

In the test case we choose $K_1 = 1/2$ and $K_2 = 20$. We want to verify the
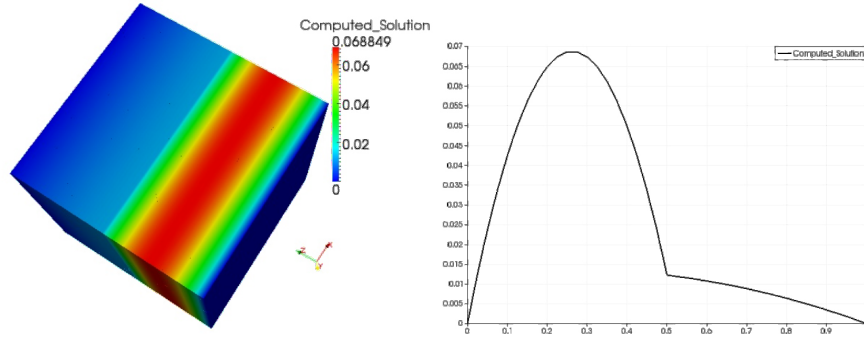
Figure 5.8: In the left figure the solution of the problem, while in the right figure the solution of the solution in a line perpendicular and crossing the level set.

quadratic convergence of the error in L^2 norm and compare the solution with that obtained with an unfitted finite element method. The volumetric mesh is the same for the XFEM simulations and the unfitted FEM simulations. The errors are presented in Table 5.2 and plotted in Figure 5.9.

h	XFEM	FEM
0.15746	$8.02 \cdot 10^{-4}$	$7.898 \cdot 10^{-3}$
0.10188	$3.03 \cdot 10^{-4}$	$5.134 \cdot 10^{-3}$
0.08242	$1.89 \cdot 10^{-4}$	$4.162 \cdot 10^{-3}$
0.05587	$8.997 \cdot 10^{-5}$	$2.824 \cdot 10^{-3}$
0.04224	$6.297 \cdot 10^{-5}$	$2.137 \cdot 10^{-3}$

Table 5.2: Comparison between the L^2 norms of the error, for the XFEM method and for the unfitted FEM method.

The results confirm the better capability of the XFEM method to capture the real solution of problems with sharp discontinuity in the data, keeping the computational costs comparable with the classic FEM.

5.2 Reduced models

We show some numerical results with the reduced models presented in chapter 3. This section is organized in the following sub-sections:
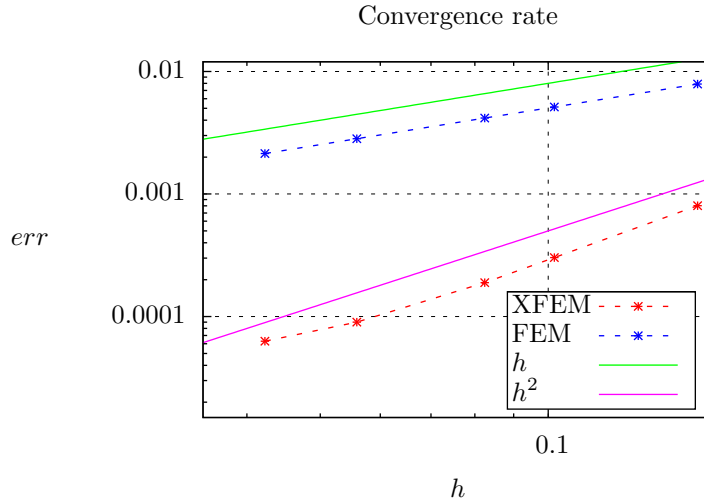
Figure 5.9: Comparison between the L^2 norms of the error between the XFEM method and the standard unfitted FEM method.

1. we will numerically evaluate the model error, *i.e.* the error we obtain if the reduced model is used instead of the complete model. We consider the reduced model with single fracture, the reduced model with intersecting fractures and the reduced model for the advection-diffusion problem;

2. we will analyse the convergence rates defining the error, taken as the difference between an exact solution of the reduced model and the numerical solution in the three cases considered above;

3. we will study the condition number and the maximum and minimum eigenvalues and the condition number of the coupled system when the fracture position changes. We treat only the Darcy reduced models since the reduced model for the tracers behaves similarly;

4. we will show some limits of the reduced model for particular values of the data and the discretization of the meshes;

5. finally we will discuss some realistic examples.

In all of the examples which involve the intersecting fractures we assume Assumption 3.6 even if the fractures involved are not exactly orthogonal.

5.2.1 Model error

The model error is the error we commit if we use the reduced model instead of solving the real equation. We define the error *err* as the difference between a reference solution, obtained using the original equations solved on a fine grid, and the reduced solution

$$err := \|p - p_{ref}\|_{L^2(\Omega)}, \tag{5.1}$$

while the relative error err_{rel} is

$$err_{rel} := \frac{err}{\|p_{ref}\|_{L^2(\Omega)}} \,. \tag{5.2}$$

For time dependent problem we investigate the errors at different time steps. Note that we are not considering the solution of the reduced model inside the fracture.

Reduced Darcy model

We consider a two-dimensional problem in a square domain cut by two fractures γ_1 and γ_2 characterized by different properties, let $\Omega = (0, 1)^2$ and

$$\gamma_1 = \{(x,y) \in \Omega : \ y = 0.27\} \,, \quad \gamma_2 = \{(x,y) \in \Omega : \ y = 0.5x + 0.34\} \,.$$

The boundary of Ω is partitioned into two parts

$$\Gamma^E = \{0, 1\} \times [0, 1] \quad \text{and} \quad \Gamma^N = [0, 1] \times \{0, 1\} \,.$$

In Γ^E we prescribe essential boundary conditions while in Γ^N we impose natural boundary conditions. We consider no flux as boundary conditions for both the fractures at $\partial\gamma_i$, for $i = 1, 2$. The computational domain is sketched in Figure 5.10. The bulk flow and the flow in the fracture are described by Problem 3.4,
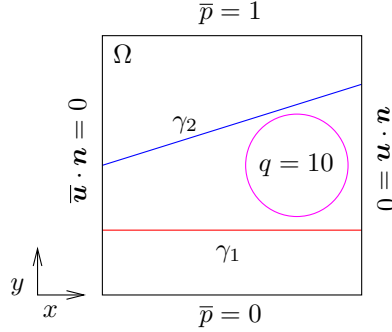
Figure 5.10: Computational domain cut by two fractures γ_1 and γ_2.

with boundary natural data $\bar{p}(x, y) = y$, for the porous medium, source term q given by

$$q(x, y) = \begin{cases} 10 & \text{if } (x - 0.75)^2 + (y - 0.5)^2 < 0.04 \,, \\ 0 & \text{otherwise} \,, \end{cases}$$

while $\hat{q}_i \equiv 0$ for both the fractures and $\boldsymbol{K} = \boldsymbol{I}$. The first fracture γ_1 is characterized by the same tangential permeability as the porous medium in Ω thus $\hat{\eta}_1 = d^{-1}$, with d the thickness of the fractures which we will choose in the sequel, while the normal permeability is variable along the fracture, namely

$$\eta_{\gamma_1}(x, y) = \begin{cases} 10d & \text{if } x < 0.5 \,, \\ 100d & \text{if } x \geq 0.5 \,. \end{cases}$$

The second fracture γ_2 is instead characterized by the same normal permeability as the porous medium in Ω *i.e.* $\eta_{\gamma_2} = d$, and a high tangential permeability $\hat{\eta}_2 = 0.01d^{-1}$.

Figure 5.11 shows the pressure field in Ω, γ_1 and γ_2, obtained with the reduced model and with the original model with a fine grid. Due to the small normal permeability of γ_1 there is a jump in the pressure across this fracture, and the gap changes along the line according to η_{γ_1}. While γ_1 acts as a barrier for the flow, γ_2 is a preferential path thanks to its high tangential permeability.
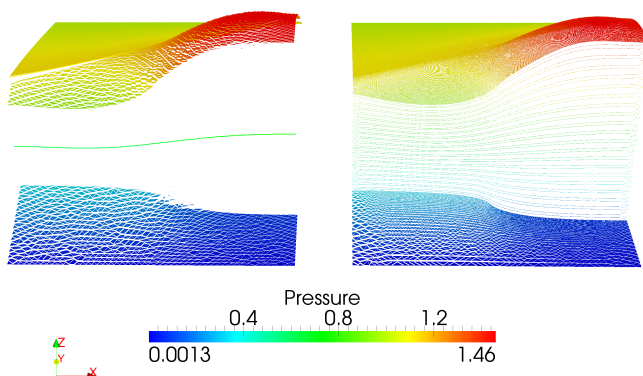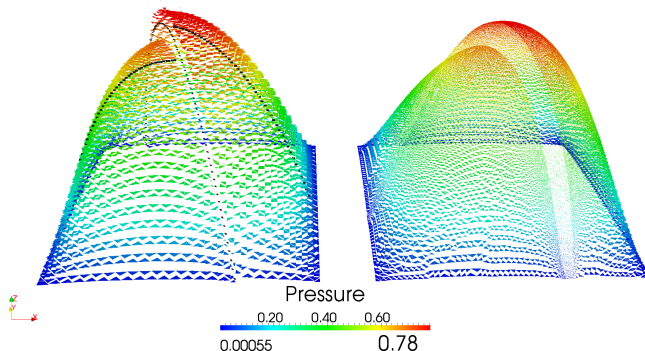

Figure 5.11: On the left the solution with the reduced model, with $\xi_0 = 0.25$ and $d = 0.05$, using 952 triangles for the medium and 100 segments for each fracture. On the right the reference solution with 125769 triangles.

Figures 5.12 and 5.13 show the model error (5.1), taking as a reference the solution of the original problem with a fine grid composed by 125769 triangles, considering the domain without both fractures. Due to the model reduction the major errors are localized near the fractures, in particular when a pressure jump occurs across a fracture. We can see comparing Figure 5.12 and 5.13 that
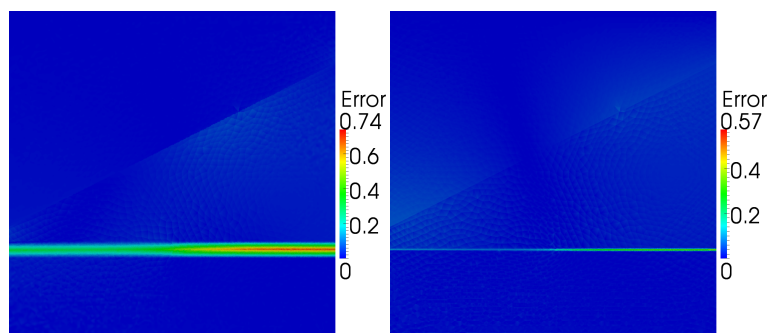
Figure 5.12: On the left image the model error (5.1) for thickness $d = 0.05$ while on the right image the model error (5.1) for thickness $d = 0.02$. In both simulation we take $\xi_0 = 0.25$.

the major error is near fracture γ_1 since the pressure jumps across it, while the error is lower near fracture γ_2 which is comparable to the error in the bulk. The global relative error (5.2) is reported in Table 5.3. We can notice that decreasing the fracture thickness d the model error decreases as expected. While changes in the shape parameter ξ_0 do not significantly affect the solution.
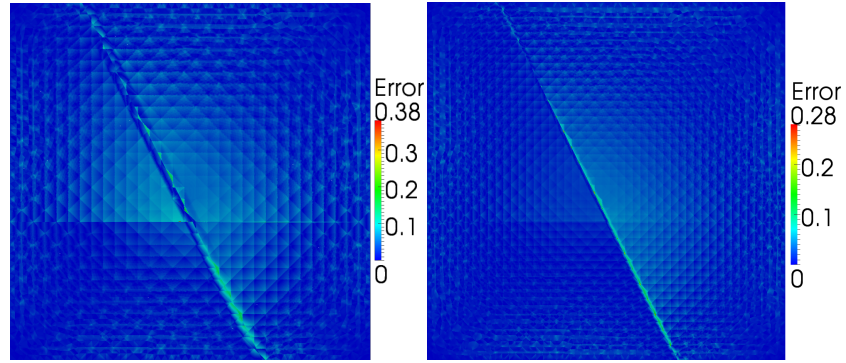
137
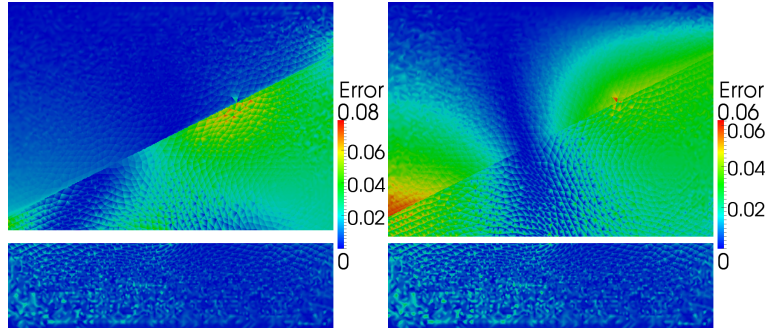
Figure 5.13: On the left image the model error (5.1) for thickness $d = 0.05$ while on the right image the model error (5.1) for thickness $d = 0.02$, with $\xi_0 = 0.25$. In both images we left out the region occupied by the fracture, now replaced by a mono-dimensional interface.

	$\xi_0 = 0$	$\xi_0 = 0.25$	$\xi_0 = 0.5$
$d = 0.02$	0.0337824	0.0279828	0.0334472
$d = 0.05$	0.0683489	0.0687755	0.0691853

Table 5.3: Global relative error err_{rel}.

Reduced Darcy model with intersection

We consider a two-dimensional problem in a square domain cut by two intersecting fractures characterized by different properties, let $\Omega = (0,\, 1)^2$ and

$$\gamma_1 = \{(x,y) \in \Omega : \ y = 0.387\} \quad \text{and} \quad \gamma_2 = \{(x,y) \in \Omega : \ y = -2x + 1.4\}\,.$$

In the boundaries for the domain $\partial\Omega$ and for each fracture $\partial\gamma_i$, for $i = 1, 2$, we prescribe homogeneous natural boundary conditions. The bulk flow and the flow in the intersecting fractures are described by Problem 3.5 with source terms $q = 10$ and $\hat{q}_i = 10d$ for both fractures and $\boldsymbol{K} = \boldsymbol{I}$, with d the thickness of the fracture. γ_1 is characterized by the same tangential and normal permeability as the porous medium in Ω thus $\hat{\eta}_1 = d^{-1}$ and $\eta_{\gamma_1} = d$. γ_2 is instead characterized by the same tangential permeability as the porous medium in Ω *i.e.* $\hat{\eta}_2 = d^{-1}$, and a low normal permeability $\eta_{\gamma_2} = 50d$. We set $\hat{\xi}_0 = 0$. The computational domain is sketched in Figure 5.14.
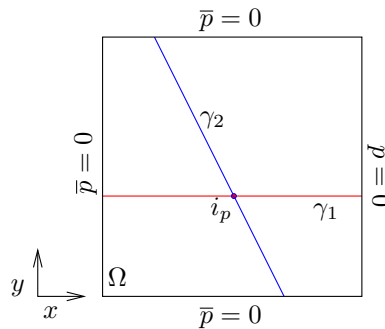
Figure 5.14: Computational domain cut by two intersecting fractures.

Figure 5.15 shows the pressure field in the domain Ω and in the fractures γ_1 and

γ_2, with and without the reduced model. Due to the small normal permeability of γ_2 there is a jump in the pressure across this fracture, furthermore the effect of fracture γ_1 is null since it has the same permeability tensor as the porous matrix.

Figure 5.15: On the left the solution with the reduced model, with $\xi_0 = 0.25$ and $d = 0.02$, using 4418 triangles for the medium, 101 segments for first fracture and 102 segments for the second fractures. On the right the reference solution with 114115 triangles.

In Table 5.4 the global relative error (5.2) defined in 5.4 is reported.

	$\xi_0 = 0$	$\xi_0 = 0.25$	$\xi_0 = 0.5$
$d = 0.02$	0.0437599	0.0440597	0.0456497
$d = 0.05$	0.072244	0.0726848	0.0724751

Table 5.4: Global relative error err_{rel} for different values of thickness d and shape parameter ξ_0.

We notice that decreasing the thickness d of the fracture the model error decreases, while changing the shape parameter ξ_0 the model error does not change significantly.

Figure 5.16 shows the model error (5.1) considering the global domain and the domain without the first fracture. We take as a reference the solution of the real problem with a fine grid composed by 114115 triangles. Due to the model reduction the major errors are localized near the fractures, in particular when a pressure jump occurs across a fracture.

In Figure 5.17 we present a zoom of the error near the intersection point $\boldsymbol{i}_p$, we can notice that the error is comparable with the neighbouring regions.

Reduced transport model

We here consider the two-dimensional problem presented in [36], with computational domain $Q_T = \Omega \times (0, T)$, where Ω is cut by a slanting fracture, see Figure 5.18. Let $\Omega = (0, 1)^2$, with boundary divided into $\Gamma^E = \{0, 1\} \times [0, 1]$ and $\Gamma^N = [0, 1] \times \{0, 1\}$.

The fracture is defined as

$$\gamma = \{(x, y) \in \Omega : y = 2x - 0.4\}.$$

The bulk flow and the flow in the fracture are described by Problem 3.4, with

Figure 5.16: On the left image the model error (5.1) for thickness $d = 0.05$ while on the right image the model error (5.1) for thickness $d = 0.02$. In both simulation the shape parameter is $\xi_0 = 0.25$.
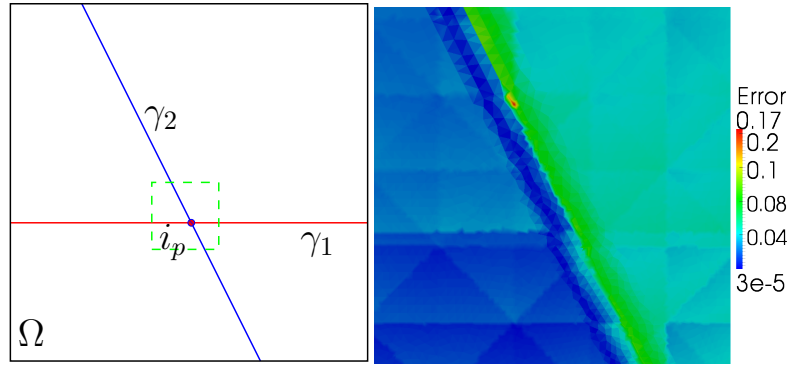
Figure 5.17: On the left image the zoom, coloured in green, of the domain Ω while on the right image the zoom of the model error for thickness $d = 0.02$, with shape parameter $\xi_0 = 0.25$.
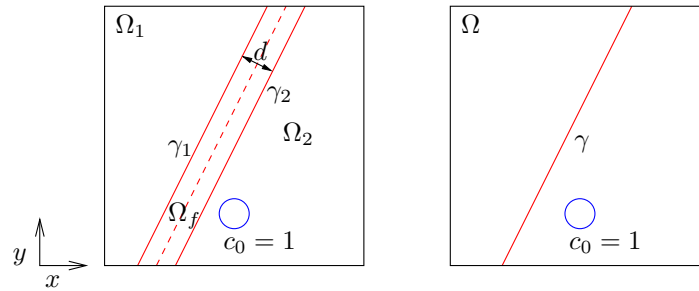
Figure 5.18: On the left, the domain Ω divided into two parts by the region Ω_f, of thickness d, corresponding to the fracture. On the right Ω_f has been replaced with the $n-1$-dimensional interface γ. The initial condition for the concentration of the tracer is also sketched in both domains.

zero scalar sources $q_i \equiv 0$ and $\hat{q} \equiv 0$, natural boundary data $\overline{p}(x, y) = 1 - y$, and thickness of the fracture $d = 0.01$. We consider full natural boundary conditions for the fracture $\hat{p} = 1 - y$ on $\partial\gamma$ with $\xi = 0.75$. The permeability tensor of the medium is isotropic, $\boldsymbol{K}_m = K_m \boldsymbol{I}$ with $K_m = 1$ while the fracture

is characterized by a high permeability in the normal and tangential directions, $\boldsymbol{K}_f = 100\boldsymbol{I}$. We want to solve Problem 3.9 where the advection field is the computed Darcy velocity which is higher in the fracture than in the porous matrix.

We set the boundary condition as $\bar{c} = 0$ and the initial data, for the concentration c, as

$$c_0(x, y) = \begin{cases} 1 & \text{if } (x - 0.5)^2 + (y - 0.2)^2 < 0.03, \\ 0 & \text{otherwise,} \end{cases}$$

as shown in Figure 5.18. The diffusion tensor is isotropic and constant, $\boldsymbol{D} = 0.05\boldsymbol{I}$ everywhere. We simulate this test case with the standard mixed FEM method and a refined mesh that is able to resolve the fracture, and compare the results with the reduced model and the XFEM approach. The time step size is $\Delta t = 0.005$ and T is set to 0.2 for both simulations. In Figure 5.19 the solutions are compared at two different times. In both cases the tracer is advected upwards and flows preferably along the fracture where the fluid velocity is higher. The two methods produce results that are qualitatively in good agreement even if a grid of only 3200 triangles for the medium and 100 segments for the fracture are used with the XFEM approach versus a much more refined grid, more than 13000 triangles, is for the standard approach. The slight mismatch between the two solutions is mainly due to the numerical diffusion associated to the coarse grid.

5.2.2 Convergence rates

In this section we investigate the convergence rates of the proposed numerical methods. In all the examples the value of the pressure in the fractures is imposed. We compute the error err for the pressure in the medium using the norm defined in (3.66) as

$$err = \|p - p_{exact}\|_{Q_h}, \tag{5.3}$$

where p is the computed pressure while p_{exact} is the exact pressure. For time dependent problem we investigate the error at the final time step.

Reduced Darcy model

To verify numerically the convergence rate presented in Theorem 3.5 of Problem 3.4 we use the same example reported in [24]. The error we compute, involves just the medium since we fix the solution inside the fracture.

We consider the domain $\Omega = (0, 1)^2$ with the fracture defined as

$$\gamma = \left\{ (x, y) \in \Omega : r^2 = \left(x - \frac{1}{2} \right)^2 + \left(y - \frac{1}{2} \right)^2 = R^2 \right\},$$

with $R = 0.21$. The computational domain is reported in Figure 5.20.
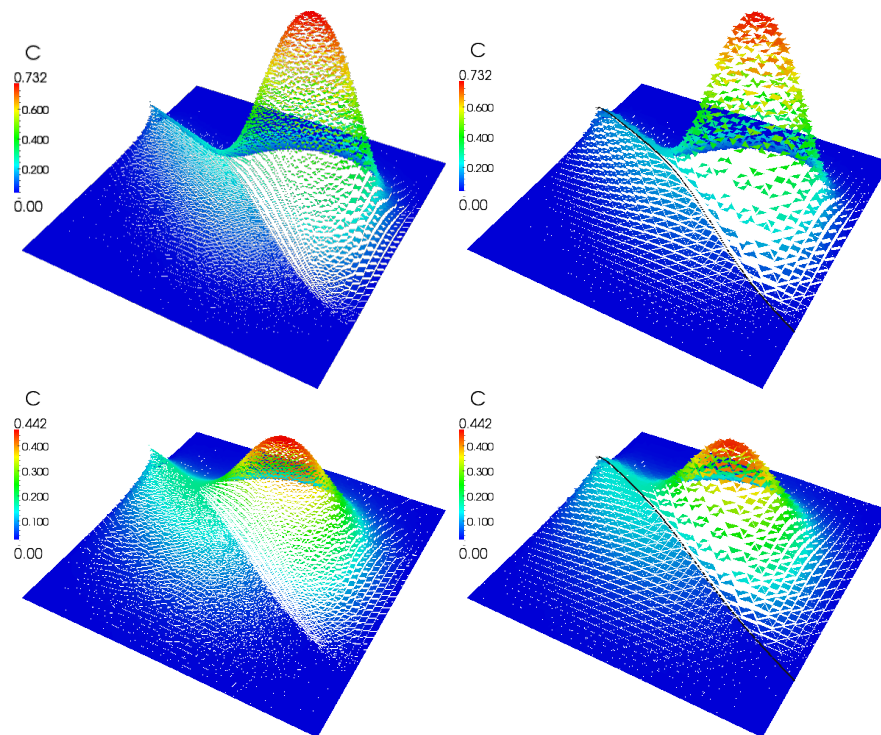
Figure 5.19: In the left images the concentration of the tracer computed with the standard mixed FEM and the fine grid is shown at time $t = 0.1$ and $t = 0.2$ respectively. While in the right images we report the solution obtained at the same time steps with the reduced approach and a coarse grid that is non matching with the fracture. The black line represents the concentration along γ.
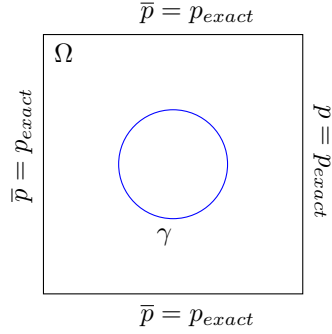
Figure 5.20: Computational domain cut by a fracture.

The data for the problem are: permeability of the medium $\boldsymbol{K} \equiv \boldsymbol{I}$, inverse of normal permeability of the fracture $\eta_\gamma \equiv \dfrac{2}{3}R$, source term

$$q(r) = \begin{cases} \dfrac{2}{R^2} & \text{if } r^2 > R^2 \,, \\[2mm] \dfrac{4}{R^2} & \text{if } r^2 < R^2 \,, \end{cases}$$

and shape parameter $\xi_0 = 0.25$. The pressure in the fracture is imposed to $\hat{p} = \dfrac{19}{12}$. We impose natural boundary condition on $\partial\Omega$ such that the exact solution is

$$p_{exact}(r) = \begin{cases} \dfrac{r^2}{2R^2} + \dfrac{3}{2} & \text{if } r^2 > R^2 \,, \\[2mm] \dfrac{r^2}{R^2} & \text{if } r^2 < R^2 \,, \end{cases}$$

Figure 5.21 shows the computed solution for 45602 triangles. Figure 5.22 shows
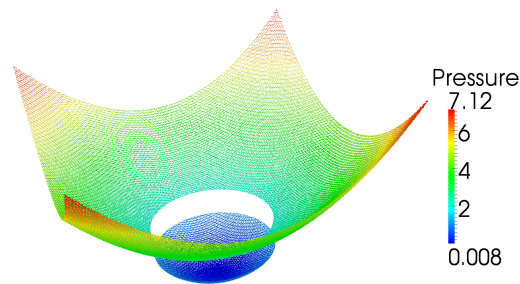
Figure 5.21: Computed solution on a mesh composed by 45602 triangles.

the convergence rate for the pressure error *err* defined in (5.3). The numerical results are in good agreement with the theoretical result.

Reduced Darcy model with intersection

For the reduced model with intersection there are no theoretical results about convergence rates for the error (3.5). However since the model presented in
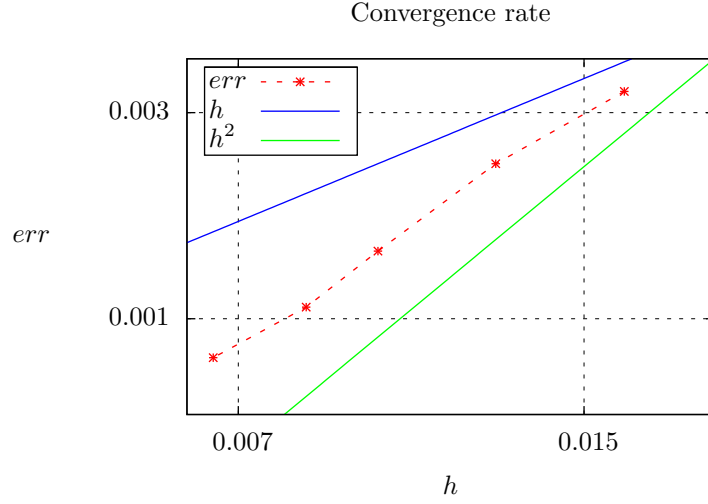
Figure 5.22: Convergence rate for the pressure error *err* of the model with a single fracture.

[Problem 3.5](#) is an extension of the one in [Problem 3.4](#), we can expect a similar behaviour for the error. The aim of this test case is to validate this assumption numerically.

We consider the domain $\Omega = (0,\, 1)^2$ with two different fractures

$$\gamma_1 = \{(x,\, y) \in \Omega : y = -2x + 1.4\} \quad \text{and} \quad \gamma_2 = \{(x,\, y) \in \Omega : y = 0.51\} \ .$$

The computational domain is reported in Figure [5.23](#) together with γ_1 and γ_2. The exact solution is
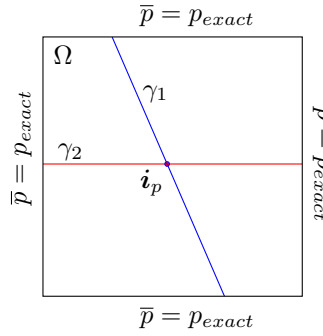
Figure 5.23: Computational domain cut by two different fractures γ_1 and γ_2.

$$p\,(x,\, y) = \begin{cases} y & \text{if } y < 0.51, \\ y + 0.5 & \text{otherwise.} \end{cases}$$

The data of the problem are: permeability of the porous medium $\boldsymbol{K} = \boldsymbol{I}$, scalar source $q \equiv 0$, shape parameter $\xi_0 = 0$ for both fractures, inverse of the normal permeability in the first fracture $\eta_{\gamma_2} \equiv 0.5$. The boundary condition $\partial\Omega$ are

natural on the top and on the bottom, and essential on the right and on the left part. The reduced pressure in γ_2 is imposed and equal to $\hat{p}_2 = 0.751$ while the reduced pressure in γ_1 is imposed and equal to the exact solution p. The penalty parameter for the Nitsche's method for the imposition of essential boundary conditions is chosen as $\mu = 7$. Figure 5.24 shows the computed solution for 17384 triangles. We analyse two different values of η_{γ_1}, first $\eta_{\gamma_1} \equiv 0$, *i.e.* perfect
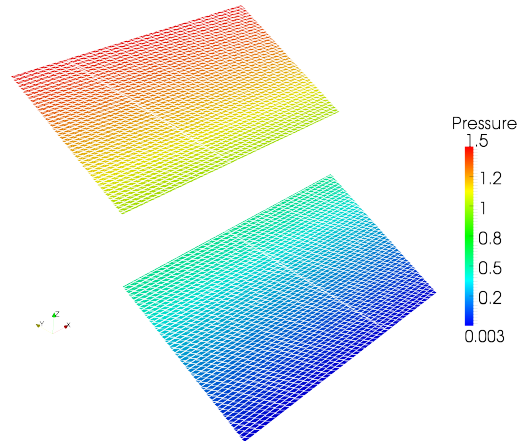
Figure 5.24: Computed solution with two fractures on a mesh composed by 17384 triangles, the first fracture has the same parameter as the bulk while the second fracture support a pressure jump.

transmission conditions are imposed to the fracture, then $\eta_{\gamma_1} \equiv 0.01$, *i.e.* the same properties as the porous medium. Figure 5.25 shows the errors for
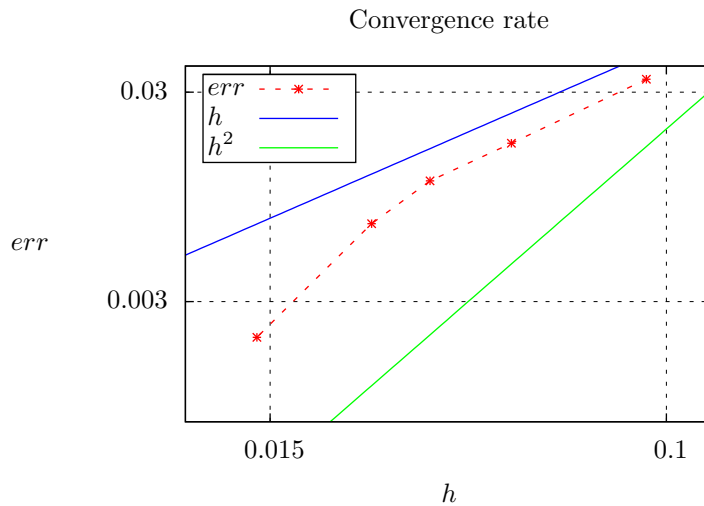
Figure 5.25: Convergence rate for the pressure error err, with $\eta_{\gamma_1} \equiv 0$, of the model with two intersecting fractures.

the first case while in Figure 5.26 are reported the errors for the second case. The numerical results are in good agreement with what we expected, indeed
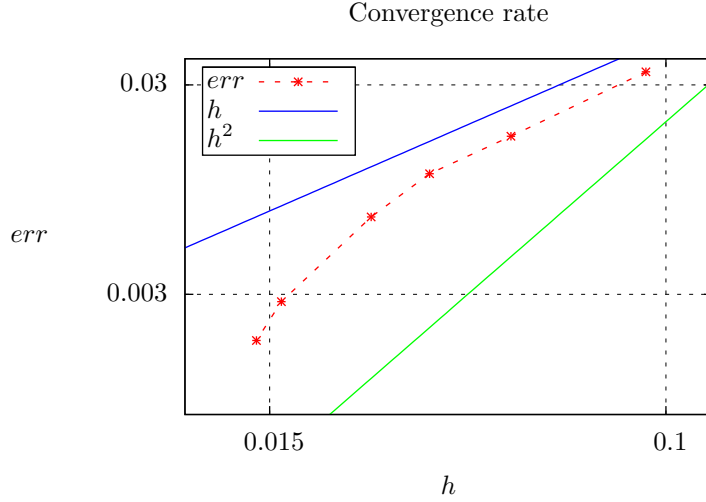
Figure 5.26: Convergence rate for the pressure error err, with $\eta_{\gamma_1} \equiv 0.01$, of the model with two intersecting fractures.

convergence is roughly quadratic in both cases.

5.2.3 Analyses of the condition number

In this part we present the behaviour of the eigenvalues in two cases: single fracture and intersecting fractures, treated with the XFEM method. In particular, in the relevant case of a cut element whose area tends to zero as in Figure 5.27. Even if there are no theoretical results on the eigenvalues of the Darcy
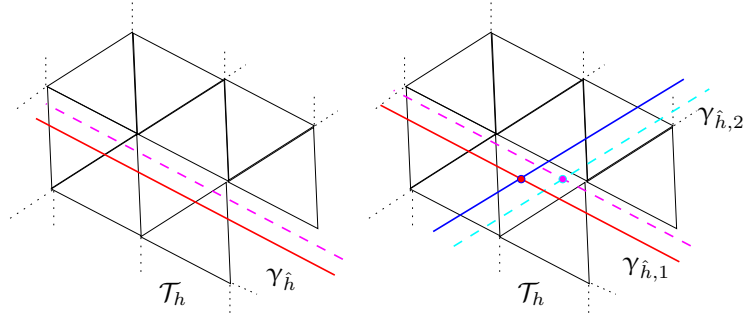
Figure 5.27: Different position of fractures respect to the mesh $\mathcal{T}_h$.

problem with fractures except for [24], where some numerical are presented. We refer to [80], [65], [15] and [45] for a detailed analysis of similar problems with the XFEM method applied to elliptic problems written in primal formulation. From the aforementioned works we have a bound for the maximum eigenvalue

$$\lambda_{max} \leq \widetilde{M} h^n \left(1 + \widetilde{C} h^{-2} \right) , \tag{5.4}$$

146

where $\widetilde{M}$, $\widetilde{C} \in \mathbb{R}^+$ are independent of the position of the fracture, n is the space dimension and h is the diameter of the smaller element of the mesh $\mathcal{T}_h$. In our tests we have two different mesh sizes: h the one associated to the mesh $\mathcal{T}_h$ and $\hat{h}$ the one associated to the fracture mesh $\gamma_{\hat{h}}$. Since in our test $n = 2$ we would expect λ_{max} to be independent of h with fixed $\hat{h}$, while $\lambda_{max} \lesssim \hat{h}^{-1}$ for fixed h. For the minimum eigenvalue we have that

$$\lambda_{min} \geq \widetilde{\alpha}_C C_{min}(h, \kappa), \tag{5.5}$$

where $\widetilde{\alpha}_C \in \mathbb{R}^+$ is related to the coercivity and Poincaré constants, while for C_{min} we have

$$C_{min}(h, \kappa) \gtrsim h^n \min(c_1, c\kappa),$$

with c_1, $c \in \mathbb{R}^+$ two constants and κ is the ratio between the minimum and maximum area or volume of the two parts of a cut element. For fixed κ and for $n = 2$ we expect that $\lambda_{min} \gtrsim h^2$ for a given $\hat{h}$ while $\lambda_{min} \gtrsim h$ for a given h. Finally, since the matrices are symmetric and positive definite, the condition number of the problem in norm 2, fixing $\hat{h}$, is $cond_2 \lesssim h^{-2}$ and $cond_2 \lesssim h^{-2}$ for a given h.

In all examples the data in the fractures are such that the pressure and velocity are continuous in all the domain Ω, thus the values of the eigenvalues and the condition number are related to the numerical method and not a particular choice of the data.

Before considering the reduced model, we analyse the behaviour of the spectrum in a transmission problem solved with the XFEM method.

XFEM

We analyse the behaviour of the spectrum of the matrix generated by the XFEM method for the classical problem presented in section 5.1.3, where the computational grid is Cartesian. We change the position of the interface γ such that the minimum ratio of volume of the cut elements decreases more and more. In Table 5.5 we present the results obtained for the spectrum of the matrix of the problem.

$\min\limits_{\mathcal{T}_h} \kappa$	λ_{min}	λ_{max}	$\lambda_{max}/\lambda_{min}$
0.125	$8.06 \cdot 10^{-3}$	3.481	$4.31 \cdot 10^2$
$1.5625 \cdot 10^{-2}$	$8.12 \cdot 10^{-3}$	3.468	$4.27 \cdot 10^2$
10^{-3}	$8.44 \cdot 10^{-4}$	3.465	$4.105 \cdot 10^3$
$1.25 \cdot 10^{-4}$	$1.02 \cdot 10^{-4}$	3.464	$3.396 \cdot 10^4$
$1.56 \cdot 10^{-5}$	$1.26 \cdot 10^{-5}$	3.460	$2.7467 \cdot 10^5$
$1.25 \cdot 10^{-7}$	$1.0029 \cdot 10^{-7}$	3.463	$3.453 \cdot 10^7$

Table 5.5: Minimum and maximum eigenvalue with respect to the ratio of the volumes.

We can observe that the maximum eigenvalue is almost constant while the minimum eigenvalue decreases linearly when the ratio between the areas of the sub-elements decreases. This result is confirmed by the theory.

We then solve the same problem but we refine the mesh leaving the interface fixed, *i.e.* with constant κ. Table 5.6 shows the values of the eigenvalues and the condition number in norm 2 for different values of the spacing of the mesh $h \approx 1/N$.

N	λ_{min}	λ_{max}	$cond_2$
5	$2.148 \cdot 10^{-2}$	4.40769	$2.05 \cdot 10^2$
11	$4.27 \cdot 10^{-3}$	1.1505	$2.67 \cdot 10^2$
19	$1.06 \cdot 10^{-3}$	1.00001	$9.51 \cdot 10^2$
29	$3.29 \cdot 10^{-4}$	1	$3.03 \cdot 10^3$
39	$1.42 \cdot 10^{-4}$	1	$7.002 \cdot 10^3$

Table 5.6: Eigenvalues and condition number for different values of $h \approx 1/N$.

We can observe that both eigenvalues are affected by the grid spacing h. The maximum eigenvalue stabilizes to 1 for decreasing values of h, while the minimum eigenvalue quadratically decreases with respect to h. Therefore the condition number grows quadratically with respect to h as the theory predicts

$$cond_2 \leq \frac{\widetilde{M}h^3(1 + \widetilde{C}h^{-2})}{h^3 \min(c_1, c\kappa)} \approx h^{-2} \,.$$

Reduced Darcy model

To analyse the behaviour of both the eigenvalues λ_{max} and λ_{min} and the condition number for coupled Darcy problem with a single fracture we consider the domain $\Omega = [0, 1]^2$, discretized with a computational grid $\mathcal{T}_h$ with 20 elements for each border, and the fracture

$$\gamma = \{(x, y) \in \Omega : y = c_i\} \,,$$

$c_i \in \{0.525, 0.5, 0.515, 0.51, 0.505, 0.5025, 0.50125, 0.500625, 0.5003125\}$, discretized with 101 segments. We set for the porous medium $\boldsymbol{K} = \boldsymbol{I}$ and $q \equiv 4$, while the data of the fracture are $d = 0.01$, $\xi_0 = 0.25$, $\hat{q} \equiv qd$, $\hat{\eta} = 1/d$ and $\eta_\gamma = d$. The boundary condition are of homogeneous natural type on the top and bottom part of $\partial\Omega$ and homogeneous essential type on the left and right part of $\partial\Omega$ and on $\partial\gamma$.

The sparsity pattern of the global matrix is reported in Figure 5.28 to show the symmetry, the different blocks medium-fracture and the extended degrees of freedom which modify the more structured pattern of the original problem. Figure 5.29 shows the behaviour of λ_{max} and λ_{min} for decreasing values of κ. As we expected, the maximum eigenvalue has a stable value while the minimum eigenvalue decreases to zero according to (5.4) and (5.5). In Table 5.7 is reported the behaviour of the eigenvalues and condition number for fixed κ but for decreasing h of the mesh and constant $\hat{h} = 1/101$ of the fracture. The position of the fracture is $c_i = 0.5$. We indicate with N the number of elements in one of the four pieces of boundary of Ω.

The results are in good agreement with what we expected. In Table 5.8 we report the behaviour of the eigenvalues and condition number for fixed κ and
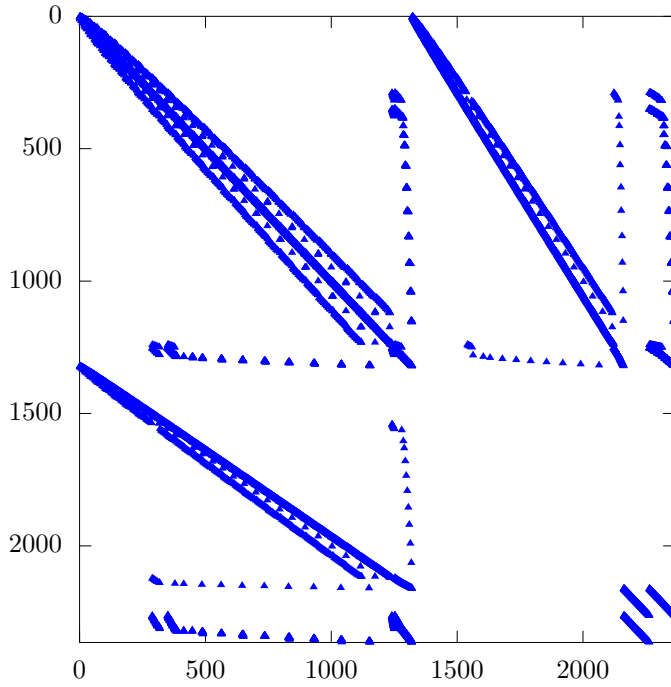
Figure 5.28: Sparsity patter of the coupled problem with 13965 non zero values.
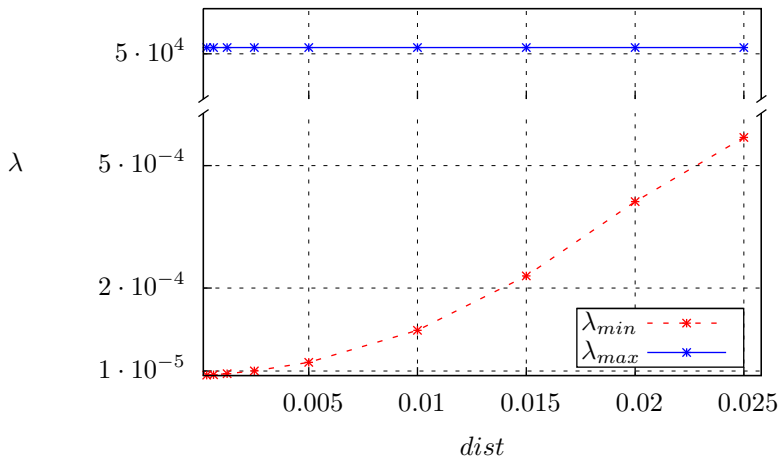
Convergence rate

Figure 5.29: Maximum and minimum of the eigenvalues for the matrix scale with *dist*.

$h \approx 1/29$ but for decreasing $\hat{h}$. The position of the fracture is $c_i = 0.5$. We indicate with M the spacing of the discretized fracture $\gamma_{\hat{h}}$, $M \approx 1/\hat{h}$.

As we expected the maximum eigenvalue scales linearly with M but the minimum eigenvalue behaves almost independent with respect to $\hat{h}$, thus the condition number seems to scale linearly with M.

N	λ_{min}	λ_{max}	$cond_2$
11	$1.9 \cdot 10^{-3}$	$5.05 \cdot 10^4$	$2.7 \cdot 10^7$
19	$5.8 \cdot 10^{-4}$	$5.05 \cdot 10^4$	$8.6 \cdot 10^7$
29	$2.5 \cdot 10^{-4}$	$5.05 \cdot 10^4$	$2 \cdot 10^8$
39	$1.4 \cdot 10^{-4}$	$5.05 \cdot 10^4$	$3.6 \cdot 10^8$
49	$8.9 \cdot 10^{-5}$	$5.05 \cdot 10^4$	$5.7 \cdot 10^8$

Table 5.7: Eigenvalues and condition number for different mesh sizes h.

M	λ_{min}	λ_{max}	$cond_2$
51	$2.3 \cdot 10^{-4}$	$2.55 \cdot 10^4$	$1.1 \cdot 10^8$
101	$2.47 \cdot 10^{-4}$	$5.05 \cdot 10^4$	$2 \cdot 10^8$
201	$2.56 \cdot 10^{-4}$	$1 \cdot 10^5$	$3.9 \cdot 10^8$
301	$2.58 \cdot 10^{-4}$	$1.5 \cdot 10^5$	$5.8 \cdot 10^8$
401	$2.59 \cdot 10^{-4}$	$2 \cdot 10^5$	$7.74 \cdot 10^8$
501	$2.59 \cdot 10^{-4}$	$2.5 \cdot 10^5$	$9.66 \cdot 10^8$

Table 5.8: Eigenvalues and condition number for different mesh sizes $\hat{h}$.

Reduced Darcy model with intersection

We analyse the behaviour of both eigenvalues λ_{max} and λ_{min} and the condition number for the reduced Darcy model with intersecting fractures not coupled with the porous medium. The fractures are

$$\gamma_1 = \{(x, y) \in \Omega : y = 0.5\} \quad \text{and} \quad \gamma_2 = \{(x, y) \in \Omega : y = -2x + 1.4\} \ .$$

The data of the fractures are $d = 0.01$, $\xi_0 = 0.25$, $\hat{q} \equiv 4d$, $\hat{\eta} = 1/d$ and $\eta_\gamma = d$, for both fractures. The boundary condition are of natural type, with zero data for γ_1 and 0.5 for γ_2. The sparsity patter of the matrix is reported in Figure 5.30 to shows the symmetry, the different blocks fracture-fracture, the reduced problem in the intersection point i_p and its transposed which express the conservation of mass and the extended degrees of freedom which modify the more structured pattern of the original problem.

Table 5.9 shows the scaling of the maximum and the minimum eigenvalue and the condition number when the number M of segments for each fractures increases. We see that λ_{min} decreases linearly with $\hat{h}$ and, when the λ_{max} approaches a fixed value, the condition number increases linearly with $\hat{h}$. This behaviour is analogous to that reported in the previous section.

5.2.4 Limitations of the reduced model

We want to investigate the occurrence of spurious oscillatory for the coupled problem of Darcy flow in a fracture and the outer porous medium, see Figure 5.31 for an example. In particular pressure oscillations in the fracture arise in the case of strong variations of the coefficients, normal and tangential permeabilities of the fracture, when the discretization of the fracture is finer than the outer medium. A similar phenomena is presented also in [34].
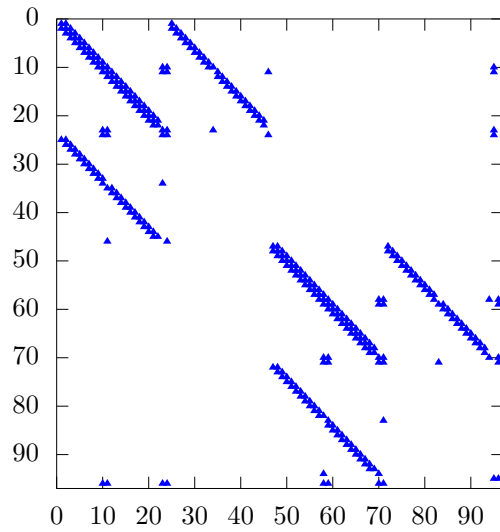
Figure 5.30: Sparsity patter of the coupled problem with 353 non zero values.

M	λ_{min}	λ_{max}	$cond_2$
11	$7.9 \cdot 10^{-3}$	9.7	$1.2 \cdot 10^3$
21	$4.3 \cdot 10^{-3}$	5.2	$1.2 \cdot 10^3$
41	$2.2 \cdot 10^{-3}$	2.7	$1.2 \cdot 10^3$
81	$1.1 \cdot 19^{-3}$	2	$1.75 \cdot 10^3$
161	$5.8 \cdot 10^{-4}$	2	$3.46 \cdot 10^4$
321	$2.9 \cdot 10^{-4}$	2	$6.88 \cdot 10^4$

Table 5.9: Eigenvalues and condition number for different mesh sizes $M \approx 1/\hat{h}_1 \approx 1/\hat{h}_2$.
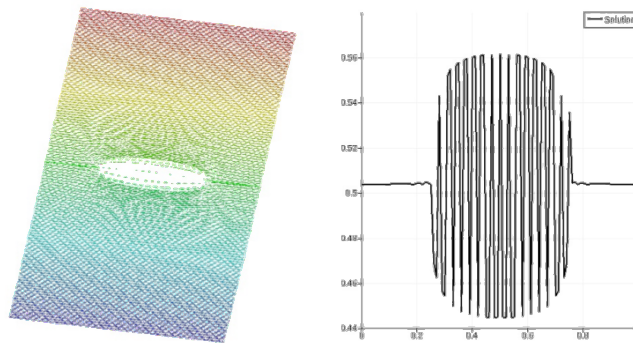
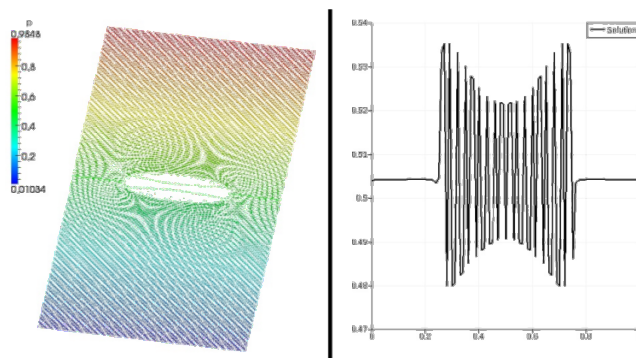**Figure 5.31:** In the left the pressure in the medium and in the fracture, we see some oscillation where the fracture acts as a barrier. In the right the pressure in the fracture, the oscillation ranges in ± 0.06. The medium is discretized with 64 triangles for each edge while the fracture with 128 segments.

In the sequel we indicate with N the number of triangles per edge of the domain, with M the number of elements in the fracture, with A the amplitude of the oscillations of pressure in the fracture and with ν the frequency of the oscillations.

The problem of interest is given on a square domain $\Omega = (0,\,1)^2$ with an horizontal fracture that cuts the domain as shown in Figure 5.32. The fracture
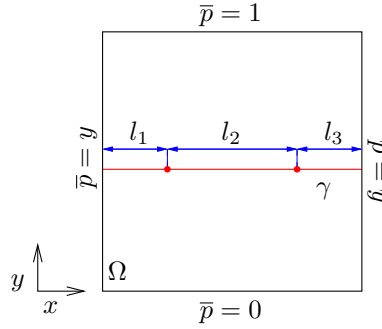
Figure 5.32: Computational domain cut by a fracture.

is

$$\gamma = \{(x,\,y) \in \Omega : y = 0.47\}\,.$$

As Figure 5.32 shows, the fracture is divided into three parts, with $|l_1| = |l_3| = 0.25$ and $|l_2| = 0.5$, where we will impose different values of fracture permeability. The fixed data are the permeability of the porous medium $\boldsymbol{K} = \boldsymbol{I}$, the scalar source $q = 4$ and the boundary conditions which are of essential type on $\partial\Omega$ and in $\partial\gamma$, in both cases we impose $\overline{p}\,(x,\,y) = y$. We present two different scenarios characterized by different permeability of the fracture. The first has $\hat{\eta} = 100$ and

$$\eta_\gamma\,(x) = \begin{cases} 10 & \text{if } x \in l_2, \\ 10^{-2} & \text{otherwise.} \end{cases}$$

The values of the oscillations are reported in Table 5.10 for different values of meshes size M and N.

	for $N = 10$				for $N = 20$			
M	10	20	40	80	10	20	40	80
A	0	$2.5 \cdot 10^{-2}$	$2.5 \cdot 10^{-2}$	$2.5 \cdot 10^{-2}$	0	0	10^{-2}	10^{-2}
ν	0	5	5	5	0	0	10	10

Table 5.10: Values of the amplitude A and frequency ν of the oscillations for different values of the meshes size M and N in the first scenario.

The second scenario has the following permeabilities in the fracture

$$\hat{\eta}\,(x) = \begin{cases} 10^3 & \text{if } x \in l_2, \\ 1 & \text{otherwise} \end{cases} \quad \text{and} \quad \eta_\gamma\,(x) = \begin{cases} 10 & \text{if } x \in l_2, \\ 10^{-2} & \text{otherwise.} \end{cases}$$

The values of the oscillations are reported in Table 5.11 for different values of meshes size M and N.

	for $N = 10$				for $N = 40$			
M	10	20	40	80	20	40	80	160
A	0	0.8	0.8	0.8	0	0	0.35	0.4
ν	0	5	5	5	0	0	20	20

Table 5.11: Values of the amplitude A and frequency ν of the oscillations for different values of the meshes size M and N in the second scenario.

The results show that the oscillations occur when the discretization of the fracture is finer than the mesh of the medium, which exhibit a frequency that depends only on the discretization of the outer medium N, in particular we found $\nu \approx N/2$. Figure 5.33 shows the same problem of Figure 5.31 with different mesh of the fracture, the frequency does not change but the amplitude decreases. Finally, if the spacing of the meshes of the porous medium and of

Figure 5.33: On the left the pressure in the medium and in the fracture, we see some oscillation in the centre where the fracture acts as a barrier. On the right the pressure in the fracture, the oscillation ranges in ± 0.03. The medium is discretized with 128 triangles for each edge while the fracture with 256 segments.

the fracture are comparable no significant oscillation are present, as Figure 5.34 shows.

It is important to notice that, even if the model develops oscillations for specific values of the parameters, the oscillations disappear when h and $\hat{h}$ go to to zero, as the theory predicts.

5.2.5 Some realistic examples

We present several realistic examples where the reduced models are applied. In particular we highlight the advantages of the reduced models compared to the complete models and the effect of the fractures to the flow. We use realistic data to prove that the reduced models behave well also for concrete applications.

Reduced Darcy model

To assess the effectiveness of the reduced model on realistic test cases we now consider the test case in subsection 5.1.1 and replace the fault with a two-
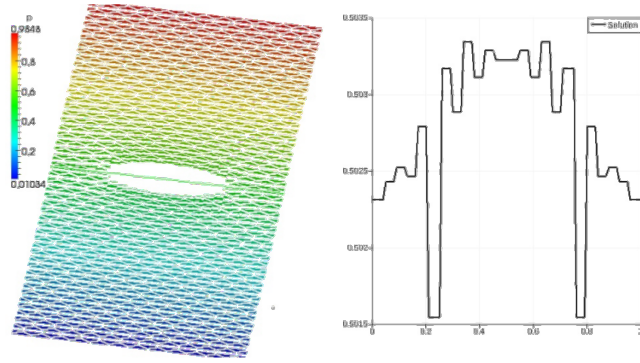
Figure 5.34: In the left the pressure in the medium and in the fracture, we see no oscillation for the fracture. In the right the pressure in the fracture, the oscillation ranges in $\pm 10^{-4}$, mainly concentrated near the discontinuity of the permeability. The medium is discretized with 24 triangles for each edge while the fracture with 24 segments.

dimensional interface, as shown in [35]. The fracture γ divides the domain in two sub-domains Ω_1 and Ω_2 as shown in Figure 5.35. We want to compare the pressure field obtained using the standard approach with a refined mesh, 72892 tetrahedra, and the pressure in the matrix and in the fault computed with the reduced model presented in Problem 3.3 with coarser grids, only 9840 tetrahedra for the matrix and 656 triangles for the fault.
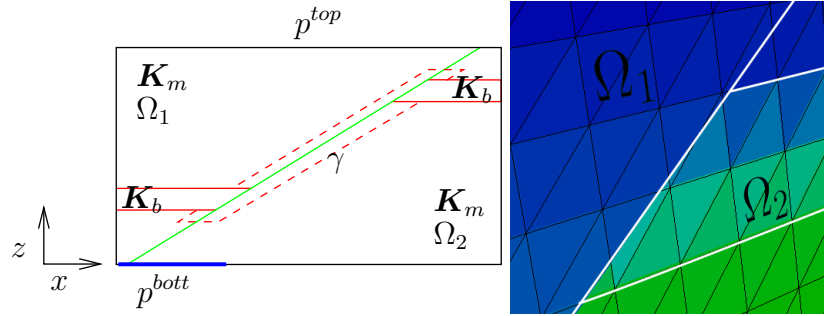
Figure 5.35: Schematic representation of the computational domain. The fault in subsection 5.1.1 is here replaced by a two-dimensional interface. On the right a zoom of the upper impermeable layer cut by the fault: XFEM allow us to reproduce a permeability field with discontinuities within the elements of the grid.

The permeability field is redefined as $\boldsymbol{K}(\boldsymbol{x}) = K(\boldsymbol{x})\,\boldsymbol{I}$, with

$$K(\boldsymbol{x}) = \begin{cases} 10^{-15} & \text{if } 200 < z < 400 \text{ and } \boldsymbol{x} \in \Omega_1, \\[2mm] 10^{-15} & \text{if } 1600 < z < 1800 \text{ and } \boldsymbol{x} \in \Omega_2, \\[2mm] 10^{-10} & \text{otherwise}, \end{cases}$$

and

$$K_{\Gamma,\boldsymbol{\tau}}(\boldsymbol{x}) = K_{\Gamma,\boldsymbol{n}}(\boldsymbol{x}) = \begin{cases} 10^{-15} & \text{if } 750 < x < 2750, \\[2mm] 10^{-10} & \text{otherwise}. \end{cases}$$

154

We point out that the extended finite element formulation allows us to represent a permeability coefficient $K(\boldsymbol{x})$ that is discontinuous across γ even if the grid is non conforming with the interface, see Figure 5.35, for further details see [38] and [45]. Since the problem in subsection 5.1.1 is a time dependent problem we here consider the pressure fields at the initial time $t = 0$, *i.e.* we solve equation (2.31) at $k = 0$, with the same boundary conditions as in Table 5.1. Results are shown in Figure 5.36. The pressure field obtained with the fine mesh is well reproduced with the coarse mesh and the reduced model for the flow along the fault. There is a slight mismatch at the top and bottom boundary, where the imposition of the natural boundary condition is less precise with a coarse grid since pressure is approximated as piecewise constant on each tetrahedron.

The reduced model has been, so far, applied only in the single-phase case, therefore a complete comparison of the resolved and reduced approaches is not possible, nevertheless the pressure fields computed at given saturation in an IMPES framework are in good qualitatively agreement.
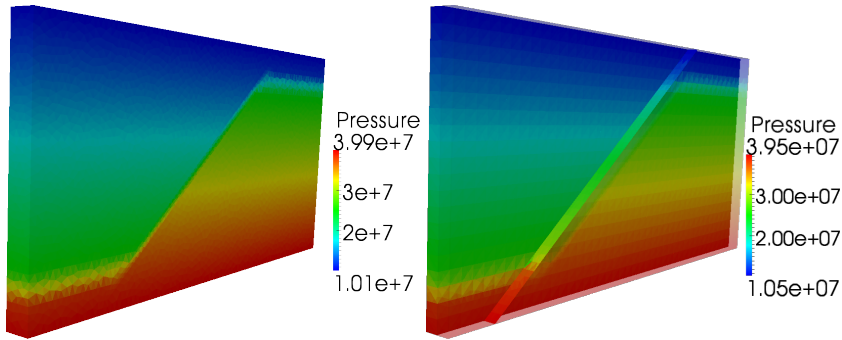
Figure 5.36: On the left, the pressure field of the problem in subsection 5.1.1 at initial time. On the right, the pressure field computed with a coarse mesh and the reduced model for the fault. The domain is clipped at $y = 100$ to visualize the pressure in the medium surrounding the fault.

Reduced Darcy model with intersection

We present a schematic example of a schematic sedimentary basin, where the flow takes place, in presence of three horizons and a fault which intersects them. The computational domain Ω, reported in Figure 5.37, is the unit square with boundary $\partial\Omega$ discretized with 2738 triangles. The horizons are represented by

$$\gamma_1 = \{(x, y) \in \Omega : y = 0.85\}, \quad \gamma_3 = \{(x, y) \in \Omega : y = 0.51\},$$
$$\gamma_2 = \{(x, y) \in \Omega : y = 0.1\sin(7x + 0.2) + 0.72\},$$

while the fault is

$$\gamma_4 = \{(x, y) \in \Omega : y = -2x + 1.4\}.$$

The boundary $\partial\Omega$ is divided into two parts where we impose for the medium and the fractures the same conditions: top and bottom homogeneous natural condition while right and left homogeneous essential condition. The source term
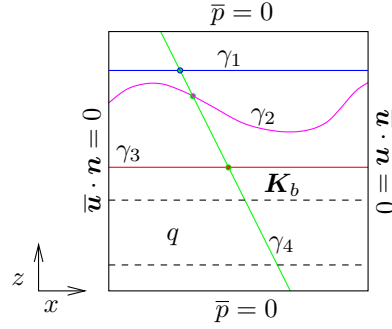
155

Figure 5.37: Schematic representation of the computational domain with four intersecting fractures.

q, present only in the medium, is

$$q\left(x,\,y\right) = \begin{cases} 4 & \text{if } 0.1 < y < 0.35, \\ 0 & \text{otherwise.} \end{cases}$$

The permeability tensor is discontinuous in the domain

$$\boldsymbol{K} = \begin{bmatrix} 1 & 0 \\ 0 & K_{2,2} \end{bmatrix} \quad \text{with} \quad K_{2,2}\left(x,\,y\right) = \begin{cases} 0.1 & \text{if } 0.35 < y < 0.51, \\ 1 & \text{otherwise,} \end{cases}$$

where, in Figure 5.37, we indicate with $\boldsymbol{K}_b$ the smaller value of $\boldsymbol{K}$. All the fractures have thickness equal to $d = 0.01$ and shape parameter equal to $\xi_0 = 0.25$ while their permeability and space discretization N are reported in Table 5.12. In Figure 5.38 is reported the net of the fractures with their pressure.

	γ_1	γ_2	γ_3	γ_4
η_γ	d	$100d$	$100d$	d
$\hat{\eta}$	$1/d$	$1/d$	$1/d$	$0.01/d$
N	41	81	41	41

Table 5.12: Different values of the permeability and space discretization for the horizons and the fault.

We can see that the pressure is discontinuous across the intersection points $\boldsymbol{i}_p$, furthermore the model can handle more then one intersection point $\boldsymbol{i}_p$ with the constraint that at most one intersection point $\boldsymbol{i}_p$ belongs to an element of the porous medium grid. Figure 5.39 compares the pressure field obtained with the reduced model, where also the fractures are presented, and the pressure field neglecting the fractures. We notice that the results are macroscopically different, therefore is important to describe accurately the horizons and the faults in simulations of subsurface flow.

Reduced transport model

We present a realistic example [36] for the reduced model of a tracer in the domain Q_T cut by the fracture γ, see Figure 5.40. The computational domain
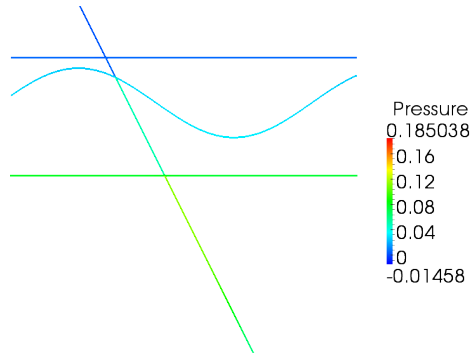
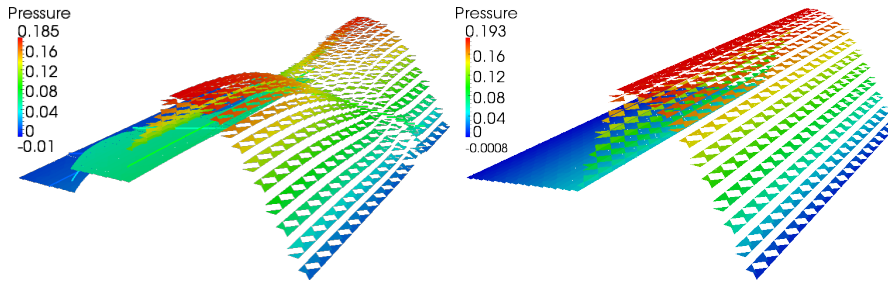**Figure 5.38:** Pressure field in the intersecting fractures.

Figure 5.39: Comparison of the pressure field with, left, and without, right, the fractures. In the left figure also the pressure in each fracture is present.
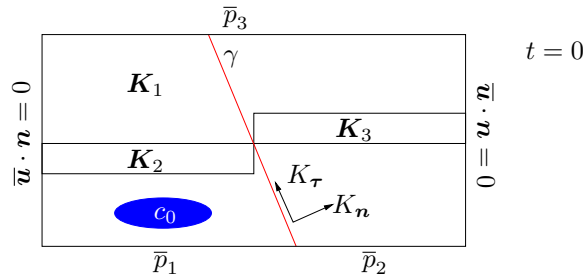

Figure 5.40: Computational domain with the data to obtain the velocity $\boldsymbol{u}$ and $\hat{\boldsymbol{u}}$.

Q_T has spatial dimensions $l_x \times l_y$, where $l_x = 6km$ and $l_y = 3km$, while the end time of the simulation is $T = 10^{13}s$, *i.e.* $\sim 0.95My$. The fracture has thickness $d = 10m$ and the shape parameter is $\xi_0 = 0.25$. To obtain the external velocity field $\boldsymbol{u}$ in the porous medium and in the fracture $\hat{\boldsymbol{u}}$ we solve a Darcy problem coupled with the reduced model in the fracture, presented in Problem 3.3. The data to obtain the velocity are reported in Table 5.13, where $\boldsymbol{K}_i = K_i \boldsymbol{I}$ and $\boldsymbol{q} = -9.81\boldsymbol{e}_2$. Note that the fracture acts as a preferential path for the flux in the tangential direction and as a barrier in the normal direction. In both problem we impose $\mu = 5 |l_x| |l_y|$ for the penalty parameter of the Nitche's method, because we use realistic dimensions of the domain Ω.

Figure 5.41 shows the pressure field in the domain and in the fracture for this problem.

$K_1 = 10^{-15}m^2$	$K_2 = 10^{-18}m^2$	$K_3 = 10^{-17}m^2$	$K_\tau = 10^{-13}m^2$
$K_n = 10^{-17}m^2$	$\bar{p}_1 = 34.53MPa$	$\bar{p}_2 = 29.53MPa$	$\bar{p}_3 = 0.1MPa$

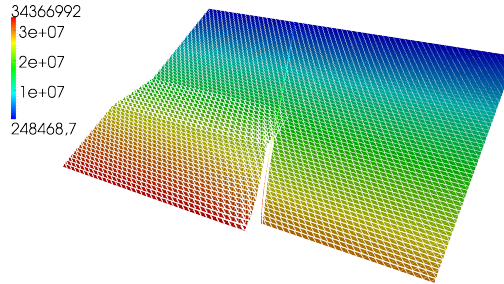**Table 5.13:** Data for the Darcy problem to obtain the external field $\boldsymbol{u}$ and $\hat{\boldsymbol{u}}$.

Figure 5.41: Pressure field of the problem.

The molecular diffusion of the tracer is homogeneous in the domain $\boldsymbol{D} = D\boldsymbol{I}$, with $D = 10^{-8}m^2/s$, while in the fracture we impose $D_{\boldsymbol{n}} = Dd$ and $D_{\boldsymbol{\tau}} = D/d$, *i.e.* the fracture has the same equivalent molecular diffusion of the medium. We impose homogeneous essential condition on the left and the right part of $\partial\Omega$ and homogeneous natural condition on the top and the bottom of $\partial\Omega$. Finally the initial condition is $c_0 = 0.3$ in the blue ellipse presented in Figure 5.40. We use $\Delta t = 5 \cdot 10^{10}s$ as the time step for the temporal scheme. We present in Figure 5.42 the concentration at two different times, on the left for $t = 1.87 \cdot 10^{-2}My$ and on the right for $t = 0.1105My$. The figures at the top are the solutions without the fracture in both the fracture and the concentration problem, while on the bottom figures are the solutions with the fracture. We can notice that the solutions are different confirming the necessity to handle in an efficient and accurate way the fracture.
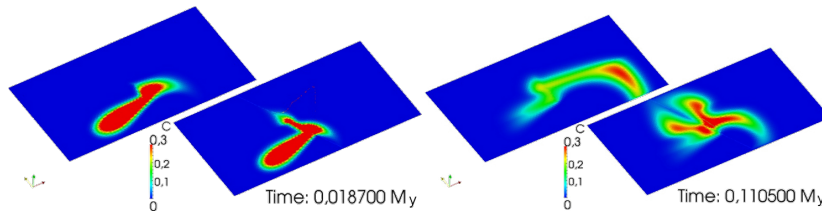

Figure 5.42: Comparison, in two different times, between the solution obtained without the fracture, the top figures, and the solution with the fracture and the reduced model, the bottom figures.

5.3 Examples of high performance computing

A very important aspect in high performance computing simulations is the scalability of the code and load balancing. Scalability is the gain we obtain if we increase the number of processes in a parallel setting. There are several different ways to measure this index. Strong scalability measures the ratio between elapsed time and number of processors for a fixed problem. To be significant

we need a problem large enough to have reasonable sized sub-problems even when the number of process is high. This often implies that the problem is too large to be solved on a single processor then the concept of weak scalability has been introduced. Weak scalability uses problems which scale as the number of processors. In this case the major difficulty is the proper scaling of the size of the problems. Our test cases involve some hundreds of processors so we can use the strong scalability concept.

The second important index is the load balancing which measures, for each part of the code, the amount of time each core requires. The best scenario is when all the processors use the same time so no time is wasted. In practice is difficult to have a perfect load balancing so we analyse the ratio between the minimum and the maximum time.

Both indices are taken into consideration for the solution of a two-phase flow and a transmission problem using LifeV.

5.3.1 Scalability

The examples we present are performed on the so called *Lagrange* super computer of the Italian computer centre CILEA with the following specifications

Type HP Cluster Intel Xeon
Nodes 208
CPU two processors Intel Xeon QuadCore 3.166GHz for each node
RAM 16 GB for each node
Hard-Disk total storage 13TB

We want to compare the strong scalability of the two-phase solver for the example presented in the subsection 5.1.1. Figure 5.43 shows the scalability, in
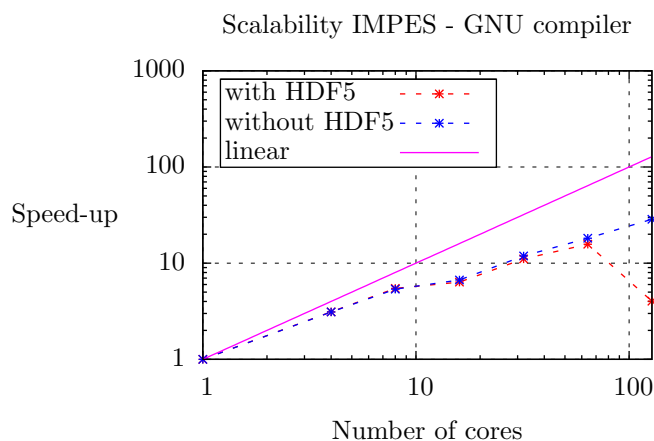

Figure 5.43: Scalability of the IMPES solver with gnu compiler.

term of speed-up, of the solver when the GNU C++ compiler version 4.1.2 is used, with and without the exporting of the solution in the HDF5 format. The speed-up is the ratio between the total time in the serial simulation and the total time in the simulation with more processors. We can see that the code scales

well, with a gain of $\sim 20\%$, except when the number of processors grows up to one hundred and the solution is exported, this is mainly due to the overhead of I/O operations. Figure 5.44 shows the scalability of the solver, with the same
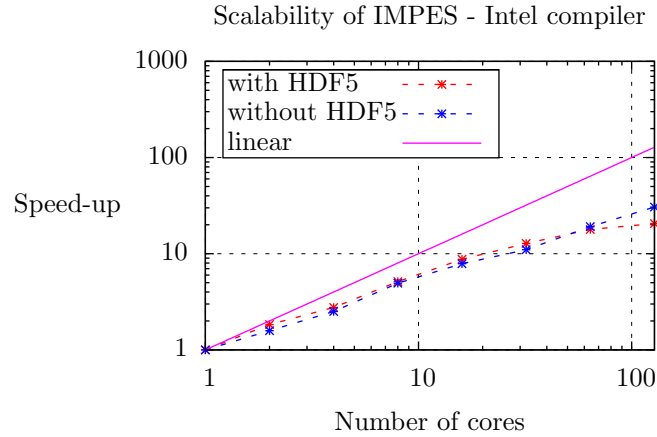

Figure 5.44: Scalability of the IMPES solver with intel compiler.

problem, if we use the intel compiler 11.1. In contrast with the previous case, we have no problems with the exporting of the solution even if the number of processors grows. With the intel compiler we have the same gain as with the GNU compiler. In Figure 5.45 we present the strong scalability of the transmis-
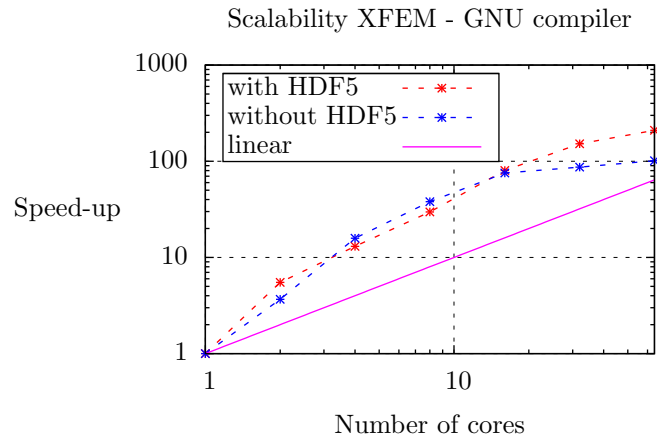

Figure 5.45: Scalability of the XFEM solver with gnu compiler.

sion problem presented in subsection 5.1.3. In this case the speed-up is greater then linear because there are some bottle necks in the serial version of the code. The gain is greater then $\sim 40\%$ in the central part of the graph, for both the compilers.

Similar behaviour are obtained with other types of super-computers like IBM BlueGene/P and IBM pSeries 575 from CINECA centre.

Processor Id	1	2	3	ratio
Read and partition the mesh	2.05	2.1	2.09	0.98
Create FEMs	1.08	1.08	1.08	1
Time step 0				
Create pressure matrix	7.86	7.86	7.86	1
Solution linear system	12.51	12.51	12.5	1
Reconstruct p and $\boldsymbol{u}$	7.42	7.43	7.43	1
Interpolation of the $\boldsymbol{u}$	1.1	1.1	1.1	1
Compute CFL	2.19	1.9	2.3	0.83
Solution of hyperbolic part of saturation	2.38	2.47	2.61	0.91
Solution export	0.31	0.88	0.92	0.34
Time step 1				
Create pressure matrix	7.98	7.98	7.99	1
Solution linear system	12.35	12.35	12.35	1
Reconstruct p and $\boldsymbol{u}$	7.53	7.53	7.53	1
Interpolation of the $\boldsymbol{u}$	1.09	1.09	1.09	1
Compute CFL	1.95	1.95	1.95	1
Solution of hyperbolic part of saturation	2.1	2.1	2.1	1
Solution export	0.31	0.75	0.77	0.4

Table 5.14: Load balancing of three processors to solve the two-phase flow. The time reported are in seconds.

We point out that in all of these cases we did not tune all the possible parameter to obtain the best performance but we used the standard ones. This is very encouraging because even better gain can be obtained with an optimal tuning.

5.3.2 Load balancing

We present the load balancing of the two-phase flow solver of the example presented in subsection 5.1.1. In particular we want to compare the balancing when three processors are used to solve the problem. In Table 5.14 we report the results for the first two time steps and the computational costs for the preprocess operations such as reading and partitioning the mesh and creating the finite elements spaces. Since we use a sub-loop to solve the hyperbolic part of the saturation equation in the table we report the average values for both the computation of the CFL condition and the solution of the hyperbolic equation. In the last column the table reports the ratio between the minimum time and the maximum time. The values suggest that the code is well balanced in almost all of its parts, in particular the solution of the pressure equation is perfectly balanced and also the solution of the hyperbolic equation in the second time step. Nevertheless the exceptions are the exporting of the solutions, where the cost grows with respect the process Id, and the hyperbolic solver in the first time step where the balance on the three processors is not perfect.

We present now the load balancing for the transmission problem presented in the subsection 5.1.3. Since the partitioning in LifeV is based on the computational grid it can happen that the level set cuts the mesh just in some sub-regions generating an unbalanced problem even if the grid is balanced. We have modi-

	Weighted [s]		Not weighted [s]	
Processor Id	1	2	1	2
Mesh reading	0.27	0.27	0.25	0.26
Mesh partitioning	0.23	0.24	0.24	0.25
Stiffness matrix	1.26	1.2	0.88	1.61
Penalty matrix	0.06	0.06	0	0.12
Jump terms	0.28	0.23	0.01	0.53
Forcing term	0.77	0.79	0.56	0.96
Global assemble	2.82	2.88	3.79	3.76
Solution	0.69	0.79	0.6	0.7

Table 5.15: Load balancing for a transmission problem with a weighted and not weighted mesh partitioning. Values taken from [45].

fied the partitioning procedure keeping the possibility to assign weights to the elements. The policy we choose is to assign weight one if the element is uncut while for the cut elements we assign weight one plus the number of level sets which intersect the element. In Table 5.15 we present the load balancing using two processors in the cases of weighted and non-weighted mesh partitioning. We tune the level set in such a way that the un-weighted case the processor 2 contains all the cut elements. We can see that the construction of all the matrices and vectors becomes unbalanced between two processors while it is balanced if we use the weighted partitioned. Also the assembly of the matrix, which is the procedure where the local parts of the global matrix are communicated to the other processors, has a greater cost in the case of the unbalanced simulation. These results suggest that the simple policy we adopted for balancing the partition is effective to recover a well balanced simulation.

Conclusion and future developments

In this thesis we developed an original numerical method for the simulation of Darcy flows at the basin scale. In particular we addressed the problem of oil migration from source to trap, which can be modelled as a two-phase flow of oil and water occurring through the sedimentary basin and focused, in particular, along strongly localized heterogeneities such as faults and horizons between layers. Following the approach proposed in [57] and [24] we adopted a model reduction strategy to account for the presence of the faults, whose thickness is very small compared to the length scale of the basin. Instead of refining the computational grid the faults are replaced by surfaces immersed in a three-dimensional domain, or lines in a bidomensional domain, yielding a coupled problem for the flow in the porous matrix and along the fractures. Moreover, following [24] we allowed the grid to be non-matching with these surfaces adopting the extended finite element method (XFEM) to this type of problems.

To extend the work of [24] to realistic cases we derived a reduced model that is able to take into account the effect of gravity, or of a generic vector source term. Moreover we extended the reduced model to the case of a domain crossed by several intersecting fractures, deriving suitable interface conditions in the intersection points, which are again non-conforming with the grids of the fractures. We presented the correct functional setting and generalized the XFEM enrichment of the finite element spaces in this general case.

Finally, we applied the same strategy used for the Darcy problem to derive a reduced model for the problem of the advection and diffusion of a tracer transported in the porous medium by a given vector field. This problem is very interesting as it can model pollutant transport in water-bearing strata. For all the mentioned problems we have presented some analytical results and a wide number of numerical simulations to support the theoretical findings. The comparison of the reduced model with the results of the classical model on a very fine grid showed that the reduced model yields correct results with a low computational cost since it does not require a mesh that is able to resolve the fractures. The error analyses showed that, as the mesh is refined the error decays as predicted by the theory. We analysed the behaviour of the condition number of the problem as a function of the position of the interface with respect to the grid finding that if the area of a sub-element tends to zero the problem becomes ill-conditioned. The development of effective preconditioners will be the subject of further investigations with a view to applying the method to complex realistic geometries. Finally we applied the reduced models to problems with realistic

data to assess the robustness of the method with real values of the coefficients and obtained solutions that exhibited the correct qualitative behaviour.

In addition to the development of reduced models a parallel and complementary work consisted in the implementation, in the framework of the LifeV library, of a two-phase solver that is three-dimensional and fully parallel. Modern programming and numerical techniques were used to obtain a general, robust solver. Some realistic problems were presented such as the flow of oil along a fault or the trapping under an impermeable cap-rock. We also tested the scalability of the code on super-computer machines.

As mentioned above, the effectiveness of the proposed models could be improved introducing stabilization techniques or appropriate preconditioners to obtain a condition number which is independent of the position of the fractures. In addition, for the transport of the tracer an important improvement would be the inclusion of stabilizations to handle advection-dominated problems without resorting to mesh refinement. Analytical properties such as well-posedness, mass conservation properties, positivity and convergence rates deserve further investigation in the case of intersecting fractures and for the scalar tracer transport model. Finally, a reduced model for the saturation equation should be derived following the work by [46] and implemented in an XFEM framework in order to obtain a two-phase solver that can be applied at the basin scale accounting for the presence of faults with a low computational cost.

Bibliography

[1] Adimurthi, Jérôme Jaffré, and G. D. Veerappa Gowda. Godunov-type methods for conservation laws with a flux function discontinuous in space. *SIAM J. Numer. Anal.*, 42(1):179–208 (electronic), 2004. (Cited in pages 40, 57, 59, 60).

[2] Clarisse Alboin, Jérôme Jaffré, Jean E. Roberts, Xuewen Wang, and Christophe Serres. *Domain decomposition for some transmission problems in flow in porous media*, volume 552 of *Lecture Notes in Phys.*, pages 22–34. Springer, Berlin, 2000. (Cited in pages 12, 61).

[3] Laila Amir, Michel Kern, Vincent Martin, and Jean E. Roberts Roberts. Décomposition de domaine et préconditionnement pour un modèle 3D en milieu poreux fracturé. In *Proceeding of JANO 8, 8th conference on Numerical Analysis and Optimization*, December 2005. (Cited in page 12).

[4] Philippe Angot, Franck Boyer, and Florence Hubert. Asymptotic and numerical modelling of flows in fractured porous media. *M2AN Math. Model. Numer. Anal.*, 43(2):239–275, 2009. (Cited in pages 12, 61, 72).

[5] Todd Arbogast. The existence of weak solutions to single porosity and simple dual-porosity models of two-phase incompressible flow. *Nonlinear Anal.*, 19(11):1009–1031, 1992. (Cited in page 48).

[6] Douglas N. Arnold, Daniele Boffi, and Richard S. Falk. Quadrilateral $H(\mathrm{div})$ finite elements. *SIAM J. Numer. Anal.*, 42(6):2429–2451 (electronic), 2005. (Cited in page 50).

[7] C. Bradford Barber, David P. Dobkin, and Hannu Huhdanpaa. The quick-hull algorithm for convex hulls. *ACM TRANSACTIONS ON MATHEMATICAL SOFTWARE*, 22(4):469–483, 1996. (Cited in page 128).

[8] Peter Bastian. *Numerical Computation of Multiphase Flows in Porous Media*. PhD thesis, Heidelberg University, 1999. (Cited in pages 18, 23).

[9] Jacob Bear. *Dynamics of Fluids in Porous Media*. American Elsevier, 1972. (Cited in pages 23, 24, 25, 26, 34).

[10] R.P. Brent. *Algorithms for Minimization Without Derivatives*. Dover books on mathematics. Dover Publications, 2002. (Cited in page 124).

[11] Franco Brezzi and Michel Fortin. *Mixed and Hybrid Finite Element Methods*, volume 15 of *Computational Mathematics*. Springer Verlag, Berlin, 1991. (Cited in pages 44, 49, 53, 55, 56, 64).

[12] R. H. Brooks and A. T. Corey. *Hydraulic properties of porous media*. Civil Engineering Dept., Colorado State Univ., Fort Collins, CO, 1964. (Cited in pages 35, 36).

[13] Erik Burman and Peter Hansbo. A unified stabilized method for stokes' and darcy's equations. *J. Comput. Appl. Math.*, 198:35–51, January 2007. (Cited in page 98).

[14] Clément Cancès. Asymptotic behavior of two-phase flows in heterogeneous porous media for capillarity depending only on space. II. Nonclassical shocks to model oil-trapping. *SIAM J. Math. Anal.*, 42(2):972–995, 2010. (Cited in pages 40, 48).

[15] Laura Cattaneo and Claudia Maria Colciago. Modelli computazionali per la crescita tissutale. Master's thesis, Politecnico di Milano, 2010. (Cited in page 146).

[16] R.E. Chapman. *Petroleum geology*. Developments in petroleum science. Elsevier, 1983. (Cited in page 21).

[17] G. Chavent. A new formulation of diphasic incompressible flows in porous media. In Paul Germain and Bernard Nayroles, editors, *Applications of Methods of Functional Analysis to Problems in Mechanics*, volume 503 of *Lecture Notes in Mathematics*, pages 258–270. Springer Berlin / Heidelberg, 1976. (Cited in page 29).

[18] Guy Chavent and Jérôme Jaffré. *Mathematical Models and Finite Elements for Reservoir Simulation*, volume 17. Elsevier, 1986. (Cited in pages 25, 42, 48).

[19] Zhangxin Chen. *Reservoir Simulation: Mathematical Techniques in Oil Recovery*, volume 77. SIAM, 2007. (Cited in pages 18, 28, 34).

[20] Zhangxin Chen and Richard E. Ewing. Comparison of various formulations of three-phase flow in porous media. *J. Comput. Phys.*, 132(2):362–373, 1997. (Cited in page 32).

[21] Zhangxin Chen, Guanren Huan, and Yuanle Ma. *Computational methods for multiphase flows in porous media*. Computational Science & Engineering. Society for Industrial and Applied Mathematics (SIAM), Philadelphia, PA, 2006. (Cited in pages 18, 32).

[22] Bernardo Cockburn and Chi-Wang Shu. Runge-Kutta discontinuous Galerkin methods for convection-dominated problems. *J. Sci. Comput.*, 16(3):173–261, 2001. (Cited in page 57).

[23] A.T. Corey. *Mechanics of immiscible fluids in porous media*. Water Resources Publications, 1994. (Cited in page 23).

[24] Carlo D'Angelo and Anna Scotti. A Mixed Finite Element Method for Darcy Flow in Fractured Porous Media with Non-Matching Grids. *Mathematical Modelling and Numerical Analysis*, 2011. (Cited in pages 12, 95, 97, 101, 102, 103, 141, 146, 163).

[25] Carlo D'Angelo and Paolo Zunino. Robust numerical approximation of coupled stokes' and darcy's flows applied to vascular hemodynamics and biochemical transport. *ESAIM: Mathematical Modelling and Numerical Analysis*, 45(03):447–476, 2011. (Cited in page 98).

[26] Clint N. Dawson. Godunov-mixed methods for advective flow problems in one space dimension. *SIAM J. Numer. Anal.*, 28(5):1282–1309, 1991. (Cited in page 57).

[27] Clint N. Dawson. Godunov-mixed methods for advection-diffusion equations in multidimensions. *SIAM J. Numer. Anal.*, 30(5):1315–1332, 1993. (Cited in page 57).

[28] Peter Dietrich, Rainer Helmig, Martin Sauter, Heinz Hötzl, Jürgen Köngeter, and Georg Teutsch, editors. *Flow and transport in fractured porous media*. Springer, 2005. (Cited in page 22).

[29] B. Durand. Present trends in organic geochemistry in research on migration of hydrocarbons. In Malvin Bjorøy, editor, *Advances in organic geochemistry*, 1981. (Cited in page 17).

[30] W. A. England, A. S. Mackenzie, D. M. Mann, and T. M. Quigley. The movement and entrapment of petroleum fluids in the subsurface. *Journal of the Geological Society*, 144(2):327–347, April 1987. (Cited in pages 16, 17).

[31] A. Ern and J.L. Guermond. *Theory and practice of finite elements*. Applied mathematical sciences. Springer, 2004. (Cited in page 128).

[32] Magne S. Espedal and Kenneth Hvistendahl Karlsen. Numerical solution of reservoir flow models based on large time step operator splitting algorithms. In *Filtration in porous media and industrial application (Cetraro, 1998)*, volume 1734 of *Lecture Notes in Math.*, pages 9–77. Springer, Berlin, 2000. (Cited in page 57).

[33] Gilles Fourestey and Simone Deparis. Lifev user manual. `http://lifev.org`, November 2010. (Cited in pages 123, 125).

[34] Najla Frih, Vincent Martin, E. Jean Roberts, and Ali Saada. Modeling fractures as interfaces with nonmatching grids. Research Report RR-7517, INRIA, February 2011. (Cited in page 150).

[35] Alessio Fumagalli and Anna Scotti. Numerical modelling of multiphase subsurface flow in the presence of fractures. *Communications in Applied and Industrial Mathematics*, December 2011. (Cited in page 154).

[36] Alessio Fumagalli and Anna Scotti. A reduced model for flow and transport in fractured porous media with non-matching grids. In *ENUMATH 2011 Proceedings Volume*. Springer, 2012. Accepted. (Cited in pages 139, 156).

[37] M.W. Gee, C.M. Siefert, J.J. Hu, R.S. Tuminaro, and M.G. Sala. *ML 5.0 Smoothed Aggregation User's Guide*, 2006. (Cited in page 123).

167

[38] Anita Hansbo and Peter Hansbo. An unfitted finite element method, based on Nitsche's method, for elliptic interface problems. *Comput. Methods Appl. Mech. Engrg.*, 191(47-48):5537–5552, 2002. (Cited in pages 129, 133, 155).

[39] Anita Hansbo and Peter Hansbo. A finite element method for the simulation of strong and weak discontinuities in solid mechanics. *Comput. Methods Appl. Mech. Engrg.*, 193(33-35):3523–3540, 2004. (Cited in page 12).

[40] Thomas Hantschel and Armin I. Kauerauf. *Fundamentals of Basin and Petroleum Systems Modeling.* Springer, 2009. (Cited in pages 18, 19, 20, 21, 27, 34).

[41] Michael A. Heroux, Roscoe A. Bartlett, Vicki E. Howle, Robert J. Hoekstra, Jonathan J. Hu, Tamara G. Kolda, Richard B. Lehoucq, Kevin R. Long, Roger P. Pawlowski, Eric T. Phipps, Andrew G. Salinger, Heidi K. Thornquist, Ray S. Tuminaro, James M. Willenbring, Alan Williams, and Kendall S. Stanley. An overview of the trilinos project. *ACM Trans. Math. Softw.*, 31(3):397–423, 2005. (Cited in page 123).

[42] Helge Holden, Kenneth Hvistendahl Karlsen, and Knut-Andreas Lie. Operator splitting methods for degenerate convection-diffusion equations. I. Convergence and entropy estimates. In *Stochastic processes, physics and geometry: new interplays, II (Leipzig, 1999)*, volume 29 of *CMS Conf. Proc.*, pages 293–316. Amer. Math. Soc., Providence, RI, 2000. (Cited in page 45).

[43] Helge Holden, Kenneth Hvistendahl Karlsen, and Knut-Andreas Lie. Operator splitting methods for degenerate convection-diffusion equations ii: numerical examples with emphasis on reservoir simulation and sedimentation. *Computational Geosciences*, 4(4):287–322, 2000. (Cited in pages 45, 57).

[44] A.G. Hunt. *Percolation theory for flow in porous media.* Lecture notes in physics. Springer, 2005. (Cited in page 21).

[45] Guido Iori. Una metodologia XFEM per problemi ellittici 3D con superfici di discontinuità. Master's thesis, Politecnico di Milano, December 2011. (Cited in pages 133, 146, 155, 162).

[46] J. Jaffré, M. Mnejja, and J.E. Roberts. A discrete fracture model for two-phase flow with matrix-fracture interaction. *Procedia Computer Science*, 4:967–973, 2011. (Cited in pages 12, 164).

[47] Jérôme Jaffré. Numerical calculation of the flux across an interface between two rock types of a porous medium for a two-phase flow. In *Hyperbolic problems: theory, numerics, applications (Stony Brook, NY, 1994)*, pages 165–177. World Sci. Publ., River Edge, NJ, 1996. (Cited in pages 40, 57).

[48] Jérôme Jaffré, Vincent Martin, and Jean E. Roberts. Generalized cell-centered finite volume methods for flow in porous media with faults. In *Finite volumes for complex applications, III (Porquerolles, 2002)*, pages 343–350. Hermes Sci. Publ., Paris, 2002. (Cited in page 12).

[49] S. G. Jennings. The mean free path in air. *Journal of Aerosol Science*, 19(2):159–166, 1988. (Cited in page 24).

[50] E. F. Kaasschieter. Solving the Buckley-Leverett equation with gravity in a heterogeneous porous medium. *Comput. Geosci.*, 3(1):23–48, 1999. (Cited in page 60).

[51] K. H. Karlsen, N. H. Risebro, and J. D. Towers. L^1 stability for entropy solutions of nonlinear degenerate parabolic convection-diffusion equations with discontinuous coefficients. *Skr. K. Nor. Vidensk. Selsk.*, (3):1–49, 2003. (Cited in page 60).

[52] K. Hvistendahl Karlsen, K.-A. Lie, J. R. Natvig, H. F. Nordhaug, and H. K. Dahle. Operator splitting methods for systems of convection-diffusion equations: nonlinear error mechanisms and correction strategies. *J. Comput. Phys.*, 173(2):636–663, 2001. (Cited in page 45).

[53] Matteo Lesinigo. Analisi di modelli multiscala per i fluidi in mezzi porosi con fratture. Master's thesis, Politecnico di Milano, April 2009. (Cited in page 61).

[54] Randall J. LeVeque. *Finite Volume Methods for Hyperbolic Problems*. Number 31 in Cambridge Texts in Applied Mathematics. Cambridge University Press, 2004. (Cited in page 40).

[55] P.-L. Lions and B. Mercier. Splitting algorithms for the sum of two nonlinear operators. *SIAM J. Numer. Anal.*, 16(6):964–979, 1979. (Cited in pages 42, 46).

[56] Leslie B. Magoon and Wallace G. Dow. *The Petroleum System: From Source to Trap*, volume 60 of *Memoir*. American Association Of Petroleum Geologists, 10 1994. (Cited in pages 15, 18).

[57] Vincent Martin, Jérôme Jaffré, and Jean E. Roberts. Modeling fractures and barriers as interfaces for flow in porous media. *SIAM J. Sci. Comput.*, 26(5):1667–1691, 2005. (Cited in pages 12, 61, 72, 79, 163).

[58] Siddhartha Mishra and Jérôme Jaffré. On the upstream mobility scheme for two-phase flow in porous media. *Comput. Geosci.*, 14(1):105–124, 2010. (Cited in pages 57, 59).

[59] Norman R. Morrow. A Review of the Effects of Initial Saturation, Pore Structure and Wettability on Oil Recovery by Waterflooding. In *North Sea Oil and Gas Reservoirs Seminar, Trondheim (December 2-4, 1985)*, pages 179–191. Graham and Trotman, Ltd., London, 1987. (Cited in page 17).

[60] M. Muskat. *Physical principles of oil production*. McGraw-Hill Book Co., New York, 1949. (Cited in page 23).

[61] Sundararajan Natarajan, Stéphane Bordas, and D. Roy Mahapatra. Numerical integration over arbitrary polygonal domains based on Schwarz–Christoffel conformal mapping. *International Journal for Numerical Methods in Engineering*, 80(1):103–134, 2009. (Cited in page 128).

[62] Alfio Quarteroni. *Numerical Models for Differential Problems.* Modeling, Simulation and Applications. Springer, Heidelberg, DE, 2009. (Cited in page 45).

[63] Alfio Quarteroni and Alberto Valli. *Numerical approximation of partial differential equations*, volume 23 of *Springer Series in Computational Mathematics.* Springer-Verlag, Berlin, 1994. (Cited in pages 42, 45, 52).

[64] P. A. Raviart and J. M. Thomas. A mixed finite element method for second order elliptic problems. *Lecture Notes in Mathematics*, 606:292–315, 1977. (Cited in pages 50, 54, 96).

[65] A. Reusken. Analysis of an extended pressure finite element space for two-phase incompressible flows. *Computing and Visualization in Science*, 11(4-6):293–305, 2008. cited By (since 1996) 6. (Cited in page 146).

[66] Amir Riaz and Hamdi Tchelepi. Stability of two-phase vertical flow in homogeneous porous media. *Physics of Fluids*, 19, 2007. (Cited in page 37).

[67] Jean E. Roberts and J.-M. Thomas. Mixed and hybrid methods. In *Handbook of numerical analysis, Vol. II*, Handb. Numer. Anal., II, pages 523–639. North-Holland, Amsterdam, 1991. (Cited in page 49).

[68] Marzio Sala and Michael Heroux. *Robust Algebraic Preconditioners using IFPACK 3.0.* Sandia National Laboratories, february 2005. (Cited in page 123).

[69] Amel Sboui, Jérôme Jaffré, and Jean Roberts. A composite mixed finite element for hexahedral grids. *SIAM J. Sci. Comput.*, 31(4):2623–2645, 2009. (Cited in page 50).

[70] Anna Scotti. *A Numerical Model for Generation, Rntention and Expulsion of Hydrocarbons from Source Rock.* PhD thesis, Politecnico di Milano, March 2010. (Cited in page 37).

[71] D. Sluijk and Marinus Herman Nederlof. Worldwide Geological Experience as a Systematic Basis for Prospect Appraisal. *Petroleum Geochemistry and Basin Evaluation*, 35:15–25, 1984. (Cited in page 17).

[72] J.G. Speight. *The chemistry and technology of petroleum.* Chemical industries. CRC Press/Taylor & Francis, 2007. (Cited in page 27).

[73] Øyvind Sylta. *Hydrocarbon migration modelling and exploration risk.* PhD thesis, Norwegian University of Science and Technology, 2002. (Cited in page 18).

[74] Øyvind Sylta. Quantifying secondary migration efficiencies. *Geofluids*, 2(4):285–298, 2002. (Cited in page 36).

[75] M. Th. van Genuchten. A closed-form equation for predicting the hydraulic conductivity of unsaturated soils. *Soil Sci. Soc. Am. J.*, 44(5):892–898, 1980. (Cited in page 34).

[76] F. Vassenden, Øyvind Sylta, and C. Zwach. Secondary migration in a $2D$ visual laboratory model. European Association of Geoscientists & Engineers, 2003. Fault and Top Seals: What do we know and where do we go? (Cited in page 131).

[77] D. H. Welte. *Migration of Hydrocarbons in Sedimentary Basins*, chapter Migration of hydrocarbons, facts and theory, page 393. Paris, Editions Technip, 1988. (Cited in page 17).

[78] Stephen Whitaker. *The Method of Volume Averaging*, volume 13 of *Theory and Applications of Transport in Porous Media*. Kluwer Academic Press, 1999. (Cited in page 23).

[79] N. N. Yanenko. *The method of fractional steps. The solution of problems of mathematical physics in several variables*. Springer-Verlag, New York, 1971. Translated from the Russian by T. Cheron. English translation edited by M. Holt. (Cited in page 42).

[80] Paolo Zunino, Laura Cattaneo, and Claudia Maria Colciago. An unfitted interface penalty method for the numerical approximation of contrast problems. *Applied Numerical Mathematics*, 61(10):1059–1076, 2011. (Cited in page 146).